



The
University
Of
Sheffield.

**INTRODUCTION AND DEVELOPMENT OF ALUMINIUM ION FREE
SILICATE BASED BIOACTIVE GLASS IONOMER CEMENT BASED ON
GLASS FLAKES AND SETTING MODIFIER (CITRATE) FOR DIRECT
POSTERIOR DENTAL RESTORATIONS**

Dr Muhammad Khawaja Hammad Uddin

Thesis submitted to the University of Sheffield for the degree of Doctor of Philosophy

Department of Material Sciences and Engineering

July 2018

Abstract

Enhanced glass ionomer cement (GIC), based on bioactive glasses, are relatively new material used in minimally invasive prevention of dental caries in the field of restorative dentistry over the past few decades. A series of aluminum ion free silicate based bioactive glasses with the substitution of calcium with strontium and barium with the admixture of poly-acrylic acid after the introduction of tartrate and citrate ions in the presence of water were produced to study for dental applications. Aluminum ion free silica based bioactive glass composition substituting 3 mole percent of calcium oxide with strontium and barium $46.14 \text{ SiO}_2.2.60 \text{ P}_2\text{O}_5.23.95 \text{ CaO}.24.35 \text{ Na}_2\text{O}.1.5\text{X}1.1.5\text{X}2$ ($\text{X}1 = \text{SrO}$ and SrF_2) and ($\text{X}2 = \text{BaO}$ and BaF_2) were synthesised using melt quenching technique. It was postulated that a change of particle size of filler content and introduction of citrate ions would enhance the mechanical, chemical and biological properties of the resultant set cement. To test this hypothesis, glass flakes of different sizes, ranging from 100 nm to 100 μm were obtained from Leeds Glass Flakes Company Ltd, UK and were characterised physically, mechanically and *in vitro* biologically. The analysis of prepared glass and cement samples as undertaken using various physical, chemical, thermal, mechanical and *in vitro* biological characterisation techniques: X-ray diffraction analysis (XRD), particle size analysis, contact angle and density measurements, Brunauer-Emmett-Teller analysis, FTIR and Raman spectroscopy, energy dispersive x-ray spectroscopy (EDX), scanning electron microscopy (SEM), differential thermal analysis, compression strength, Gilmore needle test, *in-vitro* bioactivity with stimulated body fluid

study (SBF) and biocompatibility (MTT assay and confocal microscopy).

The produced series of glasses were found to be amorphous in nature after x-ray diffraction analysis. Results of both contact angle and Brunauer-Emmett-Teller analysis revealed that calcium substitution with strontium and barium created positive change in terms of increased hydrophilicity and surface area. FTIR and Raman spectra of all glass samples (BG 1-7) revealed silicate and phosphate related peaks and thus, the presence of phospho-silicate structure. Characterisation of all ionomer cement samples with FTIR and Raman spectroscopy after the introduction of both tartaric and citric acid showed organic and inorganic peaks, endorsing the formation of resultant glass ionomer cement. Scanning electron micrographs indicated the layer formation over the surface of all prepared cement samples after 7th and 14th days in simulated body fluid solution. Similarly, the elemental analysis by energy dispersive x-ray spectroscopy revealed the presence of hydroxyl-carbonate apatite along with calcium phosphate ratio close to 1.67. The *in vitro* cell viability analysis for both glass and ionomer cement samples based on MTT assay and confocal study established the connection between improved biocompatibility after the substitution of strontium, barium and fluoride ions in glass and citrate ions in ionomer cement samples. Enhanced mechanical properties were also observed with further analysis of the resultant cement by compressive strength and Gilmore needle tests for the evaluation of working and setting time of all tartrate and citrate-based ionomer cements.

On the basis of obtained results, it was concluded that calcium ions can be substituted with strontium and barium ions effectively due to their similarity in ionic radius and charge. These ions allow the creation of an extended and more freely cross-linked glass network without altering the fundamental glass structure. Moreover, substitution significantly increases the desired properties in terms of bioactivity, biocompatibility and mechanical characteristics of the developed glass series and resultant ionomer cements. Thus, the produced series of aluminium ions free silicate based bioactive glass series can be incorporated into existing glass ionomer cement systems for both medical and dental applications with beneficial results.

Keywords: Glass ionomer cement, Silicate based bioactive glasses, Strontium and barium substitutions, Bioactivity, Biocompatibility, Mechanical properties, Citric acid.

Publications

1. Shafique, M. A., Murtaza, G., Saadat, S., Ahmed, R. and **Uddin, M. K. H.** (2017) 'Improved Cell Viability and Hydroxyapatite Growth on Nitrogen ion- Implanted Surfaces'. *The Journal Radiation Effect and Defects in Solids: Incorporating Plasma Science and Plasma Technology*, 172(7-8), 590-599.
2. Batool, R., Imran, M., Kandhro, A. H., Salahuddin, N. and **Uddin, M. K. H.** (2017) 'Resistance Patterns among Multidrug-Resistant Tuberculosis Patients: A Multi-Centre Study from Pakistan'. *The International Journal of Endorsing Health Science Research*, 5(4), 7-11.
3. Shafique, M. A., Murtaza, G., Saadat, S., Zaheer, Z., Shahnawaz, M., Ahmed, R. and **Uddin, M. K. H.** (2016) 'Study of Nickel Ion Release in Simulated Body Fluid from C⁺- Implanted Nickel Titanium Alloy'. *The Journal of Scientific Review and Letters*, 23(5).

Manuscripts (in process)

1. Shah, N., **Uddin, M. K. H.**, and et al 'Fabrication of thermally stable graphite-based poly (acrylonitrile-co-acrylic acid) composite with impressive antimicrobial properties' (submitted and accepted in to *Journal of Chemical Technology and Biotechnology*).
2. Oseghale, C. I., Abdalla, A. H., **Uddin, M. K. H.** and Hall, P. J. 'Gold based carbon supported core-shell catalysts for energy storage and biomedical applications'.
3. Tola. R, Khalid. N, Hammad. M, **Uddin, M. K. H.** and H. Saleem 'Frequency of urinary tract calculi in paediatric population'.
4. Ahmed. N, Begum. S, Hammad. M, Khan. A, Raza. Y, Imran. M and **Uddin, M. K. H.** 'Effect of cryopreservation and passage culture on proliferation, cell cycle regulation and cell injury of adult mesenchymal stem cells'.

Acknowledgment

In the name of Allah (SWT), the most beneficent, the most merciful

Foremost, I would like to express my sincere gratitude to my primary supervisor Dr Ihtesham Ur Rehman for his extraordinary kind support, valuable guidance and care towards my PhD project. His consistent and constant advice and guidance made my journey of gaining knowledge successful, for which I am truly grateful. I extend the word of thanks for him for keeping trust upon me and providing me the opportunity to become project mentor for his masters and undergraduate students.

I owe my deepest gratitude to my co-supervisor Professor Russell J Hand, and my assessors Dr Gwendolen Reilly, Professor Ian. M Reany and Dr Tom Hayward (postgraduate research tutor) for their consistent encouragement and valuable guidance. I would also like to acknowledge lab technician and staff members of Department of Material Science and Engineering and the Department of Dental School.

I am deeply indebted to our entire research group (Ceyla Yorucu, Saad, Daniela, Marcela, Nihad, Adebah, Peyman) and my Kroto Research Institute colleagues (Ahtesham Raza, Collin, Sabi Roman) for their persistent support. I would like to express my gratitude to both of master's students, Tanay B. Thakkar, Susie Zhao and Fatemah H Boaoies who helped me throughout my time at the university as graduate student.

I am grateful to the University of Sheffield, Materials Science and Engineering Department for awarding me funding and learned society for awarding me travel grants for my doctoral program.

I would also like to convey my special thanks for the spiritual support of my dearest uncle Late Dr Kamal Ahmed Ansari, my father Dr M K Imad Uddin and my mother Mrs Kausar Imad, both (maternal and paternal) grandfathers and grandmothers, my better half Mrs Mamoona Hammad, my beloved sister Dr Saba Kashif and her husband Dr S M Kashif and most importantly Mr and Mrs M Ibrahim and Mr M Rashid Hussain and my relatives for their consistent prayers, moral support, affection and assistance.

Last but not the least; I would like to pass my sincere gratitude and honour to all of my family members and family friends, who lost their lives during the completion of my degree.

Abbreviations and Nomenclatures

- % Percentage
- μl Microliters
- μm Micrometre
- mm millimetres
- mg milligrams
- $^{\circ}$ Degree
- $^{\circ}\text{C}$ Degree Celsius
- cm Centimetre
- conc Concentrated
- θ Theta angle
- λ Wave length
- $\text{\textcircled{R}}$ Registered
- Ag Silver
- Al Aluminium
- ALP Alkaline phosphatase
- Au Gold
- Ba Barium

- BET Brunauer-Emmett-Teller-analysis
- BG Bioactive glasses
- Bis-GMA bis-phenol-A-glycidyl methacrylate
- Ca Calcium
- CA Citric acid
- CPBPs Citrate based polymer blends
- CPC Calcium Phosphate Cement
- D Diameter
- DMEM Dulbecco's modified eagle's medium
- DTA Differential thermal analysis
- EDTA Ethylene diamine tetra acetic acid
- EDX Energy dispersive x –ray spectroscopy
- Eq Equation
- F Fluoride
- FA Fluorapatite
- FCA Carbonated fluorapatite
- FCS Foetal calf serum
- FTIR Fourier transform infrared spectroscopy

- GIC Glass ionomer cement
- GF Glass flakes
- gm Grams
- G Pa Giga pascals
- HA Hydroxyapatite
- HCA Carbonated hydroxyapatite
- HEMA hydroxyethyle-methacrylate
- Hg Mercury
- hrs Hours
- K₂O Potassium oxide
- kV Kilo volts
- Mg Magnesium
- min Minute
- Mol % Mole percent
- M Pa Mega pascals
- MTT [3-(4,5-dimethylethiazol-2-yl)-2,5-diphenyltetrazolium bromide]
- Na Sodium
- NMR Nuclear magnetic resonance (spectroscopy)

- O Oxygen
- OH Hydroxal ion
- OSX Osterix
- PAA Polyacrylic acid
- PBS Phosphate buffer solution
- PO₄ Phosphate
- PDL Periodontal ligament fibres
- PMMA Polymethyl-methacrylate
- RMGIC Resin modified glass ionomer cement
- rpm Rounds per minute
- SBF Simulated body fluid
- SEM Scanning electron microscope
- SiO₂ Silica
- Sr Strontium
- Sn Tin
- TA Tartaric acid
- t Time
- Ti Titanium

- UDMA Urethane di-methacrylate
- Wt % Weight percent
- XRD X-ray diffraction analysis
- Zn Zinc
- ZPC Zinc phosphate cement

Table of Contents

ABSTRACT	I
PUBLICATIONS	IV
MANUSCRIPTS (IN PROCESS)	IV
ACKNOWLEDGMENT	V
ABBREVIATIONS AND NOMENCLATURES	VI
LIST OF FIGURES	XV
LIST OF TABLES	XXIII
CHAPTER 1: INTRODUCTION	1
1.1 INTRODUCTION	1
1.2 AIMS AND OBJECTIVES	6
1.3 THESIS LAYOUT.....	7
CHAPTER 2: LITERATURE REVIEW	9
2.1 INTRODUCTION	9
2.2 STRUCTURE OF NATURAL HUMAN TOOTH	9
2.2.1 ENAMEL	10
2.2.2 DENTINE.....	11
2.3 DENTAL CARIES	12
2.4 DENTAL RESTORATIONS.....	15
2.5 LIMITATIONS OF EXISTING DENTAL RESTORATIVE MATERIALS	16
2.5.1 METAL BASED RESTORATIONS	16
2.5.2 RESIN AND POLYMER BASED RESTORATIONS	16
2.5.3 PHOSPHATE AND SILICATE BASED RESTORATIONS	17
2.6 SELECTION CRITERIA FOR DENTAL RESTORATIVE MATERIALS	18
2.6.1 MECHANICAL STRENGTH	18
2.6.2 WATER SORPTION	19
2.6.3 BIOCOMPATIBILITY	19
2.7 GLASS.....	20
2.7.1 DEFINITION AND INTRODUCTION	20
2.7.2 HISTORY AND BACKGROUND	21
2.7.3 GLASS FORMATION THEORIES	23
2.7.3.1 Structural theories.....	23
2.7.3.2 Kinetic theories.....	26
2.8 GLASS IONOMER CEMENT SYSTEM (GIC)	26

2.8.1 Introduction and dental applications.....	26
2.8.2 Composition.....	28
2.8.3 Role of setting modifiers	32
2.8.4 Structural and mechanical properties	36
2.8.5 Advantages and disadvantages	38
2.8.6 Recent modifications and their limitations.....	40
2.9 INTRODUCTION OF CITRIC ACID AS A SETTING MODIFIER	42
2.10 BIOACTIVE GLASSES.....	45
2.10.1 BACKGROUND AND HISTO-CHEMISTRY OF SILICATE BASED BIOACTIVE GLASSES	45
2.10.2 CLASSIFICATION OF BIOACTIVE GLASSES.....	48
2.10.3 USE OF SILICATE BASED BIOACTIVE GLASSES IN DENTAL APPLICATIONS	50
2.10.4 SILICATE BASED BIOACTIVE GLASS (45S5 BIO-GLASS®).....	51
2.11 ALUMINIUM IONS FREE BIOACTIVE GLASS IONOMER CEMENT	52
2.12 SIGNIFICANCE OF STRONTIUM AND BARIUM SUBSTITUTION IN BIOACTIVE GLASSES	53
2.13 SIGNIFICANCE AND RELEASE OF FLUORIDE IONS	56
2.14 THE CONCEPT OF GLASS FLAKES (GF).....	57
2.14.1 USE OF GLASS FLAKES IN MATERIAL SCIENCES AND ENGINEERING.....	57
2.14.2 PHENOMENA OF ANISOTROPIC SHRINKAGE AND ASPECT RATIO	59
2.15 SUMMARY	61
CHAPTER 3: MATERIALS AND METHODS	63
3.1 INTRODUCTION	63
3.2 GLASS PREPARATION	63
3.2.1 GLASS SAMPLE PREPARATION.....	63
3.2.2 SELECTION OF CRUCIBLE	68
3.2.3 CONTROLLING OF PARTICLE SIZE.....	69
3.3 CEMENT PREPARATION.....	70
3.3.1 CEMENT SAMPLE PREPARATION.....	70
3.4 GLASS AND CEMENT CHARACTERISATION.....	72
3.4.1 PHYSICAL CHARACTERISATION	72
3.4.1.1. X-Ray diffraction analysis	72
3.4.1.2. Contact angle measurement.....	74
3.4.1.3 Particle size analysis	75
3.4.1.4 Brunauer-Emmett-Teller analysis.....	76
3.4.1.5 Density Measurements (Archimedes and Pycnometer).....	77
3.4.2 THERMAL CHARACTERISATION.....	79
3.4.2.1 Differential thermal analysis	79

3.4.3 CHEMICAL CHARACTERISATION	81
3.4.3.1. Fourier Transform Infrared (FTIR) spectroscopic analysis.....	81
3.4.3.2. Raman spectroscopic analysis	83
3.4.4 IN-VITRO BIOLOGICAL CHARACTERISATIONS	85
3.4.4.1 IN- VITRO BIOACTIVITY ANALYSIS	85
3.4.4.1.1 Stimulated body fluid (SBF) study.....	85
3.4.4.1.2 Scanning electron microscopic (SEM) analysis	88
3.4.4.1.3 Energy dispersive x-ray spectroscopy (EDX) analysis	89
3.4.4.2 IN- VITRO BIOCOMPATIBILITY ANALYSIS	90
3.4.4.2.1 Sterilisation of both glass and cement samples	90
3.4.4.2.2 Cell culture and MTT assay of glass and cement samples	91
3.4.4.2.3 Optical and confocal microscopy	94
3.4.5 MECHANICAL CHARACTERISATION.....	95
3.4.5.1 Compressive strength analysis.....	95
3.4.5.2 Gilmore needle test.....	97
3.6 STATISTICAL ANALYSIS	98
3.7 SUMMARY	99
CHAPTER 4: RESULTS	100
4.1 INTRODUCTION	100
4.2 GLASS PREPARATION	100
4.3 CEMENT PREPARATION.....	104
4.4 GLASS AND CEMENT CHARACTERISATION.....	106
4.4.1 PHYSICAL CHARACTERISATION	106
4.4.1.1. X-ray diffraction analysis	106
4.4.1.2. Contact angle measurement.....	108
4.4.1.3 Density measurement (Archimedes and Pycnometer).....	110
4.4.1.4 Particle size analyses	112
4.4.1.5 Brunauer-Emmett-Teller analysis.....	117
4.4.2 THERMAL CHARACTERISATION.....	119
4.4.2.1 Differential thermal analysis	119
4.4.3 CHEMICAL CHARACTERISATION	121
4.4.3.1. Fourier Transform Infrared (FTIR) spectroscopic analysis.....	121
4.4.3.2. Raman spectroscopic analysis	127
4.4.4 IN-VITRO BIOLOGICAL CHARACTERISATIONS.....	135
4.4.4.1 IN- VITRO BIOACTIVITY ANALYSIS	135
4.4.4.1.1 Scanning electron microscopic (SEM) analysis	135
4.4.4.1.2 Energy dispersive x-ray spectroscopy (EDX) analysis	143
4.4.4.2 IN- VITRO BIOCOMPATIBILITY ANALYSIS	148
4.4.4.2.1 MTT assay and statistical analysis of glass and cement samples.....	148
4.4.4.2.2 Confocal microscopy of bioactive glass samples	161

4.4.5 MECHANICAL CHARACTERISATIONS	163
4.4.5.1 Compressive strength and statistical analysis	163
4.4.5.2 Gilmore needle test	166
4.4.6 SUMMARY	170
CHAPTER 5: DISCUSSION	172
5.1 INTRODUCTION	172
5.2 GLASS AND CEMENT CHARACTERISATION.....	172
5.2.1 PHYSICAL CHARACTERISATION	172
5.2.1.1. X-ray diffraction analysis	172
5.2.1.2. Contact angle measurement	173
5.2.1.3. Density measurement	177
5.2.1.4. Particle size analyses	178
5.2.1.5 Brunauer-Emmett-Teller analyses	180
5.2.2 THERMAL CHARACTERISATION.....	181
5.2.2.1 Differential thermal analysis	181
5.2.3 CHEMICAL CHARACTERISATION	183
5.2.3.1 Fourier transform infrared (FTIR) spectroscopic analysis	183
5.2.3.2. Raman spectroscopic analysis	193
5.2.4 IN-VITRO BIOLOGICAL CHARACTERISATIONS	198
5.2.4.1 IN- VITRO BIOACTIVITY ANALYSIS	198
5.2.4.1.1 Scanning electron microscopic (SEM) analysis	198
5.2.4.1.2 Energy dispersive x-ray spectroscopy (EDX) analysis	202
5.2.4.2 IN- VITRO BIOCOMPATIBILITY ANALYSIS	205
5.2.4.2.1 Cell culture and MTT assay of glass and cement samples	205
5.2.4.2.2 Optical and confocal microscopy	207
5.2.5 MECHANICAL CHARACTERISATIONS	209
5.2.5.1 Compressive strength analysis.....	209
5.2.5.2 Gilmore needle test.....	211
5.3 SUMMARY	214
CHAPTER 6: CONCLUSION AND FUTURE WORK	218
6.1 CONCLUSION.....	218
6.3 FUTURE WORK.....	220
CHAPTER 7: REFERENCES AND APPENDIX	222
7.1 REFERENCES	222
7.2 APPENDIX.....	248

List of Figures

Figure 1: Schematic diagram indicating the atomic structure of phosphor-silicate based glass indicating non-bridging oxygen (NBO) and bridging oxygen (BO) -----	23
Figure 2: Schematic diagram showing the tetrahedral structure of silica (SiO_4) and phosphate (PO_4)-----	25
Figure 3: Schematic diagram showing compositional range of glass in glass ionomer cement production -----	29
Figure 4: Acidic components currently being used in glass ionomer cement commercially --	31
Figure 5: Graphical representation of the effect of tartaric acid on cement during setting reaction of glass ionomer in terms of viscosity over time -----	34
Figure 6: Schematic diagram showing chemical and setting reaction of glass ionomer cement -----	35
Figure 7: Bone binding ability of bioactive glasses based on composition (Jones 2013). ----	49
Figure 8: Classification of bioactive glasses (BG) -----	50
Figure 9: Schematic diagram indicating the mechanism of polymerisation contraction in oil pipe lines after application of glass flakes as filler content -----	58
Figure 10: Schematic diagram showing ability of self-alignment in 0.1 to 1 μm sized glass flake particles. -----	60
Figure 11: Schematic diagram showing misalignment of 5 μm size glass flakes. -----	60
Figure 12: Photographic image of Siemens® D5000 XRD machine with specimen changer.	73

Figure 13: Photographic image of Contact Angle Goniometer measuring equipment. -----	74
Figure 14: Photographic image of Brunauer-Emmett-Teller analysis (BET) equipment. ----	76
Figure 15: Photographic image of Perkin-Elmer® Differential thermal analysis instrument.	80
Figure 16: Photographic image of Thermo scientific™ Nicolet™ iS™50 FTIR spectrometer MTEC photoacoustic cell. -----	82
Figure 17: Schematic diagram indicating the phenomena of Raman scattering -----	84
Figure 18: Photographic image of Thermo scientific™ DXR™ Raman microscope. -----	84
Figure 19: Photographical image showing experimental setup used for the preparation of conventional simulated body fluid solution (c-SBF). -----	87
Figure 20: Photographic image of Philips/FEI XL30 S-FEG microscope scanning electron microscope (SEM).-----	88
Figure 21: Schematic diagram for energy dispersive x-ray spectroscopy (EDS). -----	90
Figure 22: Light microscopic image of human oral fibroblast cultured over the surface of T- 75 flask, exhibiting the uniform cellular growth before MTT assay analysis. -----	92
Figure 23: Photographic image of spectrometer MTT plate reader (BIO-TEK, USA).-----	94
Figure 24: Photographic image of light optical microscopy (a) and confocal laser scanning microscope (CLSM) (b) respectively. -----	95
Figure 25: Photographic image of Hounsfield mechanical compression strength test equipment.-----	96
Figure 26: Schematic diagram of Gilmore Needle Instrument -----	98

Figure 27: Photographic image of produced silicate based glass sample BG 1 after casting.	
-----	101
Figure 28: Photographic image of produced silicate based glass sample BG 2 after casting.	
-----	101
Figure 29: Photographic image of produced silicate based glass sample BG 3 after casting.	
-----	101
Figure 30: Photographic image of produced silicate based glass sample BG 4 after casting.	
-----	102
Figure 31: Photographic image of produced silicate based glass sample BG 5 after casting.	
-----	102
Figure 32: Photographic image of produced silicate based glass sample BG 6 after casting.	
-----	103
Figure 33: Photographic image of produced silicate based glass sample BG 7 after casting.	
-----	103
Figure 34: Photographic image of obtained silicate based glass flakes from Leeds Glass Flakes Company Ltd. UK.	
-----	104
Figure 35: Photographic image showing discs of prepared cement samples.	105
Figure 36: Traces of x-ray diffraction analysis of all produced glass series (BG 1-7).	107
Figure 37: XRD trace of obtained glass flakes based on the composition provided from Leeds Glass Flakes Company Ltd. UK.	
-----	108

Figure 38: Contact angle measurement results analysis of silicate based bioactive glass samples (BG 1-7) by using one-way ANOVA ($p < 0.05$, * represents significant difference).
----- 109

Figure 39: Illustration of the results of density measurements of glass (BG 1-7), where (in black) indicates Pycnometer measurements and (in orange) indicates measurements Archimedes respectively.----- 111

Figure 40: Illustration of particle size analysis ($< 45 \mu\text{m}$) and SEM image of produced silicate based bioactive glass samples (BG 1-7).----- 114

Figure 41: SEM Micrographs of Glass Flakes of different sizes as obtained from Leeds Glass Flakes Company Ltd UK. ----- 117

Figure 42: BET measurement analysis of all produced glass series (BG 1-7).----- 118

Figure 43: Traces of differential thermal analysis of all produced silicate based bioactive glass series from (BG 1-7). ----- 120

Figure 44: FTIR spectrum of all produced silicate based bioactive glass series (BG 1-7).-- 122

Figure 45: In vitro bioactivity FTIR analysis of all produced silicate based bioactive glass samples (BG 1-7). ----- 123

Figure 46: FTIR spectrum of tartaric acid based glass ionomer cements samples (TA GIC 1-7)----- 124

Figure 47: FTIR spectrum of citric acid based glass ionomer cements samples (CA GIC 1-7)
----- 126

Figure 48: Raman spectrum of all produced silicate based glass series (BG 1-7) ----- 128

Figure 49: In vitro bioactivity Raman analysis of all produced silicate based bioactive glass series (BG 1-7).----- 130

Figure 50: Raman spectrum of tartaric acid based glass ionomer cement samples (TA GIC 1-7).. ----- 132

Figure 51: Raman spectrum of citric acid based glass ionomer cements samples (CA GIC 1-7). ----- 134

Figure 52: SEM micrographs of tartaric acid based cement samples (TAC1-7) at 1st day (control sample) at 10, 5 and 2 um scales before immersion in c-SBF respectively.----- 137

Figure 53: SEM micrographs of tartaric acid based cement samples (TAC1-7) at 7th day at 10, 5 and 2 um scales after immersion in c-SBF respectively. ----- 138

Figure 54: SEM micrographs of tartaric acid based cement samples (TAC1-7) at 14th day at 10, 5 and 2 um scales after immersion in c-SBF respectively. ----- 139

Figure 55: SEM micrographs of citric acid based cement samples (CAC1-7) at 1st day (control sample) at 10, 5 and 2 um scales before immersion in c-SBF respectively.----- 140

Figure 56: SEM micrographs of citric acid based cement samples (CAC1-7) at 7th day at 10, 5 and 2 um scales before immersion in c-SBF respectively.----- 141

Figure 57: SEM micrographs of citric acid based cement samples (CAC1-7) at 14th day at 10, 5 and 2 um scales before immersion in c-SBF respectively.----- 142

Figure 58: Micrograph of Leeds glass flakes Ltd UK based silicate glass sample composition energy dispersive x-ray spectroscopy (EDS) analysis.----- 144

Figure 59: Micrographs of tartaric acid based cement samples (TAC1-7) EDS analysis for 7th and 14th day after immersion in c-SBF respectively. ----- 146

Figure 60: Micrographs of citric acid based cement samples (CAC1-7) EDS analysis for 7th and 14th day after immersion in c-SBF respectively. ----- 147

Figure 61: Microscopically images of oral human fibroblasts over tissue cultured plate before MTT assay (BG 1-7) including control sample. ----- 150

Figure 62: Photographical image of 96 well plates before MTT assay for 24 hours. ----- 150

Figure 63: Photographical image of 96 well plates before MTT assay for 48 hours. ----- 151

Figure 64: Graphical illustration of in vitro biocompatibility analysis of all produced silicate based bioactive glass series (BG 1-7) with 24 and 48 hours of MTT assay with ANOVA (significant difference * $p < 0.05$). ----- 151

Figure 65: Microscopically imaged oral human fibroblasts over tissue cultured plate before MTT assay with tartaric acid based glass ionomer cement samples (TAGIC 1-7) including control sample.----- 154

Figure 66: Photographical image of 96 well plates before MTT assay for 24 hours of tartaric acid based glass ionomer cement samples (TAGIC 1-7) respectively----- 155

Figure 67: Photographical image of 96 well plates before MTT assay for 48 hours of tartaric acid based glass ionomer cement samples (TAGIC 1-7) respectively. ----- 155

Figure 68: Graphical illustration of MTT assay results with ANOVA (*p <0.05 significant different) for tartaric acid based cements (GIC TA 1-7) for 24 and 48 hours' incubation periods.----- 156

Figure 69: Microscopically imaged oral human fibroblasts over tissue cultured plate before MTT assay with citric acid based glass ionomer cement samples (CAGIC 1-7) including control (positive) sample. ----- 158

Figure 70: Photographical image of 96 well plates before MTT assay for 24 hours of citric acid based glass ionomer cement samples (CAGIC 1-7) respectively.----- 158

Figure 71: Photographical image of 96 well plates before MTT assay for 48 hours of citric acid based glass ionomer cement samples (CAGIC 1-7) respectively.----- 159

Figure 72: Illustration of MTT assay results with ANOVA (*p <0.05 significant different) for citric acid based cements (GIC CA 1-7) for 24 and 48 hours' incubation periods.----- 159

Figure 73: Illustration of MTT assay reading of obtained glass flakes from Leeds glass flakes company Ltd, UK for 24 and 48 hours' study over tissue cultured plate with immersed medium indicating decreased in cellular respond in 48 hours of study.----- 160

Figure 74: Confocal images for in vitro biocompatibility analysis of all produced silicate based bioactive glass series (BG 1-7) for 24 hours. ----- 163

Figure 75: Compressive strength results comparison between tartaric / citric acid glass ionomer cement samples. ----- 164

Figure 76: Compressive strength comparison of different sized glass flakes upon with the admixture of citric acid. Statistical analysis results indicate the significant difference $* < p < 0.005$ and ** indicates similar groups comparison in between the samples. ----- 165

Figure 77: Compressive strength comparison of different sized glass flakes upon with the admixture of tartaric acid. Statistical analysis results indicate the significant difference $* < p < 0.005$ and ** indicates similar groups comparison in between the samples. ----- 166

Figure 78: Comparison between working (black) and setting time (orange) of tartaric acid based cements. ----- 167

Figure 79: Comparison between working (black) and setting (orange) time of citric acid based cements. ----- 169

List of Tables

Table 1: Typical composition of glass ionomer cement	29
Table 2: Silicate based bioactive glass composition based on 45S5 bioactive glass having calcium substitution with strontium and barium by 3 mole % of calcium ions.....	65
Table 3: List of different chemicals used for batching of produced glasses.....	67
Table 4: Composition of Glass Flakes (GF) from Leeds Glass Flake Company Ltd. UK.	67
Table 5: Different types, sizes and shapes of Glass Flakes (GF) obtained from Leeds Glass Flake Company Ltd. UK.....	68
Table 6: Materials used for the fabrication of cement	71
Table 7: Materials used in the preparation of SBF solution for in vitro bioactivity analysis. .	85
Table 8: Density measurement analysis (Pycnometer & Archimedes) of glass samples (BG 1-7).	111
Table 9: Particle size analysis results of all milled glass samples < 45 µm in size from BG 1-7.....	115
Table 10: Calcium and phosphate ratio of tartaric acid based cement samples after 7th and 14th days of immersion in conventional stimulated body fluid solution (c-SBF).....	146
Table 11: Calcium and phosphate ratio of cement samples after 7th and 14th days of immersion in conventional stimulated body fluid solution (c-SBF).....	146
Table 12: Comparison between working and setting time of tartaric acid based cements.	168
Table 13: Comparison between working and setting time of Citric acid based cements.	169

Table 15: FTIR peak identification and their attribution with references prior to simulated body fluid solution (SBF) immersion of all prepared silicate based bioactive glass samples (BG 1-7).....	184
Table 16: FTIR peak identification and their attribution with references following SBF immersion of all prepared silicate based bioactive glass samples (BG 1-7).....	187
Table 17: FTIR peak identification and attribution with reference to all prepared silicate based bioactive glass ionomer samples with both tartaric and citric acid (TA / CA GIC 1-7).....	189
Table 18: Raman peak identification and attribution with references following SBF immersion of all prepared silicate based bioactive glass samples (BG 1-7).....	194
Table 19: Raman peak identification and attribution with references for all prepared silicate based bioactive glass ionomer samples with both tartaric and citric acid (TA / CA GIC 1-7).	195
Table 20: Ionic concentrations of various SBF in relation to human blood plasma.....	203

Chapter 1: Introduction

1.1 Introduction

Restorative dentistry is currently one of the most sought after modalities by patients and most frequently provided by clinicians. One of the most prevalent oral diseases which can be cured by adopting preventive restorative techniques (rather than surgery) is dental caries. There are various accepted treatments for the inhibition of dental caries. These include therapeutic delivery of fluoride through the drinking of fluoridated water and topical application of fluoridated agents such as fluoride gel. However, these preventive measures are insufficient for complete eradication of dental caries.

Due to the introduction of minimal invasive concept in dentistry, the criteria for selection of restorative material especially for direct restorative treatments, has changed enormously. Increasingly, patients are becoming more conscious of aesthetics causing them to prefer restoration work to look more natural in terms of blending with the residual natural anatomical land marks. Thus, demand from patients in this regard has encouraged scientists and manufacturers to design material which provides close approximation visually and functionally, to features observed naturally after fundamental compositional amendments such as glass ionomer cement (GIC) and dental composite (Salentijn. L et al. 1985; Boyde 1989; Bechtle et al. 2009).

Orthopedically, the glass ionomer cement system has been used for bone cements but not for direct tooth restoration. Due to its potential to able sustained release of fluoride ions, when compared with other dental restorative materials, it can be considered as direct tooth restoration. There are also a number of mechanical drawbacks which must be overcome to use this type of cement such as poor marginal adaptation and bonding, dissolution and disintegration, surface roughness, plaque adhesion and crack propagation. All of these issues must be considered and indeed improved before glass ionomer cement is used in the first instance for direct posterior dental restoration.

Another area for concern is the consistent leaching of aluminium ions in higher concentrations from the resultant ionomer cement, which can interfere and reduce the mineralisation process of bone at the initial stages. Aluminium ions are the least biologically acceptable inorganic species which can leach out from the resultant cement. Even more worryingly, the presence of aluminium ions in high concentration has been associated with both Alzheimer's and Parkinson's disease. Indeed, increased concentration of aluminium ions in the brain has been found to lead to aluminium ion encephalopathy. Several cases of sub-acute aluminium ion encephalopathy have been reported after the implantation of aluminium ion based glass ionomer cement during translabyrinthine otoneurosurgery. Therefore, much focus is being placed on developing a novel silicate based bioactive glass ionomer cement which is aluminium ions free and has improved mechanical and biological properties (Guillard et al. 1997; Gomes et al. 2013).

However, designing an aluminium ion free glass ionomer cement is not straightforward and has proven elusive. This is because aluminium plays a significant role in the setting of the cement. Chemically, during the setting stages, carboxylic and poly acrylic acid liberate protons in the presence of water. These, then react with the surface particles of the glass. A matrix then forms due to leaching of Al^{3+} and Ca^{2+} cations which readily form a cross linking bridge between the carboxyl ions and glass particles (Gomes et al. 2013; Jones 2013; Kim et al. 2014).

Glasses are inorganic amorphous solids that can be processed once they reach glass transition temperatures. Structurally, glass consists of network formers, network modifiers and intermediates (Shelby 2005) and can be formed of various bases such as silicate, phosphate and borate depending on the intended functions. Glasses are more readily soluble than the equivalent crystalline structures because of their presence in a higher energy state. Glass compositions can be altered to influence solubility which, in turn alters setting times. This is particularly useful for glasses that are used for *in vivo* and *in vitro* applications. Moreover, therapeutically significant ions can be integrated in basic glass composition with relative ease and in fairly significant proportions. For instance, certain applications require substituted apatite (strontium and fluoride) for setting reactions. It is hypothesised that the incorporation of these ions does not affect the resultant cement properties.

Bioactive glass which has a phosphosilicate structure was first manufactured by L. Hench and named 45S5[®] Bioglass. The composition (SiO_2 45%, Na_2O 24.5%, CaO 24.5% and P_2O_5 6.0 % *in wt percentage*) causes the ability of better quality glass ionomer cement formation upon the

admixture with poly-acrylic acid and water. Moreover, the substitution of other elements such as strontium, barium and fluoride with calcium oxide, into the main composition can improve the bonding and remineralisation ability of the formed cement (Gentleman et al. 2010; Fredholm et al. 2012).

Glass ionomer cement is basically based on a liquid powder based system which undergoes an acid base reaction upon interaction. The powder is composed of aluminosilicate based glass and the liquid consists of an aqueous solution of poly acrylic acid. The acid base reaction occurs in three different stages such as dissolution, gelation and hardening. However, setting modifiers (tartaric acid, for instance) can play a vital role in the reaction kinetics of glass ionomer cement. The reaction rate modifiers initially delay the prime reaction rate and deliver a complete set of snap at the end. Similarly, mechanical properties of resultant cements are also associated with the introduction of setting modifiers. To enhance comprehensive mechanical and biological properties of existing glass ionomer cement systems, different modifications have been suggested such as addition of chelating co-monomer acids (Nicholson 1998).

Citric acid possesses excellent potential to be used as a cross linker and a biologically active molecule capable of facilitating calcium and phosphate nucleation composites. Citrate, which was previously known for its key role in cell metabolism, has recently been reported to be present in up to 80% of human bones and scaffolds based on citric acid have been shown to induce *in vitro* nucleation of hydroxyapatite over collagen matrices. Due to the presence of hydroxyapatite over the surfaces of scaffolds, it is evident that this molecule is potentially able

to aid localised bone regeneration when studied both *in vivo* and *in vitro* (Sanchez-Ferrero et al. 2015)

Moving now to the next component of glass ionomer cement, glass flakes are small flakes of glass measuring between 0.1 to 10 μ m in size depending on the requirement. Glass flakes are manufactured commercially with blowing and spinning methods. Incorporation of glass flakes according to their aspect ratio is vitally important. Smaller sizes of glass flakes (0.1 to 1 μ m) have the inherent property of self-alignment perpendicular to the surface anisotropically as compared to larger sizes (5 to 10 μ m). Due to this inherent potential, smaller size glass flakes naturally create a smooth surface and they can increase the strength of the resulting composite by enhancing the ability of the material to resist wear, corrosion and penetration (Rexer & Anderson 1979; Dunlap 1991; Shigeki & Hidekazu 1992; Yang et al. 2004; Paul et al. 2005; Franklin et al. 2005; Simon J & Charles 2009; Uo et al. 2010).

1.2 Aims and Objectives

The aim of this thesis was to develop a novel biomaterial that can be used for direct posterior dental restorations. In order to achieve this aim, the primary objective of this research was to develop a series of bioactive aluminum ions free silica based bioactive glasses by substituting calcium with strontium and barium ions in the basic glass composition, and to study the effects of substitution by characterisation of all produced glass samples. For this purpose, an aluminum ion free series of silica based bioactive glass composition with the calcium substitution of strontium and barium with 3 mole percent of calcium oxide $46.14 SiO_2.2.60 P_2O_5.23.95 CaO.24.35 Na_2O.1.5X1.1.5X2$ ($X1= SrO$ and SrF_2) and ($X2= BaO$ and BaF_2) were synthesised through the melt quenching technique.

The secondary objective of this work was to develop a novel bioactive glass ionomer cement with the admixture of tartaric and citric acid as setting modifiers and to study the effects of citric acid based cements in comparison with tartaric acid. Similarly, the final objective of this study was to alter the particle size of filler content for which silicate based glass flakes of different sizes ranging from 100 nm to 100 μ m were obtained from Leeds Glass Flakes Company Ltd, United Kingdom and were optimised and characterised physically, mechanically and *in vitro*, biologically.

As a hypothesis, it was suggested that the introduction of citrate ions and changing the particle size of the filler content should improve the mechanical, chemical and biological properties

of the resultant set cement.

1.3 Thesis Layout

This thesis is divided into six main chapters. Chapter 1 has provided the introduction and layout of this thesis along with the aims and objectives. Chapter 2 consists of a literature review which details, the findings of existing research related to our current knowledge of the anatomy of the human tooth, dental caries and available dental restorative materials, their limitations and selection criteria. The middle part of chapter 2 comprises the definition, history and theories of glass formation followed by a description of research on glass ionomer cement systems (including background, applications, compositions, advantages and disadvantages, properties and modifications). The end of this chapter includes an explanation of the significance of citric acid and bio glass (background, histo-chemistry, classifications, applications and properties) followed by the importance of aluminum ion free silicate based bioactive glasses, substitution of strontium, barium and fluoride ions and finally the introduction to the concept of glass flakes.

Chapter 3 contains a description of the materials and methods used for preparation and characterisation techniques for the individual preparation and analysis of all produced series of silicate based bioactive glasses and glass ionomer cements (tartaric and citric acid based).

For instance, physical characterisations [XRD, Density measurements (Archimedes and

Pycnometer), Contact angle measurements, Particle size analysis and BET], thermal characterizations (DTA), chemical characterizations (FTIR and Raman spectroscopy), *in vitro* biological characterisations comprising *in vitro* bioactivity analysis (simulated body fluid (SBF) study, SEM and EDX) and *in vitro* biocompatibility analysis (MTT assay, optical and confocal microscopy) and lastly mechanical characterisations (including compressive strength analysis and Gilmore needle test).

Chapter 4 (results) and chapter 5 (discussion) provides the results followed by a detailed discussion based on the available literature and analysis of said results. Finally, Chapter 6 draws conclusion from the discussion and proposes logical avenues for future work in terms of the further analysis and development of a produced series of silicate based bioactive glasses and ionomer cements.

Chapter 2: Literature review

2.1 Introduction

This thesis investigates the development of silicate based bioactive glass ionomer cement for dental applications. The new cement substitutes calcium with strontium and barium ions with 3 mole % of calcium oxides, along with the admixture of poly acrylic acid in the presence of water after the introduction of tartrate and citrate as setting modifiers. Therefore, this chapter begins with a detailed review of the literature by introducing the anatomical structure of the human tooth, dental caries and selection criteria for dental materials. This is followed by a definition of glass and a summary of the findings of previous studies related to glass ionomer cement, silicate based bioactive glasses and the use of glass flakes as filler content. Finally, our present knowledge of the significance of strontium, fluoride and barium is provided by referring to the available literature.

2.2 Structure of natural human tooth

Naturally, the human dental hard tissues consist of enamel, dentine and cementum. Anatomically, 20% of the surface area of oral cavity consists of teeth. Teeth play a significant role in mastication, speech and normal facial aesthetics. The fully matured human tooth is composed of enamel, which is inert, acellular and hard in nature. Histologically it is epithelial

in origin. Internally, the tooth is supported by less mineralized and more resilient connective tissue called dentine. In mammals, teeth within the oral cavity after their eruption commonly attach via connective tissue known as periodontium. The periodontium consists of periodontal ligaments fibers (PDL), surrounding alveolar bone and cementum. All of these aforementioned tissues are responsible for tooth attachment and provide more flexible support against heavy mechanical wear forces as a result of mastication. Clinically, within the oral cavity, the tooth is divided into the cervical (or crown) portion which is visible and the radicular (or root) portion which is embedded in the surrounding alveolar bone and periodontium (Boyde 1989).

2.2.1 Enamel

Enamel is the hardest mineralised dental hard tissue due to its high mineral content. Anatomically, it forms the outer most part or crown portion of an individual tooth. It is thickest over cusp and incisal edges of the incisors and molars. However, it is commonly thinner over cervical or neck portion of the tooth. Fully developed enamel consists of 2% water by weight and 5-10% by volume. It also contains an extracellular mineralised matrix consisting of 96% minerals and 4% organic material. The remainder is constituted of protein (Osborn 1968; William 1995; Nanci 2003).

Histologically, enamel prism is the basic structural unit of enamel and it shows key whole appearance. Mechanically, enamel is brittle in nature and has low tensile strength. Due to its high modulus of elasticity, it provides more flexible protection against fracture to the

underlying dentine during cyclic loading of the routine masticatory process. The specific gravity of enamel is 3 and its refractive index is 1.33. It has a density of 3.021g/cm³ (William 1995; Berkowitz et al. 2002). Enamel is harder, denser and less porous at its superficial surface than at the sub surface layer which is more porous. Newly developed enamel is very thick and white in colour due to its of lower mineral content than more mature enamel. For this reason, it reflects less light compared to fully matured and developed enamel. The translucency of enamel increases with age and becomes very much paler and more yellow in colour due to the reflection of the underlying dentine (Boyde 1989; William 1995; Berkovitz et al. 2009; Nelson 2009).

2.2.2 Dentine

Dentine is biologically hydrated and complex in structure, forming the entire bulk of an individual tooth. Naturally, it can modify itself according to physiological (aging) and pathological (dental caries) behavioural changes. Due to these characteristic features various types of dentine can form. These include primary, secondary, tertiary (reparative or reactionary dentine), transparent (bruxism) and sclerotic (arrested caries) dentine (Ronald L & Sakaguchi 2012; Anusavice et al. 2012). There are different layers of matured dentine. The first layer is un-mineralised and exhibits various thicknesses, ranging from 10-50 µm. It outlines the inner pulp of the tooth known as pre-dentine. Histologically, pre-dentine consists of collagen fibres and is similar to bones known as osteoids. Layers of mineralised mature dentine are formed

from pre-dentine and consists non-collagenous matrix proteins. Fully mature dentine is composed of 10% water, 20% organic and 70% inorganic material. The organic material contains 90% collagen (type I, III & V) and non-collagenous matrix proteins. The inorganic material consists of small plates of hydroxyapatite crystals. Mechanically, dentine is softer than enamel but slightly harder than bone that can be viewed radio-graphically. Physically, dentine is flexible, a feature which provides the fracture resistance to the outer covering of brittle enamel. Microscopically, dentine and enamel join together and form a scalloped shaped structure (Nanci 2003; Nelson 2009).

Additional elements for the tooth are the pulp and the soft tissue, which consists of collagen fibrils, blood vessels and nerve cells. Cementum covers the entire root portion of the tooth. The thickness varies from 20-50 μ m at the cervix and 150-200 μ m at the apex. Compositionally, cementum is composed of organic and inorganic material in a 1:1 ratio, and water. Attached periodontal ligament fibres are composed of collagenous fibres and glycoprotein. The cementum and periodontal ligament fibres together provide flexible support and anchorage to the individual tooth during the process of mastication (William 1995).

2.3 Dental caries

The word “caries” is a Latin derivative which means rot or rotten. Dental caries can be defined as chronic contagious oral ailments resulting from the communication among oral

microorganisms in dental plaque, dietary carbohydrates and susceptible teeth. It debilitates the resistance and protection of oral well-being across all age groups and can result in serious health problems. The frequency and severity of dental caries depends upon certain factors which include age, sex, race, socio-demographic features, economic status, localities, food practice and oral hygiene habits (Yadav & Prakash 2017).

Microorganisms are the foremost causative agents of dental caries whereby numerous facultative and obligative anaerobic bacteria dominate in the microbial community. Of these, *Streptococcus mutans* has been reported as the chief etiological agent of dental caries as it is extremely acidogenic and generates short chain acids which soften dental hard tissues. When dental caries develop, dietary carbohydrates are utilised by the cariogenic bacteria present in the dental plaque. Fermentation of carbohydrates results in the formation of lactic acid, which triggers the melting of the hydroxyapatite crystal structure of the tooth (Yadav & Prakash 2017).

Symptoms such as tooth ache, difficulty eating and chewing and pulpitis due to decayed teeth are often the results of dental caries, with more serious potential complications including myocardial infarction, complication to pregnancy and diabetics, cardiovascular and respiratory diseases, oral cancer, endocarditis, erectile, cavernous sinus thrombosis and Ludwig angina (Yadav & Prakash 2017).

Dental tissue surfaces, specifically the non-shedding shell of enamel, accrue a biofilm that supports the growth of a variety of bacterial species within a protective habitat. Dental plaque

is itself a multi-layered biofilm consisting of various bacterial populations present as micro-colonies. Several microorganisms exist at the site of caries. These includes gram positive cocci such as *Streptococcus mutans*, *Streptococcus salivarius* and *Staphylococcus aureus*, gram positive rods such as *Actinomyces odontolyticus*, *Lactobacillus fermentum* and *Bifidobacterium dentium*, gram negative cocci such as *Veillonella parvula* and Neisseria species and gram-negative rods such as *Bacteriodes denticola*, *Bacteriodes melaninogenicus*, *Escherishia coli* and *Klebsiella pneumoniae* (Yadav & Prakash 2017).

There are five different stages of caries formation which are as follows:

1. Initially, yellowish or chalky white spots start to appear on the tooth surfaces due to the loss of calcium ion. This initial stage of tooth decay is reversible by treatment and has no other symptoms.
2. In the second stage, enamel starts to decay and the tooth surface begins to deteriorate as the decay continues. This stage is irreversible but does not cause pain or sensitivity.
3. In the tertiary stage, the decay progresses further than the enamel and reaches the dentine. Tooth ache begins in this stage.
4. The pulp of the tooth becomes infected due to the bacterial colonisation. Blood vessels and nerves present inside the pulp disintegrate resulting in pus formation.
5. Finally, in the last stage the root tip of the tooth becomes affected along with the surrounding bones. Severe pain along with swelling on the cheeks is commonly seen

during this phase.

2.4 Dental restorations

In an attempt to more effectively treat issues such as dental caries and due to the increase in the demand for delivery of optimal dental health care, advancements have been made to support the approach of evolving novel dental restorative materials for both direct and indirect restorations. Precisely, an ideal dental restorative material should exhibit strength, biocompatibility and adequate adhesion with the surrounding dental hard tissues (Kenneth 2007). At present, researchers are continuing their focus to those approaches which show more potential for the prevention of multi-factorial oral diseases such as dental caries and periodontal diseases. To accomplish this, various types of direct posterior dental restorative materials have been developed and introduced commercially. The formulations of these materials are based on metals (amalgam and cermet) and non-metals (compomers), resins (composites and resin modified glass ionomer cement (RMGIC), phosphates (zinc phosphate) and silicate based glass ionomer cements (GIC). However, it is evident from the literature that their collective drawbacks outweigh their advantages. As a result, their popularity has decreased over time (Maltz et al. 2010; Anusavice et al. 2012).

2.5 Limitations of existing dental restorative materials

Currently, a number of materials are being used for direct and indirect dental restorations. Existing restorative materials are compositionally based on metals and non-metals, resin and polymers, phosphates and silicates. However, the current materials exhibit certain limitations which are described briefly below according to their composition.

2.5.1 Metal based restorations

Metal-based restorations are mainly composed of either mercury (Hg), silver (Ag) and zinc (Zn), tin (Sn) and gold (Au). The most common examples of this type of restoration are amalgam and cermet. The most cited meticulous mechanical, physical and biological drawbacks are galvanism, creep, poor aesthetics, inadequate wear and corrosion resistance, cytotoxicity, neurotoxicity, surface roughness and plaque adhesion. On the other hand, these types of restorations are well understood and adequately stable (Bharti et al. 2010; Ronald & Sakaguchi 2012).

2.5.2 Resin and polymer based restorations

Resins and polymers such as hydroxyethyle-methacrylate (HEMA), urethane di-methacrylate (UDMA), bis phenol-A-glycidyl methacrylate (bis-GMA) and polymethyl-methacrylate (PMMA) are most commonly used for these restorations. Composite, compomer, giomer and

resin modified glass ionomer cement (RMGIC) are common examples. Collectively, both *in-vitro* and *in-vivo* evidence based limitations include marginal leakage, micro-cracks propagation, surface roughness, plaque adhesion, polymerisation shrinkage, inadequate wear, corrosion resistance and the risk of recurrent or secondary caries. In terms of their advantages they are economical aesthetically pleasing (Lee et al. 2010; Zhang et al. 2010).

Resin based cavity varnishes, used in dental applications, are superficial thin coatings which provides a barrier to the penetration of chemicals or to the loss of essential constituents from the surface of a filling material such as restorative materials. These varnishes are made up of a clear or yellowish fluid containing resins that could be either natural (copal and colophony) or synthetic resins (polystyrene). These resins are dissolved in a solvent (ether or acetone) and then they are smeared over the cavity floor with the help of a brush or cotton. As the solvent evaporates, a thin layer of resin coating is left behind. Varnishes must be applied up to 3 times on the filling material to ensure an even coating of resin (Noort 2013).

2.5.3 Phosphate and silicate based restorations

These restorations use calcium and zinc phosphate as a base along with silicate glasses (as filler content) with various compositions. Some common examples are glass ionomer cements (GIC), calcium phosphate cements (CPC) and zinc phosphate cements (ZPC). However, common drawbacks are marginal leakage, plaque adhesion, inadequate wear resistance, creep,

insufficient bonding ability with surrounding dental hard tissues, discoloration and staining, dissolution and disintegration of cement, and the risk of recurrent or secondary caries. However, good aesthetics and alleviate manipulation can be considered as their advantages (Tadjiev & Hand 2010; Chen et al. 2010).

2.6 Selection criteria for dental restorative materials

The study of dental restorative materials is based on material sciences and engineering. There are four categories of materials sciences such as ceramics, metals, composites and polymers. On the basis of their individual characteristic features, a large number of dental materials are currently being designed and used (O'Brien 1997). The following sections provide a brief description of the ideal properties and selection criteria for dental restorative materials.

2.6.1 Mechanical strength

Mechanical properties of material depend upon the type, concentration, size and distribution of the incorporated filler particles. Commonly used filler particles in dental restorative materials are fused silica, quartz and glasses such as alumina silicate. The geometry and shape of filler content affects the interfacial bonding ability of an individual material with the surrounding dental hard tissues. Incorporation of nano or micro-sized filler content can enhance the

mechanical characteristic features of any individual material. For instance, increase in resistance of material against creep, wear, corrosion, brittleness, distortion and disintegration (Walls 1986; O'Brien 1997; Anusavice et al. 2012).

2.6.2 Water sorption

Characteristically, dental restorative material should be able to withstand water damage and chemical effects. In the moist oral environment, materials can undergo dimensional instability due to water sorption. Principally, water molecules diffuse into the matrix and cause weakening of interfacial bonds between the matrix and filler content. Consequentially, dissolution and disintegration of set cement can occur (Anusavice et al. 2012).

2.6.3 Biocompatibility

Ideally, restorative material should be capable of minimizing the risk of multiple oral lesions and conditions such as leukoplakia and dental caries. Moreover, material should be bioactive and capable enough to act as a barrier against cytotoxicity and neurotoxicity (O'Brien 1997; Anusavice et al. 2012). Due to its numerous advantages, such as better adhesion and aesthetics with surrounding dental hard tissues by ionic bonding, and slow but sustained release of fluoride ions in an *in-vivo* environment, glass ionomer cement is one of the main dental material groups currently being researched. In spite these advantages though, glass ionomer cement exhibits certain limitations including brittleness, low tensile strength, and dissolution and

disintegration in the early stages of setting (Walls 1986). The upcoming section of the literature review provides a definition and history of this material group along with its setting and reaction chemistry.

2.7 Glass

2.7.1 Definition and introduction

Glass is a solid material which easily breaks into small pieces due to its brittleness. According to the American Society for Testing Materials (ASTM), glass can be defined as “an inorganic product of fusion which has cooled to the rigid conditions without crystallization”. An alternative description has been provided by Wong and Angell in 1976. They state that glass is an amorphous solid material which goes through the process of glass transition, when it is subjected to heat treatment. This transition process involves the continuation of the dimensions and also the change in physical properties such as thermal expansion and specific heat capacity which potentially come from the super cooled liquid state. Developmentally, the invention of borosilicate and silica phosphate-based glasses which are more chemically resistant than pure glass is fairly recent (Varshneya 1994; Shelby 2005)

2.7.2 History and background

The early Egyptians realised that glass as a very precious and valuable material found on earth evidenced by glass beads found in ancient tombs and death masks of Pharaohs. Similarly, in pre-historic periods, the cave and land dwellers used natural volcanic glass materials in the manufacturing of their tools as weapons including axes, knives, arrows and scrapers (Shelby 2005).

Production of glass from raw materials by melting has been practiced for many centuries. Therefore, there are various different school of thoughts which particularly defined the first formation and production of glass in ancient times. Some of them suggested that, the first glass was basically evolved by the combination of sea salt and calcium oxide released from bones residue which are present in the cinders of the built fire over the sand, found near the edges of the Mediterranean Sea shoreline. This helps lowering down the melting temperature of the sand and enables to produce low quality glass more commonly. Researchers of that time thought that glass which is found in the sand may have such deliberated potential that it might be helpful in the fabrication of first most frequent commercially offered glass to sell (Shelby 2005).

However, the first man made cured glass was produced in the form of beads and was also shaped into sharp edged tools especially, for hunting and self-protection rational. As through the development of the modern era many efforts have been introduced for the controlled shaped production of different types of glasses. Earlier the production of bottles was done by

meandering of the glass around the compact pattern of sand. Whereas, when the glass cooled, the pattern sand was wiped out from inside of the bottle which leaves the vacant as well as the lucent walls, which is usually asymmetrical in shape. The method for modelling and casting glass in the form of bottles and mirrors are much more refined and developed nowadays as compared to earlier. Although, it is considerably easier now to produce glass according to more desirable mechanical and physical properties but many more flaws are still in existence which requires more attention and investigation. The dramatic improvements in the glass manufacturing in terms of bottles and glass jars become very much popular. Similarly, the art of manufacturing coloured glasses has also been transferred as the family secrets from generation to generation of artisans (Varshneya 1994; Shelby 2005).

2.7.3 Glass formation theories

2.7.3.1 Structural theories

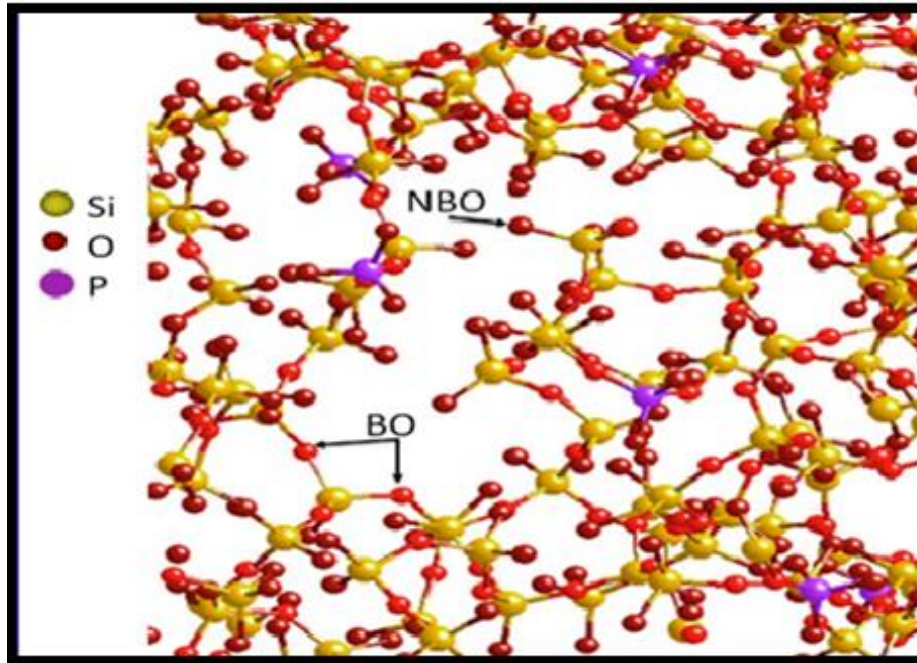


Figure 1: Schematic diagram indicating the atomic structure of phosphor-silicate based glass indicating non-bridging oxygen (NBO) and bridging oxygen (BO)

(Shelby 2005; Jones 2013)

In 1926 Goldschmidt presented the first and simplest theory of glass formation. He postulated that the common formula for glass was R_nO_m , where R_n is the number of oxygen ions arranged particularly in the range of 0.2 to 0.4 radius. He also hypothesised that, the only glass that should be able to melt must be composed of a tetrahedral cationic structure. The major drawback of this theory was that there is no explanation of the dependence on the tetrahedral ions required for glass formation (Shelby 2005).

A few years later, Zachariasen proposed extensions of Goldschmidt's work. He intended to explain how the number of ions could possibly be related to the formation of glass. Zachariasen proposed that, silicate-based glasses have a tetrahedral structure which possibly forms networks into all four corners, especially in a single crystal. However, the extension of this network is basically in all three directions (x, y and z axis) as shown in Figure 1 and 2. As a result, there is an equal behavioural change in all directions which gives rise to the isotropic property of the glass. In general, those compositions of glasses which have the ability to form networks are most able to form good quality glass (Shelby 2005).

Various other structural theories of glass formation were proposed by other scientists. Smekal proposed a theory to explain the formation of ionic and covalent bonds when glass melts. He stated that there are basically two main categories of structural theories of glass. First category states that glass is an inorganic material which contains partial ionic and covalent bonds. Similarly, the other one contains inorganic / organic chain with covalent bonds between them and they are connected by weak Vander wall forces. Following this, Stanworth proposed that the formation of glass is based on the electro-negativity of the cations. He classified oxides into three main groups. Group I oxides act as the network formers due to the formation of bonds with oxygen and ionic characteristics of nearly 50 percent. Group II act as the intermediates and contain more ionic bonds which bind with the oxygen ions. Group III are the glass modifiers because this group contains much more less electro-negativity. This means that

oxides of this group modify the crystal-latticed structure within the network of glass (Varshneya 1994; Shelby 2005).

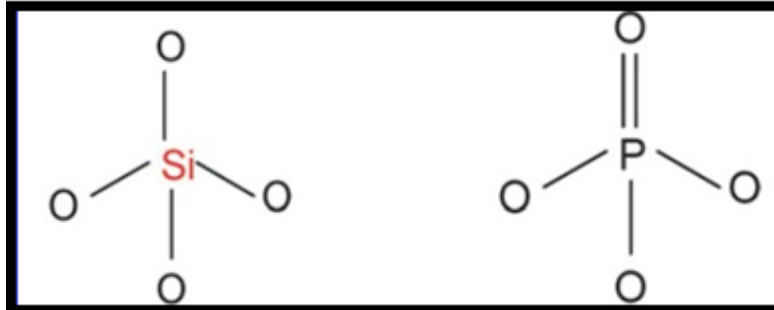


Figure 2: Schematic diagram showing the tetrahedral structure of silica (SiO₄) and phosphate (PO₄) (Arepalli et al. 2016).

On the basis of the bond strength, Sun proposed that, the formation of strong ionic or covalent bonds during melting can prevent the formation of a crystal lattice structure upon cooling. Some years later, Rawson explained the basic drawback of Sun's theory of glass formation. He concluded that Sun had overlooked the relationship between temperature and bond strength. He stated that, due to the very high melting temperature of glass, there is enough energy available to break the bonds simultaneously. Rawson explained that material which contains multiple bond strength and a low melting temperature expresses better ability of glass formulation in comparison with material with single strength of bonds with a high melting temperature (Shelby 2005).

2.7.3.2 Kinetic theories

The theory of kinetics for the formation of glass is associated to the process of crystallisation. The process of crystallisation can be described as the combination of a pattern of crystal growth and process of nucleation. The nucleus present in the formed crystal lattice structure grows to a certain size and this growth might be homogenous or heterogeneous. If the growth is spontaneous within the melt, it is referred to as homogenous nucleus growth. If the growth occurs spontaneously due to any impurities, especially with the walls or base of the crucible used, then it is referred to as heterogeneous nucleus growth pattern (Shelby 2005).

2.8 Glass ionomer cement system (GIC)

2.8.1 Introduction and dental applications

Kent and Wilson (1972) contributed greatly to dental restorative material sciences by mixing poly-acrylic acid and ion leachable glass. The resultant product was named glass ionomer cement (GIC) or aluminosilicate poly-acrylate (ASPA) by De Trey in 1976: a hybrid of carboxylate and dental silicate cement. Since its initial development, glass ionomer cement has received mixed responses from dental clinicians (Smith 1998; Anusavice et al. 2012).

Various modifications to this initial material have been suggested but without any significant mechanical or physical improvements as a result. These modifications include use of maleic

and acrylic acid, dried polymer powder, metal reinforcements and resin based modifications (Tyas 1991). Despite its remarkable advantages, the use of glass ionomer cement is still limited in terms of dental applications. The prime reason for such limitation of use is its low diametric tensile and flexural strength, early stage dissolution of cement during setting and inadequate translucency (Tiwari & Nandlal 2012). These issues have limited the use of glass ionomer cement to less stress bearing restorations such as those in Class V (gingival third of buccal, labial, lingual and palatal surfaces of teeth), as liners in composite restorations, and as luting cement. Due to more recent advancements, glass ionomer cement is now being used in Class III (cavities on proximal surface of incisors and canines but incisal angles are not involved) and Class I restorations, and core build-ups for crown and bridge placements. Glass ionomer cements have found a niche in medical applications as well. Currently, it is fairly commonly used for middle ear reconstructive surgery due to its bioactivity, the production of osteoconductive ions for instant sustained release of fluoride ions, its negligible exothermic nature, and adequate bonding ability with surrounding metal and bone. In other words glass ionomer cement is now being viewed as a suitable bone substitute (Ronald & Sakaguchi 2012; Anusavice et al. 2012).

2.8.2 Composition

Glass ionomer cement consists of poly-acrylate cross-linked chains which are reinforced by aluminosilicate particles of glass. The glass powder may contain silica, calcium, alumina, sodium and fluoride. Of these, the ratio of silica and alumina is the key factor dictating its reaction with poly-acrylic acid (Tiwari & Nandlal 2012). Other metal oxides (barium, zinc and strontium) are used in addition to increase the radio-opacity of the resultant cement. The preparation of glasses is all based on traditionally available routes of glass processing. Depending on the composition, the mixture of raw batch material of glass is fused together at a range of temperatures varying from 1100°C to 1500°C. The glass is then quickly quenched in order to avoid any devitrification. The casted glass is then ground into powder of particle size 15 to 50µm by the ball milling method and then sieved. The liquid content tends to consist poly-acrylic acid (50%) and copolymers (40%) of maleic, itaconic and tri-carboxylic acid along with water (10%) (Smith 1998; Anusavice et al. 2012).

More commonly, all commercially available glass ionomer cement compositions are based on aluminosilicate glasses along with modifications including calcium, strontium, lanthanum and phosphate oxides. The typical composition of commercially available dental glass ionomer cement is indicated in Table 1.

Table 1: Typical composition of glass ionomer cement (Ronald & Sakaguchi 2012; Anusavice et al. 2012).

Sr No	Oxides	Mole percent (Mol %)	Weight percent (Wt %)
1	SiO ₂	22.3 %	30.1%
2	Al ₂ O ₃	24.9 %	19.9%
3	AlF ₃	2.7 %	2.6 %
4	NaF	1.9 %	3.7 %
5	CaF ₂	33.2 %	34.5 %
6	AlPO ₄	15.1 %	10.0 %

Wilson and Nicholson (1993) found that two main types of glasses exist: SiO₂ – Al₂O₃ – CaO and SiO₂ – Al₂O₃ – CaF₂. All other ionomer glasses are derived from these two.

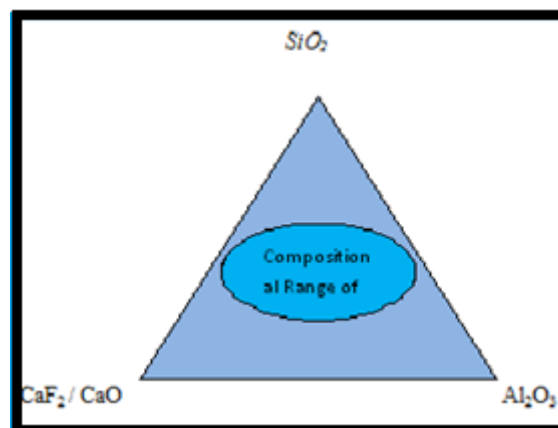


Figure 3: Schematic diagram showing compositional range of glass in glass ionomer cement production (Anusavice et al. 2012; Holand & Beall 2012).

Modifications to the basic design of glass ionomer cement have resulted in the composition of traditionally available materials. Moreover, glass ionomer composition is limited within a range, as shown in Figure 3. The formation of the glass outside this range tends to crystallise and phase separation occurs when using the quench cooling method. The knowledge of comprehensive reaction chemistry is very important for the prediction of micro structural properties of set cement. Reaction chemistry starts after manipulation of powder and liquid contents of cement. Physically, yellow colour plastic paste forms instantly. Chemically, immediately after mixing of contents the acid-base reaction starts and acid starts to dissolve the glass quickly (Bher et al. 2011; Holand & Beall 2012).

Glass ionomer cement can be formed using two different methods:

1. Mixture of glass powder with aqueous solution of poly acrylic acid.
2. Mixture of glass powder with freeze-dried poly acrylic acid and water.

Collectively, glass ionomer cements are available in various tailored forms. As a result, determination of the setting reaction is itself a challenge. Analogues of ranges of poly acrylic acid with differences in molecular weight are incorporated into available formulations. The major polymeric acids / chelating agents which are currently used in the formation of glass ionomer cements are acrylic acid, maleic acid, tartaric acid and itaconic acid as shown below in Figure 4 (Walls 1986; Anusavice et al. 2012). The determination of viscosity and handling ability merely depends upon molecular weight of poly-acid.

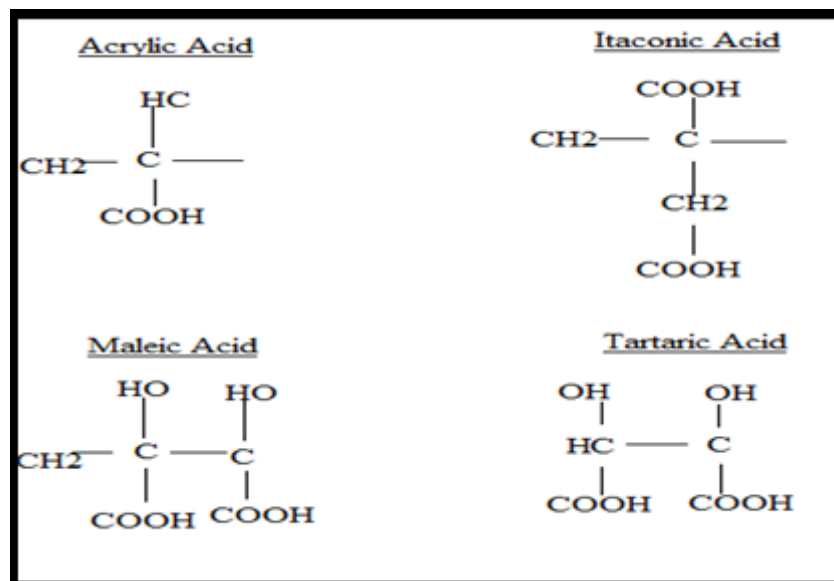


Figure 4: Acidic components currently being used in glass ionomer cement commercially (Anusavice et al. 2012).

Studies have shown that changes in the polymer component can potentially enhance the strength of the set cement but that, due to matrix instability, the disintegration and dissolution of the resultant cement could occur immediately. More specifically, the copolymer of poly vinyl-phosphonic acid is potentially capable of improving the initial setting stability of the glass ionomer cement from hydrolytic ionic invasion. Another finding is that the use of maleic acid can increase the cross-linking density within the cement and provide better mechanical strength. In this case though, the brittleness of the set cement increases. However, the addition of tartaric acid plays a positive role in the setting chemistry of glass ionomer cement, as shown in Figure 5 (Moshaverinia et al. 2009; Tiwari & Nandlal 2012).

2.8.3 Role of setting modifiers

The setting reaction of glass ionomer cement starts after the acid-base reaction between the basic glass and polymeric acid. In glass powder with aqueous solution of poly acrylic acid, the dissolution of poly-acid occurs instantly during mixing, as compared to freeze-dried poly acrylic acid glass powder mixture. The setting reaction of glass ionomer cement occurs in three different stages as a result of the release and cross-linking network formation of calcium and aluminium ions from the glass particles and maturation of the matrix polymer. These stages are dissolution, gelation and hardening and are shown in Figure 6.

Dissolution begins with the amalgamation of different constituents present in the cement. During this initial stage of cement formation, due to the presence of water molecules, hydrogen ions from polymeric acid become separated and preferentially separate carboxyl groups. Moreover, hydrogen ions detach the calcium (Ca^{2+}) and aluminium (Al^{3+}) ions from the surface of glass particles into the polymeric matrix. As a result, siliceous hydro gel forms because hydrogen ions diffuse in the glass particles and create negative charge. This negative charge creates an environment for calcium and aluminium ions to cover the surface of the glass particles and create a deficient zone of cations (Moshaverinia et al. 2009; Anusavice et al. 2012; Tiwari & Nandlal 2012).

Experimental studies have proven that silicate (Si^{4+}) ions leach out during the dissolution stage from the surface of glass particles and Hatton and Brook (1992) suggested that silicate (Si^{4+})

ions play a role in the cross linking reaction and matrix formation (Hatton & Brook 1992). In 1996, Matsuya et al proposed the reaction and setting chemistry of glass ionomer cement based on NMR and infrared spectroscopic analysis. They concluded that silicon ions play a significant role in cement matrix formation and that the reaction precedes the release of aluminium ions. This release results in aluminium ion based poly-acrylic acid gel formation.

Originally, glass aluminium ions are in tetrahedral form with oxygen but, as the setting reaction progresses, aluminium ions become octahedral. Due to this chemical shift in the silicon network, a progression in the strength of the glass ionomer cement occurs during the gelation stage (Matsuya et al. 1996). In 1998, Nicholson published work supporting the proposed theory of Hatton and Brook. He concluded from his research that during the dissolution stage when calcium and aluminium ions become soluble the release of phosphorus and silicon ions begins. As a result, at this stage, termination occurs more prominently than the exchange of ions due to inorganic network formation, which enhances the resultant cement insolubility (Nicholson 1998; Guggenberger et al. 1998). Similarly, in 1999 Maeda et al concluded, by using the SIMS technique, that silica formation only occurs in the siliceous layer which is precisely surrounded by dense non electron halo glass particles (Maeda et al. 1999).

The second and most prominent stage of the glass ionomer setting reaction is the gelation stage. This stage lasts up to a few minutes. Due to the formation of free cations of calcium (Ca^{2+}) and aluminium (Al^{3+}), a cross linking bridge forms in between the terminated groups of carboxyl ions and polycarboxylates. Calcium ions (divalent) release much more quickly than aluminium

ions (trivalent) in the polymer matrix. Finally, in the hardening stage, the cross-linking bridge forms in between aluminium ions and the depleted carboxyl group. This stage typically lasts between five to ten minutes, although some studies report a longer period of time required due to the introduction of setting modifiers as shown below in Figure 5 (Nicholson 1998; Anusavice et al. 2012)

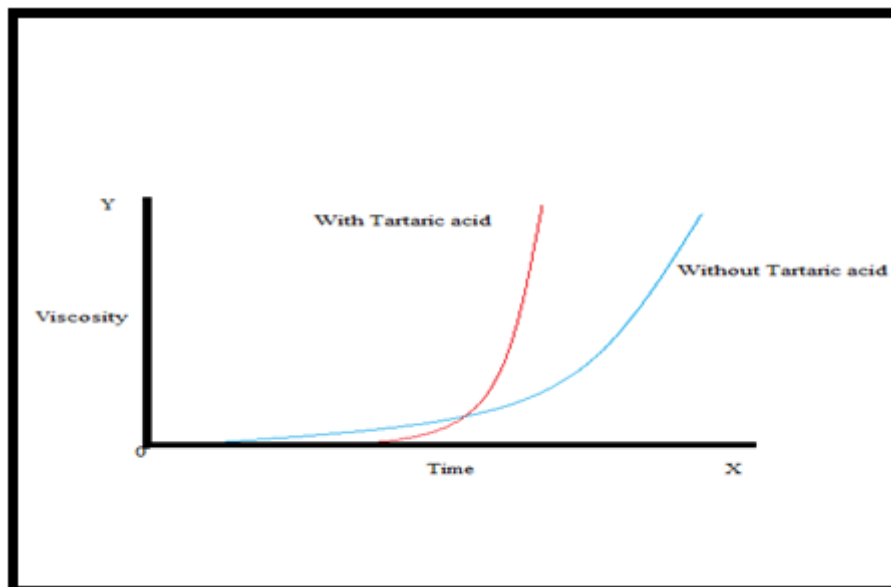


Figure 5: Graphical representation of the effect of tartaric acid on cement during setting reaction of glass ionomer in terms of viscosity over time (Noort 2013).

Significantly, the addition of tartaric acid to the liquid content can be considered as an important step towards the setting process and reaction chemistry of glass ionomer cement. Tartaric acid acts as a modifier and it controls the dissolution rate of glass particles present in the composition. As an impact, initial setting and handling characteristics of glass ionomer cement improve. Due to its high acidity, tartaric acid readily attacks the glass particles. As a

result, the influence of reactivity of glass particles towards poly-acids is decreased (Wilson et al. 1976; Nicholson 1998). Wilson et al, by using a Gilmore needle along with oscillating rheometer, analysed the potential effects of different substitutions within the composition of glass ionomer cement. They concluded that the addition of tartaric acid was quite successful, particularly in terms of the working and handling characteristics of the resultant cement (Stamboulis et al. 2004). Furthermore, Prossler et al (1982) analysed the effects of modification into glass ionomer cement by using infrared spectroscopic techniques. They found that the rate of acidity present during the setting reaction can control the degree of the acid base reaction (Prosser et al. 1982).

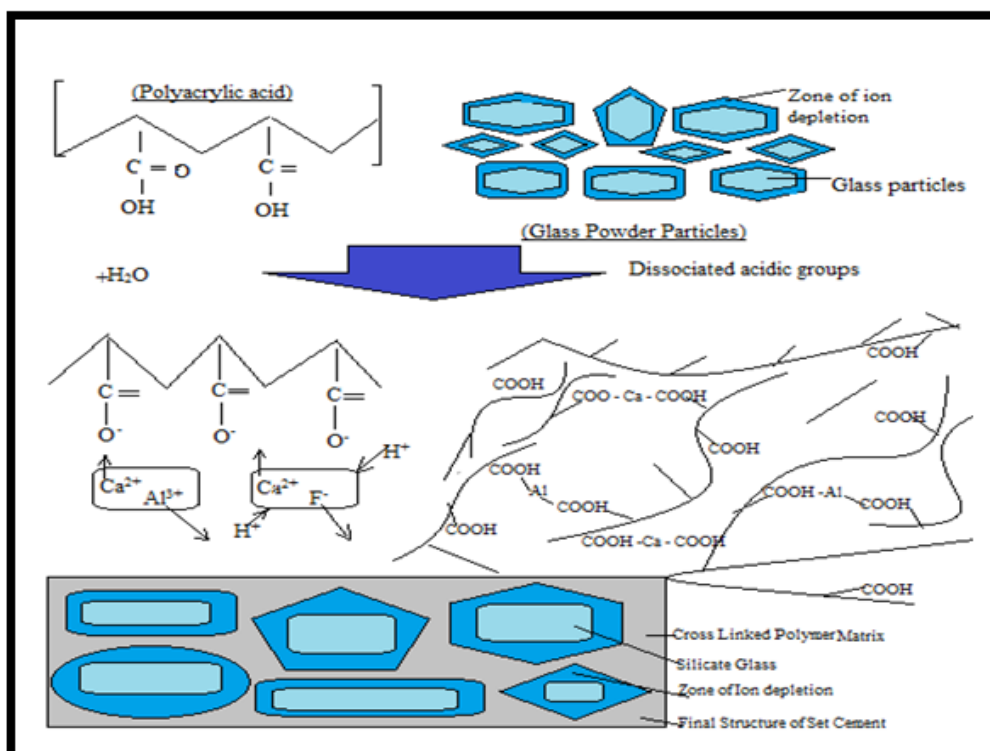


Figure 6: Schematic diagram showing chemical and setting reaction of glass ionomer cement (Noort 2013).

Generally speaking, with the addition of strong acids, the process of chemical reaction accelerates compared to when using bases. This slows down the speed of reaction. Similarly, modifications for the improvement of working time can delay the release of cations. On the other hand, alterations for setting time can lead to the formation of poly-acid base complexes. As a result, blocking of bridging occurs among the cations and poly-acids positively. This can only be converse with the rise in pH as breakdown of complexes can initiate and trapped cations can become part of a given reaction. However, applications of tartaric acid in higher concentrations (>20%) can create adverse effects such as weakening the resistance of cement against aqueous invasion and increasing the solubility of the set cement (Crisp et al. 1979). Inclusion of fluoride ions can also effect the workability due to the formation of aluminium fluoride, which can play a role in the release of cations and their premature inclusion during matrix formation (Wilson et al. 1976). However, there is no in a straight line related evidence for mentioned species along with their different structures and their bonding patterns (Nicholson 1998).

2.8.4 Structural and mechanical properties

Determination of micro structural properties is vital for successful application of glass ionomer cement. Hatton and Brook (1992) examined the microstructure using a transmission electron microscope (TEM). They found that in set cement, the alumina silicate ions of glass particles encircle the cross-linked cations of the poly carboxylic matrix (Hatton & Brook 1992). Release

of fluoride ions is a significant factor of glass ionomer cement restoration. Due to the presence of fluoride ions, ionic exchange between the hydroxyl group (OH^-) of hydroxyapatite and fluoride ions occur. As a result, fluoroapatite crystals are formed. Due to low surface energy they increase dissolution resistance of set cement and increase the anti-cariogenic effect of glass ionomer cements. Potentially, the recharge ability of fluoride ions present in glass ionomer cement, can accelerate within the complex oral environment due to the presence of sodium fluoride (NaF), especially after use of fluoridated tooth pastes and mouthwashes (Smith 1998; Anusavice et al. 2012).

Numerous *in-vivo* and *in-vitro* experimental studies have been conducted to determine the mechanical properties of glass ionomer cements. Prosser et al (1986) concluded that, in glass ionomer cements, crack propagation or fracture starts due to the inadequate tensile strength of set cement (Prosser et al. 1986). Furthering this research, Xie et al. (2000) calculated the flexural strength of conventional glass ionomer cement (10-25 MPa) in comparison with resin modified glass ionomer cements (RMGIC) (80 MPa). They postulated that disintegration of cement takes place due to incidence of fracture which may occur during glass matrix formation (Xie et al. 2000). It was finally concluded that the distortion and dissolution of set cement occurs due to inadequate matrix formation, filler particle size and shape and insufficient handling techniques (Anusavice et al. 2012).

2.8.5 Advantages and disadvantages

On the basis of *in-vivo* and *in-vitro* evidence based research and recent compositional glass ionomer cement modifications and advancements, its applications in medical and dental fields has been growing rapidly. To be more precise, it has been found that the potential bioactive bonding ability of glass ionomer cement with surrounding mineralised hard tissues, such as ionic and hydrogen bonding with the hydroxyapatite layer, is due to the presence of poly carboxylate groups (Noort 2013; Geyer et al. 1997). Various different studies have been conducted to evaluate the applications of glass ionomer cement in certain medical and dental surgical applications such as Brook et al (1991) study explaining bone substitute in oral and maxilio-facial surgery, Jonck's (1989) study of prosthetic hip replacement surgery, and Geyer's and Helms (1993) study regarding otological surgery (Brook et al. 1991; Babighian 1992; Geyer & Helms 1993). In the 90's, Renard et al presented a case report related to aluminium encephalopathy (clinical conditions due to excess accumulation of aluminium ions in the blood associated with Alzheimer's disease and neurological disorders) due to glass ionomer based cement known as Ionocem[®] used in surgeries involving the skull (Renard et al. 1994; Guillard et al. 1997). The loss of aluminium ions in early stages and their consequences pushed the use of glass ionomer cement in medical applications behind, especially in oral maxillofacial surgeries (Andersson and Dahl, 1994). However, in the United Kingdom, Sereno CEM[®] is

being used in less stress bearing areas of the middle ear in ossiculoplasty surgical procedures (Serenio CEM[®], UK).

In dentistry, due to its aesthetic qualities, radio opaque nature (radiological) and cost effectiveness, it is widely accepted as a direct restorative material for anterior / deciduous restorations, luting and lining under crown bridge restorations (Hickel et al. 1998; Croll & Nicholson 2002). In contrast, due to its inadequate resistance against strong abrasive mechanical forces (wear) during mastication, disintegration and dislodgment of set cement under cyclic loading (creep), and insufficient protection against plaque adhesion (surface roughness), the use of glass ionomer cement for posterior dental or stress bearing areas is limited. Marginal instability and micro-crack propagation along with post-operative pain and sensitivity are also considered key factors for its limited use in oral-dental applications. However, due to glass ionomer cement being fluoride releasing and the resultant recharging capability in complex oral environments it has long been the most significantly studied material by various research groups (Walls 1986; Kurkjian 1986; Naasan & Watson 1998).

Furthermore, the surface of glass ionomer cements is hydrophilic and osteoconductive. Numerous studies have been conducted by researchers to evaluate the biocompatibility of glass ionomer cement in both *in-vivo* and *in-vitro* conditions. The bioactive cellular response was observed due to the ionic releasing nature of glass ionomer cement (Oliva et al. 1996; Brentegani et al. 1997). Immediately after the gelation phase, ionic exchange starts to occur in the *in-vivo* environment, and this is directly dependent upon the compositional elements of the

glass ionomer cement. Similarly, the size of glass filler particles also plays a significant role in the promotion of good bonding and biocompatible abilities of set cement. It is known that smaller size filler particles are less toxic, and due to uniform distribution, can more easily form better bonds with surrounding hard and soft tissues than larger particles (Lucksanasombool et al. 2002; Rao 2002).

2.8.6 Recent modifications and their limitations

Certain modifications of glass ionomer cement have been suggested to overcome mechanical, physical, chemical and biological drawbacks in traditionally available glass ionomer cement. In its early stages of development, calcium fluoroalumino-silicates based glass was introduced. Since then, various commercial compositions have been introduced according to specific clinical requirements, such as the use of phosphorous and sodium ions. Similarly, to enhance the radio opacity of set cement, strontium, barium and lanthanum were introduced successfully. Structurally, alkaline based silicate glasses can be described using Zacharias's random network model. According to studies, the tetrahedral structure of silicate (SiO_4) can form a 5 to 8-membered ring structure with transformed alkaline metal ions, such as calcium ions (Ca^{2+}), which are present in interstitial spaces of the ring (Hand & Seddon 1997; Wood & Hill 1991). Pure silica (SiO_4) based glasses are electro-neutral in nature and chemically more prone to acid attack. As a result, they cannot be used as glass ionomer cements. The addition of aluminium ions (Al^{3+}) in the glass composition increase susceptibility to acid attack (Nicholson 1998;

Maeda et al. 1999). Griffin and Hill (1999) tested numerous glass components including fluoride and phosphate as major components and concluded that increased phosphate-containing glasses are susceptible to acid attack. However, due to the presence of four balanced electrons in phosphate, phosphate-oxygen bond which is hydrolytically stable can be created. They also found that the inclusion of calcium ions in the form of calcium oxide (CaO) can promote non-bridging units, which can act as glass modifiers (Griffin & Hill 1999).

The addition of fluoride content into the composition in the form of calcium fluoride (CaF₂) can be beneficial to the resultant decrease to the glass fusion temperature. Moreover, it can also increase the strength, translucency and handling characteristics of the cement. On the other hand, the addition of phosphate can increase the working and setting time of the cement whilst only providing an inconsequential improvement in strength (Anusavice et al. 2012).

The separation of phase occurs in the mixture of glass ionomer cement compositions due to difference in batch. This is commercially very beneficial in lowering the reactivity and increments in strength of glass. By controlling the structure of glass, setting properties can be controlled such as its reactivity. Due to the surface crystallisation process, the glass becomes more stable when confronted with acid attack (Wood & Hill 1991). In the same way, liquid – liquid phase separation is also a very important factor that occurs during quenching. Two different phases can occur such as the formation of residual alumina-silicate and calcium-fluoride phase. The calcium-fluoride phase is more prone to poly-acid attack during the setting

reaction. It is known that, in non-phosphate based glasses, the calcium fluoride is nucleated initially (Nicholson 1998).

Moreover, certain significant modifications have been introduced to existing glass ionomer cement system. These include the introduction of N-vinylpyrrolidone containing poly acids, fluoroapatite and nano-hydroxyapatite particles to improve mechanical properties of commercially available GC Fuji II GIC. As a result of these additions, Rehman et al found that, mechanical strength was increased (Moshaverinia et al. 2009). Furthermore, other compounds such as Chloro-hexadine gluconate (Ahluwalia et al. 2012), glycidyl meth-acrylate di-ethanoleamine derivatives and polymethyle meth-acrylate (PMMA) were introduced into the existing glass ionomer cement system (Zhang et al. 2010). However, it was observed that the properties of biocompatibility were compromised and increases in both cytotoxicity and neurotoxicity were observed (Svanberg et al. 1990; Wilson 1990; Moshaverinia et al. 2008; Yang 2012; Subramani et al. 2013; Botsali et al., 2014).

2.9 Introduction of citric acid as a setting modifier

Recent studies have suggested that citric acid has a significant ability to modulate the stress bearing function of bones. Based on these findings Tran et al. (2014) primarily suggested biodegradable, mechanically strong, and biocompatible citrate based polymers blends (CPBPs) in a polymer bio ceramic composite system which offers countless benefits because of their

capability to mimic the composition of natural bone. Introduction to these blends exposes the impact of free exogenous citrate on osteoblast culture, reflecting the ability of citrate based biomaterials to be used efficiently in orthopaedic material designing (Tran et al. 2014).

Previously, in 1960 this tricarboxylic acid molecule was reported to be up to 5% of the organic constituents of bone accountable for regulating and stabilising nano particles. Although later 90% of the total body citrate was found to be present in the skeletal system. A closely monitored nuclear magnetic resonance (NMR) study declared vigorous association of the surface of apatite nano crystals with the citrate molecule (Tran et al. 2014).

Furthermore, studies have indicated the potential of citric acid to generate hydroxyapatite crystals in simulated body fluid (SBF). It is now known as a dissolved calcium solubilising agent, firmly bound to fundamental parts of bone nano composites. Advancements in the studies related to citric acid's role suggest that it might be used in orthopaedic biomaterials and scaffold (Tran et al. 2014).

Normally, during the cyclic process of Kerb's cycle, 90% of the total body citrate is conserved by the skeletal system. More recently, research models indicate the vital role of citrate ions in bone anatomy, physiology and the development of biomaterials because of which citric acid based hydroxyapatite composites and polymers (CABP-HA)_n were introduced, which has attracted significant attention in the field of biomaterials and tissue engineering. Hue et al. (2014) and Sun et al. (2014) indicated that citrate molecules are more comprehensively studied

over the nano-crystalline structural surface of apatite and potentially can form bridges between surrounding hard tissues. Similarly, findings showing the natural occurrence of citrate ions in bone tissues, its significance in bone physiology, and recent indication of its impact on stem cell cultures have directed research into the potential impacts of citrate ions over bone development and orthopaedic biomaterial advancements (Sun et al. 2014).

Current investigations have revealed the promising attributes of citric acid supporting osteogenic development and regulation. Synthesised citrate based substitutes in contrast with autogenous bone grafts have been explained as the gold standard for bone regeneration and osteointegration because of their ideal biocompatibility. Exogenous citrate hybridized in certain biomaterials, used in culture medium and liberated from biomaterials has been demonstrated to boost the gene expression of alkaline phosphatase (ALP) and osterix (OSX). These genes are considered as the key markers for bone regeneration and formation. They are also responsible for advancements of osteogenic phenotype and support osteointegration when closely monitored. Additionally, citrate based biomaterials have been reported to support bone regeneration in cranial defects showing its remarkable osteogenic potential in implants (Sun et al. 2014).

2.10 Bioactive glasses

2.10.1 Background and histo-chemistry of silicate based bioactive glasses

Bioactive glass was developed firstly in 1969 by Larry L. Hench, a researcher from the United States of America. His first composition was known as 45S5 Bio-glass[®] and since 1985 it has been used clinically. The term bioactive glass refers to the reactive biomaterial which inherently possesses the capability of binding with mineralised tissues of surrounding bone in normal physiological environments. Early in its development, it was used in the form of small pieces, especially for prosthetic regenerative surgery of the middle ear bone. Bioactive glass is now accepted in the field of regenerative medicine and tissue engineering. Similarly, countless improvements have been made to allow the introduction of bioactive glasses in the field of dentistry, especially for endodontic, prosthodontic and implant dentistry (Hench 2006; Khan et al. 2013).

The most basic composition introduced, was based on 45% SiO₂. 24.5%Na₂O. 6%CaO and P₂O₅ and was formulated to increase the amount of CaO in combination with P₂O₅, particularly in the formed matrix of Na₂O – SiO₂. The calculated batch glass was melted, casted and then crushed into smaller rectangular shaped implants. These were successfully inserted into the femoral bone of rats for initial testing for a period of six weeks. On the basis of these findings, Hench explained that 45S5 composition of bioactive glass can successfully form a layer of hydroxyapatite (HA) which can chemically bind with collagen fibrils to form substantial

interfacial bonds (Hench 2006). Similarly, in 1977, Professor Ulrich Gross in Germany introduced a new formula based on 45S5 Bio-glass[®] with the addition of potassium oxide (K₂O) and magnesium oxide (MgO). He concluded that this glass could form strong mechanical bonds with existing bone. However, when he introduced titanium (Ti), the bond formation reduced instantly (Hench 2006; Subramani et al. 2013).

Furthermore, bioactive glass does not readily intermingle with the surrounding living tissues. Firstly, they are absorbed by the layer of matrix proteins which contains collagenous and non-collagenous proteins: vitronectin, fibronectin and fibrinogen. Cell surface receptors can enact cellular responses to organise cells to start anchoring over bioactive glass surfaces. Preliminary responses of individual cells with bioactive material are complex in nature. It begins with the adsorption of proteins into the extracellular matrix, followed by cell bonding, and cellular growth and differentiation. The biocompatibility of an individual material plays a dynamic role in further progression and success of an implanted bioactive material (Hench 2006; Khan et al. 2013).

To attain a proper balanced physical response and stimulus, stable interfacial bonding is essential between the body tissues and implant. Thus, an ideal biomaterial must have biomechanical and biochemical compatibility. Therefore, replacement of bone by an implant requires physical and mechanical matching as well as bioactivity.

Bioactive glasses can be categorised into two classes (as denoted by Hench):

1. Osteopductive materials considered as Class A. These stimulate both intracellular and extracellular responses at the interface and can bond with both hard and soft tissues. Wilson et al. described osteoproduction as the process where osteogenic stem cells colonise at a bioactive surface within a defected environment that occurs due to surgical interventions.
2. Osteoconductive materials considered as Class B. These develop biocompatibility at the interface along which bone migrates. This type of bioactive glasses only exhibits an extracellular response at the interface.

A series of reaction are involved for the formation of mechanically strong bonds between the bioactive glasses and tissues. Initially after implant, formation of SiOH bonds takes place, followed by the polycondensation of SiOH bonds to Si-O-Si bonding. Subsequently, adsorption of amorphous calcium, phosphate and carbonate ions occurs, leading to the crystallisation of carbonated hydroxyapatite (HCA). The initial reactions at the glass zone of the interface till the development of HCA layer, are independent of the presence of tissue and occur in simulated body fluid (SBF). After the formation of HCA, adsorption of biological moieties such as protein and collagen in the HCA layer takes place. Extracellular interactions are dependent on the material's surface characteristics. Surface porosity and negatively charged silonals play a vital role in the adsorption of proteins with the surface of materials. Activation

of the complement system and coagulation system leading to cellular adhesion begins after protein adsorption. The interaction among osteoblast receptors and the analogous protein ligand results in cellular attachment. In the next stage differentiation of the cells is followed by the generation and crystallisation of the matrix. The reaction stages from adsorption of biological moieties until the crystallisation of the matrix are essential for the implant to bond with the tissues mechanically (Cao & Hench 1996; Jones 2013).

2.10.2 Classification of bioactive glasses

Conventional bioactive glasses can be formed by melting different oxides at a high temperature followed by casting and sintering processes. There are four basic components of bioactive glasses: silicon dioxide (SiO_2), calcium oxide (CaO), sodium oxide (Na_2O) and phosphorus pentoxide (P_2O_5). These are different in terms of weight proportions. However, the bone bonding ability of bioactive glasses is merely related to the composition of glass. As indicated in following schematic diagram Figure 7, region 'A' corresponds to the compositional part which can form a bond with surrounding bone; region 'B' represents the part which is encapsulated with fibrous tissue at the tissue implant interface; region 'C' indicates the restorable portion of composition which can dissolve with the passage of time; and region 'D' represents the portion of composition which cannot form glass (Brauer et al. 2010; Jones 2013).

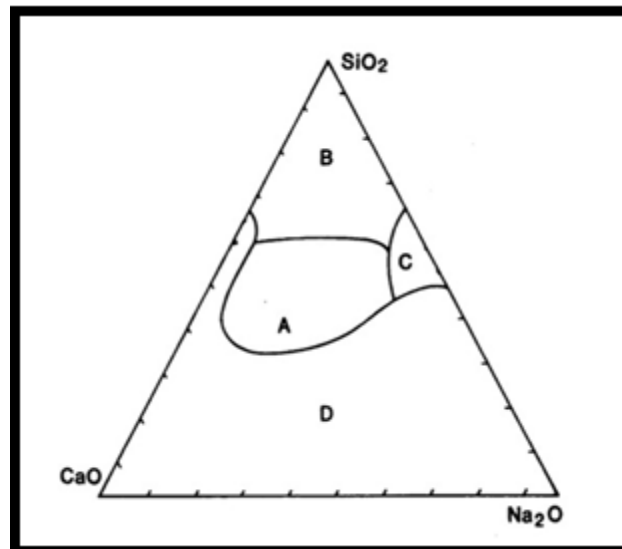


Figure 7: Bone binding ability of bioactive glasses based on composition (Jones 2013).

Moreover, bioactive glasses can be processed by either sol gel or conventional melt quench methods, as indicated in Figure 8. The sol gel method is a chemical based synthetic process where all contents of composition are processed to form a gel at room temperature and then dried to form a glass. The sol gel process does not include any melting procedure and the involvement of network modifiers is less than the melt quench method. This results in the formation of nano-porosities at the end. On the other hand, all melt quench method derived glasses are denser and have a low surface area. Degradation rate is negligible. From the literature, it is evident that all sol gel derived glasses promote less bone growth in comparison with melt quench derived glasses (Subramani et al. 2013; Noort 2013).

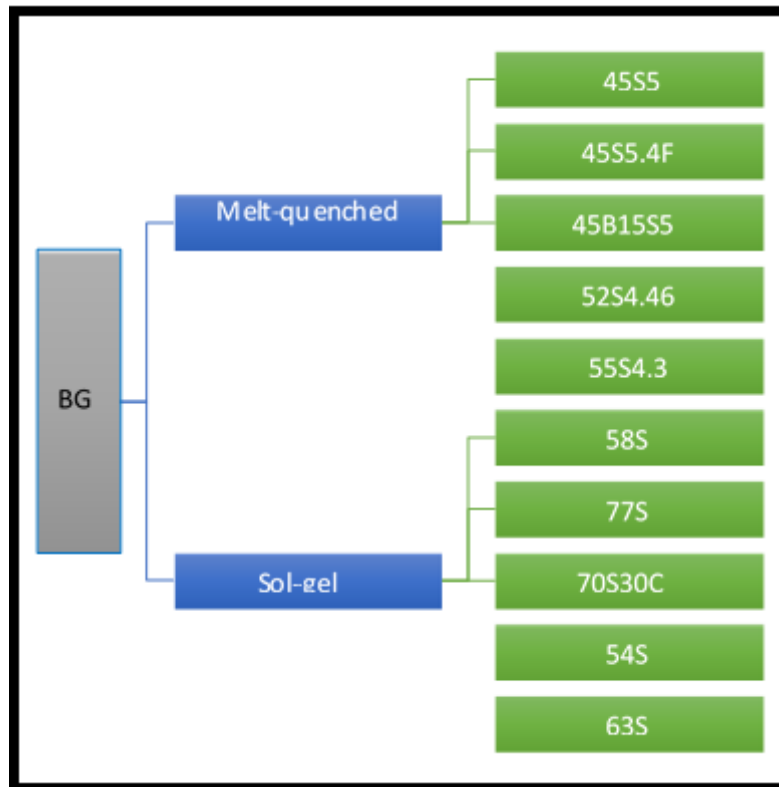


Figure 8: Classification of bioactive glasses (BG) (Cao & Hench 1996).

2.10.3 Use of silicate based bioactive glasses in dental applications

Currently, mainstream bioactive glasses used in dentistry are based on the proposed composition of Hench, in which silica is the major component of all compositions. The bioactive glass was introduced in dentistry by Dr. Clark and his research fellows in 1980. They successfully managed to preserve the edentulous alveolar ridge of patients by implanting bioactive glass. This helped the development of Bio-glass[®] commercially. Certain other bioactive glasses have since become commercially available with different brand names such as Perio-glass[®], extensively used for periodontal treatments and implant procedures. Bioactive

glasses based on batch contents $\text{SiO}_2 - \text{Na}_2\text{O} - \text{P}_2\text{O}_5 - \text{CaO}$ traditionally have inherent potential of antimicrobial activities with re-mineralisation of dental hard tissues such as enamel, dentine and cementum. Due to these unusual inherent properties they are used as coatings over implants, bone grafts and in toothpastes (Hench 2006; Khan et al. 2013).

2.10.4 Silicate based bioactive glass (45S5 Bio-glass®)

A bioactive glass has been used generally to explain the group of silicate based glasses, which may contain disrupted structure. This structure contains Q^2 chain of silica along with numerous non-bridging oxygen ions – silicon tetrahedral and as a result they can degrade into aqueous solution and liberate calcium ions (Hench 2006; Brauer et al. 2010). The 45S5 based bioactive glasses are widely being accepted to form carbonated hydroxyapatite (HCA) layer with simulated body fluids (SBF) solution, concentration of ions closely related to human blood plasma *in vitro* studies (Brauer et al. 2010). In 45S5 Bio-glass® the first two characters (45) indicates the weight percentages of silicon dioxide. Similarly, last two characters indicate the ratio of weight of calcium oxide (CaO) to phosphorous pent oxide (P_2O_5). These glasses have the ability to rapidly create strong bonds with surrounding hard tissues. Whereas, they tend to promote bone growth away from the bone and implant interface. Due to the presence of both osteogenic and osteoinductive properties and also because of the presence of silica and calcium ions in parent glass composition, helped carbonated hydroxyapatite (HCA) layer to interact and form bonds with the surrounding hard tissues (Peitl et al. 2001; Jones 2013).

2.11 Aluminium ions free bioactive glass ionomer cement

Due to its inherent biocompatibility, clinicians use glass ionomer cement with aluminium ions in various skull based and neuro-ontological surgeries. An example is in prosthetic restorations of certain skull defects such as cerebrospinal fluid fistulas (Nicholson & Czarnecka 2009; Gomes et al. 2013; Jones 2013; Kim et al. 2014).

Several *in vivo* and *in vitro* studies on commercially available glass ionomer cement containing aluminium for both medical and dental applications indicate its inhibitory effect over the process of osteoid formation and bone mineralisation. However, due to continuous leaching of aluminium ions and their accumulation far from the site of restoration, its use is limited. It has been reported that glass ionomer cement which contains aluminium potentially elicits a toxic response in bone formation and its mineralisation. Even worse, it has been suggested as causing certain neurological diseases such as, Parkinson's and Alzheimer's disease (Nicholson & Czarnecka 2009; Gomes et al. 2013; Khoroushi & Keshani 2013; Kim et al. 2014).

Several attempts have been made to develop aluminium ion free glass ionomer cement which is acceptable for a wide range of both medical and dental applications. Recently, in 2000, Kamitakahara, proposed modified aluminium free glass ionomer composition $\text{CaO-Al}_2\text{O}_3\text{-SiO}_2\text{-CaF}_2$ with $\text{CaO-Fe}_2\text{O}_3\text{-SiO}_2$ with the admixture of poly-acrylic acid and water. However, whilst the aim of cement formation was achieved, due to presence of iron ions, the bioactivity of the glass composition was compromised. In a similar attempt, in 1992 Diba et al. discovered

that bioactive glasses containing magnesium also exhibit reduced bioactivity. This research has explored the art of replacing trivalent cations (Al^{3+} and Fe^{3+}) with (Mg^{2+} and Zn^{2+}) ion divalent cations (Gomes et al. 2013; Khoroushi & Keshani 2013; Kim et al. 2014).

The effects of the addition of aluminium ions are still very contentious. At low concentrations, aluminium ions can potentially accelerate new bone formation through the formation of osteoblasts (Meyer et al. 1993). In addition, several *in vitro* studies indicate that the presence of aluminium ions in cultured osteoblasts cells have no detrimental effect. Similarly, a low concentration of aluminium ions can create the positive effect in the proliferation of osteoids. However, it can enhance further mobilisation of calcium ions through a cell independent mechanism from bone by creating an indirect effect through the inhibition of collagen synthesis of bone (Goodman and O'Connor 1991; Barreto et al. 2008).

2.12 Significance of strontium and barium substitution in bioactive glasses

Glass ionomer cement is basically an osteo-conductive material and is hydrophilic in nature. In terms of ionic release of glass ionomer cement, it is merely dependent upon glass composition (Hench 2006). The cement can form a strong bond with bone osteogenic factors (bone remodelling). More specifically, it has been found that the substitution of fluoride ions along with strontium ions provides the platform for the formation of new bone (Fredholm 2010). Hill et al. indicated that the presence of strontium ions in glass composition can also contribute

to the development of new bones and plays a vital role in the cure and prevention of osteoporosis (Fredholm et al. 2012). However, strontium ions in rat bones caused acute interference with bone formation. But, at the stage of cell differentiation, the presence of a high concentration of strontium ions indicate the interference of strontium ions in the formation of hydroxyapatite crystals. Furthermore, numerous medical studies indicate that, strontium substitution in basic glass composition with calcium ions does not create any deleterious effect on the normal physiological environment (Gentleman et al. 2010).

It has been reported that calcium ions act as a network modifier in silicate based bioactive glasses. However, due to the similarity of calcium ions in terms of ionic radius and charge, strontium can be substituted (Peitl et al. 2012; Fredholm et al. 2012). There is a low charged ratio with the size of strontium ions (large ionic radius) as compared to calcium ions that can create an extended and more freely cross-linked glass network without altering the fundamental glass structure (Gentleman et al. 2010; Mahapatra & Ku 2010). Strontium oxide (SrO) and strontium fluoride (SrF₂) are being widely used to replace or substitute calcium oxide (CaO) and calcium fluoride (CaF₂) in basic ionomer glass compositions, in order to fabricate radio-opaque glass ionomer cement. The substitution of strontium and barium into ionomer composition can increase the radio-opacity without causing the unfavourable effect on the visual properties of the produced cement. The presence of strontium and barium ions in composition can help in early radio-graphic detection of secondary caries and micro leakage. Moreover, the ability of fluoride ions release improves where complete partial substitution or

total replacement occurs (Fredholm et al. 2012; Shahid et al. 2014). Similarly, it has been observed that the presence of fluoride ions along with strontium and barium substitution can play a vital role in promoting osteoblastic activity in bones by reducing the rate of osteoclastic activity. However, it potentially promotes remineralisation of dental hard tissues by decreasing the process of demineralisation through the formation of fluoroapatite crystals with surrounding hard tissues such as enamel and dentine (Mneimne et al. 2011; Lynch et al. 2012; Kim et al. 2014; Miller 2014).

In sum, the chemical and biological effects of fluoride ions on bone and dental hard tissues are imperfectly understood due to its complexity. Both *in vivo* and *in vitro* studies reveal that the release of fluoride ions can help to increase the biocompatibility of formed cement. In addition, non-fluoride based glass ionomer cement exhibits less toxicity *in vitro* and simultaneously it also causes a decrease in osteo-conductivity *in vivo* (Fredholm et al. 2012; Shahid et al. 2014). However, incorporation of increasing amounts of fluoride ions into the basic composition can encourage adverse effects on the surrounding dental hard tissues in the form of fluoresces and fluoride staining (on deciduous teeth). Similarly, it can also be toxic to the normal physiologic environment and as a result, reduce the sub-surface structure quality of formed bone. A controlled amount of fluoride ions in the substitution can beneficially affect the maintenance of the local physiological environment and stimulation of bone remineralisation (Brauer et al. 2010; Lynch et al. 2012). It has also been found that the use of strontium and barium for substitution can significantly help in early diagnosis of dental caries and marginal leakages due

to the formation of resultant radio-opaque cement, beneficial for both medical and dental applications (Gentleman et al. 2010; Fredholm et al. 2012).

2.13 Significance and release of fluoride ions

Persistent release of fluoride ions from cement can induce osteoblastic activity (Burke et al. 2010; Sayyed et al. 2013). It can encourage the bonding abilities of the cement with surrounding hard tissues especially enamel and dentine through the formation of fluoroapatite crystals. However, fluoride, strontium and barium based substitutions are currently in practice for the treatment of osteoporosis by inhibiting osteoclastic activity and by promoting the density of trabecular bone (Brauer et al. 2010; Mneimne et al. 2011). The formation of fluoroapatite crystals provides more resistance against the process of resorption than apatite crystals, as the formation of hard tissues is a continuous process of resorption and deposition (Forsten 1990). In context of dentistry, the release and uptake of fluoride ions potentially enhances the acid resistance ability of hydroxyapatite crystals present in enamel. Significantly, because of the inherent antibacterial nature of fluoride ions, the process of demineralisation in dental caries decreases through the induced process of remineralisation by fluoroapatite crystals (Wiegand et al. 2007; Burke et al. 2010; Cabezas 2010).

2.14 The concept of glass flakes (GF)

Glass flakes are small flakes of glass which were initially used as the reinforcing agent for roof lighting panels composed of polyester resin. Glass flake incorporation causes the modulus and dimensional stability of polyester resin to be improved (Rexer & Anderson 1979; Dunlap 1991; Franklin et al. 2005; Simon et al. 2009; Uo et al.2010; Holand & Beall 2012).

2.14.1 Use of glass flakes in material sciences and engineering

Glass flakes are currently used in every domain of life. A selection of its uses are listed below (Simon et al. 2009).

- As protective wear resistance coatings, particularly in the oil and gas industry.
- As filler content in the cosmetic industry.
- As reinforcing agent in the formation of ceramics.
- In the formation of decorative purposed materials.
- As a reinforcing agent in the formation of complete dentures.
- As a reinforcing agent in composite as an optical material.

Glass flake based composite materials are so useful because they so readily bind with other materials and enhance both mechanical and physical properties. Glass flake composites are

generally used in the formation of the reinforced thermoplastic resins after consideration of their aspect ratio. For instance, glass flakes particles which were incorporated in reinforcement of thermoplastic resins, may work on phenomenal basis. Likewise, when they were used particularly in surface coatings they revealed the ability to align themselves in parallel direction along with the coating as indicated in following Figure 9. As a result, this could prevent moisture penetration as well as the influx of oxygen ion in between the arranged layers. This is due to augmented path way of both moisture and oxygen ions towards the surface of material. Moreover, this may allow the material to become more corrosion resistance (Alan & Banajee 1998; Simon et al. 2009; Motohiro et al. 2010).

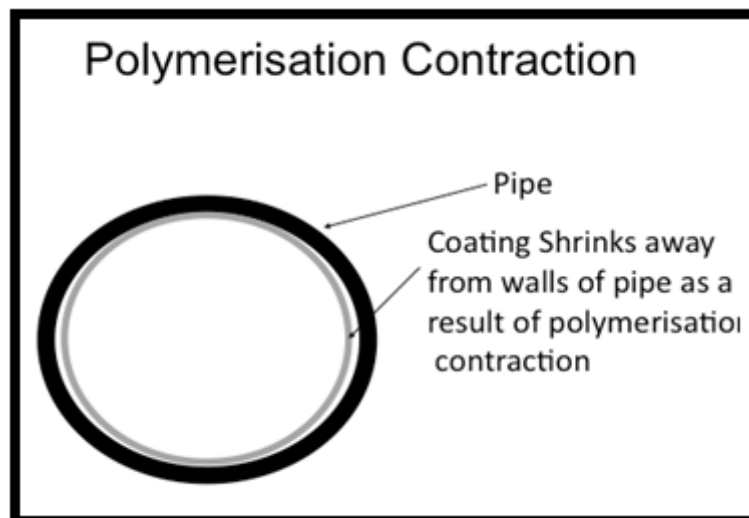


Figure 9: Schematic diagram indicating the mechanism of polymerisation contraction in oil pipe lines after application of glass flakes as filler content

As shown above, glass flake based composites are mostly used in the oil and gas industries, particularly in order to provide strength and strong wear resistance to the protective coatings

from inside of oil pipe lines. As a result, a significant decrease is noticed in terms of war-page and shrinkage of material with resulting improvements in dimension stability, surface hardness, wear resistance, tensile and flexural strength (Simon et al. 2009; Motohiro et al. 2010).

2.14.2 Phenomena of anisotropic shrinkage and aspect ratio

The incorporation of glass flakes according to their aspect ratio is key consideration. It is hypothetically evident in the available literature that glass flakes of smaller size ranging from 0.1 to 1 μ m exhibit inherent ability of self-alignment and display smooth surfaces as shown in Figure 10. Glass flakes ranging from 5 to 10 μ m in size do not self-align and can cause rough or uneven surfaces as shown in Figure 11. Due to the parallel self-alignment of small glass flake particles, the odds of influx of moisture and oxygen ions are also minimised due to anisotropic polymerisation shrinkage. As a result, the material becomes corrosion resistant and is imbued with properties such as tensile and flexural strength and surface and dimensional properties are enhanced (Rexer & Anderson 1979; Dunlap 1991; Franklin et al. 2005; Simon et al. 2009; Uo et al. 2010; Holand & Beall 2012).

Naturally, its geometrical three-dimensional design of shell formation is very closely related with the phenomenal use of glass flakes as filler content. Due to the three dimensional plate like structural nature of the shell of glass flakes, mechanical and physical strength is increased tremendously. As a result, resistance against heavy mechanical and compressive forces is promoted.

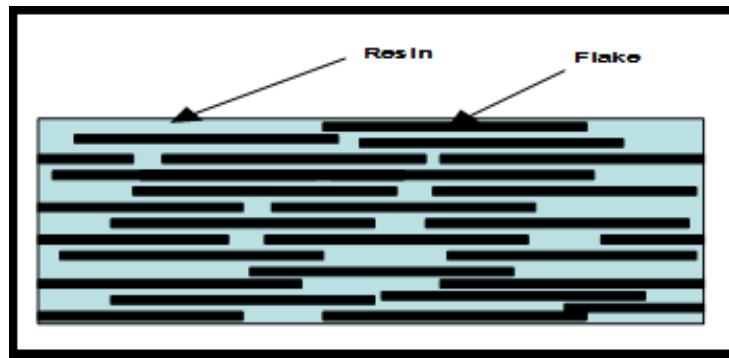


Figure 10: Schematic diagram showing ability of self-alignment in 0.1 to 1 μ m sized glass flake particles.



Figure 11: Schematic diagram showing misalignment of 5 μ m size glass flakes.

2.15 Summary

Dental caries is a multi-factorial oral condition and it is widely accepted as a primary challenge in clinical dentistry. Its rate of progression is directly related with a patient's age and their daily habits. The rate of prognosis absolutely depends upon time of initial diagnosis and adoption of adequate required restorative techniques. Glass ionomer cements (GIC) can potentially be used as a preventive and curative measure for dental caries. However, traditionally available conventional and modified glass ionomer cements have mechanical, physical, chemical and biological drawbacks. These include inadequate wear resistance, plaque adhesion over restorative surfaces, marginal leakage and micro-crack propagation, less binding ability with surrounding dental hard tissues and post-operative sensitivity which can result in recurrent or secondary caries. This project aims to overcome these existing drawbacks by developing novel bioactive conventional glass ionomer cement based on glass flakes. Smaller sized glass flakes have the potential to self-align. A series of 45S5[®] based bioactive glass compositions which substitute calcium with strontium and barium at 3 mole percent were been produced in the presence of citric acid as a setting modifier and then were characterised physically, chemically, biologically and mechanically. Furthermore, it has been observed on the basis of available results that, due to the similarity to calcium ions in terms of ionic radius and charge, strontium and barium can be substituted and exhibit the same role in the glass network. There is a low charge ratio with the size of strontium ions (large ionic radius) as compared to calcium ions

that can create extended and more freely cross-linked glass networks without altering the fundamental glass structure, as discussed in detail in the following chapters (results and discussion).

Chapter 3: Materials and Methods

3.1 Introduction

This chapter includes all materials and methodologies, which were used in this study. However, this chapter consists of two basic domains. Firstly, all material designing and compositional selection for the formation of developed silicate based bioactive glass ionomer cement and obtained silicate based glass flakes is described. Secondly, all characterisation techniques based on physical, chemical, thermal, mechanical and all *in vitro* biological properties, in relation with their background is discussed in detail.

3.2 Glass preparation

3.2.1 Glass sample preparation

The aluminium ions free series of silicate based bioactive glass (BG 1-7) composition based on 45S5 bioactive glass have been developed and fully characterised. The compositions of the glasses have calcium substitution with strontium (SrO and SrF₂) and barium (BaO and BaF₂) by 3 mole percent of calcium oxide (CaO). Details of these compositions in both mole and weight percentages respectively are given in Table 2.

In addition, all glass flakes based samples were prepared by utilizing obtained silicate based glass flake composition from Leeds Glass Flakes Company Ltd United Kingdom, for their further characterisation and analysis as shown in following Table 4. Whereas, the obtained glass flake composition is based on different particle sizes ranging from 100 nm, 100 μ m and 350 nm both milled and un-milled (as provided by the company) were used in formation of all glass flake based sample preparation as shown in following Table 5 respectively. Similarly, the silicate based glass flakes obtained from company constitutes mainly of boron, aluminium, zinc, potassium and titanium with different molar percentages accordingly as indicated in following Table 4 respectively.

Table 2: Silicate based bioactive glass composition based on 45S5 bioactive glass having calcium substitution with strontium and barium by 3 mole % of calcium ions.

SR. NO:	Composition & Additions in 100 Mole & Wt %							
BG 1	SiO ₂	P ₂ O ₅	CaO	Na ₂ O	SrO	BaO	SrF ₂	BaF ₂
(45S5)	46.14	2.60	26.91	24.35	-	-	-	-
	45.01	5.99	24.50	24.50	-	-	-	-
BG 2	SiO ₂	P ₂ O ₅	CaO	Na ₂ O	SrO	BaO	SrF ₂	BaF ₂
(45S5 with	46.10	2.60	23.95	24.35	-	1.50	-	1.50
BaO / BaF ₂)	42.72	5.69	20.71	23.28	-	3.55	-	4.06
BG 3	SiO ₂	P ₂ O ₅	CaO	Na ₂ O	SrO	BaO	SrF ₂	BaF ₂
(45S5 with	46.10	2.60	23.95	24.35	1.50	1.50	-	-
SrO / BaO)	43.44	5.79	21.06	23.67	2.44	3.61	-	-
BG 4	SiO ₂	P ₂ O ₅	CaO	Na ₂ O	SrO	BaO	SrF ₂	BaF ₂
(45S5 with	46.10	2.60	23.95	24.35	1.50	-	-	1.50
SrO / BaF ₂)	43.21	5.76	20.95	23.55	2.42	-	-	4.10
BG 5	SiO ₂	P ₂ O ₅	CaO	Na ₂ O	SrO	BaO	SrF ₂	BaF ₂
(45S5 with	46.10	2.60	23.95	24.35	-	1.50	1.50	-
BaO / SrF ₂)	43.21	5.76	20.95	23.55	-	3.59	2.94	-
BG 6	SiO ₂	P ₂ O ₅	CaO	Na ₂ O	SrO	BaO	SrF ₂	BaF ₂
(45S5 with	46.10	2.60	23.95	24.35	-	-	1.50	1.50
SrF ₂ / BaF ₂)	42.99	5.73	20.85	23.43	-	-	2.92	4.08
BG 7	SiO ₂	P ₂ O ₅	CaO	Na ₂ O	SrO	BaO	SrF ₂	BaF ₂
(45S5 with	46.10	2.60	23.95	24.35	1.50	-	1.50	-
SrO / SrF ₂)	43.72	5.83	21.20	23.82	2.45	-	2.97	-

Moreover, all series of seven batches of produced glasses were batched accordingly as mentioned in above Table 2 with pure silica sand, aluminium di-hydrogen phosphate, soda ash and lime in 46.14SiO₂ 2.60 P₂O₅ 26.91CaO and 24.35 Na₂O (mole %) as listed in Table 3 respectively. Based on calculated batch and available measured material, over automatic weighing machine 100 gm glass melt was prepared as shown in Table 2 respectively. Whereas, glass melt was performed in an electric furnace (ELITE Thermal System Ltd. UK) at 1350°C for 4 hours while maintaining continuous stirring (alumina stirrer) with (ELITE Electric Stirrer. UK) in order to achieve homogeneity and consistency throughout the whole process of melting. However, process of melting also included the pre-heating at 1050°C with 2°/min to avoid any possible thermal shock with alumina crucible. The prepared molten glass was poured into 9 litres of deionised water, particularly to form granular frit and was dried at 50°C for 2 hours. Likewise, molten glass was also poured into a pre-heated metal mould and it was annealed afterwards at 550°C for 1 hour along with 1°C cooling rate to avoid any prospect of internal stresses (Lenten Thermal Design Ltd. UK).

Table 3: List of different chemicals used for batching of produced glasses

	Material used	Source and percentage of purity
1	Sand / Silica (SiO ₂)	Loch Aline Sand.UK >99%
2	Aluminium hydroxide (Al(OH) ₃)	Acros Organics.UK >99%
3	Calcium carbonate (CaCO ₃)	Fisher Scientific.UK>98%
4	Sodium carbonate (Na ₂ CO ₃)	Sigma Aldrich.UK >99%
5	Calcium fluoride (CaF ₂)	Sigma Aldrich.UK >99%
6	Strontium carbonate (SrCO ₃)	Sigma Aldrich.UK >98%
7	Barium carbonate (BaCO ₃)	Acros Organics.UK >99%
8	Barium Fluoride (BaF ₂)	VWR Alfa Aesar UK >99%
9	Aluminium di-hydrogen Phosphate (NH ₄ H ₂ PO ₄)	VWR Alfa Aesar UK >99%
10	Strontium Fluoride (SrF ₂)	VWR Alfa Aesar UK >99%

Table 4: Composition of Glass Flakes (GF) from Leeds Glass Flake Company Ltd. UK.

Sr. No:	Name of compound	Mole %
1	Sand / Silica (SiO ₂)	64 – 70 %
2	Potassium oxide (K ₂ O)	0 – 3 %
3	Boron oxide (B ₂ O ₃)	2 – 5 %
4	Zinc oxide (ZnO)	1 – 5 %

5	Sodium oxide (Na ₂ O)	8 – 13 %
6	Magnesium oxide (MgO)	1 – 4 %
7	Calcium oxide (CaO)	3 – 7 %
8	Aluminium oxide (Al ₂ O ₃)	3 – 6 %
9	Titanium oxide (TiO ₂)	0 – 3 %

Table 5: Different types, sizes and shapes of Glass Flakes (GF) obtained from Leeds

Glass Flake Company Ltd. UK.

Sr. No:	Types	Sizes	Shape
1	Milled	100 μm	Flake
2	Un-milled	100 μm	Flake
3	Milled	100 nm	Flake
4	Un-milled	100 nm	Flake
5	Milled	350 nm	Flake

3.2.2 Selection of crucible

The selection of crucible or reaction vessel is an important factor in the formation of bioactive glasses. There were wide ranges of crucibles, which are commercially available for glass melting procedures. Generally, selection of crucible is directly related with the conditions, composition and cost of melt. However, the use of platinum crucible is considered for high

purity of glass melts as the risk of contamination is low but these are significantly expensive. Usually, use of ceramic crucibles (mullite) has been in practice especially due to their low costs. Slip-casted crucibles are slightly less porous as compared to commercially available ceramic crucibles. Whereas, platinum crucible can undergo flux line due to the presence of phosphate content (P_2O_5) in its composition. However, this ruled out the use of platinum crucible for produced series of batches for glass melts. Based on availability and cost effectiveness, alumina crucible was selected and used for glass pre-heating and till its final melting.

3.2.3 Controlling of particle size

The dry ball milling technique was considered to grind the frit of produced glass samples into fine powder of $< 45 \mu\text{m}$ as controlled size glass particles. However, the produced frit forms of glass samples were powdered by adopting zirconium ball mill along with internal volume of 1:1 ratio. Similarly, the charged volume of 0.5 l of balls having diameter ranges from 1 mm to 15 mm was applied. Whereas, the milled glass powder samples were sieved in order to obtain $< 45 \mu\text{m}$ sized glass particles according to BS EN ISO (9917) standard for dental water based cements.

3.3 Cement preparation

3.3.1 Cement sample preparation

For the process of formation of cement from both the developed series of silicate based bioactive glasses and obtained glass flake composition from Leeds Glass Flake Company Ltd UK, the mercaptan-free dried poly-acrylic acid powder (Sigma Aldrich. UK Batch No: 306223, 99%) having molecular weight of 52,000, dried tartaric acid powder (Alfa Aesar. UK Batch No: A13668, 99%) and citric acid (Alfa Aesar. UK Batch No: A13668, 99%) along with the distilled water were used, as shown in following Table 6. Similarly, cement was produced by using an 'in house' ratio of silicate based bioactive glass powder, dried poly-acrylic acid, tartaric and citric acid. The ratio of different components was used X g where, x = 1 gram of glass powdered to 0.2 grams of poly-acrylic acid (PAA) to 0.3 grams of tartaric (TA) / citric (CA) acid and 1000 μ l of distilled water. In all experiments cement samples were made by hand mixing technique on a provided mixing sheet. The resulting cements were given the nomenclature relating to the parent series of produced glasses used for instance, GIC TA / CA1 - 7 in relation with both tartaric and citric acid respectively.

Table 6: Materials used for the fabrication of cement

Sr. No:	Material used	Amount measured	Company / source
1	Poly acrylic acid (PAA)	0.2 grams	Sigma Aldrich UK
2	L-(+)-Tartaric acid (TA)	0.3 grams	Alfa Aesar UK
3	Citric acid (CA)	0.3 grams	Alfa Aesar UK
4	Water	1 gram (1000 μ l)	Normal Distilled Water

During the whole process of cement preparation each and every handling instrument was washed prior to the procedure with Isopropanol to avoid any contamination and then dried into hot air vacuumed oven up to 65° - 70° C temperature for 2 hours respectively. Whereas, for the manipulation process of cement, all required materials were measured with automatic weighing machine. Firstly, all powdered contents were mixed homogeneously together by using a stainless-steel spatula and mixing sheet. Secondly, continuous and constant adding of measured amount of water (1000 μ l) was added to form a smooth and homogeneous form of cement. Moreover, mixture of prepared cement was then shaped into disc shaped (1 cm diameter and 2 mm thickness) and cylindrical structures (4mm diameter and 6mm height) respectively, to analyse the produced silicate based bioactive glass ionomer cement samples with further characterisation techniques according to BS EN ISO (9917) standard for dental water based cements.

3.4 Glass and Cement characterisation

3.4.1 Physical characterisation

3.4.1.1. X-Ray diffraction analysis

To identify the amorphous or crystalline nature of produced series of silicate based bioactive glass samples, x-ray diffraction was employed. The prepared milled ($< 45 \mu\text{m}$) powder samples were loaded individually into a plastic specimen holder and placed into a tray chamber of Siemens[®] D5000 Cu $K\alpha$ diffraction meter with specimen changer machine as shown in following Figure 12. The copper $K\alpha$ radiation ($\lambda=1,540562\text{Å}$) with scan axis $5-70^\circ 2\theta$ along with continuous angular increment of 0.01° and the scanning speed of $2^\circ 2\theta/\text{min}$ was set in the x-ray diffraction commander software. The operating voltage of machine was 40 kV at 30 mA of current. The obtained data was recorded and analysed in the form of graphical representation with attached computer.

The x-ray diffraction analysis commonly used for structural and atomic space investigations of any specimen, wavelength of x-rays facilitates its use to analyze individual specimen at their atomic scale. Likewise, in this technique hot filament material made up of tungsten is usually used to produce electrons that would bombard onto the surface of specimen. However, in relation with the crystal structure of specimen, the incident ray would diffract in different ways. In this case, the incident ray and the diffracted ray formed a diffracted angle known as

2θ angle that was plotted against the reflected intensities correspondingly (Boyd et al. 2008a; Sharma et al. 2012).



Figure 12: Photographic image of Siemens® D5000 XRD machine with specimen changer.

Moreover, x-ray diffraction analysis is based on the principle of Bragg's law equation for instance; $n \lambda = 2 d \sin \Theta$. Where, the distance between the lattice planes is 'd', maximum diffraction angle is ' Θ ', wavelength is indicated by ' λ ' and order of wavelength is denoted by the symbol 'n' respectively. Simultaneously, this technique also provides the information regarding interatomic distance and bond angles as well. X-ray diffraction technique is a powerful phase detection technique which involves minimum sample preparation (Boyd et al. 2008b; Sharma et al. 2012).

3.4.1.2. Contact angle measurement

Wettability of all produced silicate based bioactive glass (BG 1-7) discs were determined individually by using sessile-drop contact angle method technique, with a contact angle Goniometer equipment with an optical system model number 100-00(220)[®] consisting attached micropipette, light source, microscope and a plate form for specimen as shown in following Figure 13. Whereas, a drop of 5 μ l of ultra-pure water (Millipore[®]) was placed over the prepared dry surfaced glass discs fixed on stainless steel metal substratum. Water contact angle measurements were taken after 5 seconds respectively and the temperature (22 °C) and moisture (73 %) were kept constant throughout the entire experiment. Measurements were recorded by depositing at least five drops on each prepared glass discs individually and an average measurement was taken.



Figure 13: Photographic image of Contact Angle Goniometer measuring equipment.

3.4.1.3 Particle size analysis

Particle size measurements of all prepared glass samples (BG 1-7) after ball milling technique were obtained, glass powder $< 45\mu\text{m}$ was dispersed into two litres of deionised water and the particle size distribution was analysed by using laser particle size analysis technique (Malvern Mastersizer 3000[®], UK). However, obscuration range was kept between the ranges of 5 – 10 % and 5 measurements for each sample were taken with the delay of 10 seconds in between each measurement along with the constant stirring speed of 2000 rounds per minutes (rpm) respectively. The obtained results were analysed by using Mastersizer software and plotted in Microsoft[®] word excel 2016. Similarly, for qualitative analysis of un-reacted prepared powder glass samples of $< 45\ \mu\text{m}$ were viewed under the scanning electron microscope (SEM). All prepared glass powder samples were placed over the sticky carbon discs, which was attached to metal (aluminium) stubs and were previously gold coated (SC500A EM Scope UK) for 4 minutes respectively. Whereas, prepared glass powdered samples were viewed with Philips[®] (Cam-Scan Electron Optics Ltd, USA) with operating voltage of 10 kV and secondary electron images were also captured with different magnifications.

3.4.1.4 Brunauer-Emmett-Teller analysis

Specific surface areas of all produced series of silicate based bioactive glass powder (BG 1-7) that was measured by Brunauer-Emmett-Teller analysis (BET) with nitrogen adsorption technique as shown in following Figure 14. Before analysis, samples were dried and purged with nitrogen gas at 250°C for 14 hours to remove any remaining moisture contents and contaminants.



Figure 14: Photographic image of Brunauer-Emmett-Teller analysis (BET) equipment.

3.4.1.5 Density Measurements (Archimedes and Pycnometer)

For the further evaluation of physical properties of all casted silicate based bioactive glass samples (BG 1-7), the density evaluation studies were performed by using both Archimedes and gas Pycnometer experimental techniques. For Archimedes density measurement, the cleaned produced casted square shaped silicate based bioactive glass samples of 2cm of equal width and length, were measured in liquid with an attached built-in stainless-steel basket, which was immersed into the liquid medium consist of water. Three consecutive readings were taken for all samples in air and aqueous media respectively. The average mean values were recorded in g/cm^3 .

Similarly, density of all produced silicate based bioactive glass samples, each of which was analysed individually by using Archimedes, Mettler Toledonew classic MS. USA machine respectively as well. However, before each measurement all the specimens were cleaned using isopropanol in order to remove any contaminated smear layer. Automated Archimedes machine worked on the principle based on the following equations,

$$V_{\text{glass}} = \Delta V_{\text{H}_2\text{O}} = \Delta g_w / d_{\text{H}_2\text{O}} = (g_1 - g_2) / d_{\text{H}_2\text{O}}$$

Furthermore, the mass of glass in both air and water can be denoted as ' g_1 ' and ' g_2 ' respectively. Similarly, according to the Archimedes principal the total volume of glass when it is immersed in deionised water (V_{glass}) would be equal to volume displaced ($\Delta V_{\text{H}_2\text{O}}$). Whereas, the ' $d_{\text{H}_2\text{O}}$ '

indicates density of deionised water at provided temperature and density of glass (d_{glass}) were calculated by following mentioned equation correspondingly. The precision of density meter was 0.001gcm^{-3} .

$$d_{glass} = g_1/V_{glass} = (g^1 \cdot d_{H_2O} / g_1 - g_2)$$

Likewise, Pycnometer density measurement is an effective tool for the evaluation of porous and non-porous materials in a displaced medium of gas and liquid. The inert gas such as helium, argon or nitrogen is used as the displacement medium. For this purpose, prepared powdered samples were sealed in an air tight instrument compartment of known volume, then appropriate gas was introduced and then it allowed expanding another precision for internal volume. The pressure before and after expansion was measured, which was then used to compute the volume of samples respectively. However, density measurements of all prepared glass samples were performed in an inert gas environment such as helium at 18.53°C temperature with 25 purges. All samples were placed into provided stainless steel crucible of 1cm^3 in diameter individually and the average mean values in g/cm^3 were recorded and observed respectively.

3.4.2 Thermal characterisation

3.4.2.1 Differential thermal analysis

The differential thermal analysis is a common characterization technique used to record any possible drastic changes of energy when a material is subjected to certain heating profile. However, the change in the energy of sample would be recorded against the reference material and therefore the term ‘differential’ is usually used. There can be different heating profiling rates used in this technique. The data can be observed by plotting the graph of temperature difference between sample and reference. Likewise, from the plotted graph researchers are capable of revealing the results about glass transition, crystallization and melting temperature of any sample accordingly. Whereas, other thermal events such as removal of any particular substance from produced samples can also be observed and analyzed as well (Charsley and Warrington, 1992, O’Donnell et al., 2008). Use of this technique in this project also revealed the information regarding cost effectiveness of produced glasses commercially (Fredholm et al. 2010; Gomes et al. 2013; Saadaldin et al. 2013).



Figure 15: Photographic image of Perkin-Elmer® Differential thermal analysis instrument.

To ascertain glass transition ‘T_g’ and events of crystallisation on heating, all prepared < 45 μm milled powdered glass samples were placed into Perkin-Elmer® DTA 7 USA, besides the reference material and the electronic dip sensor was placed into the sample, in order to record any change of weight and temperature during heating as shown in following Figure 15. The heating profile was set equally for each prepared glass sample for instance RT (room temperature) to 1000°C at 10°C / min ramp in normal atmospheric (air) environment. The results were observed and recorded over the attached calibrated computer in graphical representations. Similarly, alumina crucible was used instead of platinum crucible in order to avoid any chemical reaction, due to presence of phosphate content (P₂O₅) particularly during the whole process of thermal analysis of all produced samples (BG 1-7) respectively.

3.4.3 Chemical characterisation

3.4.3.1. Fourier Transform Infrared (FTIR) spectroscopic analysis

Fourier transform infrared spectroscopic (FTIR) technique is based on the phenomena of vibrational spectroscopy. However, for a material to be recognized as infrared active it must exhibit change in dipole moment when subjected to infrared radiations. Principally, the mathematical technique identified as Fourier transform is employed to obtain final spectra which could be exhibited in absorption or transmission spectrum (Rehman et al. 2012; Sathyanarayana 2015). Likewise, the photoacoustic Fourier transform infrared spectroscopic (PAS-FTIR) technique is a non- destructive technique of analysis in an inert environment (helium). Due to the optical absorption the samples get heated up and reveal thermal expansion and on cooling the sample released heat in the form of a thermal wave. Whereas, change in thermal energy could be observed to divulge the information regarding chemical composition of prepared samples (Vijayaraghavan 2008).



Figure 16: Photographic image of Thermo scientific™ Nicolet™ iS™50 FTIR spectrometer MTEC photoacoustic cell.

Photoacoustic Fourier transform infrared spectroscopy (PAS-FTIR) technique was utilized to obtain individual spectrum of all produced silicate based bioactive glasses and ionomer cement samples with different setting modifiers (tartaric and citric acid). However, all produced samples were sized into 10 mm in diameter and 2 mm in thickness respectively. Similarly, the Thermo scientific™ Nicolet™ iS™50 spectrometer with MTEC photoacoustic cell, under absorbance mode was used, between the range of 400 cm^{-1} - 4000 cm^{-1} as shown in following Figure 16. The sample chamber was purged with helium gas before collecting the spectra. Individual spectrum was obtained at resolution of 4 cm^{-1} with 256 numbers of scans. Analysis of spectra was carried out by using OMNIC® software.

3.4.3.2. Raman spectroscopic analysis

Raman and infrared spectroscopic analytical techniques are sensitive to basic structure of silicate glasses thus; it allows in determining the vibration mode changes in Si-O-Si bonds.

Both infrared and Raman spectroscopic techniques are associated with changes in vibration and rotational level of energy. However, both these techniques are non-destructive and complement to each other.

However, a molecule that can exhibit the change in its polarization could be referred as Raman active molecule was indicated by C.V. Raman in 1928. Raman spectroscopy technique is related with the laser emission which potentially is able to produce monochromatic light. Due to change in energy, an incident photon exhibits elastic scattering, inelastic or Raman scattering upon the interface with a molecule. Likewise, if the frequency of the emitted photon is higher than initial energy state, it would be more than its final energy state and known as anti-strokes. In strokes the final energy state would be higher than initial energy state as shown in following Figure 17. On the other hand, in inelastic scattering different molecules demonstrate different frequencies, known as Raman shift (cm^{-1}) or unique fingerprint region of that material. Rehman *et al.* in 1994 reported that, Raman spectroscopy indicates more sensitivity towards P-O and C-O vibrations respectively and has the benefit of having minimal sample preparation as well (Chalmers et al. 2012; Rehman et al. 2012).

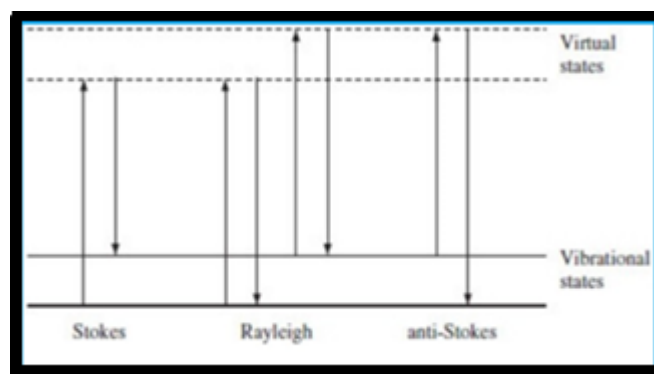


Figure 17: Schematic diagram indicating the phenomena of Raman scattering

(Smith & Dent 2013).

Raman spectroscopy technique was used to obtain spectrum of both produced silicates based glass and ionomer samples with different setting modifiers (tartaric and citric acid) samples by using Thermo scientific™ DXR™ Raman microscope under shifted spectrum (cm^{-1}) format, between 55 cm^{-1} - 3409 cm^{-1} as shown in following Figure 18. However, all spectrums were obtained by using 532 nm lasers, at 10 mW powers, 25 pinhole apertures, 50 ld objective, exposure time 15 sec and number of exposures 2. Similarly, the analysis of individual spectrum was carried out by using OMNIC® software for Raman spectroscopy.

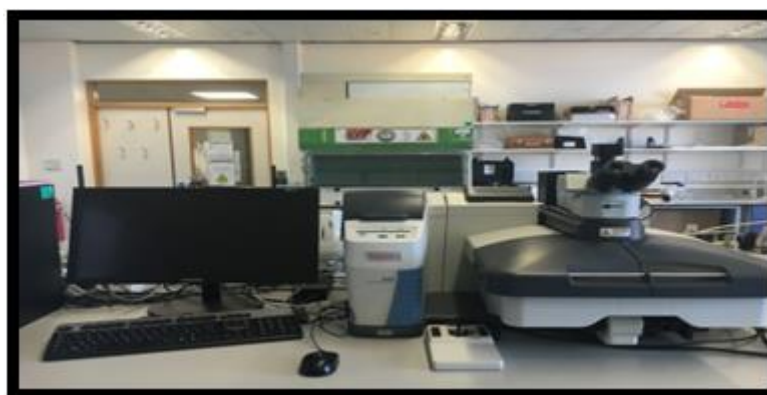


Figure 18: Photographic image of Thermo scientific™ DXR™ Raman microscope.

3.4.4 *In-vitro* biological characterisations

3.4.4.1 *In- vitro* bioactivity analysis

3.4.4.1.1 Stimulated body fluid (SBF) study

In vitro bioactivity of all silicate based bioactive glasses and produced glass ionomer cement samples with different setting modifiers (tartaric and citric acid) were analysed by immersing them in simulated body fluid solution (SBF) for 24 hours for all glass samples and for 1st, 7th and 14th days for both cement samples respectively. Simulated body fluid solution (SBF) was produced according to the procedure described by Kokubo and Takadama in 2006 and the composition is tabulated in Table 7. After the afore mentioned respective interval of time, immersed samples were collected and analysed by using inductive energy dispersive x-ray spectroscopy (EDS) and scanning electron microscope (SEM).

Table 7: Materials used in the preparation of SBF solution for in vitro bioactivity analysis (Kokubo & Takadama 2006).

Sr. No:	Compounds	Chemical formula	Amount (gm)	Source / Company
1	Sodium Chloride	NaCl	8.035 gm	Sigma Aldrich UK
2	Sodium bicarbonate	NaHCO ₃	0.355 gm	Sigma Aldrich UK
3	Potassium Chloride	KCl	0.225 gm	Sigma Aldrich UK

4	Di-potassium hydrogen phosphate trihydrate	$K_2HPO_4 \cdot 3H_2O$	0.231 gm	Sigma Aldrich UK
5	Magnesium Chloride Hexahydrate	$MgCl_2 \cdot 6H_2O$	0.311 gm	Sigma Aldrich UK
6	Calcium Chloride	$CaCl_2$	0.292 gm	Sigma Aldrich UK
7	Sodium Sulphate	Na_2SO_4	0.072 gm	Sigma Aldrich UK
8	TRIS-hydroxymethyle aminomethane	$((HOCH_2)_3CNH_2)$	6.118 gm	Sigma Aldrich UK
9	Hydrochloric acid	1.0 M HCL	0-5 ml gm	Sigma Aldrich UK

Furthermore, the simulated body fluid solution was prepared by following the prescribed method given by Kokubo and Takadama in 2006 as shown in following Figure 19. All equipment used in these experiments were washed initially with 1.0M hydrochloric acid (HCl) and deionized water to avoid any contamination. Firstly, 700 ml of deionized water was added to 1000 ml marked capacity polypropylene beaker. Then beaker was placed over the surface of hot plate magnetic stirrer (MR Hei-Tec, Heldolph Instruments) at temperature of 37⁰C. After attaining set temperature, reagents from 1 to 8 (as given in Table 7) were added in the solution. Each reagent was allowed to dissolve completely before the addition of next one. Once all reagents were dissolved completely, deionized water was added to attain the volume of 900 ml according to the protocol. The temperature was allowed to reach 37⁰C prior to the immersion of pH meter. After attaining initial pH as recorded between the range of 1.0 and 3.0, Tris hydroxymethyle aminomethane was added incrementally to the solution until pH

reached to 7.45. On the other hand, temperature was kept constant at 37⁰C along with the constant addition of 1.0M hydrochloric acid solution and volume of solution was then adjusted to 1000 ml accordingly. The obtained solution was colorless and no precipitation was observed. For final storage, the obtained solution was transferred into multiple polypropylene vials of 50 ml capacity and were stored at 4⁰C in a fridge (Oyane et al. 2003; Kokubo & Takadama 2006).



Figure 19: Photographical image showing experimental setup used for the preparation of conventional simulated body fluid solution (c-SBF).

3.4.4.1.2 Scanning electron microscopic (SEM) analysis

For further qualitative investigations scanning electron microscopic analysis were conducted for the conformation of the formation of carbonated hydroxyapatite layer upon both immersed glass ionomer cement samples with different setting modifiers (tartaric and citric acid) with certain interval of time for instance 1st, 7th and 14th days respectively. Similarly, Philips/FEI XL30 S-FEG microscope was used with beam energy of 15 kV along with different magnifications and all images were recorded on the attached computer as shown in following Figure 20. However, all produced glass ionomer cement samples before scanning electron microscopic analysis were gold coated respectively.



Figure 20: Photographic image of Philips/FEI XL30 S-FEG microscope scanning electron microscope (SEM).

3.4.4.1.3 Energy dispersive x-ray spectroscopy (EDX) analysis

For elemental analysis of all produced glass ionomer cement samples with different setting modifiers (tartaric and citric acid) with different interval of time for instance 7th and 14th days after immersion in simulated body fluid solution (SBF), energy dispersive x-ray spectroscopy (EDX) analysis was performed respectively. However, all produced samples were carbon coated and analysed by using INCAx-Sight 6650 (Oxford Instrument) with beam energy of 15 kV as shown in Figure 20. Similarly, all results were observed and analysed by using INCA software for energy dispersive x-ray spectroscopy (EDX).

However, this technique is most commonly known to be used along with scanning electron microscopy in an incorporated component. The energy beam is focused either over designated area or spotted over the surface of the sample. Similarly, the incident energy beam excites the inner shell of electrons of atoms present over the surface of specimen. As a result, atoms exhibit higher energy state after they get charged but, they became unstable in nature and eventually undergo de-excitation mode as indicated in following Figure 21. Likewise, when these electrons move back towards the lower energy states they begin to start to lose their level of energy especially in the form of x-rays. It is evident from literature survey that, emission of x-rays becomes more prominent with heavy atoms (Fratta et al. 2007; Gomes et al. 2013).

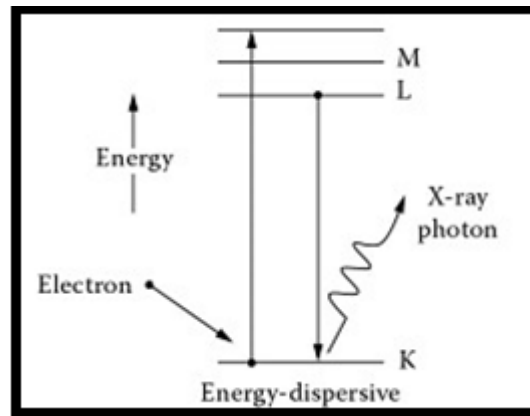


Figure 21: Schematic diagram for energy dispersive x-ray spectroscopy (EDS).

3.4.4.2 *In- vitro* biocompatibility analysis

3.4.4.2.1 Sterilisation of both glass and cement samples

All produced silicate based bioactive glass samples from BG 1-7 and glass ionomer cement samples GIC 1-7 (TA and CA) were cut and shaped into circular tablets measuring 1cm in diameter and 2mm in height respectively. Samples were firstly immersed in 70% methanol for 24 hours and then were washed with phosphate buffer solution (PBS) for 3 times, before transferring them into fresh medium for further *in vitro* cell viability analysis respectively.

3.4.4.2.2 Cell culture and MTT assay of glass and cement samples

The biocompatibility of all produced silicate based bioactive glasses and glass ionomer based cement samples with both setting modifiers (tartaric and citric acid) were investigated by using human oral fibroblasts, sub-cultured from oral mucosa of healthy donor (voluntary donation) as shown in following Figure 22. The cells used were of passage 4, batch number 315, obtained from the Kroto Research Institute tissue bank reference number 12179 and ethical reference number 003463, The University of Sheffield, UK. However, all produced samples for both glass and ionomer based cement samples were shaped into discs of 2mm in height and 1 cm of diameter were prepared and sterilized by using autoclave (15 min at 121°C/ 15 psi) (Uddin et al. 2017).

However, the cells were cultured in DMEM (Sigma Aldrich UK) media supplemented with 10% FCF serum, 1% penicillin / streptomycin, 1% glutamine. Cells were then allowed to grow to confluence over the surface of tissue culture T-75 flask (Sigma Aldrich UK) as shown in following Figure 31.

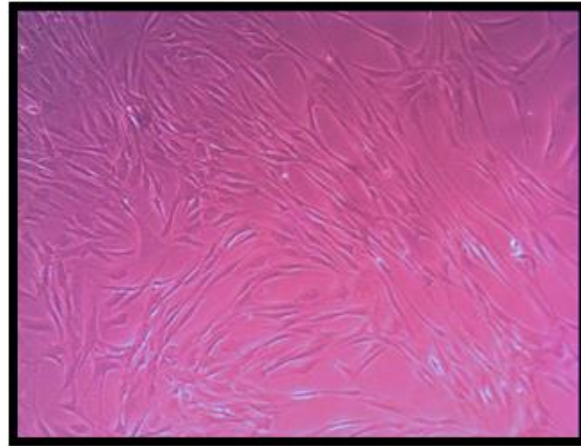


Figure 22: Light microscopic image of human oral fibroblast cultured over the surface of T-75 flask, exhibiting the uniform cellular growth before MTT assay analysis.

The glass discs were kept in prepared media (Sigma Aldrich UK) in a 24 well plate for 24 hrs before cell seeding. When the cultured oral fibroblasts reached confluency, they were detached from T-75 flask by using trypsin EDTA (Sigma Aldrich UK). These detached cells were then introduced in the 24 well tissue culture plate having the glass discs with a seeding density of 1.25×10^4 cells / ml. The material and non-material control (positive) and (negative) were introduced for the direct comparison respectively. Moreover, after seeding, cells were incubated at 37°C in a 5 % CO₂ atmosphere for 24 hours. Growth of cells were later observed on the glass samples in contact with the conditioned media by optical light microscope. The attachment and proliferation of the cells was further assessed by using confocal microscopy correspondingly (Uddin et al. 2017).

Similarly, the prepared discs of all produced cement samples were also kept in prepared DMEM (Sigma Aldrich UK) media for 24 hours in falcon tubes separately. Cells were seeded

in T-75 tissue culture flask and were then allowed to be confluent. As the cells became confluent, they were detached by using trypsin EDTA (Sigma Aldrich UK) and were seeded in a 24 well plate. These cells were allowed to proliferate in the 24 well plate until confluent after which culture media from the wells was replaced by immersed media taken from the falcon tubes having cement samples. These 24 well plates were incubated at 37°C in a 5% CO₂ atmosphere for 24 hours. The material and non-material control (positive) and (negative) were introduced for the direct comparison respectively. Growth and proliferation of the cells were observed later by optical light microscopy prior to MTT assay.

The quantitative measurement MTT assay for 24 and 48 hours was performed for both produced glass and cement samples individually, in order to determine whether the produced samples are toxic to normal cellular growth. Similarly, MTT solution (Thiazolyl blue tetrazolium bromide, Sigma Aldrich, UK) was aseptically added to each 96 well (Sigma Aldrich, UK) plate and was left for incubation at 37°C for 4 hours. The cells were then lysed with isopropanol (Sigma Aldrich, UK) as well. The intensity of colored solution was measured by using a photo spectrometer MTT plate reader (BIO-TEK, USA) at a wavelength of 570 nm as shown in following Figure 23.



Figure 23: Photographic image of spectrometer MTT plate reader (BIO-TEK, USA).

3.4.4.2.3 Optical and confocal microscopy

The cell morphology and cell attachment over the produced silicate based bioactive glass samples were observed by using confocal laser scanning microscope (CLSM) using M700 machine (Carl Zeiss Jena, Germany) and light optical microscopy (Olympus CHBS Microscope UK) as shown in following Figure 24. The all produced silicate based bioactive glass samples were shaped into discs of 2mm in height and 1 cm of diameter and were sterilized by using autoclave (15 min at 121°C/ 15 psi) individually. Similarly, after cell culture, the matured and grown cells were fixed with 3.7% paraformaldehyde and stained with prolong gold antifade reagent with 4, 6-diamidino-2-phenylindole (DAPI) molecular probes for nuclei and fluorescence signals were visualized.



Figure 24: Photographic image of light optical microscopy (a) and confocal laser scanning microscope (CLSM) (b) respectively.

3.4.5 Mechanical characterisation

3.4.5.1 Compressive strength analysis

Mechanically, the compressive strength of all produced silicate based modified bioactive glass ionomer cement with the addition of tartaric and citric acid as setting modifier samples were analysed respectively. Similarly, by using stainless steel mould of 4 mm in diameter and 6mm in height was used to make cylinder shaped samples according to British standard for dental materials (BS EN 2 9917 & 6039). The all produced cylindrical shaped samples were placed in desiccator for 24 hours for drying in normal atmospheric (air) environment. Similarly, before final mechanical testing procedure, all produced specimens for both tartaric and citric acid based samples were kept at 37°C, 100% humidity environment for 24 hours. The experiment

was conducted by using Hounsfield test equipment (UK) using 1KN load cell at crosshead speed of 1mm/min as shown in following Figure 25.

Specimens compression strength (CS) were calculated according to equation [$CS = (4p) / (\pi d^2)$].

Whereas, 'p' is the maximum applied load in (N) and 'd' is the diameter of the sample in (mm).

The compression elastic modulus (CM) was calculated as the initial slope (elastic regime) of the stress strain curves of each cement. The average values were calculated for both compression strength and compression modulus of each cement formulation and normality of the data distribution was confirmed by using Shapiro – Wilk test. The highly significant ($p < 0.001$) and significant differences ($p < 0.05$) between the different cement formulations were evaluated by using the *t* – test for their statically analysis.



Figure 25: Photographic image of Hounsfield mechanical compression strength test equipment.

3.4.5.2 Gilmore needle test

To determine, working and setting time of prepared cement as according to British standard for dental materials (BS EN 2 9917 & 6039) Gilmore needle test experiment was performed on all produced silicate based glass ionomer cement with different setting modifiers such as tartaric and citric acid respectively. Gilmore needle works on two different types and sizes of needles along with different weights placed over the surface of setting cement as indicated in following schematic Figure 26. Firstly, the large diameter (10mm) needle with 28gm weight to determine the working time until needle stops to indent any more. Secondly, the needle with smaller diameter (1mm) with the weight of 400gm is then applied and the time when the needle stops to penetrate was measured as setting time. However, both tests were being carried out in ambient temperature $21 \pm 1^\circ \text{C}$. For working time, the initial weight and indentation was recorded when cement initially starts to resist against weight. For setting time, the samples were kept into $23^\circ \text{C} \pm 1^\circ \text{C}$ according to British standard of setting time analysis and it was carried out in 37°C temperature. Whereas, according to British standards if working time was greater than 5min and less than 1min than prepared cement will be ineffective. Similarly, if setting time will exceed from 20 min then formed cement will not be viable.

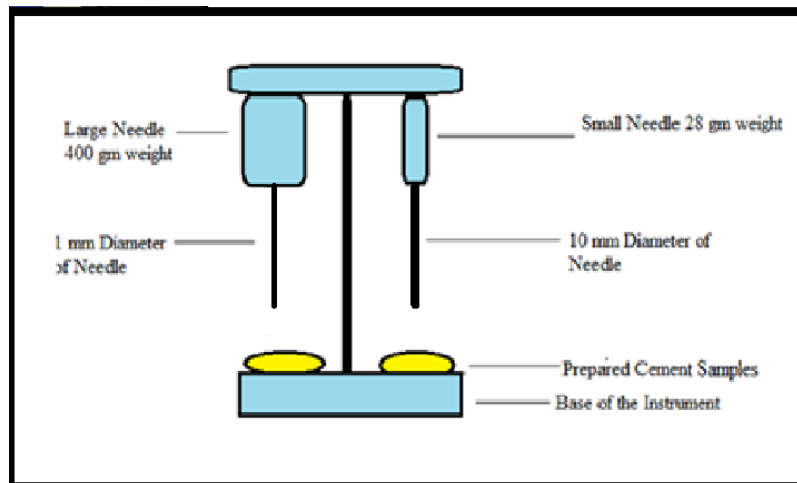


Figure 26: Schematic diagram of Gilmore Needle Instrument used.

3.6 Statistical analysis

The statistical analysis was performed by using IBM SPSS 22.0 version and graph pad prism software for graph plotting to analyse the statistical values of all the experiments individually.

All presented graphed data refer to mean \pm standard deviation (SD). The changes among the control and the treated samples were also analysed by the one-way ANOVA analysis of variance, followed by Tukey's post hoc test at 5% level. Results with p -values of ≤ 0.05 (*) were considered statistically significant.

3.7 Summary

In this chapter, detailed characteristic features and parameters were discussed, which were used in the optimised characterisations and analysis of all produced samples. The series of silicate based calcium substituted bioactive glasses (BG 1-7) with strontium and barium ions along with the 3 mole % of calcium ions and prepared company based glass flakes samples were synthesised and characterised individually. Whereas, based on produced series of silicate based bioactive glasses, ionomer cement samples were made with the introduction of different setting modifiers such as tartaric and citric acid in the presence of water and poly acrylic acid. Moreover, in the following consecutive chapters 4 and 5 all obtained results will be expressed and discussed in detail along with the references from the available literature respectively.

Chapter 4: Results

4.1 Introduction

This section of the thesis possesses all experimentally obtained results based on physical, chemical, thermal, mechanical and *in vitro* biological studies from the produced series of silicate based bioactive glass ionomer cements with the introduction of different setting modifiers such as tartaric and citric acid. However, all observed results of glass flakes based samples upon the admixture with different setting modifiers, as from the obtained composition provided from Leeds Glass Flake Company Ltd UK, are also presented in accordance with their physical, chemical and biological characterisations respectively.

4.2 Glass preparation

All developed series of silicate based bioactive glasses (BG 1-7) were melted and casted after pouring into pre- heat treated rectangular shaped metallic die as shown in following Figures 27-33 respectively. During initial pouring stage it was observed that, all glass samples (BG 1-7) were homogenous, less viscous in nature and showed an amorphous appearance upon cooling. However, there were no significant signs of establishment of bulk and surface nucleation of crystals were observed. Whereas, it was also observed that, all produced glass

samples exhibit amorphous nature and they were not undergone with devitrification upon cooling.

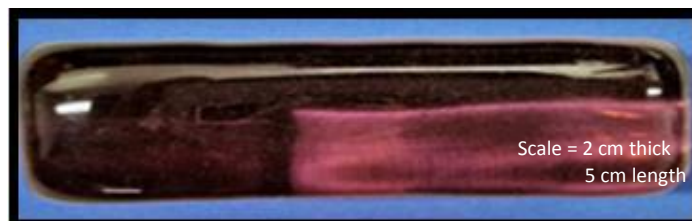


Figure 27: Photographic image of produced silicate based glass sample BG 1 after casting.



Figure 28: Photographic image of produced silicate based glass sample BG 2 after casting.



Figure 29: Photographic image of produced silicate based glass sample BG 3 after casting.

Moreover, the ‘in-house’ copy of 45S5 based bioactive glass [46.14SiO₂ 2.60 P₂O₅ 26.91CaO and 24.35 Na₂O (mole %)] as shown in Figure 27 (BG 1) was produced which was completely transparent, smooth and slightly pink in colour. Similarly, strontium and barium based glasses

were observed to be less viscous and fluidly, transparent and more glass like upon pouring than calcium based glasses like BG 1 glass sample.



Figure 30: Photographic image of produced silicate based glass sample BG 4 after casting.



Figure 31: Photographic image of produced silicate based glass sample BG 5 after casting.

This indicates that substitution of calcium ions in the basic glass composition with larger ions such as strontium and barium disrupts the glassy network more readily than others. Moreover, the calcium substitution with strontium and barium ions in composition, helps to lower the glass fusion temperature which has more economical effect in commercial applications (Fredholm et al. 2010; Shahid et al. 2014). Whereas, glass samples from 2 -7 were also completely transparent and light blue in colour as shown in Figure from 28-33 respectively.



Figure 32: Photographic image of produced silicate based glass sample BG 6 after casting.



Figure 33: Photographic image of produced silicate based glass sample BG 7 after casting.

All casted glass samples were apparently amorphous in nature with no obvious signs of crystallisation. Moreover, initial characterisations for the confirmation of amorphous or crystalline nature of produced glass samples; x-ray diffraction characterisation technique was adopted for all produced glass samples as shown in following Figure 36 respectively. Similarly, in this project we also characterised the obtained synthesised glass flakes from Leeds Glass Flakes Company Ltd. UK as shown in Figure 34.



Figure 34: Photographic image of obtained silicate based glass flakes from Leeds Glass Flakes Company Ltd. UK.

4.3 Cement preparation

During cement preparation, it was observed that, all produced silicate based bioactive glass ionomer cement samples with the introduction of different setting modifiers such as tartaric and citric acid, were homogeneously mixed upon the admixture of poly-acrylic acid in the presence of water. Whereas, the obtained silicate centred glass flakes based composition from Leeds Glass Flakes Company Ltd UK, upon the admixture of tartaric and citric acid exhibited less homogeneity with prolonged working and delayed setting time. Moreover, after mixing all cement samples appeared white in colour and opaque in nature and were shaped and sized into 1cm diameter and 2 mm thickness having round discs forms as shown in following Figure 35. The working time and setting time of all produced silicate based glass ionomer cement samples were observed and recorded for 2- 3 minutes respectively. Similarly, this was more accurately analysed with ISO standard Gilmore needle test method for dental cements.



Figure 35: Photographic image showing discs of prepared cement samples.

Likewise, upon setting all produced cement samples become hard. It was also observed that, during the process of manipulation of cement, due to acid-base nature of reaction, the cementation process was slightly exothermic in nature, which lasts up to few seconds (5 sec) and the handling characteristics of cement were found satisfactory except glass flakes based cement samples.

4.4 Glass and Cement characterisation

4.4.1 Physical characterisation

4.4.1.1. X-ray diffraction analysis

All produced silicate based bioactive glasses samples (BG 1-7) and obtained glass flakes from Leeds Glass Flakes Company Ltd. UK, were analysed by using x-ray diffraction technique in order to evaluate the extent of crystallisation that occurred during the process of rapid cooling. The result indicates that all synthesised glass samples (BG 1-7) and obtained glass flakes samples were x-ray amorphous as shown in following Figure 36 and 37 respectively. However, in produced silicate based bioactive glass samples the degree of two theta angle gradually moved towards smaller values with the increase of strontium and barium substitutions into parent composition as shown in following Figure 36. The amorphous halo shift indicates an increase in average spacing in glass structure due to larger size of strontium (Sr^{+2}) and barium (Ba^{+2}) cations and also due to ionic radius of strontium 1.16Å and barium 1.35Å which is close to calcium at 0.94Å (Fredholm et al. 2010; Mneimne et al. 2011; Fredholm et al. 2012; Lynch et al. 2012).

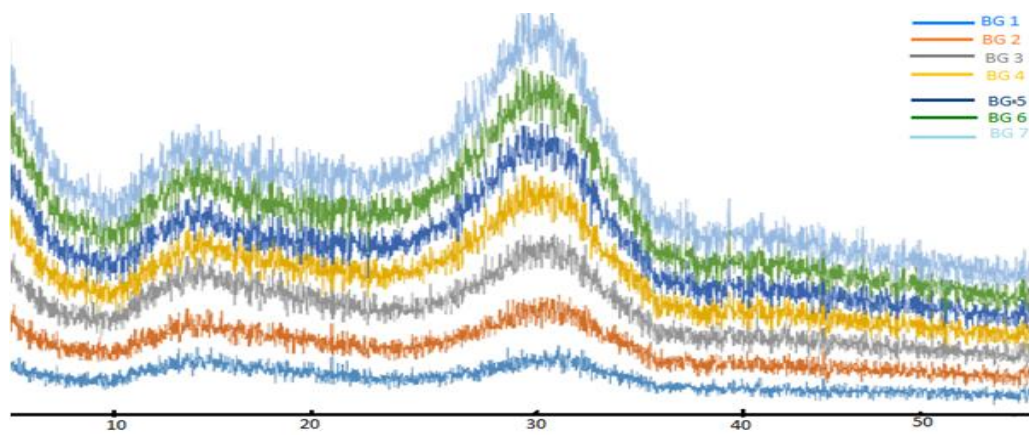


Figure 36: Traces of x-ray diffraction analysis of all produced glass series (BG 1-7). Results indicate the predominance of amorphous state and 2θ angle shifts towards smaller values with increase of strontium and barium ions substitution into the parent composition respectively. The amorphous halo shift indicates the increase in average spacing in the glass structure due to larger size of Sr^{+2} and Ba^{+2} cations, without disrupting basic structure of glass.

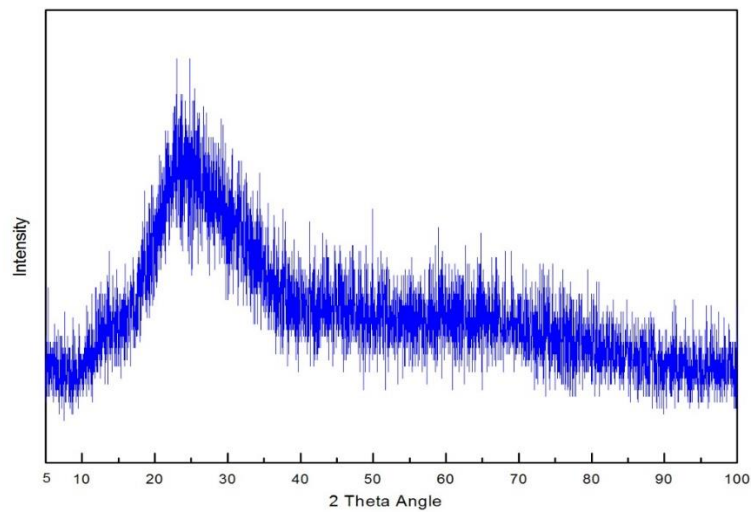


Figure 37: XRD trace of obtained glass flakes based on the composition provided from Leeds Glass Flakes Company Ltd. UK. However, results indicate the predominance of amorphous nature of glass structure.

4.4.1.2. Contact angle measurement

Wettability of bioactive glasses plays significant role with respect to cell adhesion, cell proliferation and protein adhesion (Duée et al. 2013). It can easily be observed from results that, all produced silicate based bioactive glass samples indicates more hydrophilicity except BG 1 (65°) as shown in Figure 38. The water contact angle of BG 1 (control 45S5) is under the theoretical limit of 65° but, it is very high enough to make silicate based glasses to be a potential candidate for cell adhesion (Vogler 1998). Similarly, due to the introduction of strontium and barium as substitutional component with calcium ion in the parent composition a gradual

decrease in contact angle from BG 2-7 can be observed in following Figure 38 correspondingly.

This specifically indicates the increased hydrophilic nature of developed series of silicate based bioactive glasses (Duée et al. 2013). However, significant difference was also observed statically ($p < 0.05$) with one-way ANOVA.

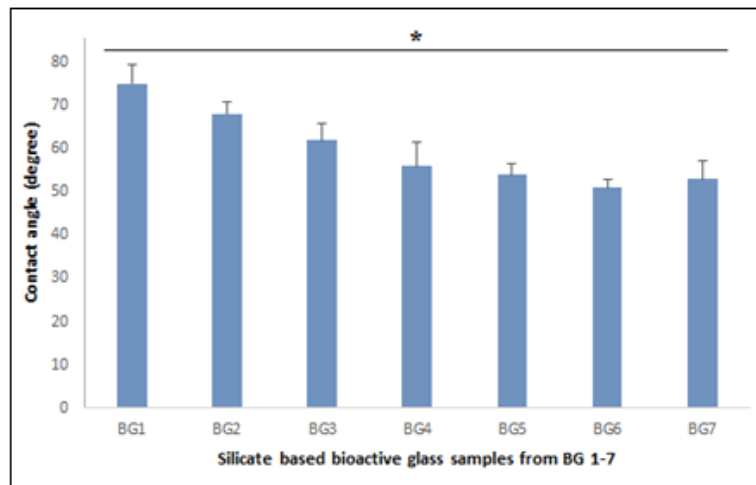


Figure 38: Contact angle measurement results analysis of silicate based bioactive glass samples (BG 1-7) by using one-way ANOVA ($p < 0.05$, * represents significant difference) and data represents mean \pm SD (n=3). However, BG 5-7 shows lower contact angle which leads to better wet ability (hydrophilic) with respect to increased biocompatibility such as protein adsorption, cell attachment and spreading respectively.

4.4.1.3 Density measurement (Archimedes and Pycnometer)

The density of each produced silicate based glass samples (BG 1-7) were analysed by adopting both Archimedes principle along with air and water as an immersion medium and also with Pycnometer analytical technique. The density measurement of all developed series of calcium substituted glass with strontium and barium exhibit an increase in the density but within the range of silicate based bioactive glasses as shown in following Figure 39 and Table 8 respectively (Fredholm et al. 2010; Jones 2013).

Likewise, the density of all produced silicate based glass samples were recorded by using Pycnometer test. This analysis was conducted in an inert environment by using helium gas at normal atmospheric room temperature 24°C. However, for each individual produced powdered glass samples of < 45 µm sized particle (BG 1-7), obtained results were recorded and observed over attached computer respectively.

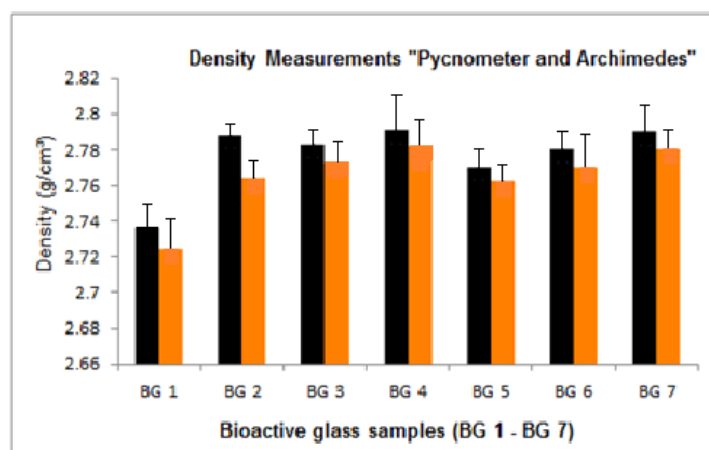


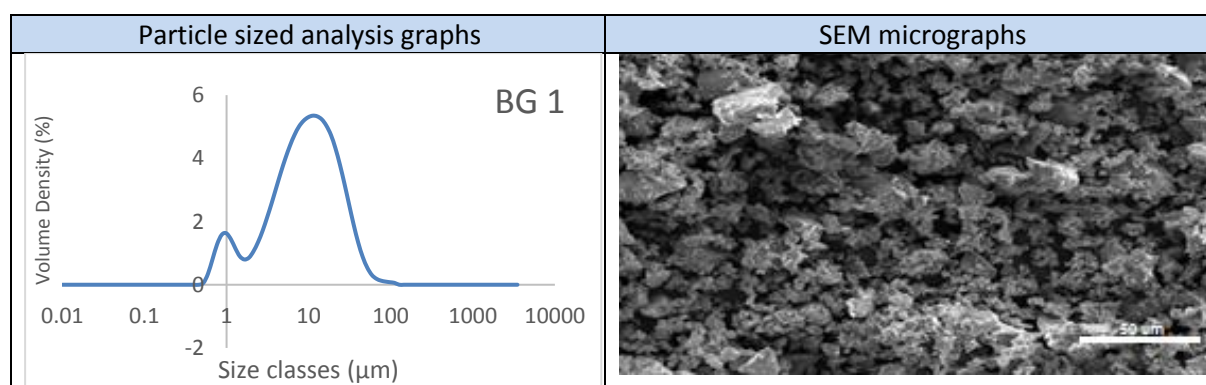
Figure 39: Illustration of the results of density measurements of glass (BG 1-7). Results represents mean \pm SD (n=3), where (in black) indicates Pycnometer measurements and (in orange) indicates Archimedes measurements respectively.

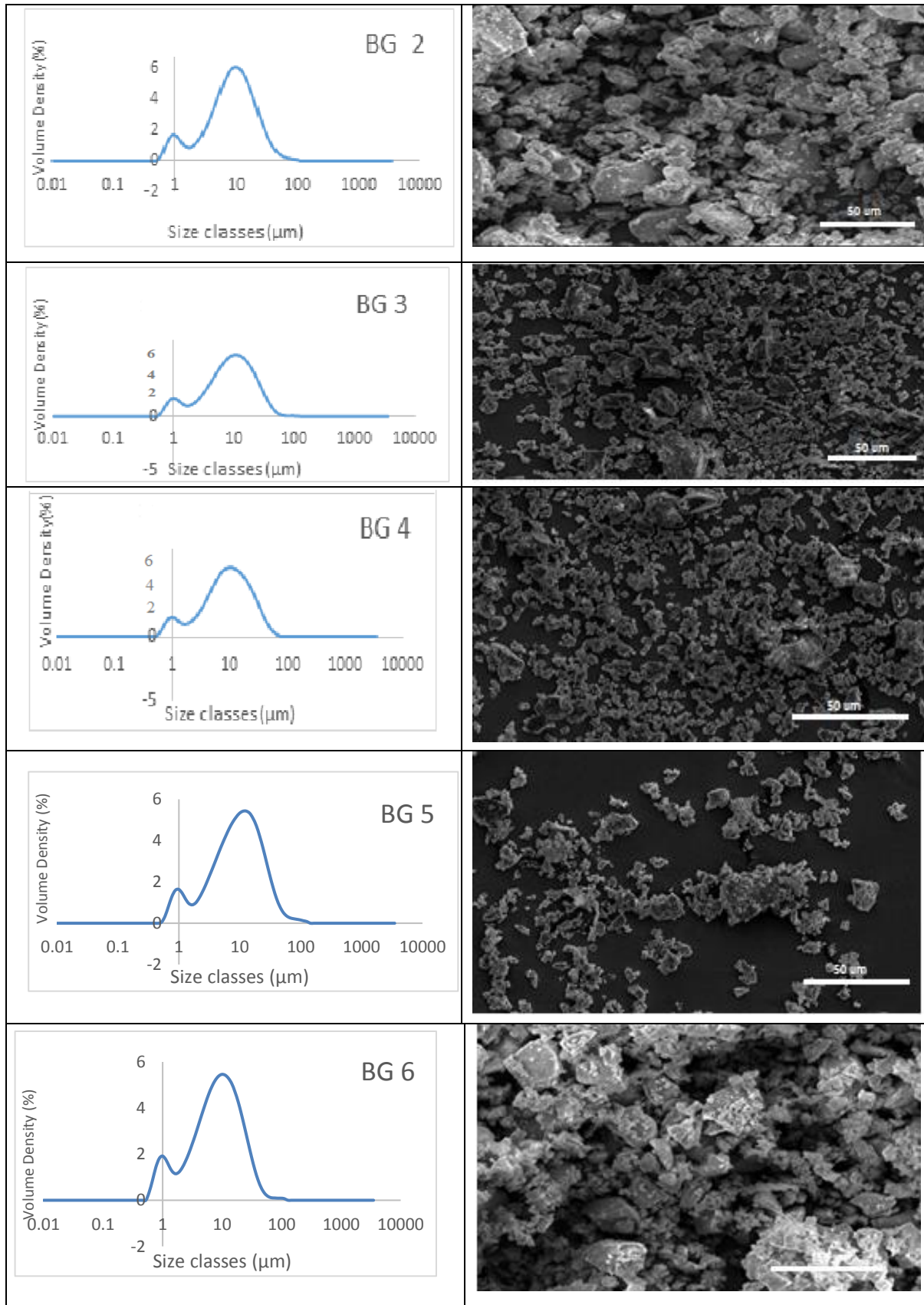
Table 8: Density measurement analysis (Pycnometer & Archimedes) of glass samples (BG 1-7).

Glass samples	Pycnometer density measurements in g/cm ³	Archimedes density measurements in g/cm ³
BG 1	2.73	2.72
BG 2	2.78	2.76
BG 3	2.78	2.77
BG 4	2.79	2.78
BG 5	2.77	2.76
BG 6	2.78	2.77
BG 7	2.79	2.78

4.4.1.4 Particle size analyses

For quantitative and qualitative analysis of all milled glass powder samples $< 45 \mu\text{m}$ size, the laser particle size analysis and scanning electron microscope (SEM) was undertaken to analyse particle size distribution and morphological structure of all produced series of silicate based bioactive glasses as shown in following Figure 40 respectively. Distinctive differences in morphology and particle size distribution governs specific characteristic features of resultant glass ionomer cement such as working and setting time as well as other mechanical properties such as compressive strength. It was observed that almost 95 % or even more particles were $< 45 \mu\text{m}$ in size. Likewise, the mean particle sizes were approximately 20-25 μm in size as tabulated in following Table 9. The laser particle size results illustrate that all produced glass samples had similar particle size distribution. Moreover, scanning electron microscopic technique was used to analyse the morphological characteristics of all milled glasses as shown in following Figures 40 respectively.





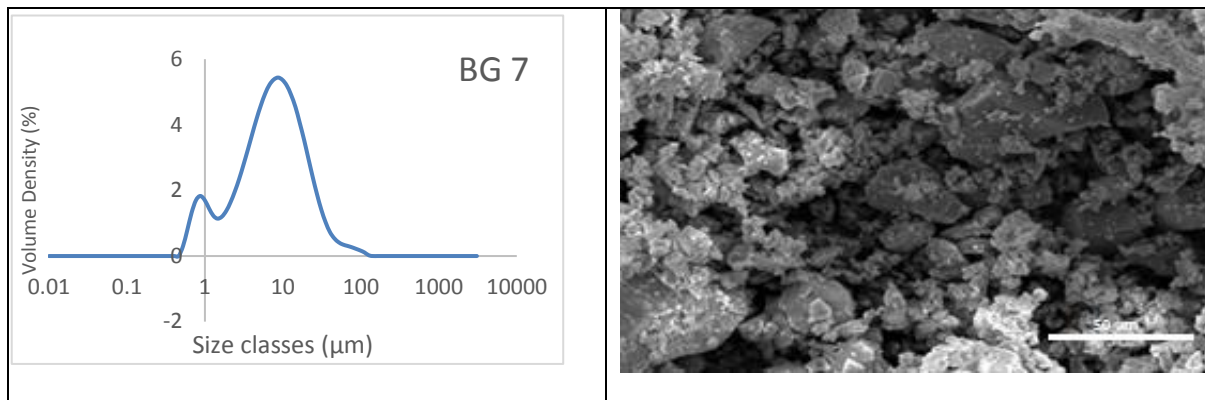


Figure 40: Illustration of particle size analysis (< 45 μm) and SEM image of produced silicate based bioactive glass samples (BG 1-7).

However, all prepared milled silicate based bioactive glass powdered samples were analyzed individually by using Malvern Mastersizer 3000 system UK to determine their particle size distribution. The wet analysis technique was adopted by using Hydro EV wet dispersion unit and water was used as the liquid medium in normal atmospheric environment 20°C. The obscuration range was kept from 5% - 10 % in total. Whereas, five measurements were taken for each individual sample, with the delay of 10 seconds between each measurement along with stirring speed of 2000 rotation per minute (rpm). Similarly, the obtained data were analyzed by using Mastersizer software[®] and Microsoft Excel 2016[®]. The surface morphology of all prepared samples was also determined by using scanning electron microscopy (SEM). All samples were gold coated prior to imaging and SEM analysis was conducted by using Philips/FEI XL30 S-FEG with beam energy of 15kV respectively.

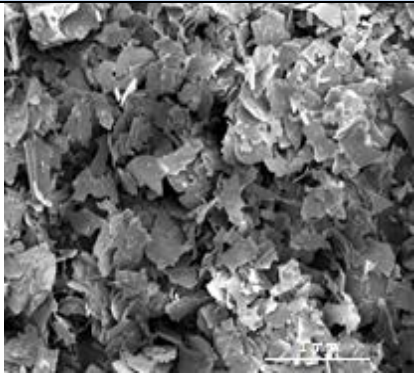
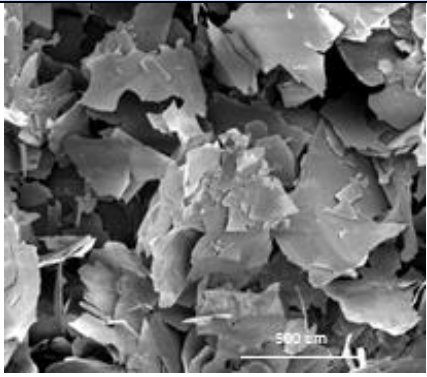
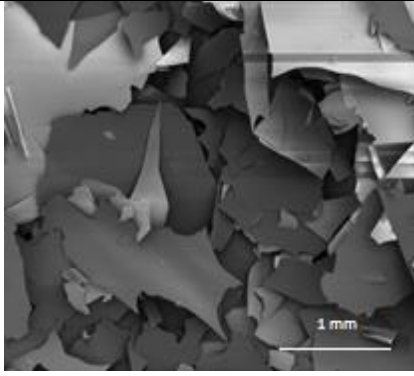
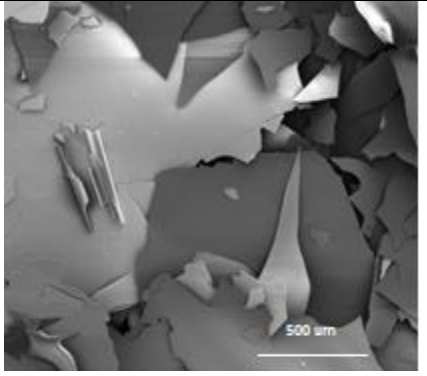
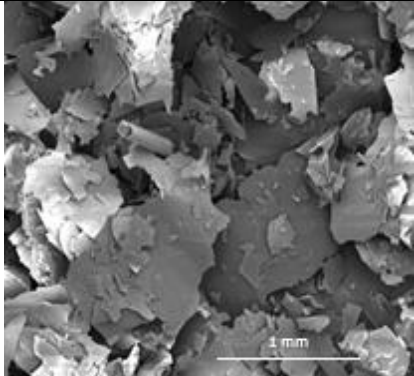
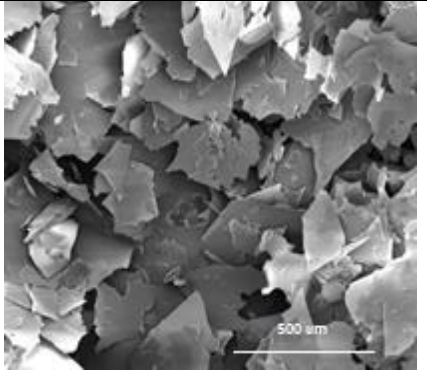
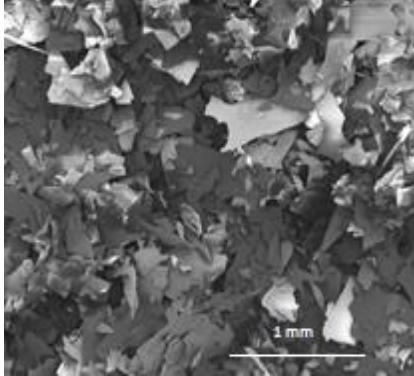
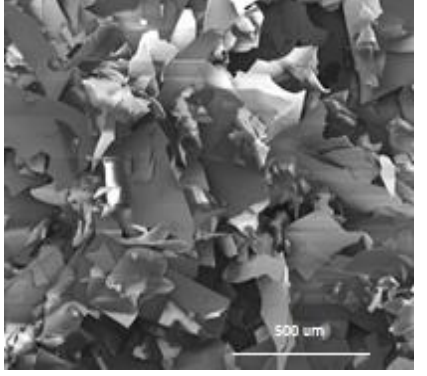
Furthermore, scanning electron microscopic (SEM) analysis was also conducted for the evaluation of particle size and morphological structure of obtained glass flakes from Leeds

Glass Flakes Company Ltd. UK. Different sizes of these obtained glass flakes were used both in nano and micro meters such that, 100 and 350 nano meter (milled and un-milled) along with 100 and 350 micro meter (milled and un-milled) glass flakes correspondingly as shown in following Figure 41 by using same optimised equipment's.

Table 9: Particle size analysis results of all milled glass samples < 45 μm in size from BG

1-7.

Sr No:	Glass Samples	Mean particle Size (μm)	Particle sizes < 45 μm %
1	BG glass sample 1	18.28	96%
2	BG glass sample 2	26.90	97%
3	BG glass sample 3	25.85	98%
4	BG glass sample 4	20.79	90%
5	BG glass sample 5	26.46	95%
6	BG glass sample 6	23.75	85%
7	BG glass sample 7	20.11	89%

Sr No.	1mm	500 μ m
100 μ m Milled	 Scanning electron micrograph showing a dense collection of small, irregular, flake-like particles. A white scale bar in the bottom right corner indicates 1 mm.	 Scanning electron micrograph showing a dense collection of small, irregular, flake-like particles. A white scale bar in the bottom right corner indicates 500 μ m.
100 μ m Unmilled	 Scanning electron micrograph showing large, irregular, flake-like particles. A white scale bar in the bottom right corner indicates 1 mm.	 Scanning electron micrograph showing large, irregular, flake-like particles. A white scale bar in the bottom right corner indicates 500 μ m.
100nm Milled	 Scanning electron micrograph showing a dense collection of small, irregular, flake-like particles. A white scale bar in the bottom right corner indicates 1 mm.	 Scanning electron micrograph showing a dense collection of small, irregular, flake-like particles. A white scale bar in the bottom right corner indicates 500 μ m.
100nm Unmilled	 Scanning electron micrograph showing a dense collection of small, irregular, flake-like particles. A white scale bar in the bottom right corner indicates 1 mm.	 Scanning electron micrograph showing a dense collection of small, irregular, flake-like particles. A white scale bar in the bottom right corner indicates 500 μ m.

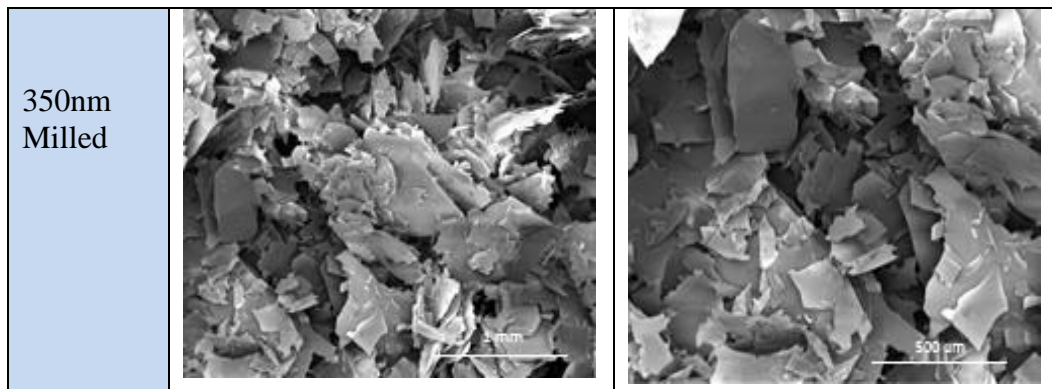


Figure 41: SEM Micrographs of Glass Flakes of different sizes as obtained from Leeds Glass Flakes Company Ltd UK.

4.4.1.5 Brunauer-Emmett-Teller analysis

All produced silicate based bioactive glass samples BG 1-7 were analysed by using Brunauer-Emmett-Teller analysis (BET) for the evaluation of surface area respectively, as shown in following Figure 42 respectively. However, the 'in house' copy of silicate based 45S5 bioactive glass without any calcium substitution indicated lower surface area as $4.4 \text{ m}^2/\text{g}$. Whereas, increase in surface area from 4.5 to $4.9 \text{ m}^2/\text{g}$ were observed in glass samples from BG 2-7 having calcium substitution with strontium and barium ions with 3 mole % of calcium oxides correspondingly.

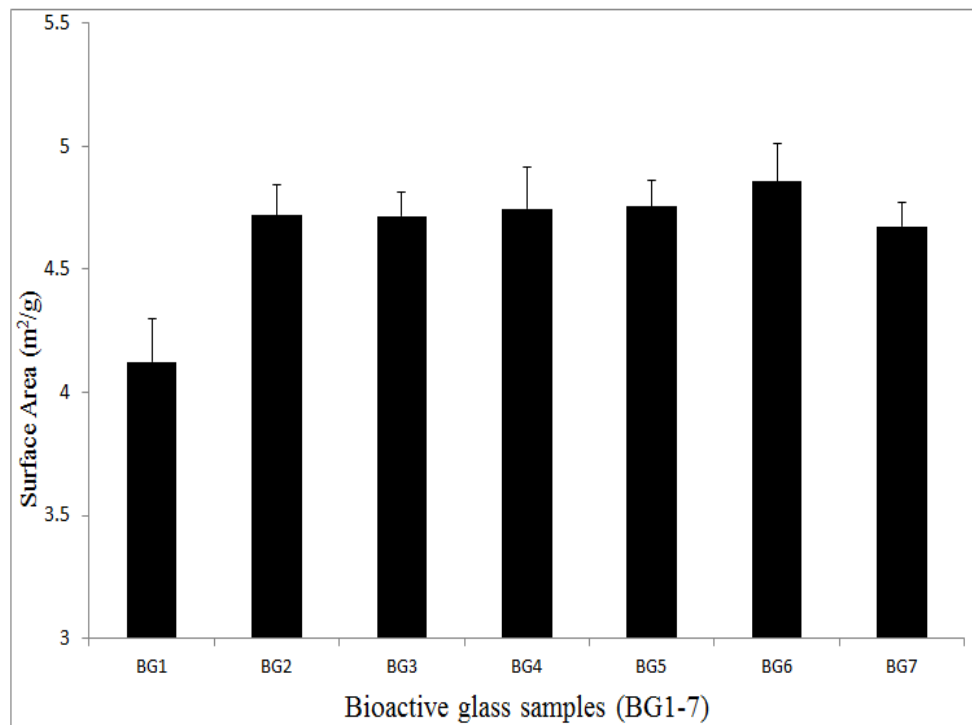


Figure 42: BET measurement analysis of all produced glass series (BG 1-7) with ANOVA ($p \leq 0.05$) and represents mean \pm SD ($n=3$). Results indicate that, substitutes increase the specific surface area of all produced bioactive glass from BG 2-7 respectively. This indicates that, more amount of surface engaged in reaction will exhibit better biological properties respectively.

4.4.2 Thermal characterisation

4.4.2.1 Differential thermal analysis

In order to analyse the glass transition 'T_g' and event of crystallisation, the differential thermal analysis was performed on all the produced silicate based bioactive glass samples in normal atmospheric environment (air). However, it was observed that, due to the substitution of calcium ions with strontium and barium in the parent composition, distinct changes occurred in the glass transition. This exchange of ions indicates the significant disruption of glassy network and as a result the decrease in glass transition temperature occurred as shown in following Figure 43. Similarly, both strontium and barium has got larger cations than calcium and it tends to disrupt the glass network more readily along with decrease in glass transition due to increase in ionic radius (Fredholm et al. 2010).

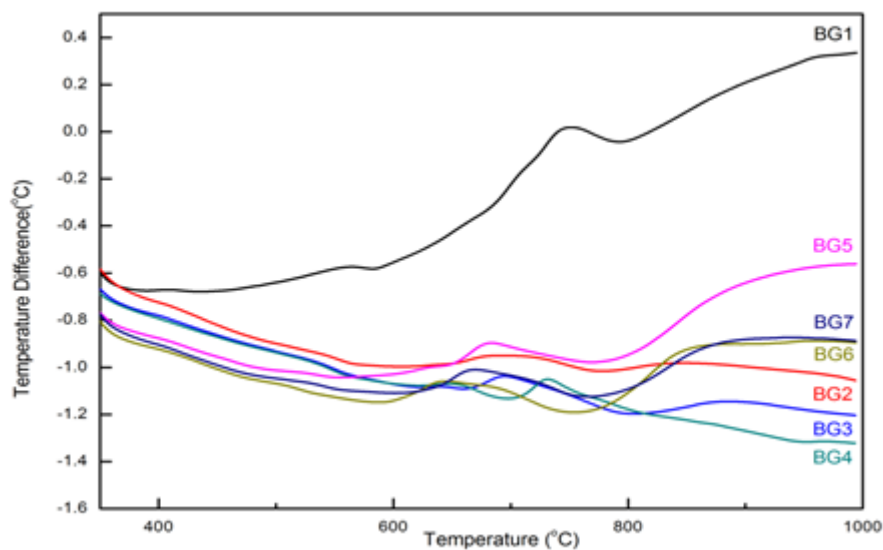


Figure 43: Traces of differential thermal analysis of all produced silicate based bioactive glass series from (BG 1-7). DTA graph indicates that, due to increase in the Sr^{+2} and Ba^{+2} substitution the distinct change in glass transition temperature occurs due to larger cationic effect of Sr^{+2} and Ba^{+2} than Ca^{+2} and the disruption of glass network initiated more readily along with decrease in glass transition temperature respectively.

4.4.3 Chemical characterisation

4.4.3.1. Fourier Transform Infrared (FTIR) spectroscopic analysis

For chemical investigation of strontium and barium supplemented, produced silicate based series of glasses (BG 1-7), Fourier transform infrared spectroscopic (FTIR) analysis was performed on Thermo scientific™ Nicolet™ iS™50 spectrometer with MTEC photoacoustic cell, under absorbance mode between the range of 400 cm^{-1} - 4000 cm^{-1} as shown in following Figure 44 respectively. However, it was observed that, the peaks appeared in between the range of $1200 - 1000\text{ cm}^{-1}$ because of Si – O asymmetric stretching. Likewise, peaks in between the range of $500 - 540\text{ cm}^{-1}$ attributed to P – O bending mode and peaks appeared within the range of $890 - 975\text{ cm}^{-1}$ attributed to the one Si – O non-bridging oxygen (NBO) per SiO_4 tetrahedron (Q^3 group). However, peaks between the ranges of $800 - 840\text{ cm}^{-1}$ can be classified due to the presence of two Si-O-2NBO functional groups (Q^2 group). Whereas, the FTIR spectrum of all produced glass samples were identical with each other. Similarly, this indicates the presence of identical Si-O bonds and Q^n species; this means that all calcium substituted glasses with strontium and barium ions, essentially have similar network connective structure as discussed in detail in the following discussion chapter 5 respectively (Fredholm et al. 2010).

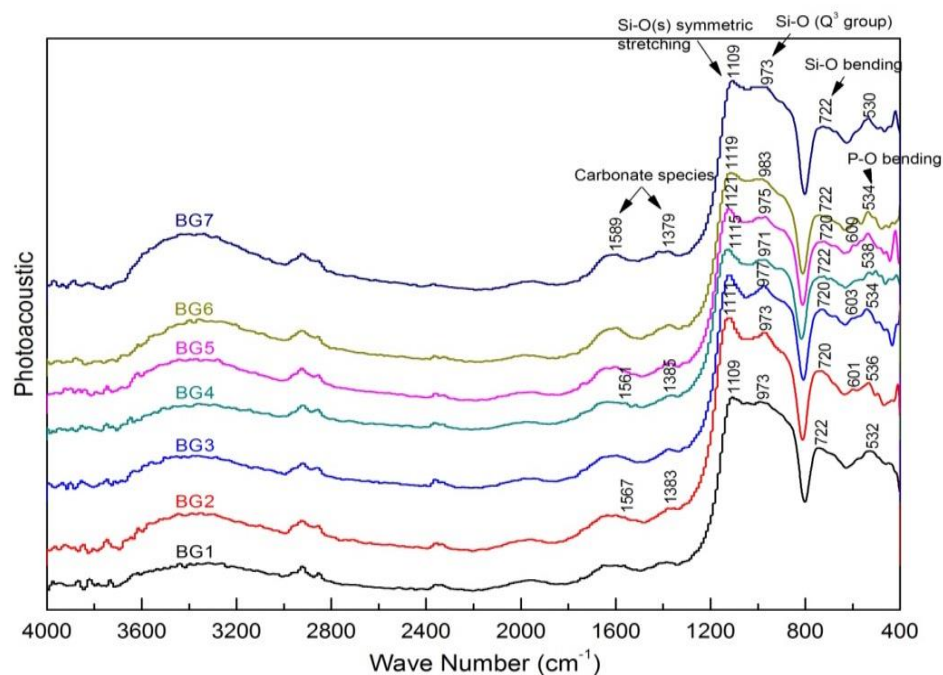


Figure 44: FTIR spectrum of all produced silicate based bioactive glass series (BG 1-7). Similarly, peaks at 1060-1040 cm^{-1} and 745 cm^{-1} were showing basic silica glass chemical structure regarding stretching mode Si-O bonds and bending mode Si-O bonds, separately. The absorption peaks of deformation mode of PO_4^{3-} groups located at around 520 cm^{-1} respectively.

Similarly, the onset of the formation of hydroxyapatite layer (HCA layer) after the immersion of produced silicate based bioactive glass samples (BG 1-7) in prepared simulated body fluid (SBF) solution for 24 hours were observed by utilizing FTIR technique respectively as shown in following Figure 45. However, the untreated produced silicate based bioactive glass samples exhibited broad peaks which were assigned to Si-O in the range of 1060 - 1040 cm^{-1} but, after 24 hours of immersion in simulated body fluid solution the stretching of P-O bond belonging

to PO_4^{3-} groups were observed in this region. Whereas, the peaks ranging in between $600 - 515 \text{ cm}^{-1}$ were attributed to P-O bending mode due to presence of PO_4^{3-} tetrahedral structure. These significant peaks attribute the formation of carbonated hydroxyapatite phase (HCA layer) in the produced silicate based bioactive glass samples respectively.

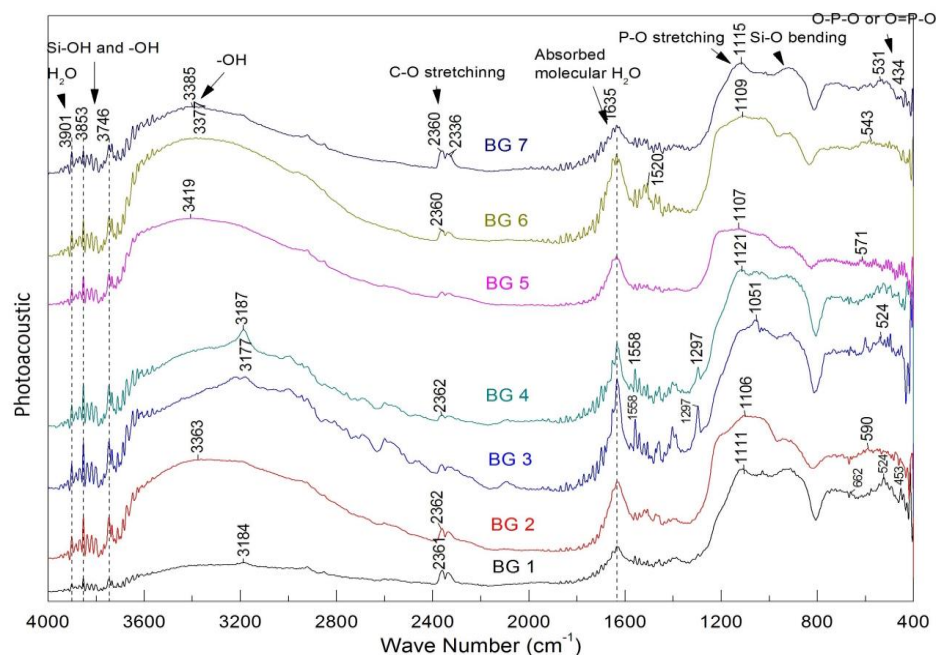


Figure 45: In vitro bioactivity FTIR analysis of all produced silicate based bioactive glass samples (BG 1-7). However, most peaks located in the region of $1121 - 1051 \text{ cm}^{-1}$ were due to asymmetric stretching vibration mode of P-O-P bonds. Whereas, the peaks in the range of $600 - 400 \text{ cm}^{-1}$ may be assigned to bridging phosphorous bending vibrations mode of O - P - O or O = P - O, this may indicate the formation HCA layer after 24 hours' immersion of produced glass samples in SBF solution.

Furthermore, the peaks which were emerged in all produced silicate based bioactive glass samples (BG 1-7) especially after immersion in the range of $920 - 912 \text{ cm}^{-1}$ indicated the appearance of Q^3 groups regarded as Si-O unit with one “non-bridging” and three bridging oxygen bonds. Similarly, all prepared specimens were stored in SBF solution for 24 hours, for drying in dry hot aired vacuumed incubator before FTIR analysis for 48 hours. However, in obtained FTIR spectrum the deformation modes of O-H groups and absorbed water molecules were observed δ (H-O-H) and attributed with the peak value of 1635 cm^{-1} and also the OH groups in stretching vibrations mode were attributed in between the range of $3419 - 3177 \text{ cm}^{-1}$.

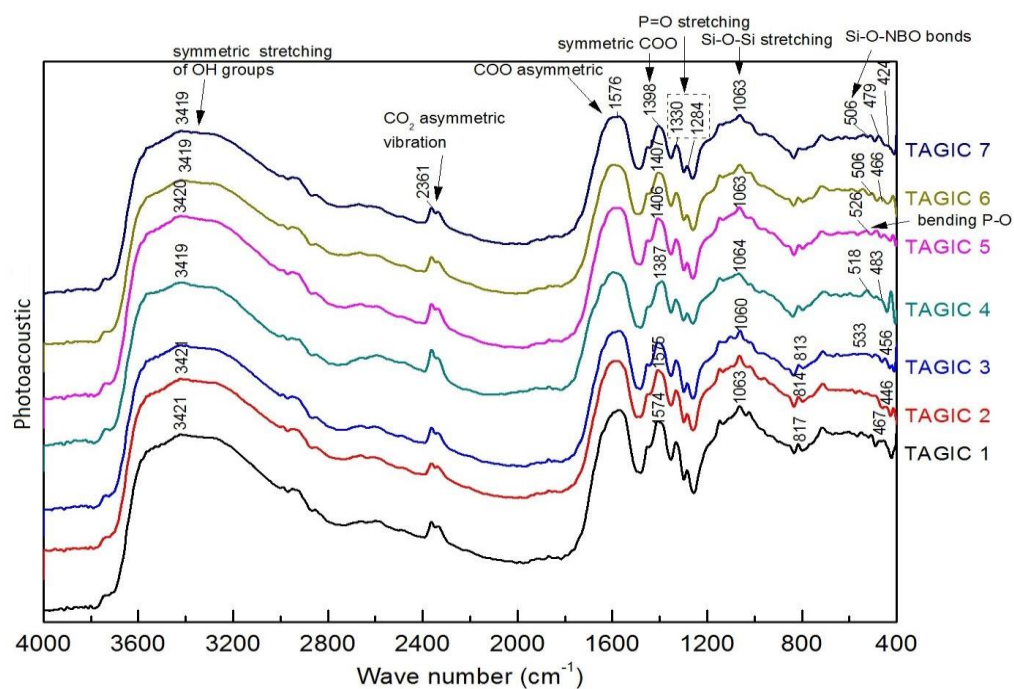


Figure 46: FTIR spectrum of tartaric acid based glass ionomer cements samples (TAGIC 1-7) indicates peaks at 1574 , 1407 and 1398 cm^{-1} was attributed to carboxylic acid

group respectively. However, peaks at around 1576 and 1586 cm⁻¹ were assigned to symmetric and asymmetric stretching vibration of O-C=O bonds.

Furthermore, all prepared silicate based glass ionomer cement samples (TA GIC 1-7) upon the admixture of poly-acrylic acid and tartaric acid as setting modifier in the presence of water were analyzed, by using FTIR technique as shown in above indicated Figure 46 respectively.

Similarly, it was observed that, peaks from 415-540 cm⁻¹ and 550-600 cm⁻¹ were attributed to Si-O-Si bending mode and P-O bend correspondingly. However, the peak attributed at 720 cm⁻¹ and 800 cm⁻¹ indicates the presence of Si-O bending mode. The phenomenon of Si-O-Si stretching was also observed between the range of 850 cm⁻¹ and 1200 cm⁻¹ and around 1066 cm⁻¹ as well (Gonzalez et al. 2003; Bellucci et al. 2011; Subramani et al. 2012).

Similarly, the shoulder of this peak was observed at 950 cm⁻¹ and this shoulder appeared due to O-H deformation vibration because of the presence of Si-OH structure in all of the tartaric acid based cement samples. This indicated the formation of silica gel around glass particles during the cement setting reaction stage. Whereas, another shoulder was seen around 1020 cm⁻¹ due to asymmetric stretching of P-O bonds as shown in Figure 47 respectively (Gonzalez et al. 2003; Bellucci et al. 2011; Subramani et al. 2012).

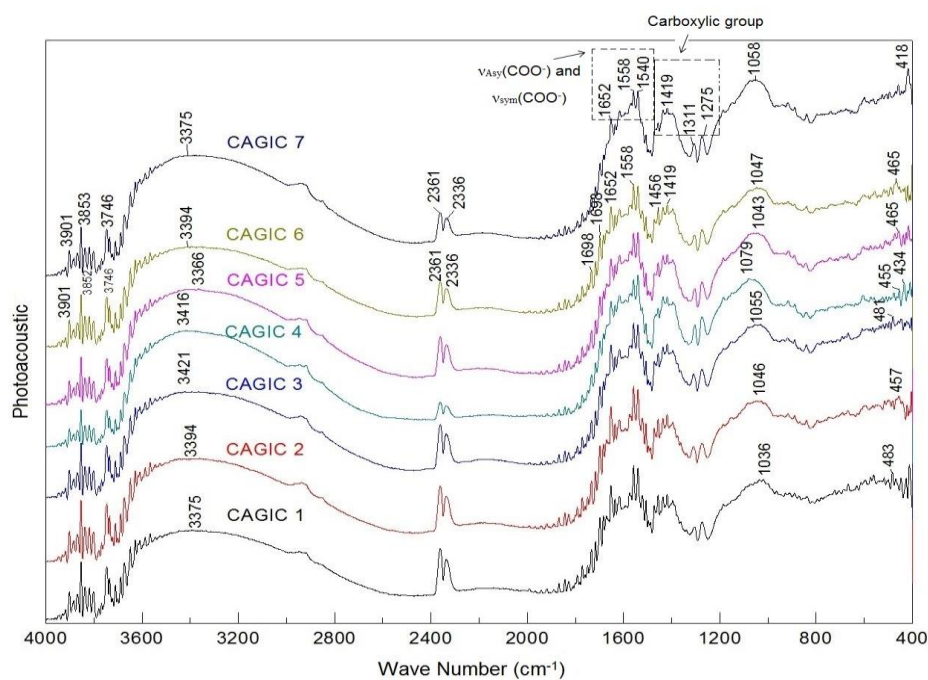


Figure 47: FTIR spectrum of citric acid based glass ionomer cements samples (CA GIC 1-7) Similarly, peaks at 1419, 1311 and 1275 cm^{-1} were attributed to carboxylic acid group. However, peaks at around 1558 and 1540 cm^{-1} were assigned to symmetric and asymmetric stretching vibration of O - C=O bonds.

Moreover, all prepared silicate based bioactive glass ionomer cement (CA GIC1-7) samples after the admixtur of poly-acrylic acid and citric acid as setting modifier in the presence of water were also analysed by adopting FTIR characterisation techniques. Similarly, in all produced citric based glass ionomer samples, peaks attributed from the range between 1079-1036 cm^{-1} indicated the Si-O-Si bonds respectively. However, absorption peaks at 1419, 1311 and 1275 cm^{-1} were attributed to carboxylic acid group. The peaks observed around 1558 and 1540 cm^{-1}

¹ were assigned to symmetric and asymmetrical vibrational stretching of O-C=O bonds. Whereas, the presence of -OH groups observed at around the peak at 3300 cm⁻¹ and the peaks at 2361-2331cm⁻¹ attributed to the asymmetrical stretching of CO₂ respectively.

4.4.3.2. Raman spectroscopic analysis

Raman spectroscopy is considered as the fundamental type of molecular spectroscopy which is basically related with inelastic scattering phenomena. Due to the inelastic scattering of photons the Raman scattering occurs. Similarly, this determines the peaks which were created by vibrational energy and because of this the identification of molecular symmetry and chemical structure could be analysed. However, it can provide qualitative information by vibrational transition of molecules along with infrared absorption.

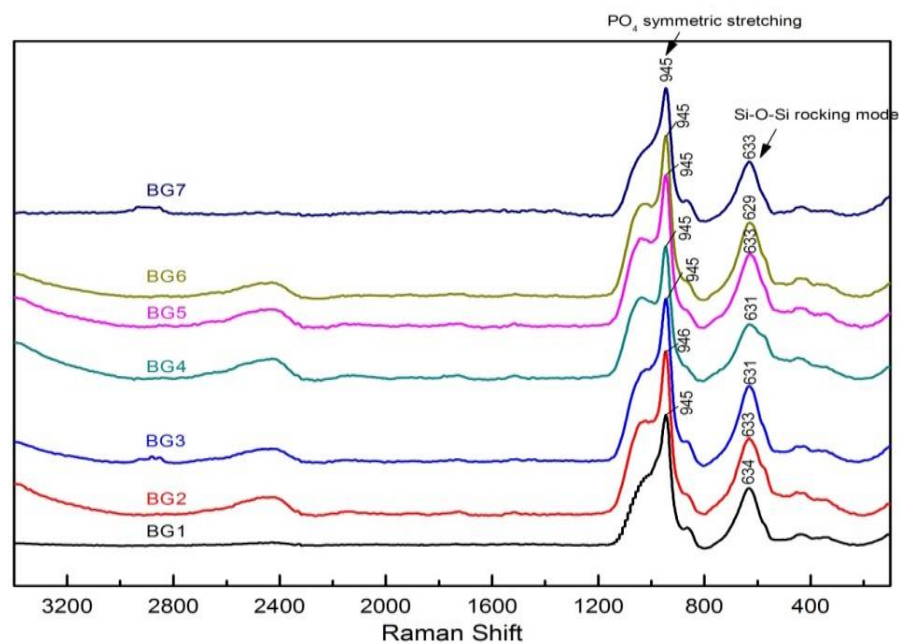


Figure 48: Raman spectrum of all produced silicate based glass series (BG 1-7) and peak at $630 - 650 \text{ cm}^{-1}$ can be ascribed as Si-O-Si group; $943-950 \text{ cm}^{-1}$ ascribed as the symmetrical stretching of phosphate group (PO_4) and $800 - 1150 \text{ cm}^{-1}$ indicates Si-O-Si tetrahedral silica with different (NBO) non-bridging oxygen units. Whereas, shifting of frequencies and variation in intensities merely associated with the addition of alkali and alkaline earth oxides to the silica network respectively.

Raman spectroscopy has been widely accepted for the analysis of anionic structure of silicate based glasses and the effect of phosphorus and other substitutions on their basic structure. Similarly, the open amorphous structure of all silicate based bioactive glasses appeared due to the addition of alkali and alkaline earth oxides into parent composition. These cations (Na^+ , Ca^+ , Sr^+ and Ba^+) play a vital role in the modification and disruption of glassy network. Due

to the presence of these cations in the basic glass structure, the reduction in the ratio of connectivity in the glassy network by replacing non-bridging silicon oxygen bonds collectively occurs. Raman spectroscopy is very sensitive to changes occur in Si-O-Si bonds and a useful technique in the detection of Si-O-NBO bonding in bioactive glasses. However, the shifting of frequencies and variation in intensities merely associated with addition of alkali and alkaline earth oxides to the silica network. Inclusion of higher ratio of network modifiers can potentially be able to increase the Raman intensities. The similar nature of behaviour has also been reported for other glasses such as phospho-silicate and borosilicate glasses (Gonzalez et al. 2003; Bellucci et al. 2011; Subramani et al. 2012).

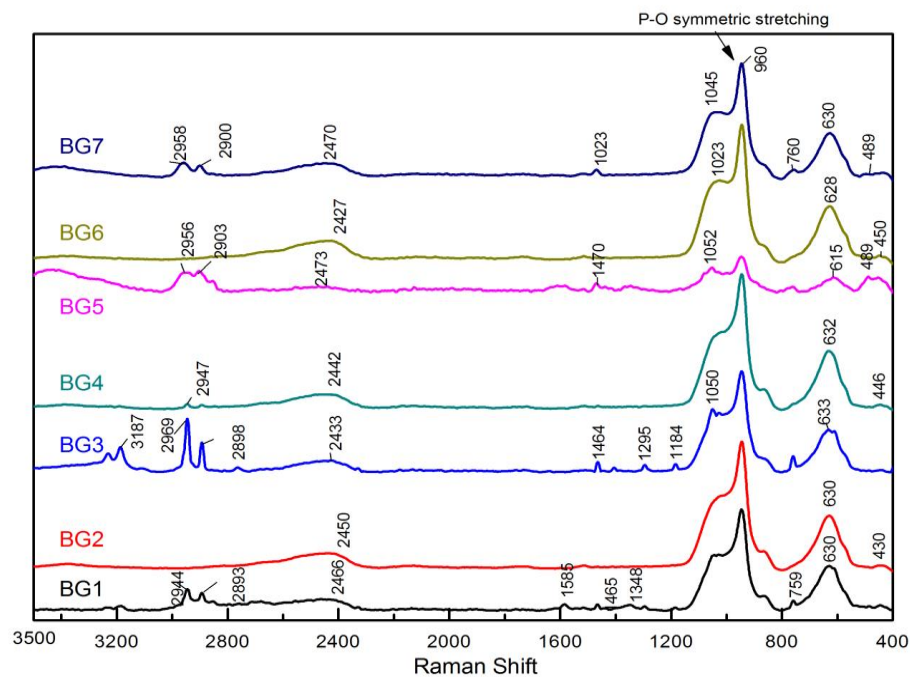


Figure 49: In vitro bioactivity Raman analysis of all produced silicate based bioactive glass series (BG 1-7). However, peaks of P-O symmetric stretching mode attributed at 945 cm^{-1} , after immersion in stimulated body fluid solution (SBF) mentioned peaks shifted towards higher wave number, exhibits hydroxyapatite growth in all produced glass samples.

For silicate and phosphate based glasses the spectral range from 200 – 1200 cm^{-1} were been considered because of the presence of main peak for silicate glasses fall within this interval. The presence of broad peak in between the range of 630 – 650 cm^{-1} can be ascribed as Si-O-Si group as shown in above Figure 48. However, this peak is usually present in $\text{P}_2\text{O}_5\text{-Na}_2\text{O-CaO-SiO}_2$ based glass system and they can potentially be able to move towards higher wave numbers with low SiO_2 containing glass compositions.

Furthermore, peaks from 800 to 1150 cm^{-1} are associated with the Si-O-Si tetrahedral silica bonds along with different (NBO) non-bridging oxygen units. Whereas, the small peaks appeared at 860 cm^{-1} , 920 cm^{-1} and 975 cm^{-1} can be ascribed to the monomers of SiO_4 (4NBO), dimmers Si_2O_7 (3NBO) and chains of Si_2O_6 (2NBO) respectively. Moreover, the peak appeared at 1030-1035 cm^{-1} can be related to vibrational changes due to the presence of two dimensional structures such as Si_2O_5 (1NBO). Similarly, the presence of intense bands within the range of 943-950 cm^{-1} ascribed as the symmetrical stretching of phosphate group (PO_4). Additionally, this peak usually hides partially at 920 cm^{-1} and it could appear within the range of 975 – 1130 cm^{-1} in the form of shoulders significantly on the right hand side of this peak (Gonzalez et al. 2003; Bellucci et al. 2011). However, after the immersion of all produced glass samples in simulated body fluid solution (SBF) the appearance of peaks between the range of 1150 – 800 cm^{-1} and also the P-O symmetric stretching mode was observed at the 945 cm^{-1} which usually shifted to higher wavenumber noticed as shown in following Figure 49 [51].

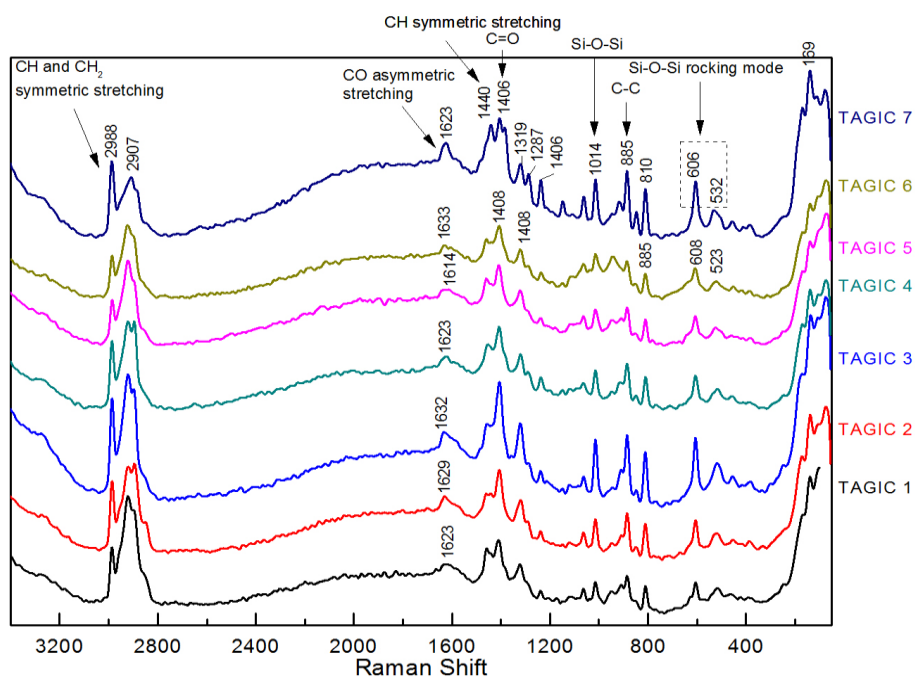


Figure 50: Raman spectrum of tartaric acid based glass ionomer cement samples (TAGIC 1-7). Similarly, peaks at 1406 cm^{-1} and 885 cm^{-1} attributed to C=O and C-C respectively. However, peaks at 2988 cm^{-1} and 2907 cm^{-1} attributes to CH and CH_2 symmetrical and peaks at around 1440 cm^{-1} were with regard to deformation of C-H bonds respectively.

Furthermore, all prepared silicate based bioactive glass ionomer cement samples with the admixture of poly-acrylic acid and tartaric acid as setting modifier in the presence of water were analyzed by using Raman spectroscopy as shown in Figure 50 respectively. However, the spectrum between the range of 500 cm^{-1} and 1700 cm^{-1} were attributed to the vibrations raised from the structural changes of organic molecules. This usually occurs due to the formation of salts during the reaction of metal oxides with poly-acrylic acid and tartaric acid.

Similarly, peaks appeared at 606 cm^{-1} , 811 cm^{-1} and 1317 cm^{-1} indicates the formation of calcium tartrate. Whereas, peak attributed at 810 cm^{-1} considered for the presence of sodium tartrate. The C - C stretched region of calcium tartrate were observed at the ranges between 885 cm^{-1} and around 1014 cm^{-1} . Moreover, peak of the low intensity is present at 950 cm^{-1} which ascribed as PO_4 symmetric stretching. A similar low intensity peak appeared around the wavelength of 1066 cm^{-1} which attributes to Si-O-Si stretching. However, the symmetric and asymmetric COO stretching were also observed for the presence of calcium tartrate and attributed at 1403 cm^{-1} and 1630 cm^{-1} respectively. The phenomenal changes for the CH_2 deformation of calcium poly-acrylate were also observed at wavelength such as 1438 cm^{-1} and peaks attributed at 2927 cm^{-1} indicates the presence of CH_2 or CH stretching mode correspondingly.

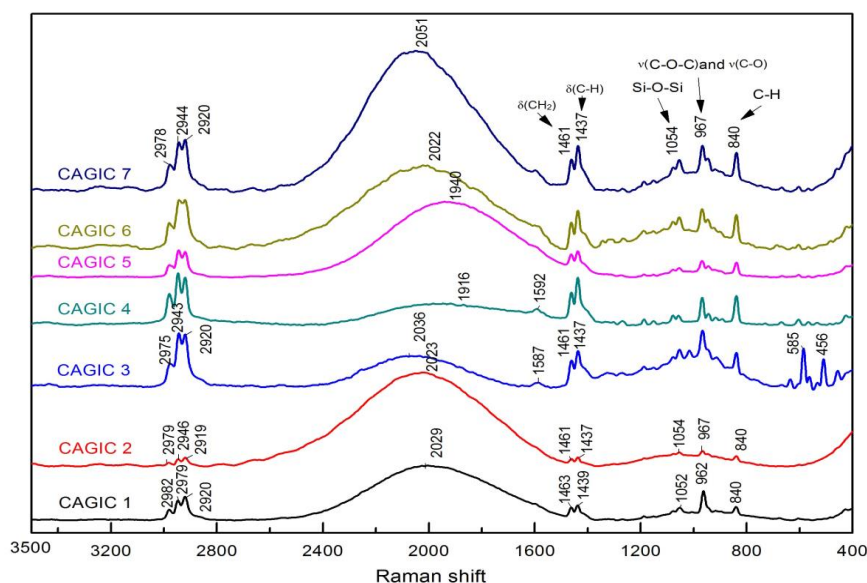


Figure 51: Raman spectrum of citric acid based glass ionomer cements samples (CAGIC 1-7). Similarly, the peaks at 967cm^{-1} was assigned to C–O–C and C–O stretching vibration mode. However, the peaks at around 840 cm^{-1} were regarding deformation of C–H bonds respectively.

Moreover, all produced silicate based bioactive glass ionomer cement samples with the admixture of poly-acrylic acid with citric acid as setting modifier in the presence of water were also characterised by using Raman technique as shown in Figure 51. Similarly, the peak appeared at around 840 cm^{-1} ascribed as with deformation of C–H bonds. However, the peak observed at wavelength 967 cm^{-1} attributed C–O–C and C–O stretching in vibrational mode. On the other hand, in the structure of citrate the presence of -CH groups are relatively noticeable. Whereas, the peaks at 1461 cm^{-1} and 1437 cm^{-1} were attributed as stretching of CO_2

and the deformation of C-H correspondingly. Likewise, peaks observed at 2978 cm^{-1} , 2944 cm^{-1} and 2920 cm^{-1} were attributed to symmetric stretching mode of CH_2 groups, which may indicate the presence of citrate chains respectively.

4.4.4 *In-vitro* biological characterisations

4.4.4.1 *In- vitro* bioactivity analysis

4.4.4.1.1 Scanning electron microscopic (SEM) analysis

For further qualitative analysis of all produced silicate based bioactive glass ionomer cement samples (TA / CA GIC) with the admixture of poly-acrylic acid in the presence of two different setting modifiers such as tartaric and citric acid and water were analysed by using scanning electron microscopic (SEM) technique as shown in following Figures from 52 till 57 respectively. However, all prepared samples (both tartaric and citric acid based samples) were immersed in produced simulated body fluid solution (SBF) for 1st, 7th and 14th days prior to analysis correspondingly. Whereas, from the obtained and observed micrographs from scanning electron microscope, there were distinct surface morphological changes occurred on 7th and 14th day immersed samples with respect to 1st day or control untreated samples. These changes or development of globular growth over surface could be referred to as the formation of hydroxyl carbonated apatite (HCA) layer. Likewise, it was also observed that, the citric acid

based modified glass ionomer cement samples morphologically exhibited more potential for the formation of carbonated hydroxyapatite in comparisons with tartaric acid based modified glass ionomer cement samples. For instance, the spherical growth of hydroxyl carbonated apatite layer (HCA) respectively.

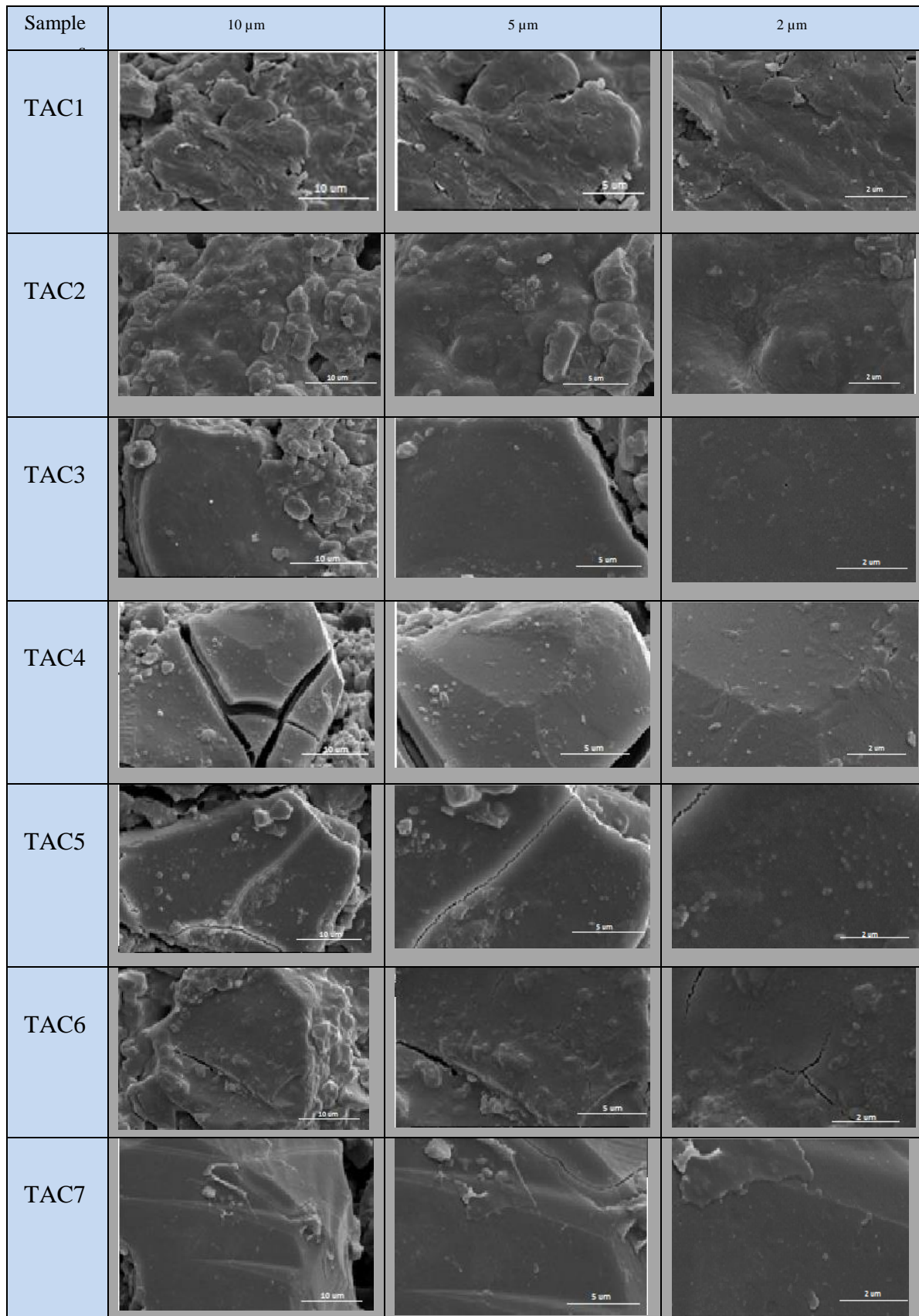


Figure 52: SEM micrographs of tartaric acid based cement samples (TAC1-7) at 1st day (control sample) at 10, 5 and 2 μm scales before immersion in c-SBF respectively.

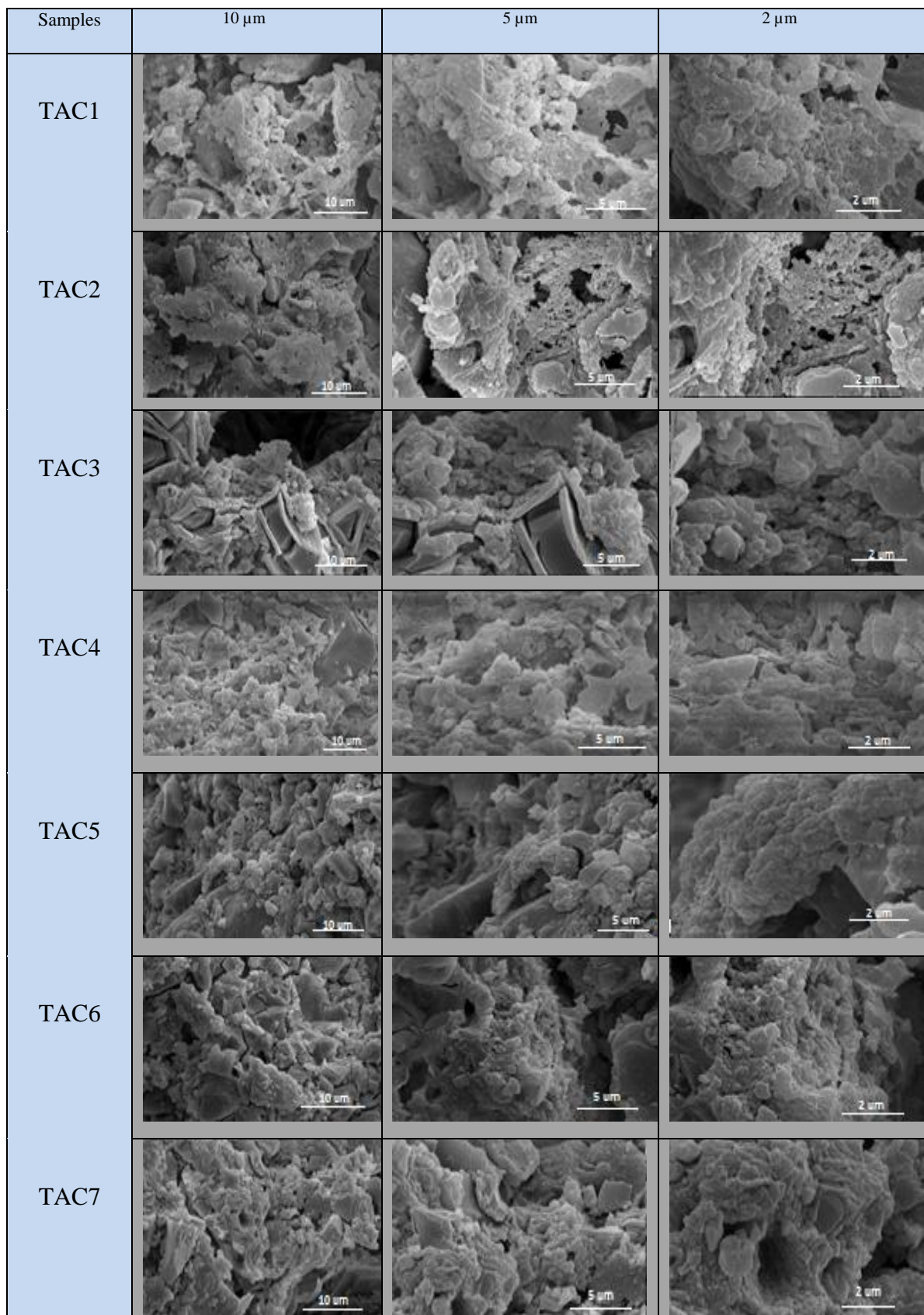


Figure 53: SEM micrographs of tartaric acid based cement samples (TAC1-7) at 7th day at 10, 5 and 2 μm scales after immersion in c-SBF respectively.

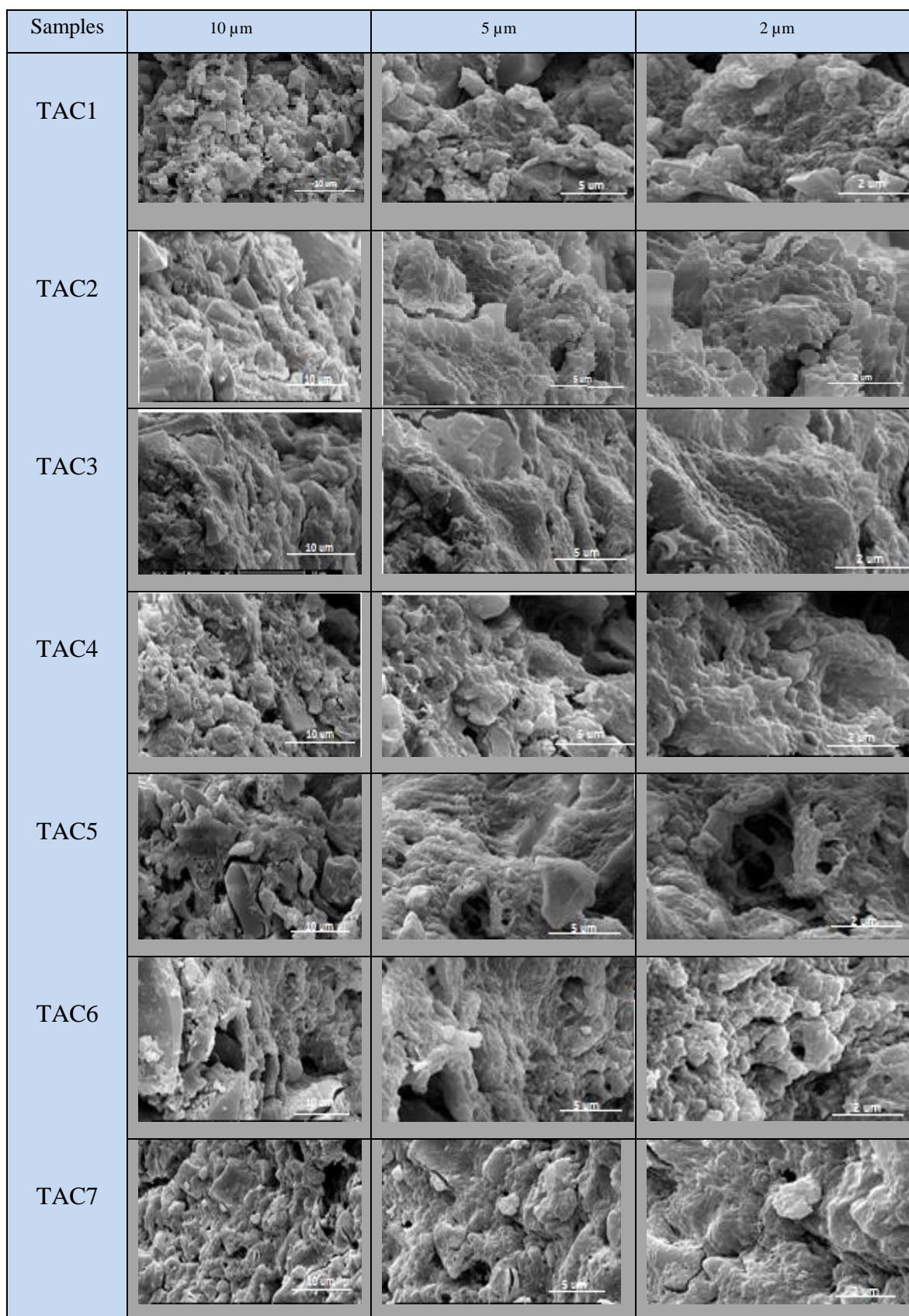


Figure 54: SEM micrographs of tartaric acid based cement samples (TAC1-7) at 14th day at 10, 5 and 2 μm scales after immersion in c-SBF respectively.

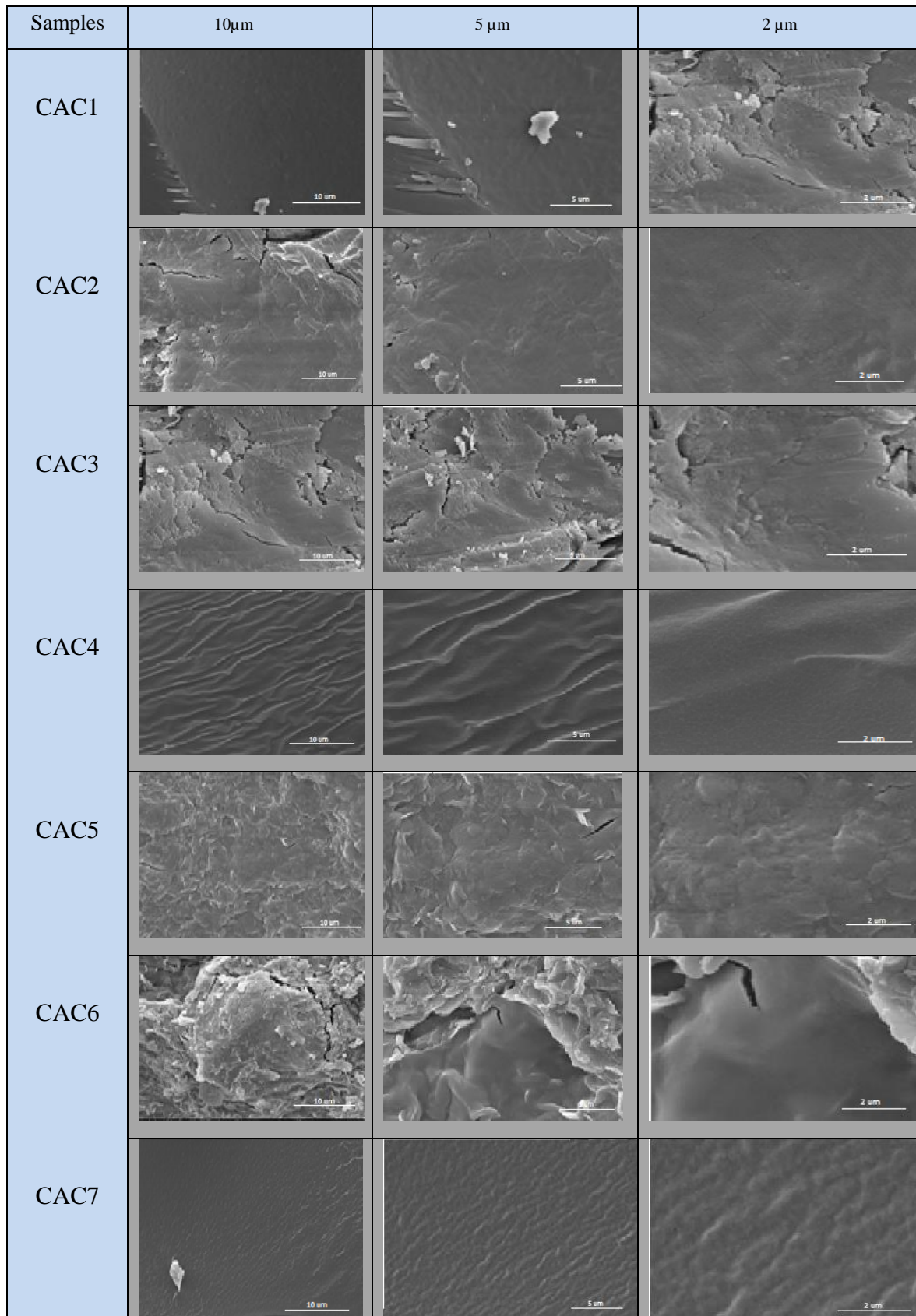


Figure 55: SEM micrographs of citric acid based cement samples (CAC1-7) at 1st day (control sample) at 10, 5 and 2 μ m scales before immersion in c-SBF respectively.

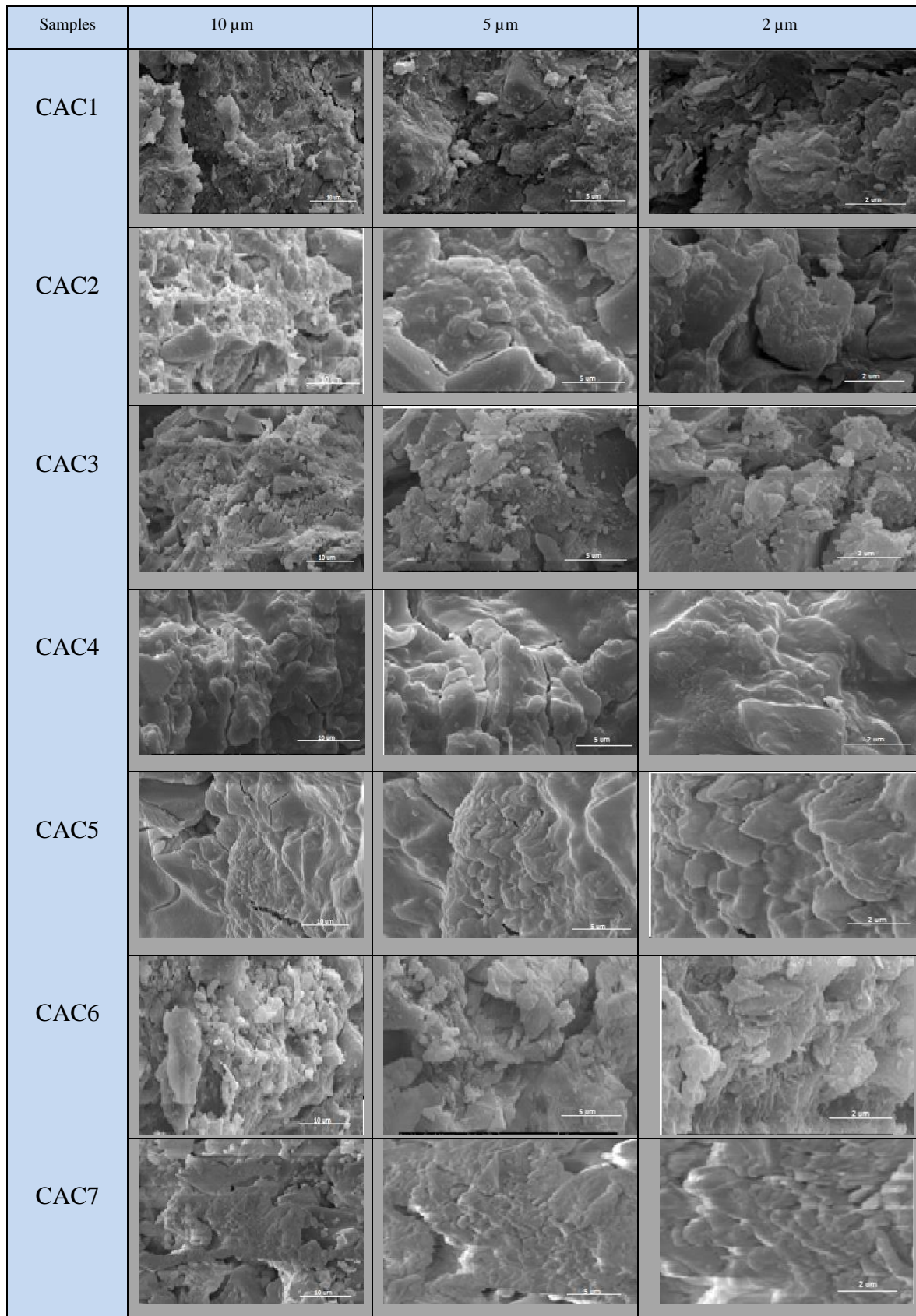


Figure 56: SEM micrographs of citric acid based cement samples (CAC1-7) at 7th day at 10, 5 and 2 μm scales before immersion in c-SBF respectively.

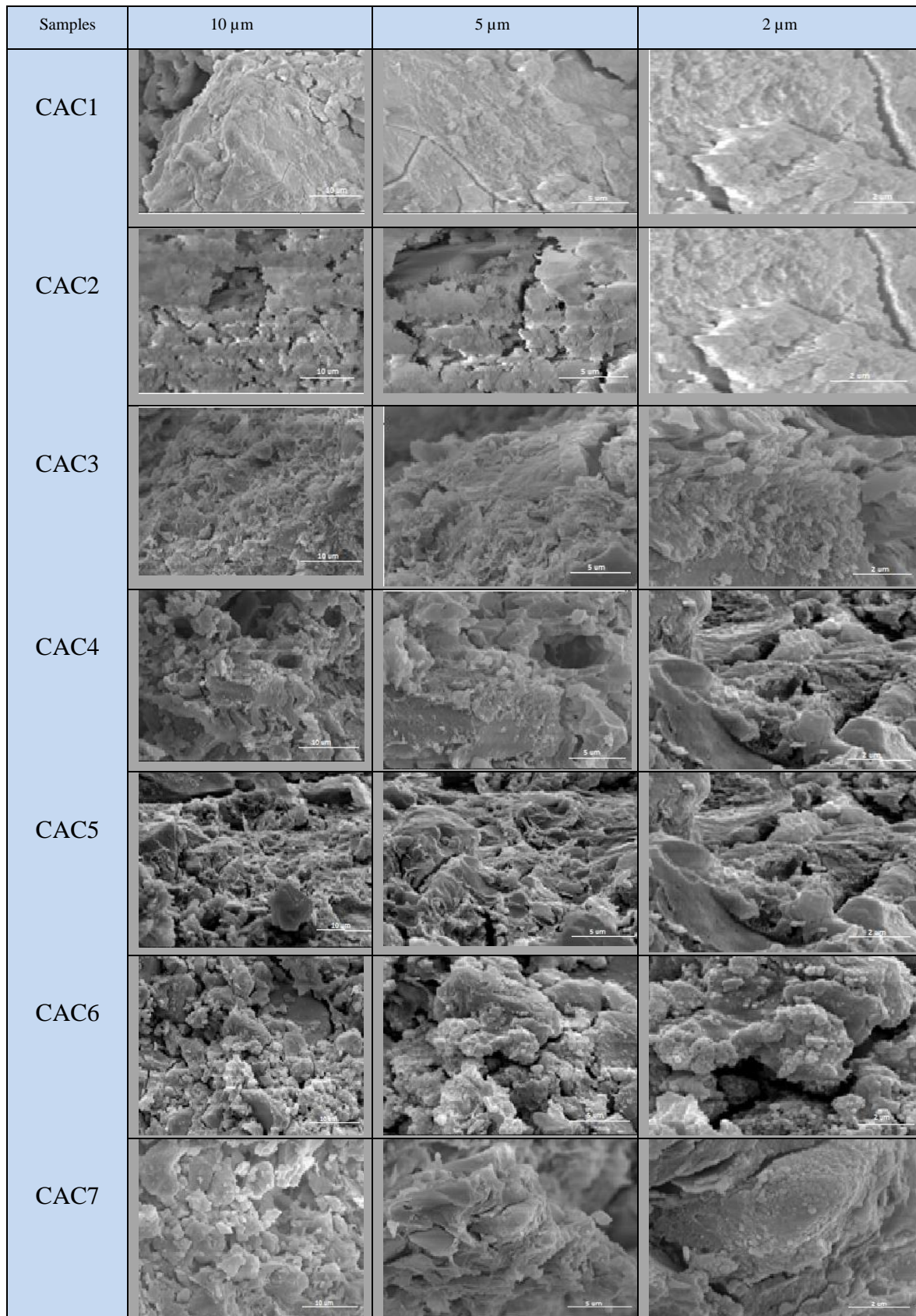


Figure 57: SEM micrographs of citric acid based cement samples (CAC1-7) at 14th day at 10, 5 and 2 μm scales before immersion in c-SBF respectively.

4.4.4.1.2 Energy dispersive x-ray spectroscopy (EDX) analysis

Energy dispersive x-ray spectroscopy (EDX) technique was adopted to exhibit the information of individual elements based on their unique atomic structure. Similarly, all produced silicate based bioactive glass ionomer cement samples upon with the admixture of poly-acrylic acid, tartaric and citric acid as setting modifier in the presence of water were analysed by using energy dispersive x-ray spectroscopy technique as shown in following Figure 59 and 60 respectively. However, the obtained energy dispersive x-ray spectroscopy spectrum was observed for all simulated body fluid (SBF) immersed cement samples after 7th and 14th days for the evaluation of calcium and phosphate ratio as shown in following Tables 10 and 11 respectively.

Moreover, it was observed that, the energy dispersive x-ray spectroscopy analysis results for both tartaric and citric acid based cement samples indicated the ratio of calcium and phosphate according to their atomic percentages and exhibited the values ranging from 1.69 to 1.86 which may confirm the presence of apatite formation at the end of 7th day of immersion. Similarly, at the end of 14th day of immersion the values ranged from 1.72 to 1.97. Yet the obtained Ca/P ratio of the produced cement samples were found to be slightly greater and lesser than the ratio of hydroxyapatite (1.67), still this did not affect the bioactivity of these samples (as discussed in detail in detail in chapter 5).

The scanning electron microscopic graphs with the increased spherical particular growth over the surface of prepared tartaric and citric acid based cement samples can be directly referred with energy dispersive x-ray spectroscopy analysis. However, the spherical particles contained high intensity of calcium, strontium and phosphate with the decrease in intensity of Si ions can possibly be correspond to the formation of carbonated hydroxyapatite layer in 7th and 14th day analysis respectively.

Likewise, after scanning electron microscopic analysis the energy dispersive x-ray spectroscopy analysis was also conducted over the obtained glass flake based samples. The presence of calcium, sodium, magnesium and silica ions in the composition was observed. as shown in following Figure 58.



Figure 58: Micrograph of Leeds glass flakes Ltd UK based silicate glass sample composition energy dispersive x-ray spectroscopy (EDS) analysis.

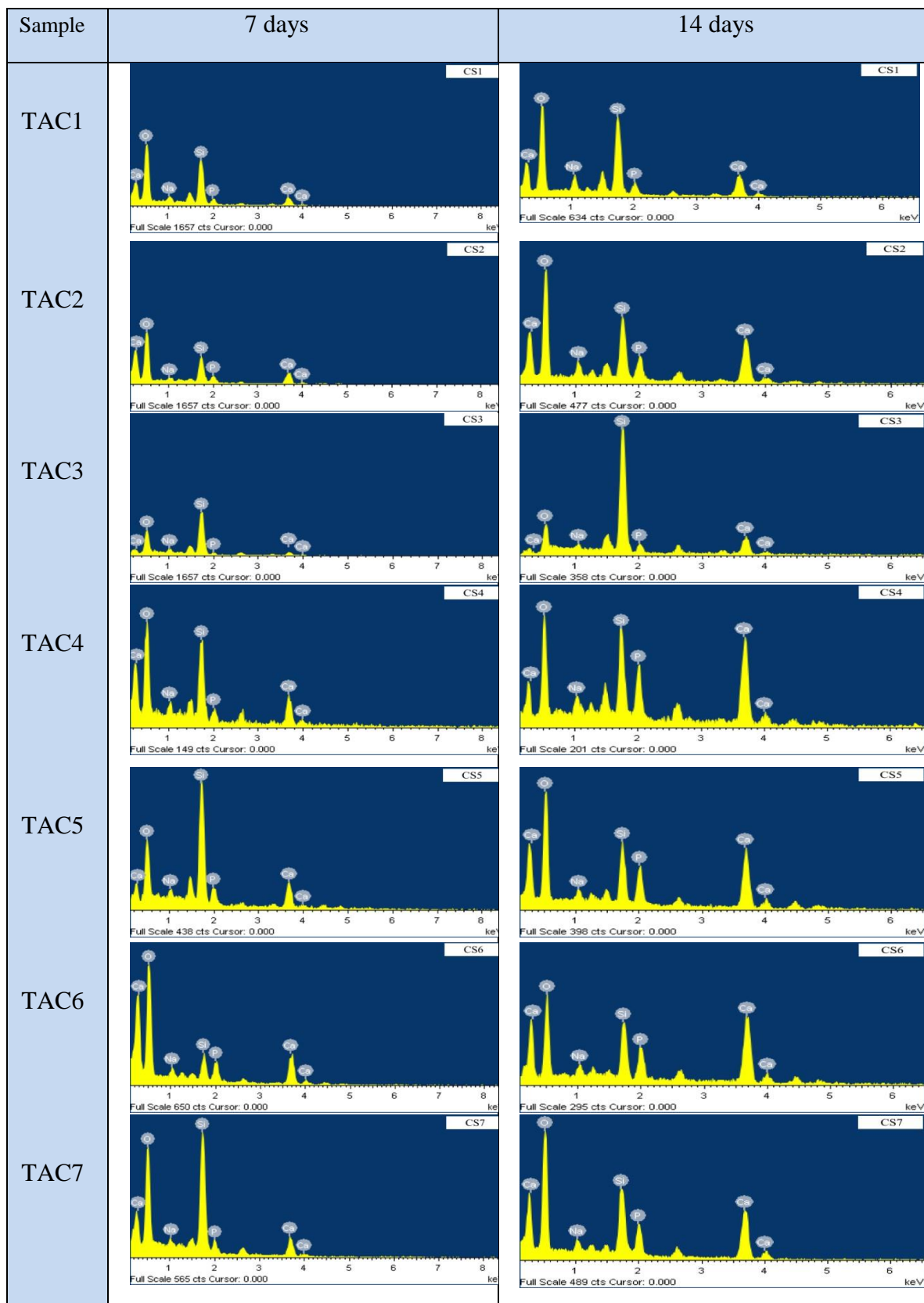


Figure 59: Micrographs of tartaric acid based cement samples (TAC1-7) EDS analysis for 7th and 14th day after immersion in c-SBF respectively.

Table 10: Calcium and phosphate ratio of tartaric acid based cement samples after 7th and 14th days of immersion in conventional stimulated body fluid solution (c-SBF).

Samples TAC	Calcium / Phosphate ratio	
	7 days	14 days
TAC1	1.69	1.72
TAC2	1.46	1.51
TAC3	1.54	1.58
TAC4	1.72	1.74
TAC5	1.72	1.75
TAC6	1.74	1.82
TAC7	1.74	1.85

Table 11: Calcium and phosphate ratio of cement samples after 7th and 14th days of immersion in conventional stimulated body fluid solution (c-SBF).

Samples CAC	Calcium / Phosphate ratio	
	7 days	14 days
CAC1	1.72	1.82
CAC 2	1.77	1.89
CAC 3	1.79	1.89
CAC 4	1.80	1.92
CAC 5	1.81	1.94
CAC 6	1.82	1.95
CAC 7	1.86	1.97

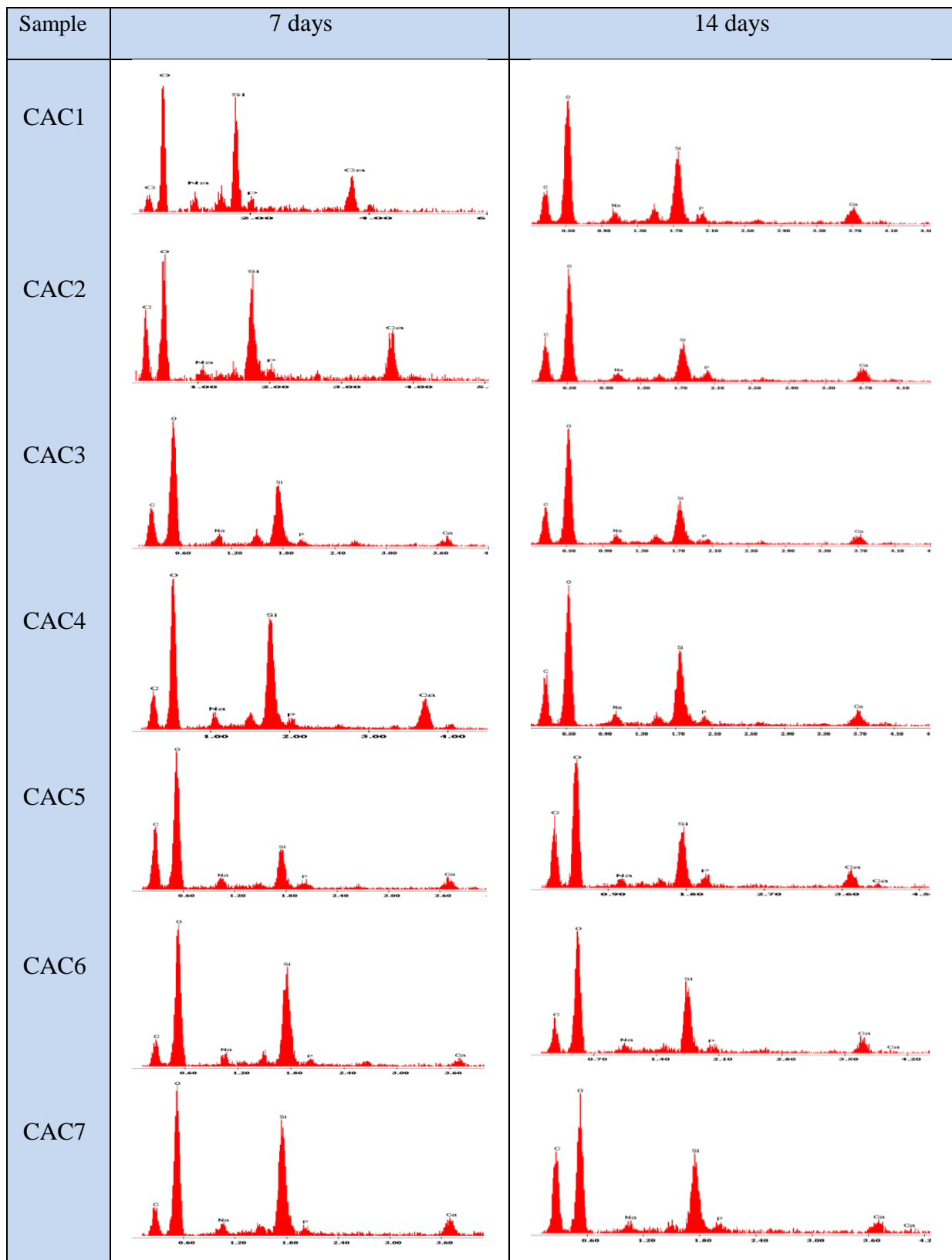


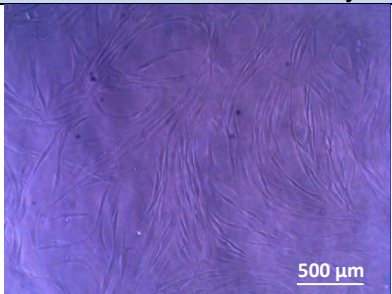
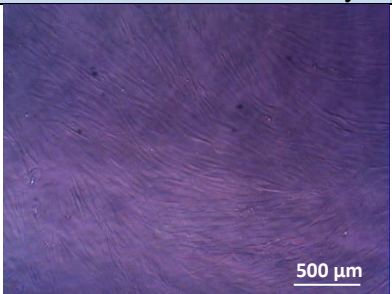
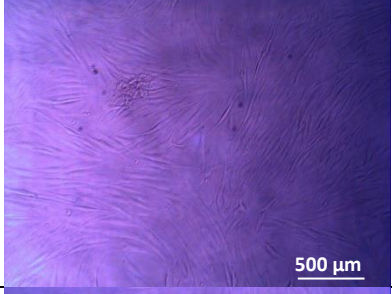
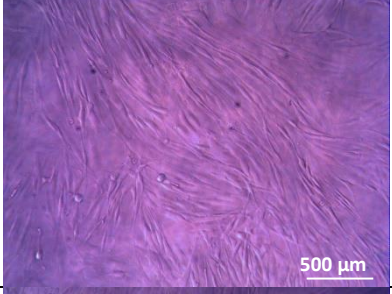
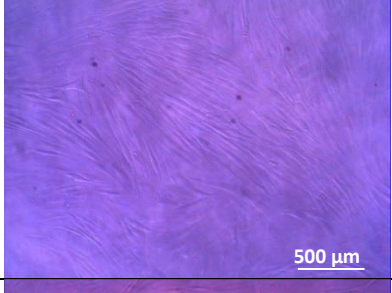
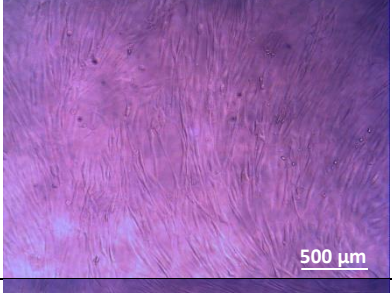
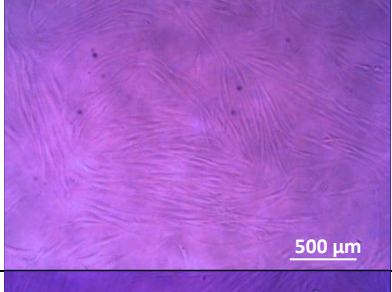
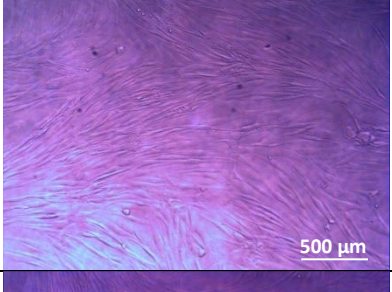
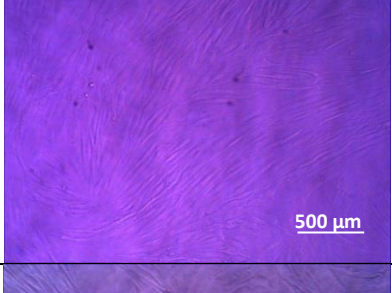
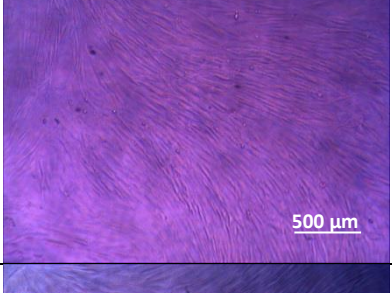
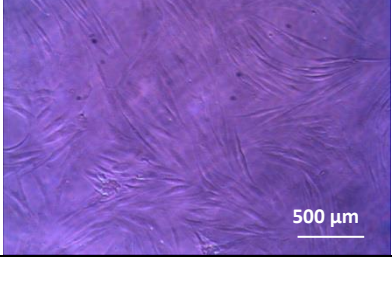
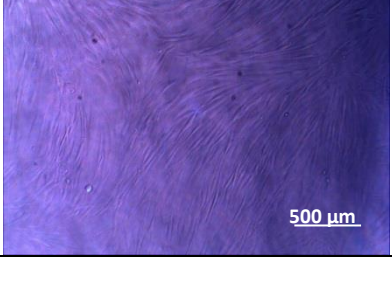
Figure 60: Micrographs of citric acid based cement samples (CAC1-7) EDS analysis for

7th and 14th day after immersion in c-SBF respectively.

4.4.4.2 *In- vitro* biocompatibility analysis

4.4.4.2.1 MTT assay and statistical analysis of glass and cement samples

Before conducting MTT assay, the growth of cultured cells in 24 well tissue culture plate in the presence of prepared silicate based glass samples (BG 1-7) and immersed medium from the prepared cement samples were observed microscopically for 24 and 48 hours independently. The proliferation of oral fibroblasts was observed on the surface of the glass samples in contact with the conditioned media inside the wells of tissue culture plate. However, the control group (positive) was also assessed as shown in following Figure 61. The increased cellular attachment and their proliferation were noticed in strontium, barium and fluoride substituted silicate based bioactive glass samples in 48 hours in comparison with 24 hours respectively.

Samples	24 hours before MTT assay	48 hours before MTT assay
Control (positive)		
BG1		
BG2		
BG3		
BG4		
BG5		

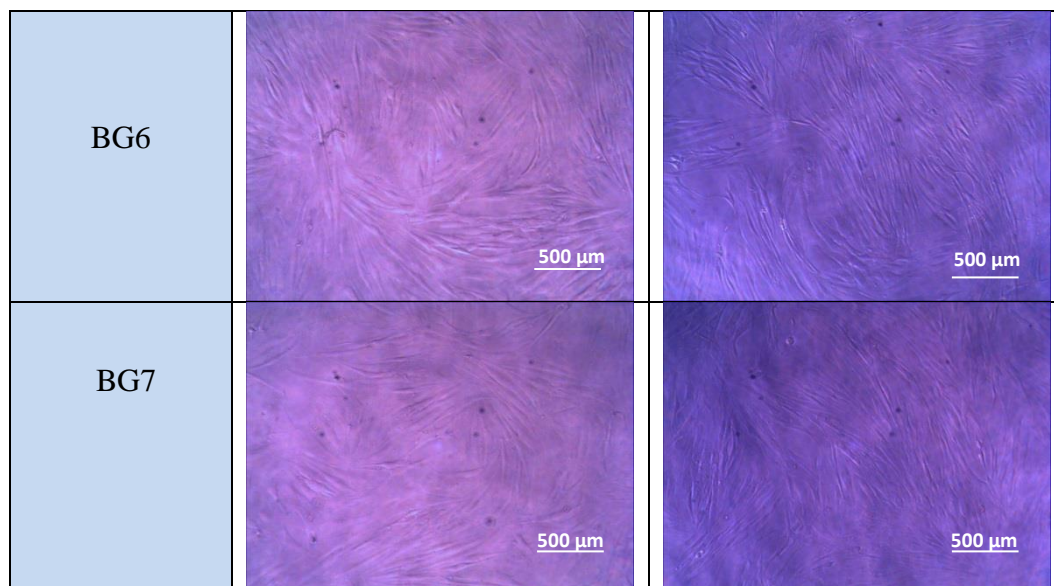


Figure 61: Microscopically images of oral human fibroblasts over tissue cultured plate before MTT assay (BG 1-7) including control sample.



Figure 62: Photographical image of 96 well plates before MTT assay for 24 hours. The presence of purple colour in assigned wells indicates the microchondrial activity of cell.



Figure 63: Photographical image of 96 well plates before MTT assay for 48 hours. The presence of purple colour in assigned wells indicates the microchondrial activity of cell.

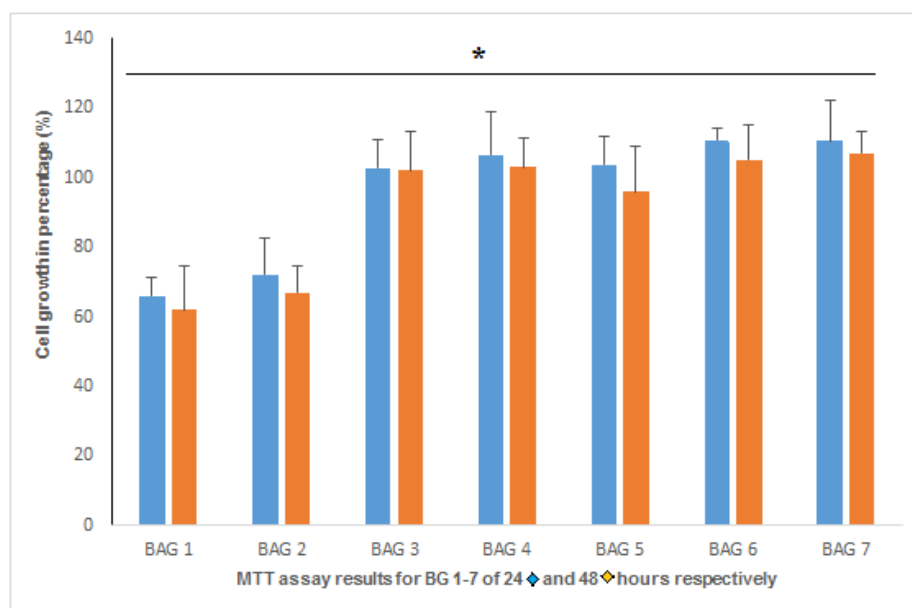


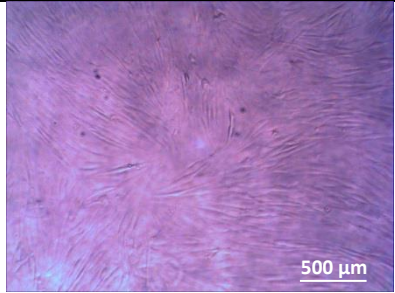
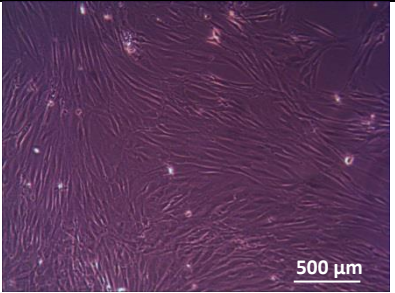
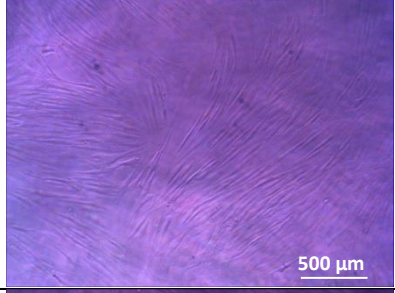
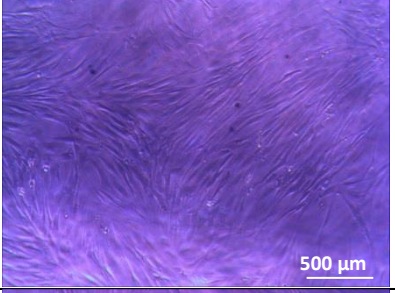
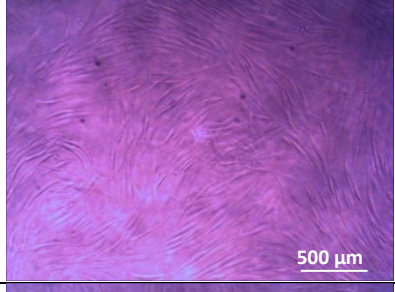
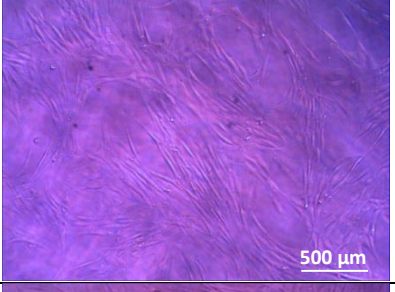
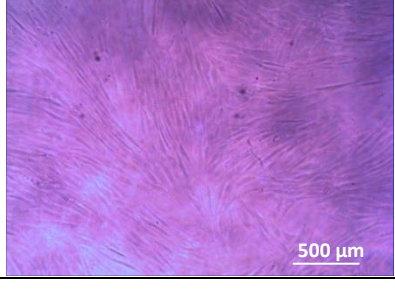
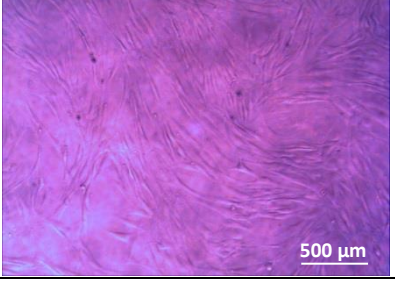
Figure 64: Graphical illustration of MTT assay results showing in vitro biocompatibility analysis of all produced silicate based bioactive glass series (BG 1-7) between 24 hours and 48 hours samples with ANOVA (significant difference * $p < 0.05$). Data represents mean \pm SD (n=3). The introduction of substitution including strontium and fluoride ions

into BG 2-7 samples allowed more cell growth after culturing for 24 hrs and 48 hrs with respectively.

For the further evaluation of mitochondrial activity of the cultured oral human fibroblasts after immersion of samples (BG 1-7) in prepared medium for 24 and 48 hours the MTT assay was performed, as shown in Figure 62 and 63 respectively. Whereas, the presence of purple colour indicates mitochondrial activity of the cells. Similarly, the obtained results for 24 and 48 hours' study were significantly analysed as well as indicated in Figure 64 respectively. Obtained results indicates that, there is significant differences ($p < 0.05$) and increase in cellular growth that has calcium substitution with strontium, and fluoride ions, in comparison with parent composition BG1 as shown in Figure 64. Similarly, it was observed that, MTT analysis of BG 2-7 samples indicated increased cellular growth for both 24 and 48 hours. This merely indicates that the calcium substitution with strontium and fluoride in parent composition may create favourable effect with respect to cellular proliferation and their attachment.

Moreover, before performing MTT assay over cultured oral human fibroblasts cells in 24 well plates, biocompatibility of prepared tartaric and citric acid based glass ionomer cement samples TAGIC / CAGIC (1-7), in the presence of immersed medium was examined carefully under the light microscope with 500 μm magnification ranged for both 24 and 48 hours, as indicated in following Figure 74 and 78 respectively. Whereas, the photographic images of 24 well plates of both 24 and 48 hours for TAGIC / CAGIC (1 – 7) samples exhibit mitochondrial activity of the cells (in purple) as indicated in Figures 66 – 67 and 70 – 71 respectively. However, the

control group (positive) was also introduced. The increased cell attachment and their proliferation were noticed in strontium and fluoride ions substituted silicate based bioactive glass ionomer cement samples in 48 hours in comparison with 24 hours and were statistically analysed by using one-way ANOVA as shown in following Figures 68 and 72 respectively.

Samples	24 hours before MTT assay	48 hours before MTT assay
Control (positive)		
TAGIC 1		
TAGIC 2		
TAGIC 3		

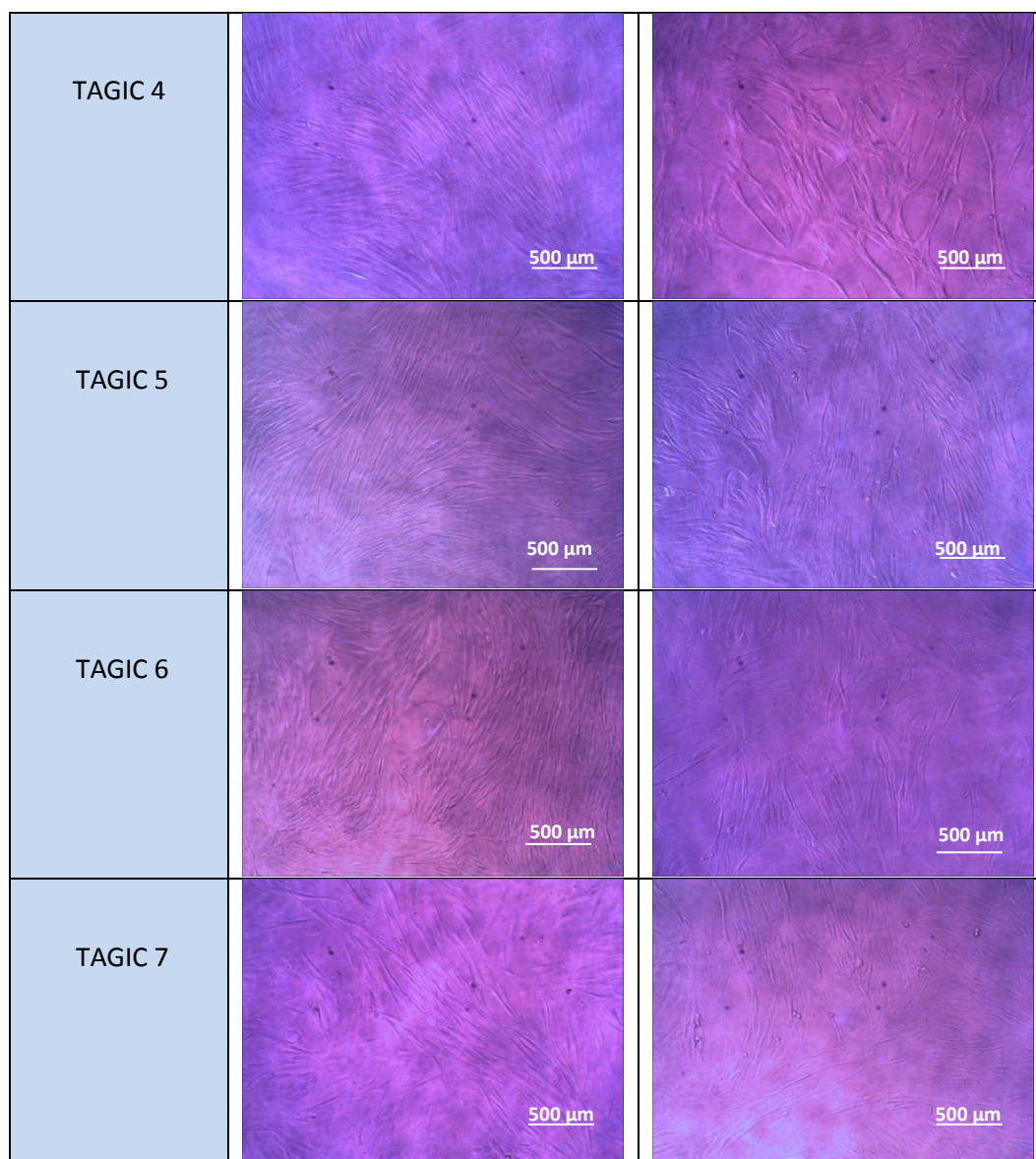


Figure 65: Microscopically imaged oral human fibroblasts over tissue cultured plate before MTT assay with tartaric acid based glass ionomer cement samples (TAGIC 1-7) including control sample.

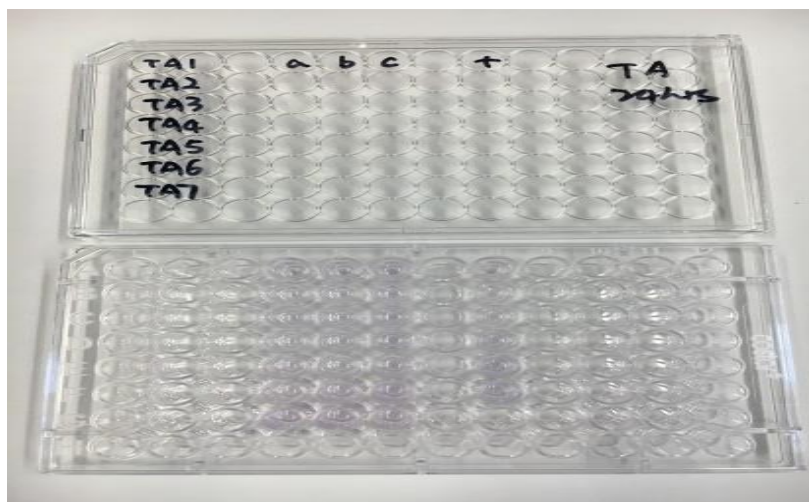


Figure 66: Photographical image of 96 well plates before MTT assay for 24 hours of tartaric acid based glass ionomer cement samples (TAGIC 1-7) respectively. The presence of purple colour in assigned wells indicates the microchondrial activity of cell.



Figure 67: Photographical image of 96 well plates before MTT assay for 48 hours of tartaric acid based glass ionomer cement samples (TAGIC 1-7) respectively. The presence of purple colour in assigned wells indicates the microchondrial activity of cell.

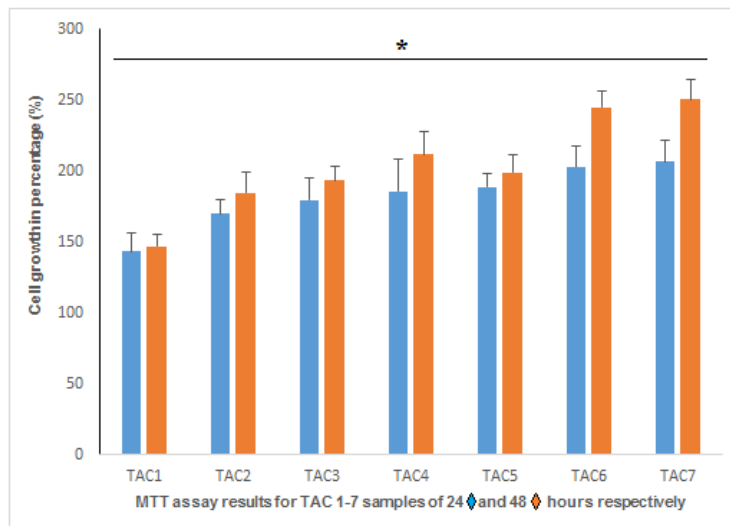


Figure 68: Graphical illustration of MTT assay results showing in vitro biocompatibility analysis of tartaric acid based cements (GIC TA 1-7) between 24 hours and 48 hours samples with ANOVA (*p < 0.05 significant different) and data represents mean ± SD (n=3). In 48 hours more cell growth observed as compared to 24 hours respectively.

Sample	24 hours before MTT assay	48 hours before MTT assay
Control (positive)		
CAGIC 1		

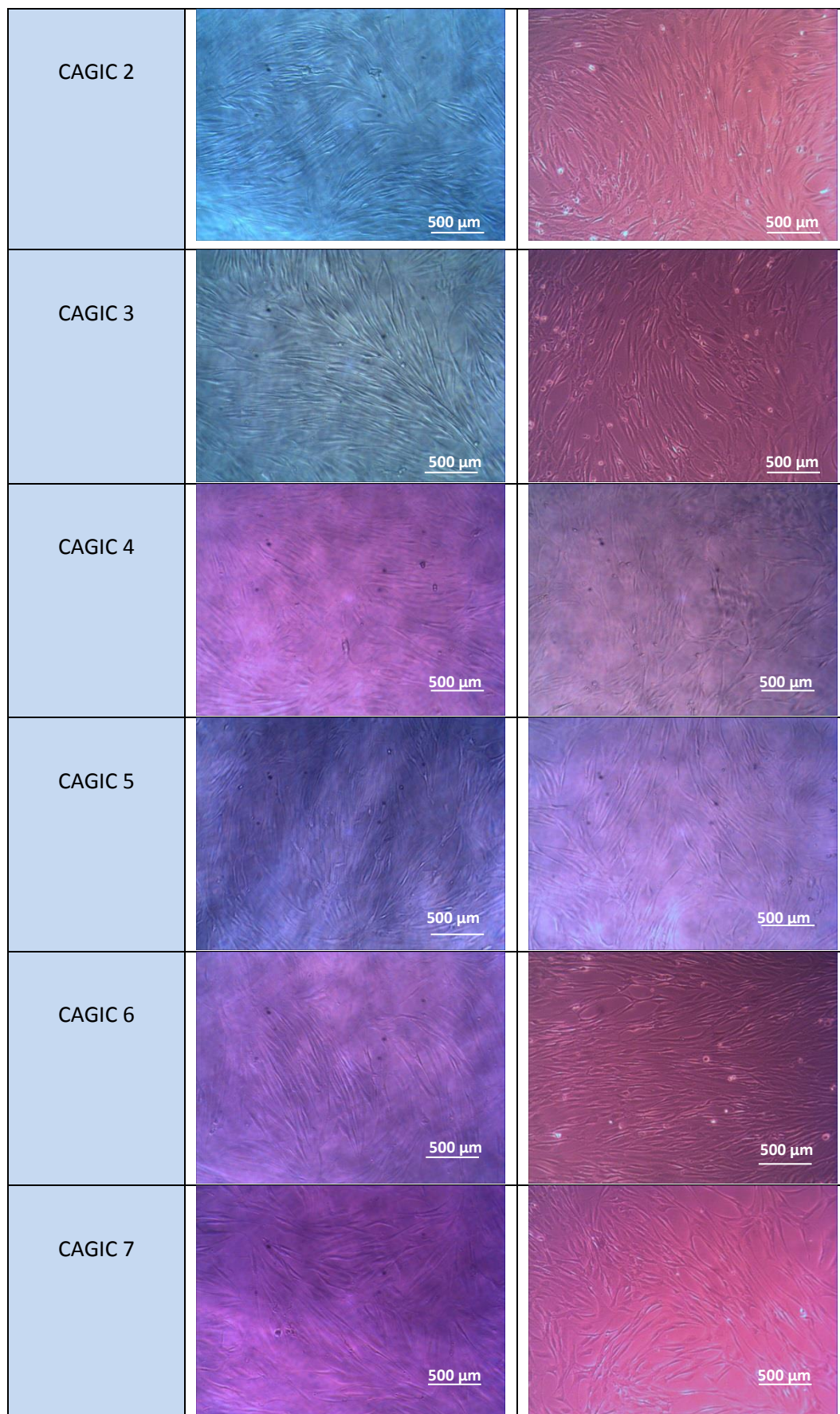


Figure 69: Microscopically imaged oral human fibroblasts over tissue cultured plate before MTT assay with citric acid based glass ionomer cement samples (CAGIC 1-7) including control (positive) sample.



Figure 70: Photographical image of 96 well plates before MTT assay for 24 hours of citric acid based glass ionomer cement samples (CAGIC 1-7) respectively. The presence of purple colour in assigned wells indicates the microchondrial activity of cell.

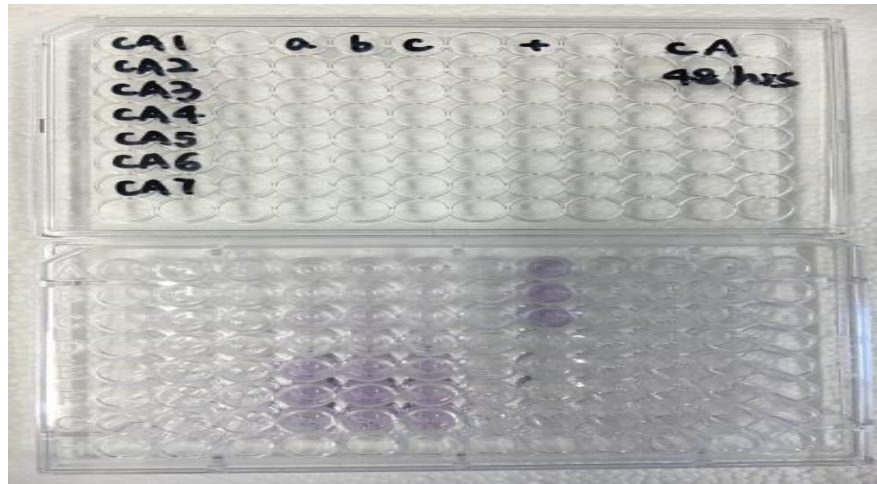


Figure 71: Photographical image of 96 well plates before MTT assay for 48 hours of citric acid based glass ionomer cement samples (CAGIC 1-7) respectively. The presence of purple colour in assigned wells indicates the microchondrial activity of cell.

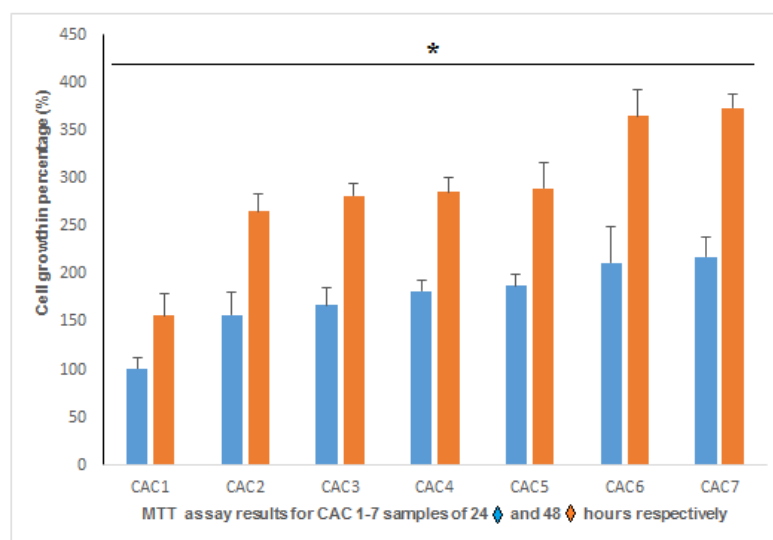


Figure 72: Illustration of MTT assay results showing in vitro biocompatibility analysis of citric acid based cements (GIC CA 1-7) between 24 hours and 48 hours samples with

ANOVA (*p <0.05 significant different). Data represents mean \pm SD (n=3). In 48 hours more, cell growth observed as compared to 24 hours.

Moreover, the obtained company based glass flake samples from Leeds glass flake company Ltd; UK were analysed for the further evaluation of their biocompatibility. The decreased cellular responses were observed in 48 hours study in comparison with 24 hours and positive control as shown in following Figure 73. However, this indicates the possible leaching of ions such as titanium, zinc, aluminium and boron into the medium which potentially created the unfavourable environment for normal cellular growth and their further proliferation.

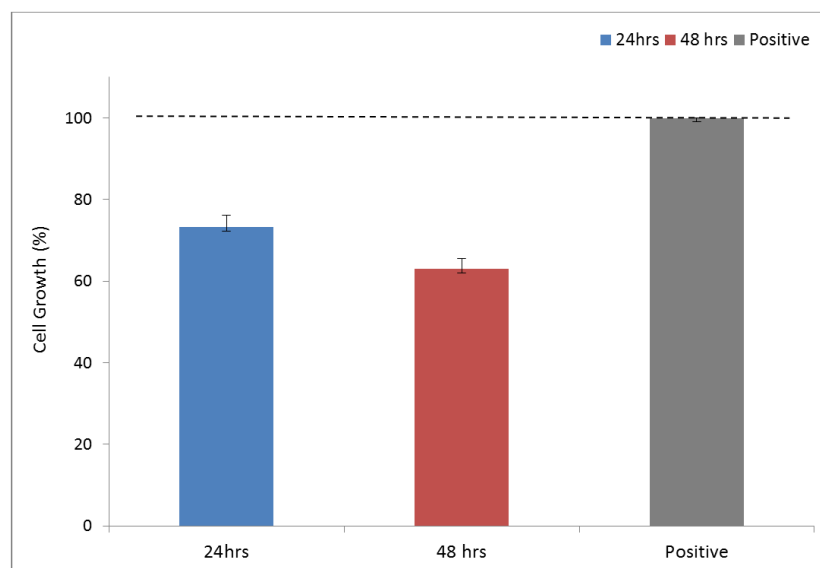
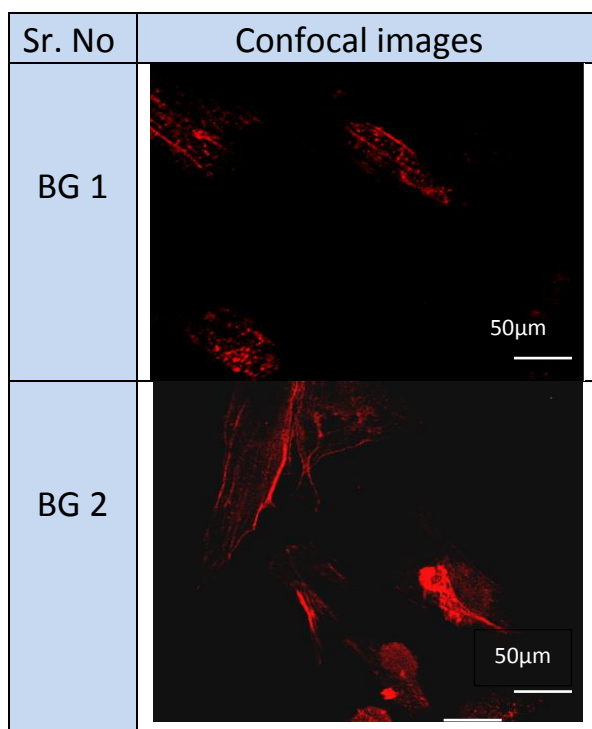


Figure 73: Illustration of MTT assay reading of obtained glass flakes from Leeds glass flakes company Ltd, UK for 24 and 48 hours' study over tissue cultured plate with immersed medium indicating decreased in cellular respond in 48 hours of study.

4.4.4.2.2 Confocal microscopy of bioactive glass samples

For the further evaluation of the attachment of cells (oral human fibroblasts) and their proliferation over the surface of all produced silicate based bioactive glass ionomer samples (BG 1-7) after 24 hours of culture, the confocal microscopy technique was utilised as indicated in following Figure 74 respectively. However, the increase in cellular attachment and their proliferation were noticed over the surface of prepared glass sample BG 2-7 as compared to BG 1 through the presence of red coloured actin fibres, possibly due to the calcium substitution with strontium and fluoride ions in composition correspondingly.



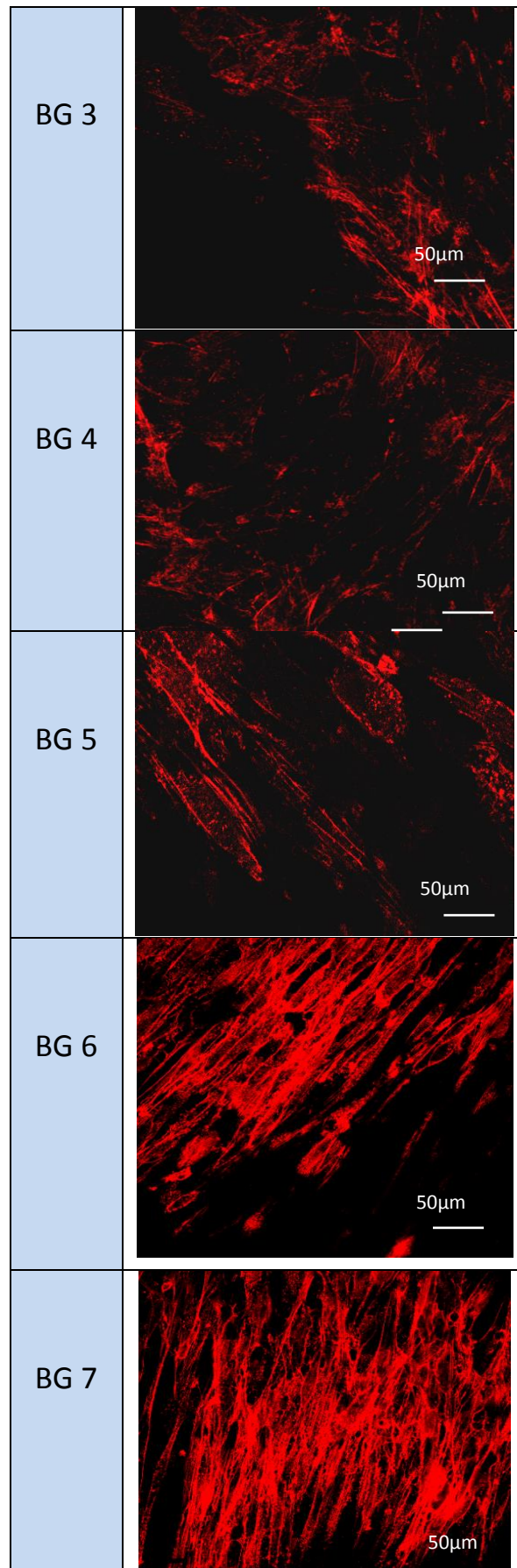


Figure 74: Confocal images for in vitro biocompatibility analysis of all produced silicate based bioactive glass series (BG 1-7) for 24 hours. However, in BG 6 and 7 indicates more cellular attachment was observed. It may be due to increased substitution of strontium ions into the parent composition.

4.4.5 Mechanical characterisations

4.4.5.1 Compressive strength and statistical analysis

The all prepared silicate based bioactive glass ionomer cement samples with the admixture of poly-acrylic, tartaric and citric acid in the presence of water were analysed mechanically by adopting compressive strength technique. The obtained results were expressed in graphical illustration as shown in following Figure 75 respectively. However, it was observed that citric acid based glass ionomer cement samples exhibit better compressive strength than tartaric acid based glass ionomer cement samples. Similarly, the obtained results were further statistically analysed by using one-way ANOVA T-test ($*p < 0.05$) significant differences were observed among both tartaric and citric acid based ionomer cements, as indicated in following Figure 75 respectively.

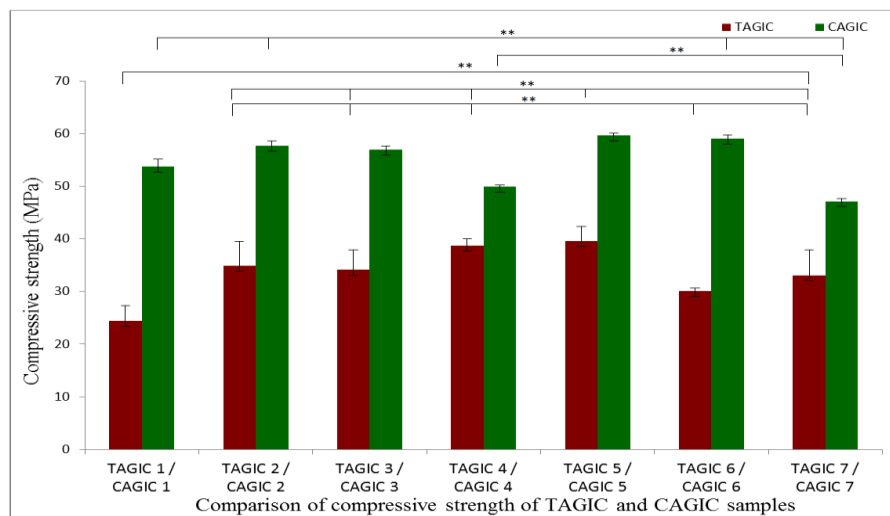


Figure 75: Compressive strength results between tartaric and citric acid glass ionomer cement samples (TAGIC/CAGIC 1-7). CAGIC samples has a higher compressive strength, However, ** indicates comparison between non significantly different TA & CA GIC samples within the same groups ($p \leq 0.05$).

Moreover, the obtained glass flakes from Leeds glass flakes company Ltd UK were mixed with tartaric and citric acid in the presence of poly-acrylic acid and water and then samples were produced and analysed mechanically as well. However, it was observed that, the 100 nm sized glass flakes exhibit decreased compressive strength (5Mpa) than the 100 μ m milled (15Mpa) in the presence of citric acid as setting modifier as shown in following Figure 76. Similarly, when the 100nm sized same batch of glass flakes were mixed with tartaric acid as setting modifier, increase in compressive strength (15Mpa). Whereas, the 100 nm and 350 nm sized glass flake based samples demonstrated decreased compressive strength (5Mpa) as indicated

in following Figure 77. All obtained results were statistically analysed for $*p < 0.05$ significant differences by using one-way ANOVA and expressed in graphical representations as shown in following Figure 76 and 77 respectively.

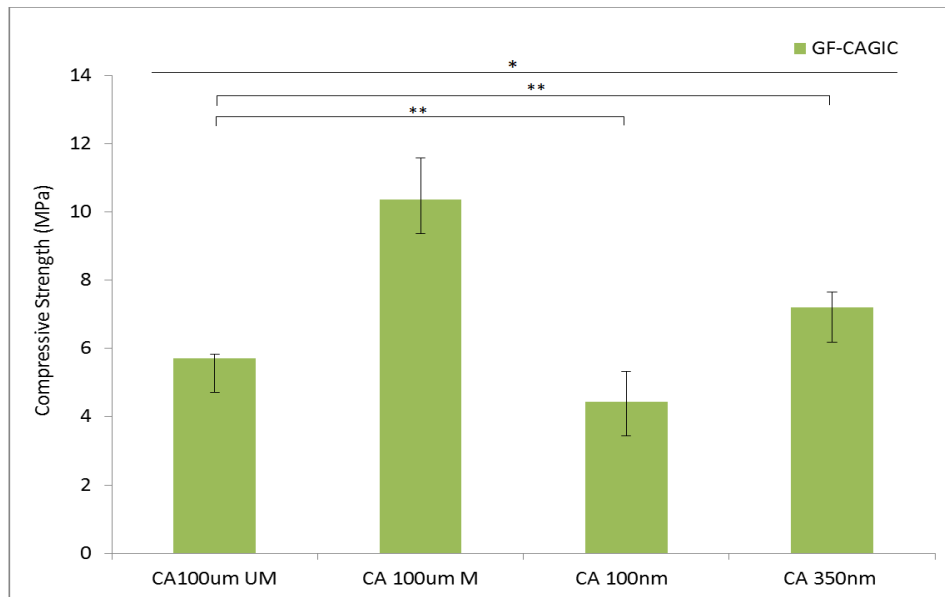


Figure 76: Compressive strength results showing comparison of different sized glass flakes upon with the admixture of citric acid. Statistical analysis results indicate (*) significant difference $< p 0.05$ and () indicates comparison between non significantly different samples within the same group.**

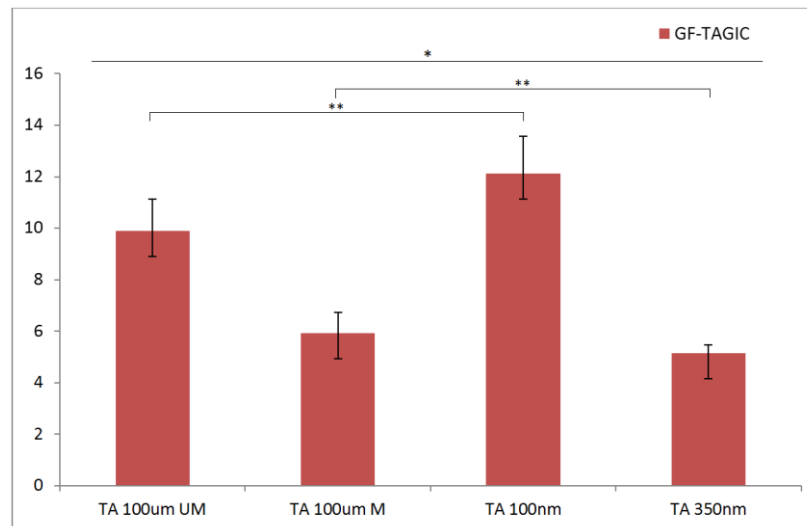


Figure 77: Compressive strength results showing comparison of different sized glass flakes upon with the admixture of tartaric acid. Statistical analysis results indicate (*) significant difference $< p 0.05$ and () indicates comparison in between non significantly different samples within the same group.**

4.4.5.2 Gilmore needle test

4.4.5.2.1 Tartaric acid based cement samples

All produced silicate based bioactive glass ionomer cement after the admixture of poly-acrylic acid and tartaric acid in the presence of water were freshly mixed individually and tested by using Gilmore needle test for the determination of their working and setting times respectively.

However, working and setting time of all prepared cement samples based on tartaric and citric acid were represented in graphs as shown in following Figures 78 and 79 correspondingly. This test has been conducted from decades for the evaluation of setting and working times of the resultant cement according to British standard (BS 6039:1981). Similarly, it was observed that, all produced series of cement samples TAGIC 1-7 were found to form cement individually. Whereas, all cement samples were experiential to be workable up to 3.5 minutes and also, they can potentially be able to set within 6 to 7 minutes as described in following Table 12. Moreover, all obtained results were determined at $23 \pm 1^\circ \text{C}$ and the arithmetic mean of 6 individual measurements with the error indicates ± 1 standard deviations individually as shown in following Figure 78.

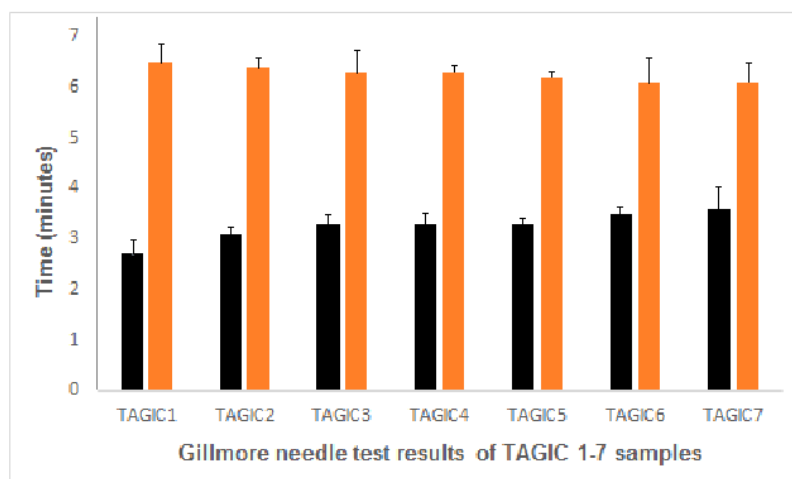


Figure 78: Comparison between working (black) and setting time (orange) of tartaric acid based cements. Tartaric acid reacts with glass component preferentially than poly-acrylic acid, as result the combination of cations like metal ions from glass and poly anion chains would be retarded.

Table 12: Comparison between working and setting time of tartaric acid based cements.

Cement samples	Working time (min)	Setting time (min)
TAGIC 1	2.7	6.5
TAGIC 2	3.1	6.4
TAGIC 3	3.3	6.3
TAGIC 4	3.3	6.3
TAGIC 5	3.3	6.2
TAGIC 6	3.5	6.1
TAGIC 7	3.6	6.1

4.4.5.2.2 Citric acid based cement samples

All produced silicate based bioactive glass ionomer cement samples were freshly mixed individually in the presence of poly-acrylic and citric acid as setting modifier and water. However, all prepared citric acid based cement samples were tested by using Gilmore needle test for their working and setting times respectively. Whereas, it was observed that, all produced series of cement samples CA GIC 1-7 were found to form cement independently. Similarly, all cement samples were experiential to be workable up to 3.5 minutes and also they can potentially be able to set within 2 to 3 minutes as described in following Table 13. Similarly, obtained results were determined at $23 \pm 1^\circ \text{C}$ and the arithmetic mean of 6 individual

measurements were taken with error indicates ± 1 standard deviations individually as shown in following Figure 79 respectively.

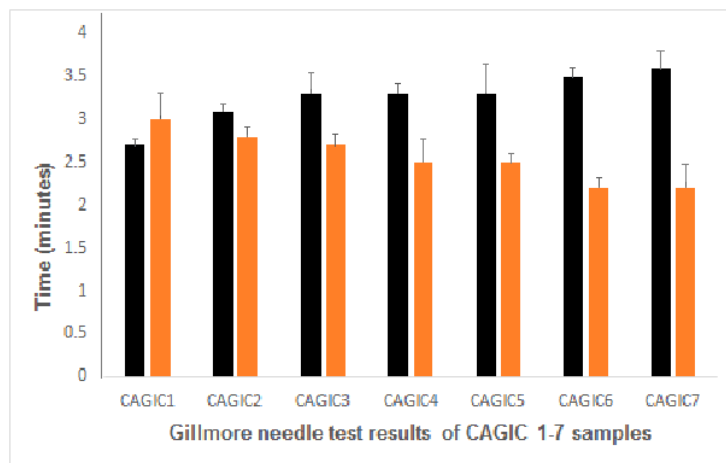


Figure 79: Comparison between working (black) and setting (orange) time of citric acid based cements. Citric acid has higher acidity than tartaric acid and it exhibited greater ability to reduce setting time than tartaric acid. In hardening stage, citric acid is able to bind metal ions preferentially and tightly, thus setting time was decreased greatly.

Table 13: Comparison between working and setting time of Citric acid based cements.

Cement samples	Working time (min)	Setting time (min)
CAGIC 1	2.7	3.0
CAGIC 2	3.1	2.8
CAGIC 3	3.3	2.7
CAGIC 4	3.3	2.5
CAGIC 5	3.3	2.5

CAGIC 6	3.5	2.2
CAGIC 7	3.6	2.2

4.4.6 Summary

In this chapter after the development and production of all silicate based bioactive glass samples (BG 1-7) that has calcium substituted with strontium, barium and fluoride (SrF_2 , BaF_2 , SrO and BaO) with 3mole % of calcium oxide (CaO) were optimised and characterised correspondingly. However, on the subject of availability of materials and crucibles (alumina) all series of glasses were batched and casted respectively. Likewise, the glass ionomer cement (GIC) samples (TA / CA GIC) with the admixture of poly-acrylic acid and water in the presence of tartaric and citric acid as setting modifier were characterised and there obtained results were analysed as well. On the other hand, all results for both silicates based bioactive glass samples and ionomer based cement samples were characterised and analysed on the basis of their developed properties for instance physical (XRD, density measurements (Pycnometer and Archimedes), contact angle and BET), chemical (FTIR and Raman), thermal (DTA), mechanical (compressive strength and Gilmore needle test) and *in vitro* biological (bioactivity and biocompatibility) respectively.

It has been observed from the obtained results that, because of the similarity of calcium ions in terms of ionic radius and charge, strontium and barium can be substituted and exhibit same role into glass network. There is low charge ratio with the size of strontium ions (large ionic radius)

as compared to calcium ions, that can create extended and more freely cross-linked glass network without altering the fundamental glass structure. Likewise, the idea of introducing glass flakes as filler content into the composition will only be beneficial, after the consideration of its aspect ratio. It is evident from the literature review that, smaller size glass flakes of 0.1 to 1 μ m have inherent potential of self-alignment and anisotropic shrinkage. As a result, smooth and even surface of restoration will be achieved. To accomplish this part of project this part of the project and to produce glass flakes (0.1 to 1 μ m), the collaboration with Leeds Glass Flake Company Ltd UK (as details mentioned in appendix) for making glass flakes on produced and selected series of composition was established. However, as part of our contract we characterised and analysed the obtained glass flakes from company based on their physical, chemical, mechanical and *in vitro* biological techniques. Moreover, in the next chapter of discussion all obtained results will be discussed in detail along with their appropriate reference from available literature review.

Chapter 5: Discussion

5.1 Introduction

In this chapter, the obtained results after the characterisation of all produced series of silicate based bioactive glasses and prepared ionomer cement samples with the introduction of different setting modifiers tartaric and citric acid are presented and discussed on the basis of their physical, chemical, thermal, mechanical and *in vitro* biological properties with close reference to the relevant available appropriate literature presented in Chapter 2.

5.2 Glass and cement characterisation

5.2.1 Physical characterisation

5.2.1.1. X-ray diffraction analysis

The produced silicate based calcium substituted bioactive glasses (BG 1-7) with strontium, barium and fluoride with 3 mole % calcium oxide in 45S5 based bioactive glass composition, and all obtained glass flake samples from Leeds Glass Flake Company Ltd UK, were x-ray diffracted for the determination and existence of any amorphous and crystalline phases. X-ray diffraction analysis is an effective and non-destructive technique, used previously for the phase determination of phospho-silicate glasses and the effect of various substitutions on its lattice structure such as strontium, barium, magnesium, iron and zinc (Brauer et al. 2010;

Fredholm et al. 2010; Gomes et al. 2013; Santocildes-Romero et al. 2015).

Results obtained from the manufactured bioactive glasses (BG 1-7) and glass flakes from Leeds glass flakes company Ltd; UK indicate the presence of an amorphous non-crystalline structure, as shown previously in Figure 36 and 37. However, the diffractograms of all silicate based bioactive glass samples indicate the presence of amorphous halo present between 25° to $35^{\circ} 2\theta$ angle and its shifting towards lower 2θ angled values. The larger 2θ angle designates the minimum distance from central atoms. This is the characteristic feature of all traditionally available bioactive glasses, especially those without any substitutions. It is known that the ionic radii of strontium, barium and calcium are 1.16 \AA , 1.35 \AA and 0.94 \AA respectively. As more strontium and barium was substituted with calcium ions, the average spacing within the basic glass structure increased noticeably due to the larger size of cations. Thus the obtained spectra moved towards smaller 2θ angled values (Boyd et al. 2008b; Brauer et al. 2010; Fredholm et al. 2010; Gomes et al. 2013; Santocildes-Romero et al. 2015).

5.2.1.2. Contact angle measurement

Water contact angle measurement analysis over the surface of silicate based bioactive glass samples provides evidence that indicate the drastic changes in physical properties such as increased specific volume, thermal expansion and decrease in viscosity. In addition, an increased effect of the relaxation rate of crystal lattice structure, decreased fatigue resistance and mechanical properties were also determined by this technique. It has previously been noted

that the density, thermal coefficient of expansion and refractive index can be enhanced due to a decrease in surface tension of glass samples (DeRosa et al. 2003). When a drop of water comes into contact with the surface of silicate based bioactive glasses, the following indicated five processes have been found to occur: Dissolution - non-preferential or superior surface dissolution of glass starts to occur with the first water contact.

- a) Exchange of alkali ions - due to the presence of water, hydrogen ions are released and an exchange of alkali ions occurs.
- b) Hydration - the process of hydration starts due to the diffusion and exchange between the water ions and glass particles.
- c) Production of reacted layer - the formation of a reacted layer over the surface of glass occurs as a by-product of chemical reaction.
- d) Hydrolysis- Finally, due to the reaction between the silicon – oxygen ionic network, the process of hydrolysis happens.

Additionally, many researchers have found that, the behaviour of silicate based bioactive glasses in aqueous environments is directly related to the composition of the glass itself. For instance, alkali ion based bioactive glasses exhibit two different stages of behaviour when they are exposed to hydrous environments. In the first stage, de-alkalisation of the surface occurs due to exchange of ions of hydrogen with alkali ions. Secondly, the dissolution of hydroxyl ions initiates because of the breakdown of Si – O – Si bonds. Perera and Doremus suggested that, due to continuous expansion and shrinkage process of the surface layer, pits and pores

start to develop slowly. However, this helps to create a positive environment which can enhance the hydrophilic nature of glass to be used in biomaterials (DeRosa et al. 2003).

Likewise, the wettability of the superficial surface layer in biomaterials plays a significant role in terms of its effects on the adsorption of proteins, attachment of cells and their proliferation.

The water contact angle of the produced series of silicate based bioactive glass samples (BG 1-7) was studied under theoretical limit (65°) between hydrophilic and hydrophobic ranges (Duce et al. 2013; Grenade et al. 2016), as shown in Figure 38. In this study, distinct differences were observed between all produced silicate based bioactive glass samples from BG 1-7, which reveals the strong relation of surface chemistry. The gradual increase in hydrophilic nature of all silicate based bioactive glasses from BG 2 – 7 indicates that, substitution of larger ionic radius elements, such as strontium and barium along with fluoride, can potentially alter the surface chemistry of the developed material. As a result, this can initiate favourable effects by increasing hydrophilicity rather than hydrophobicity. Enhanced hydrophilicity leads to increased cellular attachment and proliferation (Duce et al. 2013).

Furthermore, several authors have indicated that the wettability of a material has a great impact on the cell's behavioural properties. For example, hydrophilic surfaces $< 65^{\circ}$ have more favourable effect than hydrophobic surfaces $> 65^{\circ}$ on cellular attachment, their proliferation and growth, and also the organisation of the cytoskeleton (Schulz et al. 2012; Zheng et al. 2015; Grenade et al. 2016). (Zheng et al., 2015, Grenade et al., 2016, Schulz et al., 2012). However, Hollinger and Guelcher reported that an increased hydrophilicity of the surface of polymers

can decrease their protein binding ability whereas, hydrophobic surfaces can increase the binding ability of non-adhesive proteins such as albumin (Hollinger, 2011; Grenade et al. 2016).

It is also evident from previous literature that an increase in water contact angle is related to adsorption of carbon contents over the surface of the material. The adsorption of a carbon layer can be accredited to organic impurities such as atmospheric hydrocarbons (Schulz et al. 2012; Noro et al. 2013). Moreover, this adsorption is directly related to surface properties, micro and porous structures, atmospheric characteristics and the time of exposure for an individual specimen. These factors highlight the understanding of the typical behaviour and influence of material over cellular growth (Noro et al. 2013; Grenade et al. 2016).

The presence of silicon in the composition is considered as an essential factor for the development of normal cartilages and bones. As silicon ions can increase bioactivity and biocompatibility of any material (Qian & Liu 2015). Priya et al and Duee et al also suggested that the presence of silicate and sodium ions in the composition play a significant role in the determination of osteointegrative properties of an implant material. Due to changes in surface characteristics, an accelerated rate has been observed in the adhesion and proliferation of osteoblasts or bone forming cells (Lampin et al. 1997; DeRosa et al. 2003; Duee et al. 2013; Kalia et al. 2016).

5.2.1.3. Density measurement

For further physical analysis of all produced series of silicate based calcium substituted bioactive glass samples (BG 1-7) with strontium and barium, density measurements were performed by adopting both Archimedes and pycnometer characterisation techniques. Previously, the effects after substitution of larger cations, such as zinc and magnesium along with their potential change in structural properties, with several bioactive glasses were studied experimentally. A consistent and similar change in density after calcium substitution with strontium and barium ions can be observed from the obtained results by both Archimedes and pycnometer analysis with respect to parent 45S5 based bioactive glass composition (Doweidar 1999; Xiang & Du 2011).

Doweidar (1996) postulated that, in alkaline based silicate glasses, the volume of Q^n units is related to the presence of alkali ions in the substituted compositions. The complete addition or partial substitution of larger cationic radii elements can create the drastic change over the basic glassy structural network. This is due to the expansion of basic glass and less rigid bonded glass network because of the presence of larger cations like strontium and barium, which can be more readily attracted towards non-bridging oxygen (NBO) atoms than calcium cations (Doweidar 1996; Fredholm et al. 2010; Xiang & Du 2011).

However, Xiang et al indicated that the substitution of larger and heavier ion barium and strontium for calcium can create a consistent linear and increased change in the density of glass.

Similarly, the theoretical calculated density for the in house copy of 45S5 based bioactive glass was recorded as 2.63 g/cm². After the calcium's substitution with strontium and barium, the change was noticed between a range from 2.76 – 2.78 g/cm² as shown in Figure 39 and Table 8 (Doweidar 1999; Xiang & Du 2011). These physical structural changes were also correlated and observed in the obtained x-ray differential (XRD) analysis, as shown in Figure 36.

5.2.1.4. Particle size analyses

In order to conduct quantitative analysis of particle sizes of all produced powdered silicate based bioactive glass samples (BG 1-7) after adopting the ball milling technique, they were analysed using the laser particle sized characterisation technique, as shown in Figure 40 and Table 9. This technique is based on the principle of laser diffraction and particle interaction with the laser present in the measurement region. The dispersion of particles can be achieved by either adopting a wet (water) or dry (air) method. When the laser interacts with large particles, a smaller scattered angle is observed. Conversely, for smaller particles, a larger scattered angle is observed. The detector is able to collect data from several scattering angles and create a volume of distribution (Ma et al. 2000). Particle size analysis is important for the determination of differently shaped and sized particles for the analysis of improved mechanical and aesthetic properties of resultant glass ionomer cement. This is a complementary technique with scanning electron microscopic analysis (SEM) for the observation of different shapes and sizes of particles (Goh et al. 2013; Gomes et al. 2013a; Santocildes-Romero et al. 2015).

The particle size distribution and morphology of powdered glass also plays a vital role in the final mechanical properties of resultant cement. Dental silicate based cement with large particles (50 – 70 μm) have been found to exhibit significant degree of porosities along with compromised compressive strength of the set cement. A decrease in strength of resultant cement is also associated with the interfacial bond between glass matrixes. It has been found that larger sizes of particle can increase the interfacial bonding distance in the glass matrix (Prosser et al. 1986; Wilson 1990). In addition, larger sized filler content / particles can induce a gritty texture and unfavourable handling characteristics to the practitioner. Very fine powder can also impart detrimental properties to formed cement such as difficulty in manipulation and non-uniform structure. Thus, the distribution of similar sized particles within the cement is a fundamental factor for achieving a better quality of cement along with its related mechanical properties (Brune & Smith 1982; Singh et al. 2011).

The laser particle size results obtained in this study illustrate that all produced glass samples had a similar particle size distribution, as shown in Figure 40. Moreover, scanning electron microscopic (SEM) technique was also used to analyse the morphological characteristics of all glasses (milled and un-milled) and the obtained glass flakes of different sizes from Leeds Glass Flake Company Ltd. UK, as shown in Figure 41. As found in previous studies, the glass ‘fines’ increase the reactivity of cement by increasing the surface area, as more ions are readily available to react and release. This is eliminated in industry by the process of acid washing of cement. However, a large number of small particles can compromise the general strength of

formed cement but the presence of particles in between the range of 30 - 45 μm size can increase the strength of set cement by deflecting the crack propagation within the cement. They can also increase the availability of ions for cross-linked matrix formation and therefore can comparatively decrease the working and setting time of the resultant cement (Singh et al; Brune & Smith 1982; Shahid et al. 2014).

5.2.1.5 Brunauer-Emmett-Teller analyses

All silicate based bioactive glass samples (BG1-7) were characterised individually using Brunauer-Emmett-Teller analysis (BET) for the analysis of their surface area, as shown in Figure 42. Previous research has shown that larger surface areas (either of solids or any material) tend to help the particles interact more readily with the surrounding environment. Consequently, the higher surface area is directly related with the deposition of calcium and phosphate layer over the surface of the silicate based bioactive glass.

The obtained results show that substitution of calcium with strontium, barium and fluoride ions caused an increase in the surface area of all produced bioactive glasses as compared to the un-substituted 45S5 parent glass. Strontium and barium possess greater ionic values than calcium and phosphate in the basic glass composition. This could be a possible reason for the escalation of the surface area of all produced bioactive glasses (Sepulveda et al. 2001; Shang et al. 2010).

It is also known that the advent of bioactivity of any biomaterial with respect to the formation

of hydroxyapatite layer and its thickness is directly related to certain morphological and chemical parameters including surface area, pore volume, size and chemical composition of the glass (Sepulveda et al. 2001; Shang et al. 2010). Results from this research related to bioactivity and cell viability demonstrate an augmented cellular attachment and proliferation along with chemical changes, indicating their direct relation with the surface area of the produced glass samples.

Finally, in terms of particle size analysis, $> 45 \mu\text{m}$ sized particles exhibit a higher specific surface area and thus provide more opportunity for the ions to create a stronger matrix bond with each other.

5.2.2 Thermal characterisation

5.2.2.1 Differential thermal analysis

All silicate based bioactive glass samples (BG 1-7) were characterised and analysed using differential thermal analysis, as indicated in Figure 43. The changes in temperature were plotted against the temperature (endotherm down). The obtained differential thermal analysis traces were used for the determination of glass transition temperature ' T_g ' and the crystallisation temperature in each sample. Results indicate that the glass transition temperature value for BG 1 was higher, indicating a greater disruption in the silicate network as compared to other samples. This disruption occurred due to the presence of greater amount of network modifiers, decreasing the amount of thermal energy required for transition from

glassy state to liquid state. In addition, obtained traces revealed the presence of two discrete crystallisation exothermic events. These discrete crystallisation events could have appeared due to phase separation present in the basic glass structure which was observable in the x-ray diffraction analysis results. Crystallisation peaks represent the presence of phospho-silicate phase of glasses and all bioactive glass samples exhibited the formation of these two distinct phases (Clupper & Hench 2003; Donnell et al. 2008; Fredholm et al. 2010; Saadaldin et al. 2013; Taygun et al. 2013; Romero et al. 2015).

Furthermore, the strontium and barium based glass samples showed a gradual increase in crystallisation temperature due to the change in crystalline phase (Jones et al. 2006). This decrease in glass transition temperature evidences the mixed cationic effect in glass which may reduce the melting temperature of ionomer based glasses (Bretcanu et al. 2009; Fredholm et al. 2010). Existing research showing linear fall in glass transition temperature occurring with an increase in CaF_2 content was suggested to be due to disruption of the glassy network (Barra & Hill 2000; Clifford et al. 2001). However, Griffin and Hill also reported that a reduction in glass transition temperature occurs with an increase in phosphate content and that this causes weakening of the glass network. Similarly, it has also been shown that, strontium and barium play an identical role as calcium in both glass transition and crystalline phases of glass (Griffin & Hill 2000; Clifford et al. 2001; Fredholm et al. 2010).

5.2.3 Chemical characterisation

5.2.3.1 Fourier transform infrared (FTIR) spectroscopic analysis

All silicate based bioactive glass samples (BG 1-7) were characterised chemically, as indicated in Figure 44. The method used is FTIR spectroscopic analysis which is sensitive to changes in Si – O – Si vibrational mode and was thus ideally suited analysis of chemical and structural changes in the produced silicate based bioactive glass samples. The literature indicates that changes are predominantly seen in the fingerprint region in between 1500 cm^{-1} - 400 cm^{-1} in obtained spectra as indicated in Table 14 (Serra et al. 2002). The structure of silicate glass can be described in terms of the Q^n structured model. In this case, the single Q^n species consists of one Si^{4+} , $n/2$ bridging oxygen (BO), $4-n$ non-bridging oxygen (NBO) and alkaline earth cations $(4-n)/2$ or alkali metal ions $(4-n)$ (Fredholm et al. 2010). It was observed that peaks occurred in the region between the ranges of 415 cm^{-1} - 540 cm^{-1} related to Si – O – Si bending mode. Less intense peaks were also observed around 600 cm^{-1} in BG 5 and BG 6 glass samples, which could relate to P – O bending respectively. Presence of this peak seems simply to confirm that the produced series of silicate based bioactive glasses are basically based on a phospho-silicate structure. Si – O bending modes were also observed at the range of 700 cm^{-1} - 800 cm^{-1} . Peaks appearing in between the range of 1200 cm^{-1} - 1000 cm^{-1} can be ascribed to Si – O symmetric stretching. Si – O – 2 non-bridging oxygen (NBO) functional group (Q^2 groups) and Si – O with 1NBO per SiO_4 tetrahedron (Q^3 groups) were observed near

840 cm^{-1} and in between the range at 890 cm^{-1} - 975 cm^{-1} respectively. Presence of these groups may indicate the presence of network modifiers in the basic glass composition which can potentially disrupt the local symmetrical structure of pure vitreous silica without altering the basic glassy structure (Kim et al. 1989; Peitl et al. 2001; Serra et al. 2002; Sepulveda et al. 2002; Donnell et al. 2009; Fredholm et al. 2010).

Table 14: FTIR peak identification and their attribution with references prior to simulated body fluid solution (SBF) immersion of all prepared silicate based bioactive glass samples (BG 1-7). FTIR peak identification and their attribution with references prior to simulated body fluid solution (SBF) immersion of all prepared silicate based bioactive glass samples (BG 1-7) (Peitl et al. 2001; Serra et al. 2002; Donnell et al. 2009; Fredholm et al. 2010).

Sr No	Peaks	Peak Assignment
1	415-540 cm^{-1}	Si – O – Si bending mode
2	550-560 cm^{-1}	P – O bend
3	602 cm^{-1}	P – O bend (ν_4)
4	720 cm^{-1}	Si – O bending
5	800 cm^{-1}	Si – O (b) bending mode
6	840 cm^{-1}	Si – O – 2 NBO functional group (Q^2 group)
7	890-975 cm^{-1}	Si – O (s) with 1 NBO per SiO_4 tetrahedron (Q^3 group)
8	1200-1000 cm^{-1}	Si – O (s) symmetric stretching mode

Furthermore, the presence of carbonated species was also observed from the obtained spectrum of all produced silicate based bioactive glass samples in between the range of 1370 cm^{-1} - 1560 cm^{-1} . Perhaps carbonates formed due to the reaction of calcium or strontium oxide with the atmospheric carbon dioxide. It has been reported in the literature that surface reactivity of silicate based bioactive glasses increase along with the incorporation of strontium. Thus, it is noteworthy that these phases were not detected in x-ray diffraction (XRD) analysis because they were either present in a very insignificant amount or were non-crystalline in nature. The peaks witnessed at 3420 cm^{-1} and 2950 cm^{-1} were related to O – H stretching and CH_2 or CH stretching, respectively (Nicholson et al. 1988; Dong et al. 1997; Fredholm et al. 2010).

Additionally, all prepared bioactive glass samples were individually characterised after immersion in simulated body fluid (SBF) solution for *in vitro* bioactivity analysis, as indicated in Figure 45. It has been confirmed in previous research that a material which is known to be bioactive can create a bond between material (non-living) and tissue (living). This particular biological reaction occurs with the natural bonding junction provided by the mineralising interface of an individual material. Thus, the developed interface should be sufficient to form a hydroxyl-carbonate apatite (HCA) layer independently. In short, all bioactive materials are commonly able to create an environment favorable for osteogenesis (Cao & Hench 1996; Hench 2006).

In terms of its mechanism, bioactivity merely depends upon the composition and nature of an individual material. It is evident from the literature that eleven different stages were present in the formation of bonds between silicate based bioactive glasses and host tissues. Among these, five occur over the surface of glass depending on its composition. When silicate based bioactive glass has been immersed in a simulated body fluid (SBF) solution, these five stages (explained below) are induced immediately. As a result, a carbonated hydroxyapatite and hydroxy-fluoroapatite (HCA/HCFA) layer forms over the surface of specimens (Cao & Hench 1996; Hench 2006).

At the initial stages of the formation of the carbonated hydroxyapatite (HCA) layer, the change in pH occurs over the surface of the material due to the formation of silanol bonds (Si – OH). This is due to rapid ionic exchange of $\text{Ca}^{2+}/\text{Na}^+$ with H^+ in the prepared solution. Secondly, after the change in pH, the hydroxyl group (OH) attacks the glass structure and potentially leads to the dissolution of the soluble silica layer. Thirdly, the re-polymerisation of the SiO_2 rich layer over the surface of the glass occurs due to condensation of Si – OH groups. In the fourth stage the calcium and phosphate groups can migrate above the developed silica rich layer and, as a result, the new layer with an amorphous rich film composed of $\text{CaO-P}_2\text{O}_5$ is formed. Finally, the OH^- , CO_3^{2-} or F^- starts to integrate with the developed amorphous film and leads to crystallisation and formation of a hydroxyapatite and hydroxy-fluoroapatite (HCA/HCFA) layer.

Table 15: FTIR peak identification and their attribution with references following SBF immersion of all prepared silicate based bioactive glass samples (BG 1-7) (Kim et al. 1989; Peitl et al. 2001; Donnell et al. 2009; Fredholm et al. 2010).

Sr.No	Peak Number	Peak Assignment
1	415-540 cm^{-1}	Si – O – Si bending mode
2	550-560 cm^{-1}	P – O bend/glass
3	600-610 cm^{-1}	P – O bend/crystal
4	720 cm^{-1}	Si – O bending
5	800-890 cm^{-1}	C – O stretch
6	910 cm^{-1}	Si – O (s) with 2 NBO (Q^2 group)
7	1200-1000 cm^{-1}	Si – O (s) symmetric stretching mode
8	1080-1350 cm^{-1}	P = O stretch
9	1560-1370 cm^{-1}	Carbonate species

The Fourier transform infrared (FTIR) technique has also been reported as being used for the analysis of phospho-silicate based glasses due to its sensitivity towards Si – O – Si bonds and change in chemical nature of silicate based glasses when they are immersed in SBF solution (Peitl et al. 2001; Fredholm et al. 2010). For this research, all prepared silicate based bioactive glass samples (BG 1-7) were immersed in simulated body fluid (SBF) and analysed after 24 hours using FTIR technique, as shown in Figure 45. It was observed that the onset and the formation of hydroxyl-carbonate apatite peak was more obvious in comparison with the presence of silicate glassy network designated intensities (Peitl et al. 2001). However, Si – O – Si and P – O bending modes were observed in between the range of 415 cm^{-1} - 540 cm^{-1} and

560 cm^{-1} , respectively. The presence of a peak at 720 cm^{-1} is attributed to Si – O bending. Additionally, the formation and presence of a crystalline HCA layer can be observed in between the range of 800 cm^{-1} - 890 cm^{-1} , which generally corresponds to the C – O stretching mode. The appearance of a peak shoulder at 900 cm^{-1} can be attributed to the presence of Si-O stretching vibrational mode due to the presence of non-bridging oxygen (NBO). The presence of a peak near 1050 cm^{-1} – 1120 cm^{-1} region is an indication of the P-O stretching and an indicator of crystalline HCA phases formation (Kim et al. 1989; Peitl et al. 2001; Donnell et al. 2009; Fredholm et al. 2010). The appearance of singular peaks around 500 cm^{-1} – 600 cm^{-1} indicate the presence of P – O bonds due to the expected crystalline HCA layer, as indicated in Table 15. C – O asymmetric stretching (ν_3) can also be observed in between the range of 1410 cm^{-1} and 1450 cm^{-1} (Peitl et al. 2001; Fredholm et al. 2010). Similarly, for further analysis and for the evaluation of the establishment of P – O and C – O bonds, Raman spectroscopy technique was used due to its sensitivity towards P – O and C – O vibrations (Rehman et al. 1994; Bellucci et al. 2011).

Table 16: FTIR peak identification and attribution with reference to all prepared silicate based bioactive glass ionomer samples with both tartaric and citric acid (TA / CA GIC 1-7) (Dong et al. 1997; Deb & Nicholson 1999; Young et al. 2000; Bellucci et al. 2011).

Sr.No:	Peak Number	Peak Assignment
1	606 cm ⁻¹	Calcium tartrate
2	811 cm ⁻¹	Calcium tartrate
3	885 cm ⁻¹	C – C stretch region
4	950 cm ⁻¹	PO ₄ symmetric stretching
5	1014 cm ⁻¹	C – C stretch region
6	1066 cm ⁻¹	Si – O – Si stretching
7	1317 cm ⁻¹	Calcium tartrate
8	1403 cm ⁻¹	Symmetric COO stretch
9	1438 cm ⁻¹	CH stretch
10	1458 cm ⁻¹	CH ₂ deformation
11	1630 cm ⁻¹	Asymmetric COO stretch
12	2927 cm ⁻¹	CH ₂ or CH stretching

Next, all prepared silicate based bioactive glass ionomer cement samples (TA / CA GIC 1-7) were chemically analysed using FTIR technique after admixture with poly-acrylic acid and water in the presence of tartaric and citric acid as setting modifiers, as shown in Figure 46 and 47. From the obtained spectra it is suggested that the appearance of peaks in between the range of 500 cm⁻¹ and 1700 cm⁻¹ were due to the absorption of vibrations. This might be because of

the structure of organic molecules, such as the formation of salts due to the reaction of metal oxides with poly-acrylic, tartaric and citric acid. Peaks observed at around 606 cm^{-1} , 810 cm^{-1} , 811 cm^{-1} , 885 cm^{-1} , 1014 cm^{-1} and 1317 cm^{-1} which can be ascribed to the formation of calcium and sodium tartrate with C – C stretching. The appearances of peaks of low intensity were also observed at 950 cm^{-1} , attributed to the PO_4 symmetric stretching mode, as indicated in Table 16. Another low intensity peak was also noticed at 1066 cm^{-1} , relating to with the Si – O – Si stretching mode. Symmetric and asymmetric stretching of COO was also observed at 1403 cm^{-1} and 1630 cm^{-1} because of the formation of calcium tartrate. Similarly, CH_2 deformation of calcium poly-acrylate was observed at 1438 cm^{-1} and a peak at 2927 cm^{-1} , representing CH_2 or CH stretching (Dong et al. 1997; Deb & Nicholson 1999; Young et al. 2000; Bellucci et al. 2011).

Furthermore, in all prepared citric acid based glass ionomer cement samples, peaks were visible between the range of 1079 cm^{-1} - 1036 cm^{-1} , indicating the presence of Si – O – Si bonds. Absorption mode peaks at 1419 cm^{-1} , 1311 cm^{-1} and 1275 cm^{-1} were attributed to the carboxylic acid group, with peaks at 1558 cm^{-1} and 1540 cm^{-1} attributed to symmetric and asymmetrical vibrational stretching of O – C = O bonds. The presence of – OH groups was also observed around the region at 3300 cm^{-1} with peaks at 2361 cm^{-1} - 2331 cm^{-1} . These were ascribed as the asymmetrical stretching of CO_2 (Dong et al. 1997; Deb & Nicholson 1999; Young et al. 2000; Bellucci et al. 2011).

Apatite is an inorganic component of hard tissues consisting of hydroxide ion surrounded by calcium-ion-lined channels which offers a unique and vast area for the substitution of other ions. Inclusion of carbonate into the apatite structure is specifically significant for bone (Yoder et al. 2011).

Silicate based bioactive glasses are of great importance to be used as bone grafts and implant coatings, in aluminium ion free glass ionomer cement system. However, the addition of fluoride in such applications appears to be more promising, especially in the field of dentistry (Brauer et al. 2010a). Fluorapatite ($\text{Ca}_{10}(\text{PO}_4)_6\text{F}_2$) is homologous to hydroxyapatite ($\text{Ca}_{10}(\text{PO}_4)_6(\text{OH})_2$; HAP) which is related to the basic mineral component of hard tissues. However, fluorapatite is known to be more stable at lower pH when compared to hydroxyapatite (Chen et al. 2014).

Nuclear magnetic resonance spectroscopy (NMR) is widely accepted technique through which the structural components of any material can be studied comprehensively. In order to differentiate HCA and FA, various types of NMR depending upon the respective constituents of the apatite must be carried out. For instance, ^{19}F MAS-NMR spectroscopy is a technique used to detect fluoride content and ^{31}P MAS-NMR spectroscopy is used to analyse hydroxyapatite within a specimen. Similarly, designated NMR peaks for fluorapatite and carbonated hydroxyapatite present in the available literature can also help to differentiate between the apatite structures. ^{19}F MAS-NMR spectroscopy is the finest method for the identification of fluorapatite. Peaks for the confirmation of fluorapatite usually appear at -

101ppm (Brauer et al. 2010). Similarly, a sharp peak reflecting fluorapatite is reported to be found at -103ppm by Chen et al (2014). Mixed substituted fluorapatite (either with OH⁻ or Cl⁻ groups) can also be distinguished from pure stoichiometric fluorapatite (Chen et al. 2014).

Silicate based bioactive glasses are well known for the formation of carbonated hydroxyapatite layer *in vitro* within SBF. This HCA layer is capable of accelerating protein attachments, such as collagen, fibronectin and vitronectin, to which osteoblasts bind and allow intimate bonding with bone (Brauer et al. 2010).

Hydroxyapatite is a desired product during cement formation and it can be identified by ³¹P MAS-NMR spectroscopy at 2.8ppm spectra (Hachulska et al. 2003). In ³¹P-MAS NMR, the peaks at 2.3 ppm is attributed as typical for hydroxyapatite. A strong peak at 5.5ppm detected by ¹H-MAS NMR is indicative of water and a narrow peak at 0.1ppm for OH group (Brauer et al. 2010)

The integration of carbonate in the structure of apatite is highly significant, especially for bone, where the apatite incorporates up to 8 wt% CO₃²⁻. Substitution of carbonate is of two types either for hydroxyl ions (known as Type A substitution) or for phosphate ions (known as Type B substitution) (Yoder et al. 2011). It has been found that NMR peaks close to 0 ppm due to the (OH) group in hydroxyapatite (Panda et al. 2003).

The inorganic components of hard tissues consist of nanometre sized particles of hydroxyapatite containing different concentrations of carbonate (□8 wt%). Hydroxyapatite in

the presence of carbonate traces exhibit changes in reactivity and solubility because of which it has been investigated under the fields of material sciences and geochemistry. Formation of AB-type substituted carbonated hydroxyapatite with both A and B sites substituted can also be produced in aqueous suspensions. Various studies have proposed that HCA be synthesised under increased temperature and pressure conditions in order to gain crystals to be examined under X-ray and neutron diffraction techniques. The literature reveals that peaks at 170.2 and 166.5 ppm occur due to Type B and Type A carbonated hydroxyapatite, respectively. Kolmas et al. (2010) explained peaks at 169.5 ppm for carbonates of Type B and showed peaks for mixed A and B type carbonated hydroxyapatite at 168.2 ppm, assigning them as labile surface carbonates (Kolmas et al. 2010).

FTIR spectroscopy can also be used to distinguish A and B type substituted carbonated hydroxyapatite. In ν_3 carbonate mode, these substitutions exhibit a discrete splitting pattern, where both A and B types generate well-defined peaks at 880 and 875 cm^{-1} , respectively. Similarly, peaks obtained at ν_2 region from 1545 to 1410 cm^{-1} have been reported to distinguish these substitution sites (Masson et al. 2008).

5.2.3.2. Raman spectroscopic analysis

Following the introduction of tartaric and citric acid as setting modifiers, all produced silicate based bioactive glass and ionomer substituted cement samples, were chemically characterised using Raman spectroscopy, as shown in Figure 48- 51. It is evident from the literature that

both Raman and Fourier transform infrared spectroscopic (FTIR) techniques are complementary (Young et al. 2000; González et al. 2003).

Table 17: Raman peak identification and attribution with references following SBF immersion of all prepared silicate based bioactive glass samples (BG 1-7) (Young et al. 2000; González et al. 2003).

Sr.No.	Peak Number	Peak Assignment
1	437 cm^{-1}	Symmetric oxygen stretching of Si – O – Si or O – Si – O angular deformation of SiO_4 network
2	530-660 cm^{-1}	Si – O – Si rocking mode
3	750 cm^{-1}	Si – O – Si bending vibration
4	860 cm^{-1}	Si – O – 4 NBO monomer
5	870 cm^{-1}	Si – O – 2 NBO stretching vibration
6	920 cm^{-1}	Si – O – 3 NBO dimer
7	950 cm^{-1}	PO_4 symmetric stretching
8	975 cm^{-1}	Si – O – 2 NBO rings and chains
9	900-970 cm^{-1}	Si – O – NBO stretching vibration
10	1030 cm^{-1}	$\text{Si}_2\text{O}_5^{2-}$ (1 NBO) vibration
11	1000-1200 cm^{-1}	Si – O – Si asymmetric stretching mode

Raman spectroscopy showed an increased sensitivity to the changes in frequencies occurred due to stretching and rocking vibrations, indicating the presence of SiO_2 . This change might also confirm the presence of an alkali-earth element in the parent composition, leading to the formation of Si – O – NBO (Chalmers et al. 2012; Rehman et al. 2012). Symmetrical vibrational peaks were also observed at 950 cm^{-1} due to the presence of a PO_4 group, as shown

in Figure 48. The overlapping Si – O – Si asymmetrical stretching of PO_4 peak partially reveals the presence of Si – O – Si NBO features with the advent of shoulder observed at 1030 cm^{-1} . Peaks in the range of $2000 \text{ cm}^{-1} - 200 \text{ cm}^{-1}$ correspond to the fingerprint region of functional groups for silicate based bioactive glass (Duée et al. 2013). Peaks located in the range of $646 \text{ cm}^{-1} - 626 \text{ cm}^{-1}$ were attributed to Si – O – Si groups. The symmetrical vibration of 2-D structure of $\text{Si}_2\text{O}_5^{2-}$ was identified at the range of 1078 cm^{-1} , with peaks around 945 cm^{-1} ascribed to the presence of PO_3^{4-} groups with symmetrical stretching of P – O bonds. However, after the immersion of all produced silicate based bioactive glass samples in simulated body fluid solution (SBF), the appearance of peaks between the range of $1150 \text{ cm}^{-1} - 800 \text{ cm}^{-1}$ and P – O symmetric stretching mode observed at the 945 cm^{-1} which usually shifted towards the higher wavenumber were also noticed, as shown in Figure 49 and Table 17 (González et al. 2003; Bellucci et al. 2011).

Table 18: Raman peak identification and attribution with references for all prepared silicate based bioactive glass ionomer samples with both tartaric and citric acid (TA / CA GIC 1-7).

Sr.No.	Peak Number	Peak Assignment
1	606 cm^{-1}	Calcium tartrate
2	811 cm^{-1}	Calcium tartrate
3	885 cm^{-1}	C-C stretch region
4	950 cm^{-1}	PO_4 symmetric stretching
5	1014 cm^{-1}	C-C stretch region
6	1066 cm^{-1}	Si-O-Si stretching

7	1317 cm ⁻¹	Calcium tartrate
8	1403 cm ⁻¹	Symmetric COO stretch
9	1438 cm ⁻¹	CH stretch
10	1458 cm ⁻¹	CH ₂ deformation
11	1630 cm ⁻¹	Asymmetric COO stretch
12	2927 cm ⁻¹	CH ₂ or CH stretching

Raman spectroscopy was also used to analyse all prepared silicate based bioactive glass ionomer cement samples after the introduction of tartaric and citric acid in the presence of poly-acrylic acid and water, as shown in Figures 50 and 51. For tartaric acid based glass ionomer cement samples, the obtained spectra indicate peaks in between the range of 500 cm⁻¹ and 1700 cm⁻¹. These peaks were caused by vibrations of the structure of organic molecules, which in this case were salts formed due to the chemical reaction between metal oxides, poly-acrylic and tartaric acid. The appearance of peaks at around 606 cm⁻¹, 811 cm⁻¹ and 1317 cm⁻¹ indicate the formation of calcium tartrate. Additionally, the peak for sodium tartrate occurred at 810 cm⁻¹ and overlapping of peaks in this region are common. C – C stretching for calcium tartrate can be observed at 885 cm⁻¹ and around 1014 cm⁻¹. The related peak of low intensity is present at around 950 cm⁻¹ which corresponds to the PO₄ symmetrical stretching mode. Another low intensity peak is visible at around 1066 cm⁻¹ which could indicate Si – O – Si stretching mode. The symmetrical and asymmetrical – COO stretching raised from calcium tartrate can be perceived at 1403 cm⁻¹ and 1630 cm⁻¹ respectively. However, the CH₂ deformation of calcium poly-acrylate is seen at 1438 cm⁻¹ as well. The peak at 2927 cm⁻¹

represents the presence of CH₂ or CH stretching mode. In general, the obtained results reveal the presence of organic molecules and formation of calcium tartrate as indicated in Table 18 (Dong et al. 1997; Deb & Nicholson 1999; Young et al. 2000; Bellucci et al. 2011).

Formation of citrate during the setting reaction of citric acid based glass ionomer cement samples can be assumed from the obtained results. The peak present at 967 cm⁻¹ is attributed to C–O–C and C–O stretching vibrational mode. The peak at 840 cm⁻¹ can be ascribed to the deformation of C – H bonds, with peaks at 1461 cm⁻¹ and 1437 cm⁻¹ indicating the presence of CH groups and attributed to stretching of CO₂ and deformation of C – H bonds. The peaks observed at 2978 cm⁻¹, 2944 cm⁻¹ and 2920 cm⁻¹ can be attributed to the symmetrical stretching mode of –CH₂ groups due to the presence of citrate chain structures (DeRosa et al. 2003; Shih 2003).

In sum, FTIR and Raman spectroscopic techniques are both vibrational imaging methods and are complementary to each other. They are used to study the biochemical parameters and molecular structure of tissues and biomaterials. FTIR is a routine technique that relies on the absorption of infrared radiations, used largely for the characterisation of biomaterials. It is known that the frequencies of numerous molecules (both organic and inorganic) lies within the infrared region. Therefore, FTIR spectroscopy is extensively approached by researchers to carry out biochemical analysis in biomedical samples. Similarly, Raman spectroscopy is a significant analytical technique in biomedical applications used for biomaterial characterisation. It detects the alterations in the polarization of molecules and supports detailed

investigations of functional groups, molecular confirmations and bonding type (Lopes et al. 2018).

According to our understandings, FTIR is widely used for chemical analysis and it refers to the absorption of infrared radiations whereas, Raman is a scattering technique. A combined approach and the direct comparison between the data of these two techniques, leads us to evaluate chemical composition of the proposed material efficiently. Some constituents can be more sensitively detected by FTIR (such as C-O, C=O, O-H and Si-O-Si vibrations). However, other constituents have more sensitivity towards Raman technique (such as P-O and C-O vibrations). An advantage of Raman spectroscopy over FTIR is that it carries the spectral analysis in “Reflection mode”, so the samples can be probed in their native state or with minimal preparation. It is able to analyse wet samples to mimic physiological conditions.

5.2.4 *In-vitro* biological characterisations

5.2.4.1 *In- vitro* bioactivity analysis

5.2.4.1.1 Scanning electron microscopic (SEM) analysis

Morphologically, following the introduction of tartaric and citric acid as setting modifiers, all prepared silicate based glass ionomer cement samples (TA / CA GIC 1-7) were analysed using secondary scanning electron microscope (SEM) after immersion in simulated body fluid (SBF) solution. Analysis was conducted on the 1st (control sample), 7th and 14th days, as shown

in Figure 52 till 57. Qualitatively, the surface morphology was studied individually using secondary electron with different magnification range. With secondary electrons, photons of different energies, characteristic x-rays and back scattered electrons were generated potentially when incident beam ray interacted with the surface of the sample. The secondary and backscattered electrons are usually of more interest to researchers due to the shadowing relief effect which permits the conception of three-dimensional image. In addition, secondary electrons are useful to produce high-resolution images (Goldstein et al. 2012; Gomes et al. 2013; Romero et al. 2015).

It was observed from the obtained results that there were no depositions of calcium-phosphate apatite layers present over the surface of the control or 1st day samples. Further morphological analysis of the developed layer of spherical and globular structures over the surface of immersed cement samples was conducted using SEM technique individually for TA and CA GIC samples. The obtained SEM micrographs demonstrate morphological changes upon SBF immersion. However, the produced cement samples (TA/CA GIC 1-7) before immersion, as indicated in Figure 52 and 55, presented smooth and even surfaces. After 7 and 14 days of immersion, Ca/P layer formation was observed (Gomes et al. 2013).

Previous research suggested that the appearance of globular structures of various shapes and sizes observed through SEM indicates the formation of apatite layer. The appearance of the spherical globules at the surface of cement samples occurs due to the nucleation of a carbonated hydroxyapatite layer. The mechanism of apatite nucleation involves an initial instant cationic

exchange of sodium and calcium ions with H_3O^+ so that the formation of Si-OH bonding can take place on the glass surface. This reaction changes the pH of the solution, creating a silica rich zone close to the surface. Phosphate and calcium ions present in the suspension combine with the Si-OH groups forming calcium silicates which subsequently form amorphous CaO- P_2O_5 on the silica rich layer. Following this, the incorporation of hydroxyls and carbonates from the solution results in the crystallisation of CaO- P_2O_5 , leading to the formation of spherical bone-like apatite crystals (Kokubo et al. 2003; Jones 2013).

All produced and analysed samples exhibited the formation of micro sized circular structures similar to bone like apatite (Goh et al. 2013; Arepalli et al. 2016). The EDX technique was used to evaluate the spherical or globular surfaces as mentioned above and the results reflected the presence of calcium and phosphorous peaks which confirmed the formation of apatite layer (Goh et al. 2013). Similarly, the obtained EDX results revealed that these structures are composed of a carbonated hydroxyapatite layer with constituents including C, Ca, P along with low Si intensity peaks as compared to the initial surfaces. The significant increase in C, Ca, P and decrease in the intensities of Si demonstrated the formation of an HCA layer (Arepalli et al. 2016).

It was also noticed that certain areas samples had no layer. This implied that the growth of the apatite layer was not evenly distributed over the whole surface of the samples causing a rough texture. It is known that, the rough surface can provide increased surface area than a smooth surface. Therefore, the growth of apatite formation possibly increased. Notably, in both

tartaric and citric acid based samples, the formation of certain shielding pockets over the surface of set cement prevents the surface from being exposed to the solution, thus rendering these sites incapable of forming a hydroxyapatite carbonated (HCA) layer.

However, experiments have shown that citric acid based samples exhibit regions for the increased growth and development of layers of apatite nuclei which were fully developed and clustered together in a uniformed pattern. This indicates that the release of citrate ions from the prepared citric acid based silicate based bioactive glass ionomer cement samples may be able to create more drastic changes in the development of hydroxyapatite carbonated (HCA) layer after immersion in simulated body fluid solution than tartaric acid based glass ionomer cement samples. This is possibly due to the presence of an additional functional group in citric acid (three functional groups) in comparison with tartaric acid (two functional groups) (Sarda et al. 2002; Qiu et al. 2006; Fredholm et al. 2010; Chung et al. 2011; Ferrero et al. 2015).

In sum, the literature reveals that apatite mineralisation of bioactive glass based cement samples play a vital role in sustaining their biological properties. Apatite mineralisation of biomaterials fully supports the integration with recipient's hard tissues. Moreover, formation of apatite layer over the surface of biomaterial augments osteoblastic activity together with proliferation and differentiation (Yun et al. 2010).

5.2.4.1.2 Energy dispersive x-ray spectroscopy (EDX) analysis

All prepared silicate based glass ionomer cement samples (TA / CA GIC 1-7) and obtained glass flake samples from Leeds Glass Flakes Ltd were analysed using energy dispersive x-ray spectroscopy (EDX) following the introduction of tartaric and citric acid as setting modifiers for the analysis of elemental composition, as shown in Figures 58 till 60.

EDX is a useful analytical tool for the conformation and the presence of carbonated hydroxyapatite (HCA) layers after immersion in simulated body fluid (SBF) solution in *in vitro* bioactivity analysis. Indeed, in 1993 Gomes et al. showed that by using this technique the atomic percentages retrieved from the obtained data can be constructive in the calculation of calcium and phosphorous ratios along with various intervals of time (Goh et al. 2013; Gomes et al. 2013).

The empirical molecular formula of un-substituted hydroxyapatite can be expressed as $\text{Ca}_{10}(\text{PO}_4)_6\text{OH}_2$. However, it has been reported that in hydroxyapatite, the calcium and phosphorus ratio is usually greater than 1.67 (Gomes et al. 2013). The basis for the use of simulated body fluid solution for the formation of apatite layer is well established and it is directly related to the composition of simulated body fluid solution (SBF). Conventional simulated body fluid (c-SBF) solution exhibits a closely similar ionic composition to human blood plasma, the only difference being in the ratio of Cl^- and HCO_3^- ions present in the parent composition. This subtle difference leads to the formation of apatite layer with structural differences from the

actual bone apatite. In 2003, Oyane et al. found that only the modified simulated body fluid solution (m-SBF) and conventional simulated body fluid solution (c-SBF) were more stable than human blood plasma and had equal concentrations to it. In their research, concentration of HCO_3^- was kept equal to the saturation level with respect to calcite formation. Similarly, the ionic concentration of these simulated body fluid solutions in relation to human blood plasma are indicated in the Table 19 (Oyane et al. 2003; Kokubo & Takadama 2006; Goh et al. 2013; Gomes et al. 2013).

Table 19: Ionic concentrations of various SBF in relation to human blood plasma (Oyane et al. 2003).

Sr No:	Ionic Concentration	Blood Plasma	c-SBF	m-SBF
1	Na^+	142.0	142.0	142.0
2	K^+	5.0	5.0	5.0
3	Mg^{2+}	1.5	1.5	1.5
4	Ca^{2+}	2.5	2.5	2.5
5	Cl^-	103.0	147.8	103.0
6	HCO_3^-	27.0	4.2	10.0
7	HPO_4^{2-}	1.0	1.0	1.0
8	SO_4^{2-}	0.5	0.5	0.5

An increased concentration in calcium and phosphate ratio can be observed from the obtained results after energy dispersive x-ray spectroscopy analysis of both prepared silicates based glass ionomer cement samples (TA / CA GIC 1-7) after introduction of tartaric and citric acid as setting modifier. In addition, the ratio of calcium and phosphate (Ca/P) based calculated

atomic percentages were tabulated and indicated in Table 10 and 11 for both tartaric and citric acid based glass ionomer cement samples. The observed values range from between 1.69 - 1.74 and 1.72 – 1.86, indicating the presence of apatite at the end of 7th day of immersion of both tartaric and citric acid based cement samples. The values observed in between the range of 1.72 - 1.85 and 1.82 – 1.97 also indicate the presence of apatite at the end of 14th day of immersion of both tartaric and citric acid based cement samples respectively. As a point of comparison, Goh et al. (2013) concluded that zinc ion based bioactive glass showed the range of accepted calcium phosphate (Ca/P) ratio for bioactivity ranged from 1.438 to 2.477.

Previous studies have shown that a distinct proportion of calcium deficient hydroxyapatite ($\text{Ca}_{10-x}(\text{PO}_4)_{6-x}(\text{HPO}_4)_x(\text{OH})_{2-x}$, $0 \leq x \leq 1$) based on its formulation with ratios of 1.50-1.71 display greater bioactivity than hydroxyapatite (Goh et al. 2013; Gomes et al. 2013). Furthermore, Gomes et al. examined various combinations of cement samples with Ca/P ratios in between 1.55-1.79 that exhibited much improved bioactivity as compared to those with a ratio of 1.67. In the same vein, Goh et al (2013) examined Ca/P ratios of pure and substituted bioactive glass from 1.762-1.857. Results showed that, following the introduction of tartaric and citric acid, all prepared glass ionomer cement samples were bioactive. In addition, there were no emerging trends in change of calcium and phosphate ratios in both prepared samples between the 7th and 14th days. However, results obtained from scanning electron microscope also provide morphological confirmation for the development of apatite layer over the surface of prepared samples to some extent (Goh et al. 2013; Gomes et al. 2013).

5.2.4.2 *In- vitro* biocompatibility analysis

5.2.4.2.1 Cell culture and MTT assay of glass and cement samples

The biocompatibility of any material could be the degree to which it can interact with a living system without creating any drastic changes in the normal physiological environment. For the further analysis of cell viability of all produced silicate based bioactive glasses and prepared glass ionomer cement samples with the introduction of tartaric and citric acid, MTT assay was conducted for which human oral fibroblasts were cultured separately. Previously, Doherty et al. (1991) studied the biocompatibility of glass ionomer cement using mice fibroblasts. They analysed and observed cellular behaviour of disc shaped glass and ionomer based cement samples with microscopy (directly) and also with MTT assay (indirectly) in an immersed medium (Doherty 1991; Kokubo et al. 1991). By using the yellow tetrazolium MTT assay known as (3-(4, 5-dimethylthiazolyl-2)-2, 5- diphenyltetrazolium bromide), the increase or decrease in cellular number can be observed. The MTT assay measures the mitochondrial activity of the cell. It should be noted that MTT assay reader machine analyses results corresponding to a wavelength of 570nm (Tyas 2006).

The obtained MTT assay results of this study show that all calcium substituted strontium and barium glasses and ionomer based cement samples were able to support higher cellular growth at both 24 and 48 hours'. The results were observed to be significantly different (* $p < 0.05$) after their statistical analysis, as shown in Figure 64 and 69. However, it is evident from

literature review that strontium plays a vital role in bone reformation and remodelling through the stimulatory effect on pre-osteoblastic cells (White et al. 1989; Gentleman et al. 2010). The decrease in cellular response was also observed after 24 and 48 hours of MTT assay analysis for Leeds Glass Flake Company Ltd UK glass composition. The decreased cellular response of glass composition can be concluded as related to the addition of zinc and titanium ions in the composition. It is evident from the literature review that the presence of zinc and titanium in higher ratios can create a deleterious effect on cellular response because of their toxic behaviour (Boyd et al. 2008a).

The release of fluoride ions has been shown to create beneficial effects on the remineralisation of dental hard tissues during the onset of dental caries. It is also known that sodium ions are capable of forming strong bond with fluoride ions. Previously, studies have shown the effects of sodium fluoride ions on the human osteoblastic cell line with the conclusion that the addition of fluoride ions in the presence of sodium ions has a drastic effect over cellular growth and their further proliferation (Lanford et al. 1979; Neel et al. 2009; Velazco et al. 2014).

Several cell viability assays are currently being used. One of them is the Alamar blue assay (Borra et al. 2009). Alamar blue is known to be a significant indicator of redox reaction and it is used widely to assess cellular health, cell cycle functions, testing of toxic compounds, metabolic functions and antimicrobial risk assessment. Resazurin, the basic constituent of Alamar blue, is water soluble, non-toxic and permeable through cell membranes. As it is important to assess the biocompatibility of any newly constructed material, we carried out the

MTT assay in order to monitor the cell viability of all produced silicate based bioactive glasses and ionomer cement samples. Alamar blue assay can also be used as an effective tool to monitor cells over an extended period (Rampersad 2012).

Resazurin provides incessant monitoring of cells and is highly sensitive, rapid and reliable. It helps to keep the cells intact, permitting more advanced evaluation and analysis of messenger RNA, cytogenecity, apoptosis and immunophenotyping. Resazurin is a non-fluorescent blue dye that is reduced to the pink coloured highly fluorescent dye, resorufin. Reaction levels can be detected using spectrophotometers with appropriate filters. Generally, the absorption peaks for resazurin are obtained at 600nm wavelength (Borra et al. 2009).

The reduction during Alamar blue might be indicative of impaired cellular metabolism. This reduction from the oxidized state permits the flexibility for the detection of presence or absence of viable cells (Rampersad 2012).

5.2.4.2.2 Optical and confocal microscopy

For further biological quantitative analysis before final MTT assay experiments were conducted on all prepared silicate based bioactive glasses and ionomer cement samples, optical light microscopy and confocal microscopic techniques (only for glass samples) were carried out, as shown in Figures 61, 65, 69 and 74. Generally speaking, optical and confocal microscopic techniques facilitate the evaluation of cellular growth and proliferation over the

surface of any specimen or given material. In terms of the cellular response for unsubstituted glass and prepared glass ionomer cement samples (BG 1, TA / CA GIC 1) the results indicate less cellular growth (qualitatively supported by MTT results). In addition, the calcium substituted barium and strontium glasses and glass ionomer cement samples exhibited improved biocompatibility along with an increase in cellular proliferation and adhesion (Oliva et al. 1996; Kim et al. 2014). Johal et al concluded that strontium ion glass ionomer cements are more osteo-conductive and provide a more beneficial environment for further bone growth. It has also been shown that the slow release of strontium ions encourages the process of osteo-integration by decreasing the progression of bone resorption (Fredholm et al. 2010; Gentleman et al. 2010; Kim et al. 2014).

Moreover, the signs of significant biocompatibility through the confluent sheet of cells over the surface of glass samples can be seen from obtained confocal CLSM results (BG 1-7), as shown in Figure 74. A decreased cellular response is evident over the 'in house' copy of 45S5 silicate based bioactive glass sample (BG 1). However, the substituted glass samples (with strontium and barium) showed improved biocompatibility with increased cellular proliferation, growth and attachment. This could be due to improved surface reaction between cells and the surface of the prepared glass samples (Oliva et al. 1996; Kim et al. 2014). The obtained results are more consistent; therefore, it can be assumed that decreased ionic release occurred in the cell culture medium. Finally, the presence of highly extensive cytoskeletal extensions (in red),

reflects the cell viability of all produced silicate based bioactive glass samples (Fredholm et al. 2010; Gentleman et al. 2010; Kim et al. 2014).

5.2.5 Mechanical characterisations

5.2.5.1 Compressive strength analysis

The mechanical strength of dental restorative materials has become of great concern for both researchers and clinicians, in order that the longevity of restorative materials in complex oral environment is increased as they are subjected to multifaceted loading during masticatory processes including compressive, tensile and shear stress. Of these forces, compressive stress is the most impacting particularly cyclic compressive stresses. It is known that a normal person performs approximately 2700 chewing cycles daily and about 10^6 per year. Thus, dental restorative materials age quickly, especially as they are within a humid oral environment. Hence, researchers suggested that, it is very important to take this into account before designing of any dental restorative material (Khoroushi & Keshani 2013; Kalia et al. 2016).

In terms of enhancing mechanical strength of water based silicate glass ionomer cements, particle size and the ratio of introduction of setting modifier are most significant. Most studies suggest that particle sizes with $< 45 \mu\text{m}$ form a better quality of glass ionomer cement in this regard. The substitution of larger cationic elements, such as zinc, strontium, magnesium and barium, can create a more extended glassy network with the admixture of poly-acrylic acid,

water and different introduced setting modifiers such as tartaric and citric acid. Sampath et al have shown that an increase in the proportion of calcium ions substituted with strontium and barium ions increases the mechanical strength of resultant glass ionomer cement due to their larger cationic effect. This is most likely due to ready occupation of interstitial structural spaces. This structural behavioural change was also observed with x-ray diffraction (XRD) analysis (Gomes et al. 2013; Arepalli et al. 2016; Kalia et al. 2016).

The obtained mechanical compressive strength results of this study show that citric acid based glass ionomer cement samples exhibited an increase in compressive mechanical strength in comparison with tartaric acid based glass ionomer cement samples, as shown in Figure 75 respectively. Moreover, the obtained data were compared and statistically analysed for further evaluation of significant differences (* $p < 0.05$) in between the samples, as indicated in Figure 75. Due to acidic nature of citric acid, the compressive strength of the resultant cement enhanced significantly. Perhaps this is because of structural difference of citric acid in comparison with tartaric acid in terms of the availability of functional groups. In citric acid there are three carboxylic acid functional groups present which may create a more freely cross-linked structure from the disrupted glassy gel matrix which is developed. In addition, it is known that tartaric acid is a dicarboxylic acid and structurally it has two carboxylic functional groups as compared to poly-acrylic acid. In the final setting reaction, the tartaric acid readily starts to interact preferentially with metal ions due its higher acidity but also creates more cross linking structures than poly-acrylic acid. As a result, the capability of resulting glass ionomer

cement to withstand applied mechanical load increases due to increased number of cross linkages within the formed gel matrix.

The obtained glass flakes from Leeds Glass Flake Company Ltd. UK were also analysed mechanically and statistically upon the admixture of both tartaric and citric acid in the presence of poly-acrylic acid and water, as shown in Figures 76 till 77. It was observed from the obtained results that the desired target for the formation of cement was difficult to achieve. This is possibly due to the presence of increased substitution with boron, titanium, zinc and magnesium ions in the basic glass composition. As a result, matrix polymers were not formed properly with the admixture of poly-acrylic acid and water. This created a negative effect on the desired mechanical properties (Sanati & Andersson 1993; Noort 2013; Chen et al. 2016).

5.2.5.2 Gilmore needle test

The Gilmore needle indentation test is known to be the best method for the determination of working and setting time of glass ionomer cement specimens in this research. This is due to the results being reliant on operator interpretation and handling skills. By using this technique, the possibility of repeating same samples in a more appropriate way and the establishment of a direct correlation between working and setting time with the available data became feasible (Prentice & Tyas 2006; Yang et al. 2012; Noort 2013).

Another advantage of this technique is that it can provide immediate and direct results related to handling characteristics of the cement *in situ*. It is important to note that there were various

factors which can directly affect working and setting time of any cement. These include particle size and their distributions, chemical composition of the glass and cement, environmental testing and the choice of chelating agents and setting modifiers (Khoroushi & Keshani 2013; Noort 2013; Shahid et al. 2014).

All silicate based glass ionomer cement samples were analysed using the Gilmore needle test after the introduction of tartaric and citric acid as setting modifiers in the presence of polyacrylic acid and water. The effect and role of the setting modifiers in setting and working time of any cement is usually significant. In this case, it was observed that the control (TA / CA GIC 1) cement sample evidenced a slightly shorter working and delayed setting time compared to both tartaric and citric acid-based glass ionomer cement samples, as shown in Figures 78 and 79, and Tables 12 and 13.

The compositions of calcium substituted glasses with strontium and barium ions exhibited slightly increased working and setting times. This is due to the effect of larger cationic ratios or possibly due to the mixture of various sizes of cations released during the process of development of a cross linking network. The ability of cross linking of ions can determine the working and setting rate of any formed cement. Moreover, in commercially available glass ionomer cements, they are acid washed to increase the working time by weakening the progression of cross linking of bonds within the polymeric matrix by cations (Xie et al. 2000; Gomes et al. 2013; Khoroushi & Keshani 2013).

Inclusion of tartaric and citric acid during cement formation can increase the working time of cement but with rapid setting time. Furthermore, addition of increased amounts of copolymeric acid can cause the resultant cement to be more brittle and also affect the solubility of set cement (Singh et al. Xie et al. 2000). Howard et al. (2014) demonstrated that the working time and setting time of resultant cement samples tend to decrease when the proportion of strontium oxide is increased. Generally, due to increased substitution of calcium with strontium and barium ions more electronegative environment is created during the setting reaction (Howard et al. 2014).

The results of this study show somewhat similar working times of both tartaric and citric acid based cement. This is due to citric acid playing a similar role to tartaric acid in the setting reaction of glass ionomer cement. However, the acidic group from citric acid attacks radially with powdered glass particles and forms metal gel. Citric acid has the potential to more significantly reduce setting time than tartaric acid, possibly because citrate molecules have three functional groups but tartaric acid molecules have only two functional groups. Citric acid creates a more acidic environment than tartaric acid.

In final stages of hardening, cations leach from the glass component, combining readily with polyanionic chains. On the other hand, due to increased acidity of the environment because of citrate ions, metal ions binds more strongly with the released ions from glass and create a drastic effect lowering the setting time. With tartaric acid based glass ionomer cement samples, even after the calcium's substitution with strontium and barium ions, an extended working time

and shortened setting time was observed. This is possibly because tartaric acid was enabled to react with the glass component more readily than poly-acrylic acid. However, as a result, the formation of cations (such as metal ions) liberated from the glass were possibly retarded, delaying the progression of poly-anionic chains, ultimately resulting in an increased working time (Howard et al. 2014).

5.3 Summary

In this chapter, results obtained from the study of the produced series of silicate based bioactive glasses, glass flakes from Leeds glass flake company Ltd. UK and ionomer based cement samples with calcium substitution for strontium and barium ions and the introduction of tartaric and citric acid were fully characterised, analysed and discussed according to their developed physical, chemical, thermal, mechanical and *in vitro* biological properties. The findings from the Fourier transformed infrared and Raman spectroscopic analysis revealed the attribution of Si – O – Si and P – O related peaks, therefore confirming the phospho-silicate structure of all produced glass samples (BG 1-7). The particle size and scanning electron microscopic (SEM) analysis results exhibited a range of particle sizes with > 45 µm as an average, which played vital role in the enhanced mechanical properties of the resultant cement.

X-ray differential diffractograms (XRD) revealed the amorphous nature of all silicate based bioactive glasses and obtained glass flakes with the presence of an amorphous halo hump

between 2θ angles $25 - 35^\circ$ respectively. Due to effect of strontium and barium substitution on the produced series of bioactive glasses, a shift of 2θ angle to lower values was observed. Differential thermal analysis results exhibited a gradual decrease in glass transition temperature due to the larger cationic effect and the disruption of the glassy network, showing the potential for industrial acceptance in terms of cost effectiveness. Moreover, the silicate based bioactive glass samples with the calcium substitution for strontium, barium and fluoride indicated a lower contact angle (hydrophilicity) and greater surface area after Brunauer-Emmett-Teller (BET) analysis. These features can increase the cellular growth, proliferation and attachment.

Furthermore, chemical spectroscopic analysis with FTIR and Raman techniques, revealed the inorganic and organic related ionomer peaks from all produced glass ionomer cement samples. *In-vitro* bioactivity was studied with simulated body fluid (SBF) solution separately on the prepared bioactive glass and ionomer based cement samples. Scanning electron microscopic (SEM) micrographs for ionomer based cement specimens discovered drastic changes in surface morphology at the end of 7th and 14th days by indicating a surface growth of hydroxyapatite layer. The energy dispersive spectrometer (EDX) results revealed the presence of calcium and phosphate ratio of analysed samples at 1.67 which likely confirms the development of a hydroxyl carbonated apatite layer (HCA). *In-vitro* bioactivity analysis was also performed on silicate based bioactive glass samples individually in order to reveal any possible change in their chemical structure, such as appearance of phosphate and carbonated

peaks, at an interval of 24 hours.

The biocompatibility analysis of all silicate based bioactive glass, glass flakes and prepared cement samples were compared with results from the available literature for the conformation of cell viability. This experiment was performed using human oral fibroblasts (OHFb's) cultured in extracted medium with respect to the positive and control group. The tartaric acid based cement samples were observed to be highly biocompatible at 24 and 48 hours. Similarly, the citric acid based cement samples indicated an increased rate in cellular growth and proliferation as compared to tartaric acid cements at both 24 and 48 hours in cell culture. However, the obtained company based glass flake composition exhibited a gradual decrease in cellular response at 24 and 48 hours.

All silicate based bioactive glass samples indicated enhanced cellular attachment and were analysed with the help of optical and confocal microscopy independently. The improved cell viability was attributed to the presence of strontium, barium and fluoride ions. Conversely, a decrease in cellular responses was recorded for the glass flake composition because of the presence of increased substitution of zinc and titanium ions. Furthermore, after the introduction of tartaric and citric acid as setting modifiers in both produced silicates based bioactive glass compositions and glass flake compositions, the mechanical properties of the resultant cements were analysed. The citric acid based ionomer cement samples indicated improved signs of compressive strength in the produced glass composition.

Due to challenging handling properties of the obtained glass composition, the variation in mechanical compressive strengths was observed simultaneously with the admixture of poly-acrylic, tartaric and citric acid in the presence of water. Furthermore, the working and setting time of all prepared glass ionomer cement samples were observed using Gilmore needle test. A marked increase in working time and decrease in setting time were perceived in citric acid based ionomer cement samples due to increased cationic ratio in the basic glass structure after the calcium substitution with strontium and barium ions.

On the basis of these results and their contribution to and relation with available literature, the following and final chapter presents the conclusion of this present work ending with suggestions for future work to enhance our understanding in this field.

Chapter 6: Conclusion and Future work

6.1 Conclusion

This study has provided data on the performance of ionomer glasses and GICs which will allow the improvement of their formulation for medical applications. The specific composition created through melt quenching technique (BG 1- 7) and studied was aluminium ion-free silicate-based bioactive glass with substitution of 3 mole % of CaO with the strontium and barium ions $46.14 \text{ SiO}_2.2.60 \text{ P}_2\text{O}_5.23.95 \text{ CaO}.24.35 \text{ Na}_2\text{O}.1.5\text{X}1.1.5\text{X}2$ ($\text{X}1 = \text{SrO and SrF}_2$) and ($\text{X}2 = \text{BaO and BaF}_2$). The principal conclusions reached regarding bioactive glasses and GICs are following:

- The larger ionic radius of strontium and barium compared to calcium ions aided in the creation of an extended and more freely cross-linked glass network without altering the fundamental glass structure.
- Ca substituted glasses with strontium and barium exhibited alterations in the crystallisation behaviour and display a reduction in the glass transition temperatures. This suggests the mixed cationic behaviour of the glasses and could be a possible economic advantage, indicating a route to produce lower glass transition temperature bioactive glasses commercially.

- The produced series of Al ions free silicate based bioactive glasses played a significant role in the phases of cement formation through the release of calcium, phosphate and strontium ions upon with the admixture of poly-acrylic acid and water with the introduction of tartaric and citric acid as setting modifiers.
- Substitution of calcium ions by strontium and barium in the basic glass composition had no deleterious effects on handling, biological and mechanical properties of the experimental ionomer cement samples.
- All produced silicate based ionomer cement samples with the amalgamation of citrate ions (CA GIC 1-7) as a setting modifier exhibited enhanced mechanism and *in vitro* biological properties in comparison with tartaric acid based cement samples (TA GIC 1-7).
- The produced series of Al ions free silicate based bioactive glasses (BG 6 and 7) can be incorporated along with the admixture of citric acid in the existing glass ionomer cement system to be used in medical and dental application.
- The proposed Al ions free silicate based glass ionomer cement is designed for the direct posterior dental restoration. It is a fluoride liberating, intrinsically adhesive, bulk-filling restorative material that readily bonds to the dentine and enamel. It is able to blend thoroughly with the surrounding tooth tissues. Whereas, cavity varnish coatings are recommended to be applied over the restorative GIC fillings, Therefore it is better to

use our prepared Glass ionomer cement as restorative material rather than using it as varnish.

6.3 Future work

Despite the data produced in this research and the conclusions reached as a result representing progress, there continues to be much which can be done to advance the field in the future. The following suggestions are therefore provided to guide future researchers:

- The analysis of radiopacity of the produced aluminium ion free silicate based bioactive glasses could be done which may help to detect recurrent or secondary caries and post-operative detections.
- To determine the content of fluorine, an X-ray fluorescence (XRF) and X-ray photon spectrometry (XPS) might be conducted on all produced aluminium ion free silicate based bioactive glasses.
- A multinuclear MAS-NMR study could be used to study the atomic environments of substituted ions such as strontium, barium and fluoride in the produced series of glasses which would give more insight into the structure made of these.
- The addition of transition metal ions could be introduced in the produced series of bioactive glasses that would possibly result in coloured ionomer cements that would be easier to use for surgical purposes due to their increased visibility.

-
- Based on improved *in vitro* results, the produced series of bioactive glasses could be further analysed by adopting various *in vivo* characterisations before implantation within the normal human body.
 - Both prepared glass and ionomer based cement samples could be further analysed by adopting *in vitro* hardness studies such as Vickers hardness, tensile and flexural toughness studies.
 - Temperature dependent Fourier transform infrared and Raman spectroscopic studies could be performed for further analysis of chemical changes resulting from heat treatment.

Chapter 7: References and Appendix

7.1 References

Ahluwalia, P., Chopara, S. and Thomas., AM. (2012) 'Strength characteristics and marginal sealing ability of chlorhexidine-modified glass ionomer cement: An in vitro study' . *Journal of the Indian Society of Pedodontics & Preventive Dentistry*, 30(1), 41-46.

Alan, B. and Banajee, A. (1998) 'Autofluorescence and Mineral Gontent of Carious Dentine: Scanning Optical and Backscattered Electron Microsoopic Studies'. *Caries Reserarch*, 32, 19-22

Andersson, O.H and Dahl, J.E. (1994) 'Aluminium release from glass ionomer cements during early water exposure in vitro'. *Biomaterials*, 15(11), 882-888.

Anusavice, K. J., Shen, C. and Rawals, H. R.(2012). *Phillips' science of dental materials*. 12th Ed. Elsevier Health Sciences. Oxford University Press.

Arepalli, S. K, Tripathi, H., Hira, S. K., Manna, P. P, Pyare, R. and Singh, S. P. (2016) 'Enhanced bioactivity,biocompatibility and mechanical behavior of strontium substituted bioactive glasses'. *Materials Science and Engineering: C*, 69, 108-116.

Babighian, G. (1992) 'Use of a glass ionomer cement in otological surgery. A preliminary report'. *The Journal of Laryngol Otology*, 106(11), 954-959.

Baelum, V., Heidmann, J. and Nyvad, B. (2006) 'Dental caries paradigms in diagnosis and

diagnostic research'. *European journal of oral sciences*, 114(4), 263-277.

Barra, E.D. and Hill, R.G. (2000) 'Influence of glass composition on the properties of glass polyalkenoate cement Part 3 Influence of Flourine Content'. *Biomaterials*, 21(6), 563-9.

Barreto, F. C., Barreto, D. V., Moyses, R. M. A., Neves, K. R., Canziani, M. E. F., Draibe, S. A., Jorgetti, V., and Carvalho, A. B. (2008) 'K/DOQI-recommended intact PTH levels do not prevent low-turnover bone disease in hemodialysis patients'. *The Journal of Kidney international*, 73(6), 771-777.

Batool, R., Imran, M., Kandhro, A. H., Salahuddin, N. and Uddin, M. K. H. (2017) 'Resistance Patterns among Multidrug-Resistant Tuberculosis Patients: A Multi-Center Study from Pakistan'. *The International Journal of Endorsing Health Science Research*, 5(4), 7-11.

Bher, M., Meier, S., Hahnel, S., Burgers, R., Handel, G. and Rosentritt, M. (2011) 'Glass ionomer layer thickness and its influence on zirconia failure'. *Journal of the mechanical behavior of biomedical materials*, 4(7), 1567-1570.

Bellucci, D., Bolelli, G., Cannillo, V., Cattini, A. And Sola, A. (2011) 'In Situ Raman spectroscopy investigation of bioactive glass reactivity: Simulated body fluid solution vs Tris-Buffered solution'. *Materials Characterisation*, 62, 1021-10228.

Berkovitz, B. K., Holland, G. R. and Moxham, B. J. (2009) *Oral anatomy, histology and embryology*. 5th Ed. Mosby/Elsevier. Oxford University Press.

- Bharti, R., Wadhvani, K. K., Tikku, A. P. and Chandra, A. (2010) 'Dental amalgam: An update'. *Journal of conservative dentistry: JDC*, 13(4), 204-208.
- Borra, R.C., Lotufo, M.A., Barros Fde, M. And Andrade, P.M. (2009) 'A simple method to measure cell viability in proliferation and cytotoxicity assays. *Brazilian Oral Research*, 23(3), 255-62.
- Botsali, M. S., Kusgoz, A., Altintas, S. H., Ulker, h. e., Tanriver, M., Kilic, S., Basak, F. and Ulker, M. (2014) 'Residual HEMA and TEGDMA release and cytotoxicity evaluation of resin-modified glass ionomer cement and compomers cured with different light sources'. *The Scientific world Journal Hindawi*, 2014, 218295, 1-7.
- Boyde, A. (1989) 'Enamel'. *Teeth Springer Journal*. 5/6, 309-473.
- Boyd, D., Clarkin, O.M., Wren, A.W and Towler, M.R. (2008a) 'Zinc-based glass polyalkenoate cements with improved setting times and mechanical properties'. *Acta biomaterialia*, 4(2), 425-431.
- Boyd, D., Towler, M.R., Watts, S., Hill, R.G., Wren, A.W. and Clarkin, O.M. (2008b) 'The role of Sr²⁺ on the structure and reactivity of SrO–CaO–ZnO–SiO₂ ionomer glasses'. *Journal of Materials Science: Materials in Medicine*, 19(2), 953-957.
- Brauer, D. S., Karpukhina, N., O'Donnell, M. D., Law, R. V. and Hill, R. G.(2010) 'Fluoride containing bioactive glasses: effect of glass design and structure on degradation, pH and apatite formation in simulated body fluid'. *Acta Biomaterialia*, 6(8), 3275-3282.

- Bretcanu, O., Chatzistavrou, X., Paraskevopoulos, K., Conradt, R., Thompson, I. And Boccaccini, A.R. (2009) 'Sintering and crystallisation of 45S5 Bioglass® powder'. *Journal of the European Ceramic Society*, 29(16), 3299-3306.
- Brentegani, L. G., Bombonato, K. F. and Carvalho, T. L. L. (1997) 'Histological evaluation of the biocompatibility of a glass-ionomer cement in rat alveolus'. *Biomaterials*, 18(2), 137-140.
- Brook, I. M., Craig, G. T. and Lamb, D. J. (1991) 'Initial in-vivo evaluation of glass-ionomer cements for use as alveolar bone substitutes'. *Clinical Materials*, 7(4), 295-300.
- Brune, D. and Smith, D. (1982) 'Microstructure and strength properties of silicate and glass ionomer cements'. *Acta Odontol Scand*, 40(6), 389-96.
- Burke, F. M., Ray, H. J. and McConnell, R. J. (2010) 'Fluoride- containing restorative materials'. *International Dental Journal*, 56(1), 33-43.
- Bechtle, S., Habelitz, S., Klocke, A., Fett, T. and Schneider, G.A. (2009) 'The Fracture Behaviour of Dental Enamel'. *Biomaterials*, 31(2), 375-84.
- Cao, W and Hench.L.L. (1996) 'Bioactive materials'. *Ceramics international*, 22, 493-507.
- Chalmers, J.M., Edwards, H.G.M. and Hargreaves, M.D. (2012). *Infrared and Raman spectroscopy in forensic science*. John Wiley & Sons.
- Charsley, E.L and Warrington, S.B. (1992). *Thermal analysis: techniques and applications*. Royal Society of Chemistry, 106(4).
- Chen, X., Cuijpers, V., Fan, M. and Frencken, J. E. (2010) 'Marginal leakage of two newer

glass-ionomer-based sealant materials assessed using micro-CT'. *The Journal of Dentistry*, 38(9), 731-735.

Chen, S., Ohman, C., Jefferies, S.R., Gray, H., Xia, W. and Engqvist, H. (2016) 'Compressive fatigue limit of four types of dental restorative materials'. *Journal of the mechanical behavior of biomedical materials*, 61, 283-289.

Chen, X., Chen, X., Brauer, D.S., Wilson, R., Hill, R.G. and Karpukhina, N. (2014) 'Novel Alkali Free Bioactive Fluorapatite Glass Ceramics'. *Non-crystalline Solids*, 402, 172-177.

Chung, E.J., Sugimoto, M.J. and Ameer, G.A. (2011) 'The role of hydroxyapatite in citric acid-based nanocomposites: Surface characteristics, degradation, and osteogenicity in vitro'. *Acta biomaterialia*, 7(11), 4057-4063.

Cabezas, C. G. (2010) 'The chemistry of caries: remineralization and demineralization events with direct clinical relevance'. *The Dental Clinics North America*, 54(3), 469-478.

Crisp, S., Lewis, B. G. and Wilson, B. G. (1979) 'Characterization of glass-ionomer cements. 5. The effect of the tartaric acid concentration in the liquid component'. *The Journal of Dentistry*, 7(4), 304-312.

Croll, T. P. And Nicholson, J. W. (2002) 'Glass ionomer cements in pediatric dentistry: review of the Literature'. *The Journal of Pediatric dentistry*, 24(5), 423-429.

Clifford, A., Hill, R., Rafferty, A., Mooney, P., Wood, D., Samuneva, B. and Matsuya, S. (2001) 'The influence of calcium to phosphate ratio on the nucleation and crystallisation of apatite Glass-Ceramics'. *Material Science and Engineering: C Mater Biol Appl*, 12(5), 461-469.

- Clupper, D. and Hench, L.L. (2003) 'Crystallization kinetics of tape cast bioactive glass 45S5'. *Journal of non-crystalline solids*, 318, 43-48.
- Deb, S. and Nicholson, J.W. (1999) 'The effect of strontium oxide in glass - ionomer cements'. *Journal of Materials Science: Materials in Medicine*, 10(8), 471-474.
- Derosa, R.L., Schader, P.A. and Shelby, J. (2003) 'Hydrophilic nature of silicate glass surfaces as a function of exposure condition'. *Journal of non-crystalline solids*, 331(1), 32-40.
- Doherty, P.J. (1991) 'Biocompatibility evaluation of glass ionomer cement using cell culture techniques'. *Clinical materials*, 7(4), 335-340.
- Dong, J., Ozaki, Y. and Nakashima, K. (1997) 'Infrared, Raman, and near-infrared spectroscopic evidence for the coexistence of various hydrogen-bond forms in poly (acrylic acid)'. *Macromolecules*, 30(4), 1111-1117.
- Duee, C., Grattepanche-Lebecq, I., Desanglois, F., Follet-Houttemance, C., Chai, F. and Hildebrand, H.F. (2013) 'Predicting bioactive properties of phosphosilicate glasses using mixture designs'. *Journal of Non-Crystalline Solids*, 362, 47-55.
- Dunlap, P. N. (1991) 'Glass flake reinforced composites as optical materials'. *The Journal of Applied Optics*, 30(13), 1701-1710.
- Doweider, H. (1996) 'The density of alkali silicate glasses in relation to the microstructure'. *Journal of non-crystalline solids*, 194(1-2), 155-162.
- Doweider, H. (1999) 'Density-structure correlations in silicate glasses'. *Journal of non-crystalline solids*, 249(2), 194-200.

Erol-Taygun, M., Zheng, K. and Boccaccini, A.R. (2013) 'Nanoscale bioactive glasses in medical applications'. *International Journal of Applied Glass Science*, 4(2), 136-148.

Forsten, L. (1990) 'Short- and long- term fluoride release from glass ionomers and other fluoride- containing filling materials in vitro'. *The European Journal of Oral Sciences*, 98(2), 179-185.

Franklin, P., Wood, D.J. and Bubb, N.L. (2005) 'Reinforcement of poly (methyl methacrylate) denture base with glass flake'. *Dental materials*, 21(4), 365-370.

Fratta, D., Aguetant, J. and Roussel-smith, L. (2007). *Introduction to soil mechanics laboratory testing*. CRC press.

Fredholm, Y.C., Karpukhina, N., Law, R.V. and Hill, R.G. (2010) 'Strontium containing bioactive glasses: glass structure and physical properties'. *Journal of Non-Crystalline Solids*, 356(44), 2546-2551.

Fredholm, Y.C., Karpukhina, N., Brauer, D.S., Jones, J.R., Law, R.V. and Hill, R.G. (2012) 'Influence of strontium for calcium substitution in bioactive glasses on degradation, ion release and apatite formation'. *Journal of the Royal Society Interface*, 9(70), 880-9.

Gentleman, E., Fredholm, Y. C., Jell, G., Lotfibakhshaiesh, N., O'Donnell, M. D., Hill, R. G. and Stevens, M. M. (2010) 'The effects of strontium-substituted bioactive glasses on osteoblasts and osteoclasts in vitro'. *The Journals of Biomaterials*, 31(14), 3949-3956.

Geyer, G. and Helms, J. (1993) 'Ionomer-based bone substitute in otologic surgery'. *The Egyptian Journal Society of Neurosurgery / European Archives of Oto-Rhino-Laryngol*, 250(5), 253-256.

- Geyer, G., Dazert, S. and Helms, J. (1997) 'Performance of ionomeric cement (Ionocem) in the reconstruction of the posterior meatal wall after curative middle-ear surgery'. *The Journal of Laryngology Otolaryngology*, 111(12), 1130-1136.
- Goh, Y.F., Alshemary, A.Z., Akram, M., Kadir, M.R.A. and Hussain, R. (2013) 'In vitro study of nano-sized zinc doped bioactive glass'. *Materials Chemistry and Physics*, 137(3), 1031-1038.
- Goldstein, J., Newbury, D.E., Echlin, P., Joy, D.C., Romig, A.D.J., Lyman, C.E., Fiori, C. and Lifshin, E. (2012). *Scanning electron microscopy and X-ray microanalysis: a text for biologists, materials scientists, and geologists*, Springer Science & Business Media.
- Goodman, W. G. and O'Connor, J. (1991) 'Aluminum alters calcium influx and efflux from bone in vitro'. *The Official Journal of the International Society of Nephrology*, 39(4), 602-607.
- Gomes, F.O., Pires, R.A. and Reis, R.L. (2013) 'Aluminum-free glass-ionomer bone cements with enhanced bioactivity and biodegradability'. *Material Science and Engineering. C Mater Biol Appl*, 33(3), 1361-70.
- Gonzalez, M.P., J.S., Lite, S., Chiussi, S., Bleon, M. and Perez-Amor, M. (2003) 'Raman spectroscopic study of bioactive silica-based glasses'. *Journal of Non-Crystalline Solids*, 320, 92-99.
- Grenade, C., Pauw-Gillet, M.C.D., Gailly, P., Vanheusden, A. and Mainjot, A. (2016) 'Biocompatibility of polymer-infiltrated-ceramic-network (PICN) materials with Human Gingival Fibroblasts (HGFs)'. *Dental Materials*, 32(9), 1152-64.

Griffin, S.G. and Hill, R.G. (2000) 'Influence of glass composition on the properties of glass polyalkenoate cement Part 2, Influence of Phosphate Content'. *Biomaterials*, 21(4), 399-403.

Griffin, S. G and Hill, R. G. (1999) 'Influence of glass composition on the properties of glass polyalkenoate cements. Part 1: Influence of aluminium to silicon ratio'. *The Journal of Biomaterials*, 20, 1579-1586.

Guggenberger, R. May, R. and Stefan, K. P. (1998) 'New trends in glass-ionomer chemistry'. *The Journal of Biomaterials*, 19(6), 479-483.

Guillard, O., Pineau, A., Fauconneau, B., Chobaut, J. C., Desaulty, A., Angot, A., Borgne, E. Le. and Furon, O. (1997) 'Biological levels of aluminium after use of aluminium-containing bone cement in post-Otoneurosurgery'. *The Journal of Trace Elements in Medicine and Biology*, 11(1), 53-56.

Hand, R. J. and Seddon, A. B. (1997) 'An hypothesis on the nature of Griffith's cracks in alkali silicate and silica glasses'. *The Society of Glass Technology, Physics and Chemistry of Glasses*, 38(1), 11-14, 4.

Hatton, P.V, and Brook, I. M. (1992) 'Characterisation of the ultrastructure of glass-ionomer (poly-alkenoate) cement'. *The British Dental Journal*, 173, 275-277.

Hench, L.L. (2006) 'The story of Bioglass®'. *The Journal of Materials Science: Materials in Medicine*, 17(11), 967-978.

Hickel, R., Dasch, W., Janda, R., Tyas, M. and Anusavice, K. (1998) 'New direct restorative

materials*'. *The International Dental Journal*, 48(1), 3-16.

Holland, W. and Beall, G. H. (2012) '*Glass Ceramic Technology*', John Wiley & Sons.

Hollinger, J.O. (2011). 2011. *An introduction to biomaterials*. 2nd Ed. CRC press.

Howard, L., Weng, Y. and Xie, D. (2014) 'Preparation and evaluation of a novel star-shaped polyacid-constructed dental glass - ionomer system'. *Dental Materials*, 30(6), 644-653.

Jones, J.R., Ehrenfried, L.M. and Hench, L.L. (2006) 'Optimising bioactive glass scaffolds for bone tissue engineering'. *Biomaterials*, 27(7), 964-973.

Jones, J.R. (2013) 'Review of bioactive glass: from Hench to hybrids'. *Acta Biomaterialia*, 9(1), 4457-86.

Jonck, L. M., Grobbelaar, C.J. and Strating, H. (1989) 'Biological evaluation of Glass Ionomer Cement (ketac-0) as an interface material in total joint replacement. A screening test'. *The Journals of Clinical Materials*, 4(3), 201-224.

Kalia, P., Brooks, R.A., Kinrade, S.D., Morgan, D.J., Brown, A.P., Rushton, N. and Jugdaohsingh, R. (2016) 'Adsorption of amorphous silica nanoparticles onto hydroxyapatite surfaces differentially alters surfaces properties and adhesion of human osteoblast cells'. *PloS one*, 11, e0144780.

Kenneth, R. S. J. (2007) 'Biocompatibility of Dental Materials'. *The Journal of Dental Clinics of North America*, 51(3), 747-760.

- Khan, A.S., Khan, M. and Rehman, Ur. Ihtesham. (2013) Chapter 5- Nanoparticles, Properties, and Applications in Glass Ionomer Cements. *Nanobiomaterials in Clinical Dentistry*. William Andrew. Pages 93-108.
- Khoroushi, M. and Keshani, F. (2013) ‘A review of glass-ionomers: From conventional glass-ionomer to bioactive glass-ionomer’. The *Dental Research Journal (Isfahan)*, 10(4), 411-20.
- Kim, C.Y., Clark. And Hench, L.L. (1989) ‘Early stages of calcium-phosphate layer formation in bioglasses’. *Journal of Non-Crystalline Solids*, 113(2-3), 195-202.
- Kim, D.A., Abo-Mosallam, H.A., Lee, H.Y., Kim, G.R., Kim, H.W. and Lee, H.H. (2014) ‘Development of a novel aluminum-free glass ionomer cement based on magnesium/strontium-silicate glasses’. *Material Science and Engineering. C Mater Biol Appl*, 42, 665-71.
- Kokubo, T. (1991) ‘Bioactive glass ceramics: properties and applications’. *Biomaterials*, 12(2), 155-163.
- Kokubo, T., Kim, H.M. and Kawashita, M. (2003) ‘Novel bioactive materials with different mechanical properties’. *Biomaterials*, 24(13), 2161-2175.
- Kokubo, T. and Takadama, H. (2006) ‘How useful is SBF in predicting in vivo bone bioactivity?’. *Biomaterials*, 27(15), 2907-2915.
- Kolmas, J., Jaklewicz, A., Zima, A., Bucko, M., Paszkiewicz, Z., Slosarczyk, A. and Kolodziejcki, W. (2010) ‘Incorporation of carbonate and magnesium ions into synthetic hydroxapatite: the effect on physico chemical properties’. *Molecular structure*, 987(1-3), 40-50.
- Koulourides, T. and Cameron, B. (1980) ‘Enamel remineralization as a factor in the

pathogenesis of dental caries'. *The Journal of Oral Pathology & Medicine*, 9, 255-269.

Krafft, C., Codrich, D., Pelizzo, G. and Sergo, V. (2008) 'Raman and FTIR imaging of lung tissue: Methodology for control samples'. *Vibrational Spectroscopy*, 46, 141-149.

Kurkjian, C. R. (1986) 'The physics and chemistry of glass (Glass science: a personal view)'. *The Journal of Non-Crystalline Solids*, 84(1-3), 1-6.

Lampin, M., Warocquier-Clerout., Legris, C., Degrange, M. and Sigot-luizard, M.F. (1997) 'Correlation between substratum roughness and wettability, cell adhesion, and cell migration'. *Journal of biomedical materials research*, 36(1), 99-108.

Lanford, W.A., Davis, K., Lamarche, P., Laursen, T., Groleau, R. and Doremus, R.H. (1979) 'Hydration of soda-lime glass'. *Journal of non-crystalline solids*, 33(2), 249-266.

Lee, J. J., Keun, Y., Jai, B., Ho, J., Jun, C. H., Kyu, H., Won, J. H., Kim. and Oh, S. (2010) 'Physical properties of resin-reinforced glass ionomer cement modified with micro and nano-hydroxyapatite'. *The Journal of nanoscience and nanotechnology*, 10(8), 5270-5276.

Lopes, C.C.A., Limirio, P.H.J.O., Novais, V.R. and Dechichi, P. (2018) 'Fourier transform infrared spectroscopy (FTIR) application chemical characterisation of enamel, dentin and bone'. *Applied Spectroscopy Review*, 53(9), 747-769.

Lucksanasombool, P., Higgs, W. A. J., Swain, M. V. and Howlett, C. R. (2002) 'Effects of Glass Ionomer cements on bone tissue'. *The Journal of Materials Science: Materials in Medicine*, 13(2), 203-210.

- Lynch, E., Brauer, D.S., Karpukhina, N., Gillam, D.G. and Hill, R.G. (2012) 'Multi-component bioactive glasses of varying fluoride content for treating dentin hypersensitivity'. *Dental Materials*, 28(2), 168-78.
- Mahapatra, M. K. and Lu, K. (2010) 'Glass based seals for solid oxide fuel and electrolyzer cells – A review'. *The Materials Science and Engineering: R: Reports*, 67(5-6), 65-85.
- Maeda, T., Mukaeda, K. and Shimohira, T. (1999) 'Ion distribution in matrix parts of glass-polyalkenoate cement by SIMS'. *The Journal of Dental Research*, 78(1), 86-90.
- Maltz, M., Jardim, J. J. and Alves, L. S. (2010) 'Health promotion and dental caries'. *The Brazilian Oral Research Journal*, 24 (1), 18-25.
- Marthaler, T. M. (2004) 'Changes in dental caries 1953–2003'. *The Journal of Caries research*, 38, 173-181.
- Matsuya, S. Maeda, T. and Ohta. (1996) 'IR and NMR analyses of hardening and maturation of glass-ionomer cement'. *The Journal of Dental Research*, 75(12), 1920-1927.
- Mason, H.E., Kozlowski, A. and Phillips, B.L. (2008) 'Solid-state NMR study of the role of H and Na in AB Type carbonate hydroxylapatite'. *Chemical Material*, 20(1), 294-302.
- Ma, Z., Merkus, H.G., DeSmet, J.G., Heffels, C. and Scarlett, B. (2000) 'New developments in particle characterization by laser diffraction: size and shape'. *Powder Technology*, 111(1), 66-78.
- Meyer, U., Szulczewski, D. H., Barchaus, R. H., Atkinson, M. and Jones, D. B. (1993) 'Biological evaluation of an ionomeric bone cement by osteoblast cell culture methods'. *The*

Journal of Biomaterials, 14(12), 917-924.

Miguez-Pachecco, V., Hench, L.L. and Boccaccini, A.R. (2015) 'Bioactive glasses beyond bone and teeth: emerging applications in contact with soft tissues'. *Acta biomaterialia*, 13, 1-15.

Mitchell, L. David, A. M. (2016) '*Clinical Dentistry Oxford Book*. The Oxford University Press.

Mneimne, M., Hill, R. G., Bushby, A. J. and Brauer, D. S. (2011) 'High phosphate content Significantly increases apatite formation of fluoride-containing bioactive glasses'. *Acta Biomaterialia*, 7(4), 1827-34.

Moshaverinia, A., Ansari, S., Movasaghi, Z., Billington, R. W., Darr, J. A. and Rehman, I. U. (2008) 'Modification of conventional glass-ionomer cements with N-vinylpyrrolidone containing polyacids, nano-hydroxy and fluoroapatite to improve mechanical properties'. *The Dental Materials Journal*, 24(10), 1381-1390.

Moshaverinia, A., Roohpour, N., Ansari, S., Moshaverinia, M., Schricker, Scott., Darr, J. A. and Rehman, I. U. (2009) 'Effects of N-vinylpyrrolidone (NVP) containing polyelectrolytes on surface properties of conventional glass-ionomer cements (GIC)'. *The Journal of Dental Materials*, 25(10), 1240-1247.

Mayo, G. C. (1960) 'Gray's Anatomy of the Human Body'. *The Journal of Medical Education Academic Medicine*, 35(1), 90.

- Miller, C., Hatton, P. V. and Mirvakily, F. (2014) 'A Novel Glass Ionomer Cement'.
- Motohiro, U.O., Sasaki, A., Masuda, J., Ino, J and Watari, F. (2010) 'Application of flake shaped glass (Glass Flake®) filler for dental composite resin. *Journal of the Ceramic Society of Japan*, 118(1378), 425-427.
- Nanci, A., (2003) *Ten Cate's Oral Histology, Development, Structure, and Function*. 9th Ed. Elsevier Oxford University Press.
- Nassan, M. A. and Watson, T. F. (1998) 'Conventional glass ionomers as posterior restorations. A status report for the American Journal of Dentistry'. *The American Journal of Dentistry*, 11(1), 36-45.
- Nelson, S.J. (2009) '*Wheeler's Dental Anatomy, Physiology and Occlusion*'. 75th Ed, Elsevier Health Sciences. The Oxford University Press.
- Neel, E.A.A., Pickup, D.M., Valappil, S.P., Newport, R.J. and Knowles, J.C. (2009) 'Bioactive functional materials: a perspective on phosphate-based glasses'. *Journal of Materials Chemistry*, 19(6), 690-701.
- Nicholson, J.W., Brookman, P.J., Lacy, O.M. and Wilson, A.D. (1988) 'Fourier transform infrared spectroscopic study of the role of tartaric acid in glass-ionomer dental cements'. *Journal of dental research*, 67(12), 1451-1454.
- Noro, A., Kaneko, M., Murata, I. and Yoshinari, M. (2013) 'Influence of surface topography and surface physicochemistry on wettability of zirconia (tetragonal zirconia polycrystal)'. *Journal of Biomedical Materials Research Part B: Applied Biomaterials*, 101(2), 355-363.
- Nicholson, J.W. and Czarnecka, B. (2009) 'Review paper: role of aluminum in glass-ionomer

Dental cements and its biological effects'. *The Journal of Biomaterials Applications*, 24(4), 293-308.

Nicholson, J.W. (1998) 'Chemistry of glass-ionomer cements: a review'. *Biomaterials*, 19(6), 485-94.

Noort, R.V. (2013) 'Introduction to Dental Materials4: Introduction to Dental Materials', 4th Ed, Elsevier Health Sciences. The Oxford University Press. UK.

O'Donnell, M.D., Watts, S.J., Law, R.V. and Hill, R.G. (2008) 'Effect of P 2 O 5 content in two series of soda lime phosphosilicate glasses on structure and properties–Part II: Physical properties. *Journal of Non-Crystalline Solids*, 354(30), 3561-3566.

O'Donnell, M.D., Watts, S.J., Hill, R.G. and Law, R.V. (2009) 'The effect of phosphate content on the bioactivity of soda-lime-phosphosilicate glasses'. *Journal of Materials Science: Materials in Medicine*, 20(8), 1611-1618.

O'Brien, W. J. (1997) 'Dental materials and their selection', 3rd Ed, 69(4), 47-48, Quintessence Publishing Press. Chicago. USA.

Olivia, A., Ragione, F. D., Salerno, A., Riccio, V., Tartaro, G., Cozzolino, A., D'Amato, S., Pontoni, G. and Zappia, V. (1996) 'Biocompatibility studies on glass ionomer cements by primary cultures of human Osteoblasts'. *The Journal of Biomaterials*, 17(13), 1351-1356.

Osborn, J. W. (1968) 'Directions and interrelationship of prism in cuspal and cervical enamel of human teeth'. *The Journal of Dental Research*, 47(3), 395-402.

- Oyane, A., Kim, H.M., Furuya, T., Kokubo, T., Miyazaki, T. and Nakamura, T. (2003) 'Preparation and assessment of revised simulated body fluids. *Journal of Biomedical Materials Research Part A*, 65(2), 188-195.
- Panda, R.N., Hsieh, M.F., Chung, R.J. and Chin, T.S. (2003) 'FTIR, XRD, SEM and solid-state NMR investigations of carbonate containing hydroxapatite nano particles synthesised by hydroxide gel technique'. *Physics and chemistry of solids*, 64(2), 193-199.
- Peitl, O., Zanotto, E. D. and Hench, L.L. (2001) 'Highly bioactive P₂O₅-Na₂O-CaO-SiO₂ glass ceramics'. *The Journal of Non-crystalline Solids* 292(1-3), 115-126.
- Peitl, O., Zanotto, E. D., Serbena, F. C. and Hench, L. L. (2012) 'Compositional and microstructural design of highly bioactive P₂O₅-Na₂O-CaO-SiO₂ glass-ceramics'. *Acta Biomaterialia*, 8(1), 321-332.
- Prentice, L.H., Tyas, M and Burrow, M.F. (2006) 'The effect of oxalic acid incorporation on the setting time and strength of a glass-ionomer cement'. *Acta biomaterialia*, 2(1), 109-112.
- Prosser, H. J., Jerome, S. M. and Wilson, A.D. (1982) 'The effect of additives on the setting properties of a glass-ionomer cement'. *The Journal of Dental Research*, 61(10), 1195-1198.
- Prosser, H. J. Powis, D. R. and Wilson, A.D. (1986) 'Glass-ionomer cements of improved flexural strength'. *The Journal of Dental Research*, 65(2), 146-148.
- Qian, S. and Liu, X. (2015) 'Cytocompatibility of Si-incorporated TiO₂ nanopores films'. *Colloids and Surfaces B: Biointerfaces*, 133, 214-220.

Qiu, H., Yang, J., Kodali, P., Koh, J. and Ameer, G.A. (2006) 'A citric acid-based hydroxyapatite composite for orthopedic implants'. *Biomaterials*, 27(34) 5845-5854.

Rampersad, S.N. (2012) 'Multiple application of alamar blue as an indicator of metabolic function and cellular health in cell viability bio assays'. *Braz Oral Res*, 12(9), 12347.

Rao, K. J. (2002) 'Structural chemistry of glasses', Elsevier.

Rehman, I., Hench, L.L., Bonfield, W. and Smith, R. (1994) 'Analysis of surface layers on bioactive glasses. *Biomaterials*, 15(10), 865-870.

Rehman, I., Movasaghi, Z. and Rehman, S. (2012). *Vibrational spectroscopy for tissue analysis*, CRC Press.

Renard, J.L., Felten, D. and Bequet, D. (1994) Post-otoneurosurgery aluminium encephalopathy. *The Lancet*, 344, 63-64.

Rexer, J. and Anderson, E. (1979) 'Composites with planar reinforcements (flakes, ribbons)—A review. *Polymer Engineering & Science*, 19(1), 1-11.

Robinson, C., Shore, R. C. and Brookes, S. J. (2000) 'The chemistry of enamel caries. *Critical Reviews in Oral Biology & Medicine*', 11(4), 481-495.

Ronald, L., Sakaguchi, J. M. P. (2012) '*Craig's Restorative Dental Materials*', Elsevier. 13th Ed, The Oxford University Press. UK.

Robinsal. (1983) 'Alteration in the composition of the permanent human teeth during various attack in the demineralization and remineralization of the teeth', Leah SA, Edgar WM, editors Oxford IRL press. The Oxford University.

Saadaldin, S.A., Dixon, S.J., Costa, D.O. and Rizkalla A.S. (2013) 'Synthesis of bioactive and machinable miserite glass-ceramics for dental implant applications'. *Dental Materials*, 29(6), 645-655.

Sathyanarayana, D.N. (2015). *Vibrational spectroscopy: theory and applications*. New Age International.

Sanati, M. and Andersson, A. (1993) 'DRIFT study of the oxidation and the ammoxidation of toluene over a TiO₂ (B)-supported vanadia catalyst'. *Journal of molecular catalysis*, 81(1), 51-62.

Sanchez-Ferrero, A., Mata, A., Mateos-Timoneda, M.A., Rodriguez-Cabelo, J.C., Alonso, M., Planell, J. and Engel, E. (2015) 'Development of tailored and self-mineralizing citric acid-crosslinked hydrogels for in situ bone regeneration'. *Biomaterials*, 68, 42-53.

Santocildes-Romero, M.E., Crawford, A., Hatton, P.V., Goodchild, R.L, Reaney, I.M. and Miller, C.A. (2015) 'The osteogenic response of mesenchymal stromal cells to strontium-substituted bioactive glasses'. *Journal of tissue engineering and regenerative medicine*, 9(5), 619-631.

Sarda, S., Fernandez, E., Nilsson, M., Balcells, M. and Planell, J.A. (2002) 'Kinetic study of citric acid influence on calcium phosphate bone cements as water- reducing agent'. *Journal of Biomedical Materials Research Part A*, 61(4), 653-659.

Salentijn, L. M., Hendric-Klyvert, M. (1985). 'Dental and oral tissues; an introduction'. Philadelphia Lea and Febiger. 236.

Sayyeddan, F. S., Fathi, M. H., Edris, H., Mohammadi, A. D., Mortazavi, V. and Shirani, F.

- (2013) 'Fluoride release and bioactivity evaluation of glass ionomer: Forsterite nanocomposite'. *The Dental Research Journal*, 10(4), 452-459.
- Sepulveda, P., Jones, J.R. and Hench, L.L. (2002) 'In vitro dissolution of melt- derived 45S5 and sol- gel derived 58S bioactive glasses'. *Journal of Biomedical Materials Research Part A*, 61(2), 301-311.
- Sepulveda, P., Jones, J.R. and Hench, L.L. (2001) 'Characterization of melt- derived 45S5 and sol- gel - derived 58S bioactive glasses'. *Journal of biomedical materials research*, 58(6), 734-740.
- Serra, J., Gonzalez, S., Liste, S., Chiussi, B., Leon, M., Perez-Amor, H.O. and Ylanen, M. and Hupa. (2002) 'Influence of the non-bridging oxygen groups on the bioactivity of silicate glasses'. *Journal of Materials science: Materials in medicine*, 13(12), 1221-1225.
- Shang, S.M., Li, Z., Xing, Y., Xin, J.H. and Tao, X.M. (2010) 'Preparation of durable hydrophobic cellulose fabric from water glass and mixed organosilanes'. *Applied Surface Science*, 257, 1495-1499.
- Shih, P. (2003) 'Properties and FTIR spectra of lead phosphate glasses for nuclear waste immobilization'. *Materials chemistry and physics*, 80, 299-304.
- Singh, T.M., Suresh, P., Sandhyarani, J. and Sravanthi, J. (2011) 'Glass Ionomer Cements (GIC) in Dentistry: A REVIEW.
- Selwitz, R. H., Ismail, A. and Pitts, N. B. (2007) 'Dental caries'. *The Lancet Journal*, 369(9555), 51-59.

Schulz, S., Tomakidi, P., Mauth, C., Kohal, R. and Steinberg, T. (2012) 'Interactive fibroblast-keratinocyte co-cultures: an in vivo-like test platform for dental implant-based soft tissue integration'. *Tissue Engineering Part C: Methods*, 18(10), 785-796.

Shafique, M. A., Murtaza, G., Saadat, S., Zaheer, Z., Shahnawaz, M., Ahmed, R. and Uddin, M. K. H. (2016) 'Study of Nickel Ion Release in Simulated Body Fluid from C⁺- Implanted Nickel Titanium Alloy'. *The Journal of Scientific Review and Letters*, 23(5).

Shafique, M. A, Murtaza, G., Saadat, S., Ahmed, R. and Uddin, M. K. H. (2017) 'Improved Cell Viability and Hydroxyapatite Growth on Nitrogen ion- Implanted Surfaces'. *The Journal Radiation Effect and Defects in Solids: Incorporating Plasma Science and Plasma Technology*, 172(7-8), 590-599.

Shahid, S., Hassan, U., Billington, R.W., Hill, R. G. and Anderson, P. (2014) 'Glass ionomer cements: effect of strontium substitution on esthetics, radiopacity and fluoride release'. *The Journal of Dental Materials*, 30(3), 308-313.

Sharma, R., Bisen, D., Shukla, U. and Sharma, B. (2012) 'X-ray diffraction: a powerful method of characterizing nanomaterials'. *Recent Research in Science and Technology*, 4.

Smith, E and Dent, G. (2013). *Modern Raman spectroscopy: a practical approach*. John Wiley & Sons.

Smith, D. C. (1998) 'Development of glass-ionomer cement systems'. *The Journal of Biomaterials*, 19(6), 467-478.

Sereno CEM® commercial brochure. Corinthian Medical Ltd, Nottingham, UK.

Shelby, J.E. (2005). *Introduction to glass science and Technology*. 2nd ed. Royal Society of Chemistry.

Shimada, S., Tanaka, H. and Nakagawa, T. (1992) 'Glass Flake Composite'. Patent, Nippon Glass Fiber Co Ltd. Japan.

Simon, J., Charles. B. and Watkinson. (2009) *Understanding and use of glass flake (Paint and Coatings Industry*. Special Chemistry. The Oxford University Press. UK.

Smith, C. D. and Williams, D. F. (1982) 'Biocompatibility of Dental Materials: Biocompatibility of preventive dental materials and bonding agents'. *Journal of Dental Materials*, 4, 33431.

Stamboulis, A., Law, R. V. and Hill, R. G. (2004) 'Characterisation of commercial ionomer glasses using magic angle nuclear magnetic resonance (MAS-NMR)'. *The Journal of Biomaterials*, 25(17), 3907-3913.

Subramani, K., Ahmed, W. and Hartsfield, J.K. (2012). *Nanobiomaterials in Clinical Dentistry*. William Andrew.

Sun, D., Chen, Y., Tran, R. T., Xu, S., Xie, D., Jia, C., Wang, Y., Guo, Ying., Zhang, Z., Guo, J., Jang, Y., Jin, D. and Bai, X. (2014) 'Citric acid based hydroxapatite composite scaffolds enhance calvarial regeneration'. *The Journal of Scientific Reports* 4 ; 6912.

Svanberg, M., Mjor, I. A. and Orstavik, D. (1990) 'Mutans streptococci in plaque from argins of amalgam, composite, and glass-ionomer restorations'. *The Journal of Dental Research*, 69(3), 861-864.

- Tadjiev, D. R. and Hand, R. J. (2010) 'Surface hydration and nanoindentation of silicate glasses'. *The Journal of Non-Crystalline Solids*, 356(2), 102-108.
- Tiwari, S. and Nandlal, B. (2012) 'Comparative evaluation of fluoride release from hydroxyapatite incorporated and conventional glass ionomer cement: an in vitro study'. *The Journal of Indian Society of Pedodontics and Preventive Dentistry*, 30(4), 284-287.
- Tyas, M.J. (2006) 'Clinical evaluation of glass-ionomer cement restorations'. *Journal of Applied Oral Science*, 14, 10-13.
- Tyas, M. J. (1991) 'Cariostatic effect of glass ionomer cement: a five- year clinical study'. *The Australian Dental Journal*, 36(3), 236-239.
- Tran, R. T., Wang, L., Zhang, C., Huang, M., Tang, W., Zhang, C., Zhang, Z., Jin, D., Banik, B., Brown, J. L., Xie, Z., Bai, X. and Yang, J. (2014) 'Synthesis and characterization of biomimetic citrate based biodegradable composites'. *The Journal of Biomedical Materials Research Part A*, 102 (8), 2521-2532.
- UO, M., Sasaki, A., Mausda, J., INO, J. and Watari, F. (2010) 'Application of flake shaped glass (Glass Flake®) filler for dental composite resin'. *The Journal of the Ceramic Society of Japan*, 118(1378), 425-427.
- Varshneya, A. K. (1994) 'Fundamentals of inorganic glasses', Elsevier, Gulf Professional Publishing.

Velazo, G., Almanza, J.M., Cortes, D.A., Escobedo, J.C. and Escalante-Garcia, J.I. (2014) 'Effect of citric acid and the hemihydrate amount on the properties of a calcium sulphoaluminate cement. *Materiales de Construcción*, 64, 036.

Vijayaraghavan, R. (2008). *Nondestructive FTIR-photoacoustic spectroscopy studies on carbon fiber reinforced polyimide composite and water diffusion in epoxy resin*. ProQuest.

Vogler, E.A. (1998) 'Structure and reactivity of water at biomaterial surfaces'. *Advances in colloid and interface science*, 74, 69-117.

Walls, A. W. G. (1986) 'Glass polyalkenoate (glass-ionomer) cements: a review'. *The Journal of Dentistry*, 14(6), 231-246.

Wanpeng, C. and Hench, L. L. (1995) 'Bioactive Materials'. *The Journal of Ceramic International*, 22, 493-507.

Wiegand, A., Buchalla, W. and Attin, T. (2007) 'Review on fluoride-releasing restorative materials-fluoride release and uptake characteristics, antibacterial activity and influence on caries formation'. *The Journal of Dental Materials*, 23(3), 343-362.

Wilson, A. D., Crisp, S. and Fener, A. J. (1976) 'Reactions in glass-ionomer cements: IV. Effect of chelating comonomers on setting behavior'. *The Journal of Dental Research*, 55, 489-495.

Wilson, A.D. (1990) 'Resin-modified glass-ionomer cements'. *International Journal of Prosthodontics*, 3(5), 425-429.

White, G.J., Beech, D.R. and Tyas, M.J. (1989) 'Dentin smear layer: an asset or a liability for bonding?' *Dental Materials*, 5(6), 379-383.

Wood, D. and Hill, R. G. (1991) 'Glass ceramic approach to controlling the properties of a glass-ionomer bone cement'. *The Journal of Biomaterials*, 12(2), 164-170.

Williams, P. L. (1995). *Grays Anatomy: The Anatomical Basis of Medicine and Surgery*, 38e. PJ-73278 Oxford University Press.

Xiang, Y. and Du, J. (2011) 'Effect of strontium substitution on the structure of 45S5 bioglasses'. *Chemistry of Materials*, 23(11), 2703-2717.

Xie, D., Brantley, W. A., Culbertson, B. M. and Wang, G. (2000) 'Mechanical properties and microstructures of glass-ionomer cements'. *The Journal of Dental Materials*, 16(2), 129-138.

Yadav, K. and Prakash, S. (2017) 'Dental Caries: A microbiological approach'. *Journal of Clinical Infectious Diseases and Practice*, 2(1), 1-15.

Yang, X., Ma, G. and Nie, J. (2012) 'Synthesis and characterization of diethanolamine-containing glass ionomer cement'. *Journal of Applied Polymer Science*, 125(2), 1330-1338.

Yang, C., Smyrl, W.H., Cussler, E.L. (2004) 'Flake alignment in composite coatings'. *Journal of membrane science*, 231(1-2), 1-12.

Yoder, C.H., Pasteris, J.D., Worcester, K.N. and Schermerhorn, D.V. (2011) 'Structural water in carbonated hydroxylapatite and fluorapatite: confirmation by solid state ^2H NMR'. *Calcified Tissue International*, 90(1), 62-67.

Young, A.M., Sherpa, A., Pearson, G., Schottlander, B. and Waters, D.N. (2000) 'Use of Raman spectroscopy in the characterisation of the acid - base reaction in glass-ionomer cements'. *Biomaterials*, 21(19), 1971-1979.

Yun, H.S., Kim, S.H., Lee, S. and Song, I.H. (2010) 'Synthesis of high surface area mesoporous bioactive glass nano spheres'. *Materials Letters*, 64(16), 1850-1853.

Zhang, W., Masumi, S.I. and Song, X. M. (2010) 'Bonding property of two resin-reinforced glass-ionomer cements to zirconia ceramic'. *The Quintessence International Journal*, 41, 132-140.

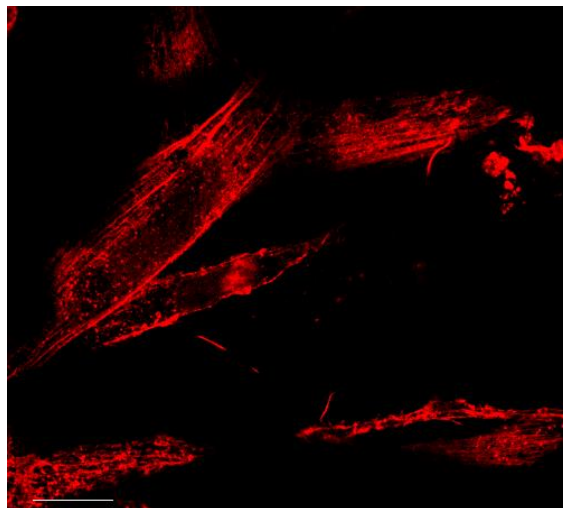
Zheng, M., Yang, Y., Lui, X.Q., Liu, M.Y., Zhang, X.F., Wang, X., Li, H.P. and Tan, J.G. (2015) 'Enhanced Biological Behavior of In Vitro Human Gingival Fibroblasts on Cold Plasma-Treated Zirconia'. *PloS one*, 10(10), e0140278.

7.2 Appendix

Poster Presentations and Image Competitions

1. Kroto Research Institute (KRI) image competition.
2. Material Sciences and Engineering (MSE) image competition.
3. Poster presented in Kroto Research Institute, Sir Harry Kroto Visit to University.
4. Poster presented in Department of Material Sciences and Engineering competition.
5. Poster presented at the University of Sheffield Engineering Conference (USES).
6. Poster presented at the Doctoral Academy Conference of the University of Sheffield.

Images Selected for Departmental (MSE) Competitions



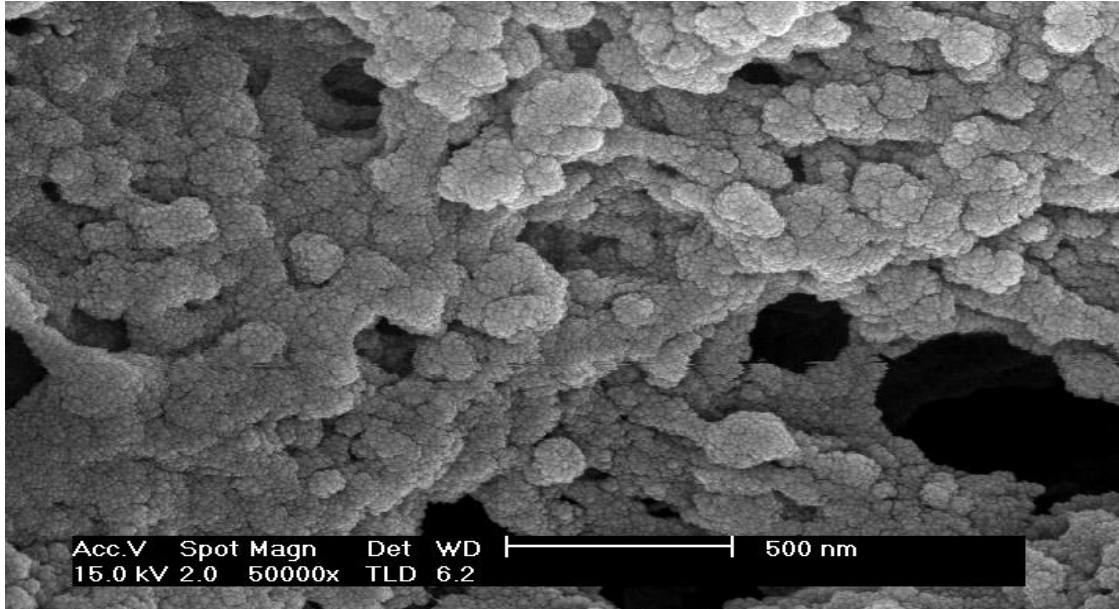
Title: *Anchoring of Cell over Biomaterial*

(Material Sciences and Engineering (MSE)

Image competition)

Title: *Blossoming of Nascent Bone over Biomaterials*

Kroto Research Institute (KRI) Image Competition

**Awards & Achievements**

1. Awarded fee waiver / scholarship from the Department of Material Sciences and Engineering, The University of Sheffield. UK.
2. Represented (Department of Material Sciences and Engineering) in Doctoral Academy Research Conference at the University of Sheffield. UK.
3. Chair sessions over ‘Advancement in Sciences’ in Doctoral Academy Research Conference at the University of Sheffield. UK.
4. Facilitator from the Department of Material Sciences and Engineering, for Research Ethics and Integrity Course from 2014 – 2016.
5. Demonstrator / Laboratory mentor for undergraduate and post-graduate taught courses students for the Departments of Material Science and Engineering,

Chemical and Biological Engineering and Biomaterials and Tissue Engineering (2014 – 2017) at The University of Sheffield. UK.

6. Graduate Teaching Assistant for the departments of Material Sciences and Engineering, Chemical and Biological Engineering and Biomaterials and Tissue Engineering (2014 – 2017).

Mentoring and Project Supervision

Mentor MSc (taught) students from the Department of Material Sciences and Engineering and the Department of Clinical Medicine and Dentistry (2013 – 2017).

- Mr Shariq Najeeb (MSc 2013 – 2014)
- Mr Shehriar Hussain (MSc 2013 – 2014)
- Mr Arqam Najmi (MSc 2014 – 2015)
- Mr Ahmed Rafikan (MSc 2014 – 2015)
- Mr Tannay. B. Thakkur (MSc 2014 – 2015)
- Miss Nisha Nair (MSc 2014 – 2015)
- Miss Daniella L. P (MSc 2014 – 2015)
- Miss Xuzi Zhao (MSc 2015 – 2016)
- Miss Bella (MSc 2015 – 2016)
- Mrs Fatemah H Boaoies (MSc 2016 – 2017)

RADIATION EFFECTS & DEFECTS IN SOLIDS, 2017
VOL. 172, NOS. 7–8, 590–599
<https://doi.org/10.1080/10420150.2017.1367296>



Improved cell viability and hydroxyapatite growth on nitrogen ion-implanted surfaces

Muhammad Ahsan Shafique^a, G. Murtaza^a, Shahzad Saadat^a, Muhammad K H Uddin^b and Riaz Ahmad^a

^aCentre for Advanced Studies in Physics, Government College University, Lahore, Pakistan; ^bKroto Research Institute, University of Sheffield, Sheffield, UK

ABSTRACT

Stainless steel 306 is implanted with various doses of nitrogen ions using a 2 MV pelletron accelerator for the improvement of its surface biomedical properties. Raman spectroscopy reveals incubation of hydroxyapatite (HA) on all the samples and it is found that the growth of incubated HA is *greater in higher ion dose samples*. SEM profiles depict uniform growth and greater spread of HA with higher ion implantation. Human oral fibroblast response is also found consistent with Raman spectroscopy and SEM results; the cell viability is found maximum in samples treated with the highest (more than 300%) dose. XRD profiles signified greater peak intensity of HA with ion implantation; a contact angle study revealed hydrophilic behavior of all the samples but the treated samples were found to be lesser hydrophilic compared to the control samples. *Nitrogen implantation yields greater bioactivity, improved surface affinity for HA incubation and improved hardness of the surface.*

ARTICLE HISTORY

Received 29 September 2016
Accepted 7 August 2017

KEYWORDS

Nitrogen ion; implantation;
stainless steel; cell viability;
hydroxyapatite

1. Introduction

Biomaterial is a natural or synthetic material which is used to make a bio-implant or any device for *in vivo* use. The purpose of *in vivo* use may be the treatment or replacing of some damaged or dysfunctional tissue organ. The history of metals used as biomaterial is more than 100 years old. Lane was the first person who introduced a metal plate inside a body for bone fracture fixation in 1895. Metallic materials have been employed for diverse biomedical applications in various fields of biomedical science. The examples of metallic materials as biomaterials include the mesh of stainless steel or nickel alloy as coronary heart stent, stainless steel or cobalt as artificial femoral head for total hip replacement, stainless steel and titanium as bone plates and screws, etc. Therefore, there is an earnest need to improve the relevant properties of candidate biomaterials (1–4). Stainless steel (SS) is an important alloy for many biomedical applications because SS is stable (appropriately corrosion resistant), bioactive and has good mechanical properties, but there are always some associated deficiencies with every material. The deficiencies of SS include toxic ion (Ni, Cr) release from the surface and miss-match of mechanical properties with bone (hardness, tensile), etc. (5–7).

CONTACT Muhammad Ahsan Shafique  muhammadahsan@gcu.edu.pk

© 2017 Informa UK Limited, trading as Taylor & Francis Group

Original Article

doi: 10.29052/IJEHSR.v5.i4.2017.07-11

Resistance Patterns among Multidrug-Resistant Tuberculosis Patients: A Multi-Center Study from Pakistan**Rabab Batool¹, Muhammad Imran^{2,3}, Abdul Hafeez Kandhro³, Zainab Barry⁴,
Naseem Salahuddin⁴ & Muhammad K H Uddin⁵**¹The Aga Khan University Hospital, Karachi, Pakistan.²The College of Medical Technology, Zia Uddin Medical University, Karachi, Pakistan.³Healthcare Molecular and Diagnostic Laboratory Hyderabad, Pakistan.⁴The Indus Hospital, Karachi, Pakistan.⁵The Department of Material Sciences and Engineering, Kroto Research Institute, The University of Sheffield, United Kingdom.

*Corresponding Author Email ID: imranmuhammad@zu.edu.pk

Received 23/11/17; Accepted 20/12/17; First Published 30/12/17

Abstract

Background: The high burden of multi-drug resistance tuberculosis (MDR TB) is a matter of great concern. The increasing resistance to anti tuberculosis drugs has been the area of growing concern and are posing threats to TB control. The aim of this study was to evaluate the drug resistance patterns for the first line and second line anti-Tuberculosis drugs in multiple drug resistant tuberculosis (MDR-TB) patients.

Method: The study was retrospective, observational, employing purposive, non-random sampling technique for data collection conducted at the TB Clinic- of the different healthcare centers in the provinces of Pakistan Sindh and Baluchistan from December 2010 to May 2016. All bacteriologically confirmed TB patients who were found to be Rifampin Resistant (RR) on Genotypic drug susceptibility testing (GXP), or detected to be drug resistant on phenotypic Universal drug susceptibility testing were enrolled into the study.

Results: Out of total 3776 patients, 96.3% were resistant to Rifampicin and 94.7% were resistant to Isoniazid. 25.5% isolates were resistant to all five first line drugs. Resistances against Pyrazinamide and Ethambutol was 54.2% and 51.6% respectively. 36.3% patients were resistant to Fluoroquinolones (FQ), 9.7% were resistant to Ethionamide (Eto) and 4.1% were resistant to both FQ and Eto. 33.5% patients were MDR plus resistant to FQ. However, the resistance to both FQ plus Aminoglycosides was quite low, 2.7%.

Conclusion: The drug resistance rates are quiet high in MDR-TB for both first line and second line drugs. The standardized MDR TB regimen needs to be updated, based on the prevalence of drug resistance patterns in the community for the effective management of drug resistant TB.

Keywords

Multiple drug resistant tuberculosis, Resistance, Genotypic drug susceptibility testing, Phenotypic Universal drug susceptibility testing, Aminoglycosides.

Introduction

Drug resistance pattern among MDR-TB patients is of critical importance for its role in designing of individualized regimen and the control of TB¹⁻². Pakistan ranks five

among the 22 high burden countries in the world for MDR TB^{3,4}. The results of a recent drug resistance surveillance carried out in Pakistan by the National TB Control Program (NTP), estimated MDR TB in

Surface Review and Letters | Vol. 23, No. 05, 1650045 (2016) | Regular Articles

STUDY OF NICKEL ION RELEASE IN SIMULATED BODY FLUID FROM C⁻-IMPLANTED NICKEL TITANIUM ALLOY

MUHAMMAD AHSAN SHAFIQUE ✉, G. MURTAZA, SHAHZAD SAADAT, ZEESHAN ZAHEER, MUHAMMAD SHAHNAWAZ, MUHAMMAD K. H. UDDIN and RIAZ AHMAD

<https://doi.org/10.1142/S0218625X16500451> |

Abstract

Nickel ion release from NiTi shape memory alloy is an issue for biomedical applications. This study was planned to study the effect of C⁻ implantation on nickel ion release and affinity of calcium phosphate precipitation on NiTi alloy. Four annealed samples are chosen for the present study; three samples with oxidation layer and the fourth without oxidation layer. X-ray diffraction (XRD) spectra reveal amorphization with ion implantation. Proton-induced X-ray emission (PIXE) result shows insignificant increase in Ni release in simulated body fluid (SBF) and calcium phosphate precipitation up to 8×10^{13} ions/cm². Then Nickel contents show a sharp increase for greater ion doses. Corrosion potential decreases by increasing the dose but all the samples passivate after the same interval of time and at the same level of V_{SCE} in ringer lactate solution.

Hardness of samples initially increases at greater rate (up to 8×10^{13} ions/cm²) and then increases with lesser rate. It is found that 8×10^{13} ions/cm² ($\approx 10^{14}$) is a safer limit of implantation on NiTi alloy, this limit gives us lesser ion release, better hardness and reasonable hydroxyapatite incubation affinity.

Keywords: Surface modification · nitinol · carbon ions · hardness · ion release · PIXE



Vol. 23, No. 05

Metrics

Downloaded 10 times

History

Received 22 October 2015

Revised 8 March 2016

Accepted 23 March 2016

Published: 19 May 2016

